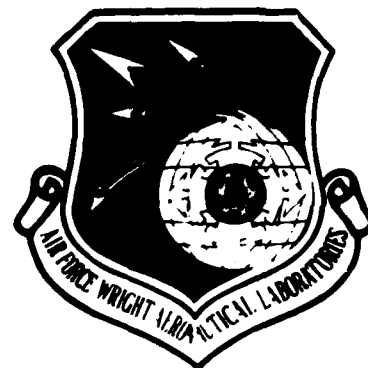


AD A118295

AFWAL-TR-81-3092
VOLUME I



**IMPROVED METHODS FOR PREDICTING
SPECTRUM LOADING EFFECTS**

Volume I - Technical Summary

**J. B. Chang
R. M. Hiyama
M. Szamossi**

**Rockwell International
North American Aircraft Operations
P.O. Box 92098
Los Angeles, CA 90009**

NOVEMBER 1981

*Copy available to DTIC does not
permit fully legible reproduction*

FINAL REPORT FOR PERIOD JANUARY 1979 TO NOVEMBER 1981

Approved for public release; distribution unlimited

**DTIC
ELECTE
AUG 17 1982
S D F**

DTIC FILE COPY

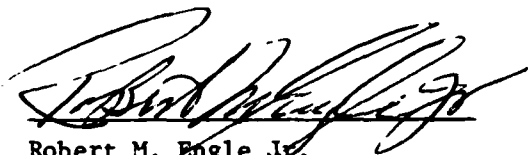
**FLIGHT DYNAMICS LABORATORY
AIR FORCE WRIGHT AERONAUTICAL LABORATORIES
AIR FORCE SYSTEMS COMMAND
WRIGHT-PATTERSON AIR FORCE BASE, OHIO 45433**

82 08 17 011

NOTICE

When Government drawings, specifications, or other data are used for any purpose other than in connection with a definitely related Government procurement operation, the United States Government thereby incurs no responsibility nor any obligation whatsoever, and the fact that the government may have formulated, furnished, or in any way supplied the said drawings, specifications, or other data, is not to be regarded by implication or otherwise as in any manner licensing the holder or any other person or corporation, or conveying any rights or permission to manufacture, use, or sell any patented invention that may in any way be related thereto.

This technical report has been reviewed and is approved for publication.

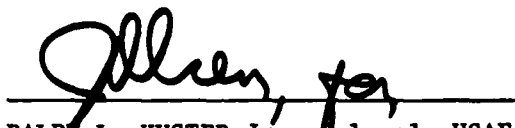


Robert M. Engle Jr.
Project Engineer



Davey L. Smith, Chief
Structural Integrity Branch

FOR THE COMMANDER:



RALPH L. KUSTER Jr., Colonel, USAF
Chief, Structures & Dynamics Division

"If your address has changed, if you wish to be removed from our mailing list, or if the addressee is no longer employed by your organization please notify AFWAL/FIBE, W-P AFB, OH 45433 to help us maintain a current mailing list".

Copies of this report should not be returned unless return is required by security considerations, contractual obligations, or notice on a specific document.

DISCLAIMER NOTICE

**THIS DOCUMENT IS BEST QUALITY
PRACTICABLE. THE COPY FURNISHED
TO DTIC CONTAINED A SIGNIFICANT
NUMBER OF PAGES WHICH DO NOT
REPRODUCE LEGIBLY.**

UNCLASSIFIED

SECURITY CLASSIFICATION OF THIS PAGE (When Data Entered)

REPORT DOCUMENTATION PAGE		READ INSTRUCTIONS BEFORE COMPLETING FORM
1. REPORT NUMBER AFWAL-TR-81-3092	2. GOVT ACCESSION NO. AD-A118 295	3. RECIPIENT'S CATALOG NUMBER
4. TITLE (and Subtitle) IMPROVED METHODS FOR PREDICTING SPECTRUM LOADING EFFECTS - VOLUME I - TECHNICAL SUMMARY		5. TYPE OF REPORT & PERIOD COVERED Final Report - 16 Jan 1979 to 30 Nov 1981
7. AUTHOR(s) J.B. Chang, R.M. Hiyama, M. Szamossi		6. PERFORMING ORG. REPORT NUMBER NA-81-234, Vol. I
9. PERFORMING ORGANIZATION NAME AND ADDRESS Rockwell International North American Aircraft Division P.O. Box 92098 Los Angeles, CA 90009		8. CONTRACT OR GRANT NUMBER(s) F33615-77-C-3121
11. CONTROLLING OFFICE NAME AND ADDRESS		10. PROGRAM ELEMENT, PROJECT, TASK AREA & WORK UNIT NUMBERS 62201F 2401 0120
14. MONITORING AGENCY NAME & ADDRESS (if different from Controlling Office) Air Force Wright Aeronautical Laboratories Flight Dynamics Laboratory (AFWAL/FIBE) Wright-Patterson Air Force Base, Ohio 45433		12. REPORT DATE November 1981
		13. NUMBER OF PAGES 217
		15. SECURITY CLASS. (of this report) Unclassified
16. DISTRIBUTION STATEMENT (of this Report) Approved for Public Release; Distribution Unlimited		15a. DECLASSIFICATION/DOWNGRADING SCHEDULE
17. DISTRIBUTION STATEMENT (of the abstract entered in Block 20, if different from Report)		
18. SUPPLEMENTARY NOTES This report consists of two volumes. Volume II - Test Data		
19. KEY WORDS (Continue on reverse side if necessary and identify by block number) fatigue crack growth, random spectrum loading, load interaction effects, over- load retardation, fatigue crack life prediction, 2219-T851 aluminum, compres- sive load acceleration, preliminary design, individual aircraft tracking		
20. ABSTRACT (Continue on reverse side if necessary and identify by block number) This report presents the technical details of improved methods for pre- dicting the load interaction effects on crack growth under flight spectrum loading developed in a research effort sponsored by the USAF. These include the cycle-by-cycle crack-growth prediction method used in the detail design stage, the flight-by-flight crack-growth analysis method for individual air- craft tracking usage, and preliminary design trade-off studies. Results of the experimental verification program are also presented in this document.		

UNCLASSIFIED

SECURITY CLASSIFICATION OF THIS PAGE (When Data Entered)

FOREWORD

Volume I of this report presents the technical details of the crack-growth prediction methodology developed in a research program entitled "Improved Methods for Predicting Spectrum Loading Effects." This program was administered by the Flight Dynamics Laboratory of the Air Force Wright Aeronautical Laboratories, Wright-Patterson Air Force Base, Ohio, under Contract F33615-77-C-3121, Project 2401, "Structural Mechanics," Task 240101. "Structural Integrity for Military Aerospace Vehicles," Work Unit 24010120. Robert M. Engle (AFWAL/FIBE) was the Air Force project engineer.

This research program was primarily conducted by personnel from the Fatigue and Fracture Mechanics Group, Dynamics Technology, Structure Systems, supervised by George E. Fitch, Jr., supervisor, Joseph S. Rosenthal, manager, and Dr. Leslie M. Lackman, director. James B. Chang was the program manager and the principal investigator of this research program. Principal contributors to the program in addition to the authors were Edward Lkein and Ko-Wei Liu. Drs. Masanobu Shinozuka, Rimas Vaicaitis, and Jan-Nan Yang contributed to phase I, Spectrum Loading Characterization Methodology Development Task.

In addition to this Technical Summary, five other reports have been prepared documenting test data and the resulting computer programs described in this report. Three reports are available upon request from AFWAL/FIBE, Attn: R.M. Engle, W-PAFB, OH 45433. The additional reports are:

AFWAL-TR-81-3092, Volume II, "Improved Methods for Predicting Spectrum Loading Effects: Test Data"

AFWAL-TR-81-3093, Volume I, "A User's Manual for a Detailed Level Fatigue Crack Growth Analysis Computer Code: The CRKGRO Program"

AFWAL-TR-81-3093, Volume II, "A User's Manual for an Interactive Graphics Crack Growth Analysis Program: INTERACTIVE CRKGRO"

AFWAL-TR-81-3094, "A User's Manual for a Computer Program to Predict Fatigue Crack Growth on a Flight-by-flight Basis: FLTGRO"

AFWAL-TR-81-3095, "Revised Structural Technology Evaluation Program (STEP) User's Manual for Structural Synthesis"



Accession For	
NTIS GRA&I	<input checked="checked" type="checkbox"/>
DTIC TAB	<input type="checkbox"/>
Unannounced	<input type="checkbox"/>
Justification	
By _____	
Distribution/	
Availability Codes	
Avail and/or	
Dist	Special
A	23 4

TABLE OF CONTENTS

Section		Page
1.0	INTRODUCTION	1
	1.1 Background	1
	1.2 Program Objective and Scope	1
2.0	PROGRAM SUMMARY	3
3.0	DEVELOPMENT OF DETAILED CRACK GROWTH ANALYSIS METHODOLOGY	6
	3.1 Selection of Fatigue Crack-Growth Rate Relationship	7
	3.2 Load Interaction Model Selection	14
	3.3 Selection of the Damage Accumulation Scheme	24
	3.4 Two-Dimensional (2-D) Crack Growth Approach Evaluation	28
	3.5 Cycle Counting Technique	32
	3.6 Computer Program Input and Output Format Development	35
	3.7 Crack Tip Stress-Intensity-Factor Library	36
	3.8 Plotting Module Development	37
4.0	DEVELOPMENT OF LIFE-PREDICTION METHODOLOGY FOR INDIVIDUAL AIRPLANE TRACKING	38
	4.1 Flight-By-Flight Crack-Growth Method	39
	4.2 Mission-Mix Life Prediction Methodology	42
	4.3 Multisegment-Per-Flight Method Development	45
	4.4 Crack Growth Updating Scheme	50
5.0	DEVELOPMENT OF LIFE-PREDICTION METHODOLOGY FOR PRELIMINARY DESIGN	51
	5.1 Introduction	51
	5.2 Preliminary Design Level Crack-Growth Analysis Program (PRDGRO)	52
	5.3 Preliminary Design-Level Crack Growth Analysis Program (PREGRO)	54
	5.4 Selection of the Crack Growth Analysis Module	57
	5.4.1 Transport Case	59
	5.4.2 Fighter Case	60

Section	Page
5.5 APAS III Program Revision	61
5.5.1 Fracture Mechanics Material Property Library	61
5.5.2 Load Spectrum Generation	62
5.5.3 Stiffened Panel Crack Library	64
5.5.4 Crack-Growth Analysis for Plate Construction Concepts	64
6.0 EXPERIMENTAL VERIFICATION	66
6.1 Experimental Test Program	66
6.1.1 Fighter and Transport Spectrum Development	66
6.1.2 Material and Specimens	68
6.1.3 Testing Procedures	68
6.1.4 Experimental Verification Test Results	69
6.2 Analytical Prediction and Crack Growth Data Correlations	72
6.2.1 Analytical Predictions	72
6.2.2 Crack Growth Test Data Correlations	73
6.2.3 Refinement of Analytical Predictions	74
7.0 CONCLUSIONS AND RECOMMENDATIONS	79
7.1 Conclusions	79
7.2 Recommendations	80
REFERENCES	199

LIST OF ILLUSTRATIONS

Figure	Title	Page
1	Wide-Range Fatigue Crack-Growth-Rate Data of 2219-T851 Aluminum Alloy at Various Stress Ratios	82
2	Coefficients A_1 (R) and A_2 (R) in the Three-Component Model for 2219-T851 Aluminum.	82
3	Wide-Range Fatigue Crack-Growth Rate Data of 2219-T851 Aluminum Alloy Plotted in da/dN Versus $(1-R)^m K_{max}$ Format for $m = 0.4$	83
4	Wide-Range Fatigue Crack-Growth Rate Data of 2219-T851 Aluminum Alloy Plotted in da/dN Versus $(1-R)^m K_{max}$ Format for $m = 0.6$	83
5	Comparison of Crack-Growth Behavior Predictions for Cracks with Small Initial size ($C_i = 0.005$ Inches) Subjected to $\sigma_{max} = 20$ ksi, $R = 0.1$, Constant-Amplitude Loading.	84
6	Comparison of Crack-Growth Behavior Predictions for Crack With Small Initial Size ($C_i = 0.005$ inches) Subjected to $\sigma_{max} = 20$ ksi, $R = 0.3$, Constant-Amplitude Loading	84
7	Fatigue Crack-Growth-Rate Data of 2219-T851 Aluminum Alloy ($da/dN \geq 10^{-7}$ inches/cycle) at Various Stress Ratios	85
8	Fatigue Crack-Growth-Rate Data of 2219-T851 Aluminum Alloy ($da/dN \geq 10^{-7}$ inches/cycle) Plotted in da/dN Versus $(1-R)^m K_{max}$ Format for $m = 0.6$	85
9	Comparison of Crack-Growth Behavior Predictions for a Through-Crack ($C_i = 0.013$ inches) Subjected to $\sigma_{max} = 20$ ksi, $R = 0.1$ Constant-Amplitude Loading	86
10	Comparison of Crack-Growth Behavior Predictions for a Through-Crack ($C_i = 0.016$ inches) Subjected to $\sigma_{max} = 20$ ksi, $R = 0.3$, Constant-Amplitude Loading.	86
11	Comparison of Crack-Growth Behaviors Predicted by Willenborg/Chang and Willenborg Models.	87
12	Four Slopes Used in Runge-Kutta Method.	87
13	Boeing 2219-T851 Aluminum Baseline Crack-Growth-Rate Data Plotted in da/dN Versus $(1-R)^m K_{max}$ Format.	88
14	Boeing 9Ni-4Co-0.2C Steel Baseline Crack-Growth-Rate Data Plotted in da/dN Versus $(1-R)^m K_{max}$ Format.	88
15	Boeing Ti-6Al-4V Baseline Crack-Growth-Rate Data Plotted in da/dN Versus $(1-R)^m K_{max}$ Format.	89
16	Range-Pair Technique of Counting Spectrum Load Cycles	90
17	Range-Pair Counting of Nondefined Load Cycles	90
18	Program Flow Chart of CRKGRO.	91
19	Sample CRKGRO CRT Plot, C Versus N.	92
20	Sample CRKGRO CRT Plot, dc/dF Versus C.	92

Figure	Title	Page
21	Sample CRKGRO CRT Plot, dc/dF Versus N	93
22	Sample CRKGRO CRT Plot, dc/dF Versus K_{max}/Flight	93
23	Comparisons of Predicted Crack-Growth Behavior Under Equivalent Constant Amplitude to Random Spectrum Test Data	94
24	A Sample History of Air-to-Air Maneuver Spectra	95
25	A Sample History of Air-to-Ground Maneuver Spectra.	95
26	A Sample History of Instrumentation and Navigation Maneuver Spectra.	95
27	Comparisons of Predicted Crack-Growth Behaviors to Test Data for Center-Through Crack Subjected to A Composite Fighter Spectrum, $\sigma_{lim} = 20$ ksi	96
28	Comparisons of Predicted Crack-Growth Behaviors to Test Data for Center-Through Crack Subjected to a Composite Fighter Spectrum, $\sigma_{lim} = 30$ ksi	96
29	Comparisons of Predicted Crack-Growth Behaviors to Test Data for Center-Through Crack Subjected to a Composite Fighter Spectrum, $\sigma_{lim} = 40$ ksi	97
30	Spectrum Schematic.	97
31	Comparison of Crack-Growth Predictions Using Various Approaches.	98
32	FLTGRO Tracking Program Crack-Growth Analysis M-91 With Different Mission Parameters.	98
33	Program Flow Chart of PRDGRO.	99
34	Program Flow Chart of PREGRO	100
35	Sample Transport Wing Geometric Parameters.	101
36	Crack-Growth Prediction for a Transport Spectrum Using the Different Crack-Growth Moduels in APAS.	101
37	Crack-Growth Prediction for a Transport Spectrum Using PRDGRO.	102
38	Crack-Growth Prediction for a Transport Spectrum Using PREGRO	102
39	Crack-Growth Prediction for a Transport Spectrum, Including Overload Retardation Effects.	103
40	Sample Fighter Wing Geometric Parameters.	103
41	Crack-Growth Prediction for a Fighter Spectrum Using the Different Crack Growth Modules in APAS.	104
42	Crack-Growth Prediction for a Fighter Spectrum Using PRDGRO.	104
43	Crack-Growth Prediction for a Fighter Spectrum Using PREGRO.	105
44	Crack-Growth Prediction for a Fighter Spectrum, Including Overload Retardation Effects.	105
45	Crack-Growth Prediction Using PROGRO and PREGRO for Library Fighter Spectrum, 1 Flight Block.	106

Figure	Title	Page
46	Crack-Growth Prediction Using PROGRO and PREGRO for Library Fighter Spectrum, 50 Flight Blocks.	106
47	Crack-Growth Prediction Using PROGRO and PREGRO for Library Fighter Spectrum, 100 Flight Blocks	107
48	Crack-Growth Prediction Using PROGRO for Library Fighter Spectrum.	107
49	Crack-Growth Prediction Using PREGRO with Retardation and Acceleration Effects for Library Fighter Spectrum	108
50	Weight Penalty Versus Load Spectrum Block Size.	108
51	Crack-Growth Prediction Based on Actual and Generalized Stress Intensity Correction Factors	109
52	Test Specimen Configuration	109
53	500 KIP Materials Test System	110
54	Schematic of MTS/Datum System 70.	110
55	Fighter Baseline Crack Growth Comparison.	111
56	Fighter A-A Mission Spectrum Variation Crack-Growth Comparison.	111
57	Fighter A-G Mission Spectrum Variation Crack-Growth Comparison.	112
58	Fighter I-N Mission Spectrum Variation Crack-Growth Comparison.	112
59	Fighter Composite Spectrum Variation Crack-Growth Comparison.	113
60	Mission Mix Variation for Short Fighter Spectra	113
61	Fighter Composite Mission-Mix Variation Crack-Growth Test Data Comparison.	114
62	Comparison of Transport Spectrum Variation to Baseline.	114
63	Crack-Growth Correlations, Fighter A-G Baseline	115
64	Crack-Growth Correlations, Fighter I-N Baseline	115
65	Crack-Growth Correlations, Fighter A-A Mission with Compressive Loads Set to Zero	116
66	Crack-Growth Correlations, Fighter Composite Spectrum - DLS = 25 ksi.	116
67	Crack-Growth Correlations, Fighter Composite Spectrum - High Loads Clipped at 85 Percent.	117
68	Crack-Growth Correlations, Fighter Composite Spectrum - 45-Percent Low-Load Truncation.	117
69	Correlation of Fighter Spectrum Test Results, CRKGRO With Load Interaction Predictions (Old Equation)	118
70	Histogram, CRKGRO Life Predictions Correlated With Fighter Spectrum Test Data.	119

Figure	Title	Page
71	Correlation of Combined Fighter and Transport Spectrum Test Results, CRKGRO With Load Interaction Predictions (New Equation)	119
72	Histogram, CRKGRO Life Predictions Correlated With Combined Fighter and Transport Spectrum Test Data (New Equation)	120

LIST OF TABLES

Table	Title	Page
1	Summary - Comparisons of Predicted Crack Lives Obtained From EFFGRO and CPACKS	121
2	Summary, Crack Growth Data Correlations	122
3	Summary of Computer Cost Comparison - Runge-Kutta Method Versus Linear Approximation Method	131
4	Summary - Incremental Interval Size Sensitivity Study . . .	132
5	Summary of Assumptions in Each Analysis Approach	133
6	Crack Growth and Fracture Properties	133
7	Material - 2219-T851 Aluminum Alloy	134
8	Material - 9Ni-4Co-.2C Steel	135
9	Material - Ti-6Al-4V Beta Annealed	136
10	Comparison of Predictive Accuracies - Cycle-Counting Effect Study.	137
11	CRKGRO Program Input Echo, Material Properties, And Crack Geometries	138
12	Typical CRKGRO Program Input Echo Stress Spectrum	139
13	Typical CRKGRO Program Output	140
14	CRKGRO Program Outputs - Summary of Crack Growth	141
15	Input Echo of CYCGRO Program for Determining C, λ , $(\Delta\sigma^b)^{1/b}$	142
16	Parametrics Calculated by CYCGRO Program	143
17	Input Echo of FLTGRO	144
18	Summary of Parameters Determined by FLTGRO for A-A, A-G, and I-N Missions at $\sigma_{lim} = 20, 30, \text{ and } 40 \text{ Ksi}$	145
19	Predicted Crack-Growth Behavior by FLTGRO, M-90	146
20	Predicted Crack-Growth Behavior by FLTGRO, M-91	147
21	Predicted Crack-Growth Behavior by FLTGRO, M-92	148
22	Summary, Comparison of CRKGRO and FLTGRO Program Predictive Accuracies and Costs	149
23	FLTGRO Input Echo	150
24	Sample Transport Detailed Sizing Data	151
25	Sample Transport-Design Stresses	152
26	Flaw Growth Analysis Results Using PROGRO - Transport Spectrum	153
27	Flaw Growth Analysis Results Using PRDGRO Without Retardation - Transport Spectrum	154
28	Flaw Growth Analysis Results Using PRDGRO With Retardation - Transport Spectrum	155
29	Flaw Growth Analysis Results Using PREGRO Without Retardation - Transport Spectrum	155
31	Sample Fighter-Detail-Sizing Data	156
32	Sample Fighter-Design Stresses	157

Table	Title	Page
33	Flaw Growth Analysis Results Using PROGRO - Fighter Spectrum	158
34	Flaw Growth Analysis Results Using PRDGRO Without Retardation - Fighter Spectrum	159
35	Flaw Growth Analysis Results Using PRDGRO With Retardation - Fighter Spectrum	159
36	Flaw Growth Analysis Results Using PREGRO Without Retardation - Fighter Spectrum	160
37	Flaw Growth Analysis Results Using PREGRO With Retardation - Fighter Spectrum	160
38	Preliminary Fracture Mechanics Material Property Library Data	161
39	Typical Lightweight Fighter Air-to-Air Combat Mission	162
40	Cumulative Occurrences per 1,000 Flight Hours of Supersonic Air-To-Air Combat	162
41	Typical Air-to-Air Fighter Fatigue Spectrum - Cycles Per 1,000 Flights	163
42	APAS - Generated Air-To-Air Fighter Spectrum Excluding Fractional Cycles, 1-Flight Block	164
43	APAS-Generated Air-to-Air Fighter Spectrum Excluding Fractional Cycles, 1-Flight Block	165
44	APAS-Generated Air-to-Air Fighter Spectrum Excluding Fractional Cycles, 100 Flight Block	166
45	APAS Program Results - Air-To-Air Fighter Spectrum	167
46	Flaw-Growth-Analysis Results Using PROGRO - Library Fighter Spectrum, 1-Flight Block	168
47	Flaw-Growth-Analysis Results Using PREGRO Without Load Interaction Effects - Library Fighter Spectrum, One Flight Block	168
48	Flaw-Growth-Analysis Results Using PREGRO With Retardation And Acceleration Effects - Library Fighter Spectrum, 1-Flight Block	169
49	Flaw-Growth-Analysis Results Using PREGRO With Retardation Effects - Library Fighter Spectrum, 1 Flight Block	169
50	Flaw-Growth Analysis Results Using PROGRO - Library Fighter Spectrum, 50 Flight Block	170
51	Flaw Growth Analysis Results Using PREGRO Without Retardation Effects Library Fighter Spectrum, 50 Flight Blocks	170
52	Flaw-Growth-Analysis Results Using PREGRO With Retardation And Acceleration Effects - Library Fighter Spectrum, 50 Flight Blocks	171

Table	Title	Page
53	Flaw-Growth-Analysis Results Using PREGRO With Retardation Effects - Library Fighter Spectrum 50 Flight Blocks	171
54	Flaw-Growth-Analysis Results Using PREGRO - Library Fighter Spectrum, 100 Flight Blocks	172
55	Flaw-Growth-Analysis Results Using PREGRO Without Load Interaction Effects - Library Fighter Spectrum, 100 Flight Blocks	172
56	Flaw-Growth-Analysis Results Using PREGRO With Retardation And Acceleration Effects - Library Fighter Spectrum, 100 Flight Blocks	173
57	Flaw-Growth-Analysis Results Using PREGRO With Retardation Effects - Library Fighter Spectrum, 100 Flight Blocks . .	173
58	Fighter Spectrum Variation Test Program	174
59	Fighter Spectrum Mission-Mix Test Program	175
60	Divided Unitblock For (A-A) ^I (A-G) ^I And (I-N) ^I Missions . .	176
61	Group III - a Mission Mix Variation For Fighter Spectra . .	176
62	Divided Unitblocks of (A-A) ^{III} (A-G) ^{III} and (I-N) ^{III} Missions	177
63	Transport Composite Baseline Spectrum G-A-G	178
64	2219-T851 Aluminum Chemical Contents	179
65	2219-T851 Aluminum Physical Properties	179
66	Summary of Test Results For Fighter Baseline Spectra . . .	180
67	Summary of Test Results for Fighter Spectrum Variations	180
68	Comparison Of Crack Lives for A-A Mission Spectrum Variations To A-A Baseline Spectrum	181
69	Comparison Of Crack Lives For A-G Mission Spectrum Variations To A-G Baseline Spectrum	181
70	Comparison Of Crack Lives For I-N Mission Spectrum Variations To I-N Baseline Spectrum	181
71	Comparison Of Crack Lives For Composite Mission Spectrum Variations To Composite Baseline Spectrum	182
72	Comparison Of Mission-Mix Crack Growth Lives To The Baseline	183
73	Summary of Test Results For Mission Mix Variations - Group A	184
74	Summary Of Transport Spectrum Variation Test Results.	185

Table	Title	Page
75	Fighter Baseline and Spectrum Variation Tests, Comparison of Prediction Accuracies CRKGRO Versus FLTGRO	186
76	Comparison Of Prediction Accuracy For Transport Spectra Cases - CRKGRO Versus FLTGRO.	189
77	Summary of Correlation Results	190
78	Comparison Of Prediction Accuracy For Fighter Spectra Cases - New Versus Old Equations	191
79	Comparison Of Prediction Accuracy For Transport Spectra Cases - New Versus Old Equations	194
80	Results Of Sensitivity Study Of R_{cut} Values To Prediction Ratio, N_p/N_T	195
81	Comparison Of Prediction Accuracy For Fighter Spectra Cases - With Varying Negative Stress Ratio Cutoff Values	196
82	Comparison Of Prediction Accuracy For Transport Spectra Cases - With Varying Negative Stress Ratio Cutoff Values	198

1.0 INTRODUCTION

1.1 BACKGROUND

Implementation of current Air Force structural integrity philosophy as defined in Military Standard MIL-STD-1530A, Aircraft Structural Integrity Program (ASIP), Airplane Requirements,⁽¹⁾ requires the capability for accurate and efficient prediction of crack-growth under exceedingly complex service loadings, in either ordered spectrum or random spectrum format. A considerable amount of experimental data exist which demonstrate significant increase in fatigue crack-growth life due to the presence of tensile overloads in spectrum loading. More recent data have shown that compressive loads reduce the retardation effects caused by overloads. Several analytical models have been developed for predicting these load interaction effects. They rely on processing the load history on either the stress level by stress level basis for ordered spectra, or the cycle-by-cycle basis for random spectra. For complex and long flight load histories, the data preparation time and computer cost become excessive.

Furthermore, since the current ASIP requires implementation of damage-tolerance control procedures throughout the life cycle of any aircraft system, the capability for assessing the impact of damage-tolerance requirements is needed from the preliminary design stage, through the detailed stress analysis stage, to the tail number tracking and life extension programs for production system. Usually, there are different requirements on the predictive accuracy in the performance of crack-growth analysis in each of the aforementioned stages. For instance, it is not cost-effective to perform a very detailed crack-growth analysis when only an order-of-magnitude-type comparison between flight spectra is needed in the preliminary design stage. Trade-offs should be made between the accuracy of the prediction needed and the sophistication of model used in the analytical prediction methodology. Hence, the need for the development of different levels crack-growth prediction methodology is obvious.

1.2 PROGRAM OBJECTIVE AND SCOPE

The objective of this program was to develop the improved crack-growth prediction methodology required for implementation of the damage-tolerance control procedure, from the preliminary design stage, through the detailed design analysis stage, to the force management stage of any weapon system. This program developed analytical models for characterizing spectrum loading relative to its effects on crack growth. Trade-offs were identified between life prediction sensitivity and model sophistication. Three levels of crack-growth analysis were considered:

1. Detailed crack-growth analysis which would be capable of predicting the load interaction effects commensurate with the cycle-by-cycle capability.
2. Parametric crack-growth analysis which would be capable of predicting effects due to change in aircraft usage or mission mix.
3. Preliminary design analysis which would provide rapid comparative analysis which realistically accounts for spectrum load interaction effects on crack growth.

2.0 PROGRAM SUMMARY

To accomplish the program objective, a research effort which consists of the following three phases has been conducted at Rockwell International, North American Aircraft Division (Rockwell/NAAD):

Phase I - Identification of Controlling Damage Parameters

Phase II - Development of Prediction Methodology

Phase III - Experimental Verification

In phase I, three interrelated tasks were performed. Task I-1 conducted an evaluation of the state-of-the-art of currently used methods for analyzing fatigue crack-growth behavior under spectrum loading. Experimental data generated from research programs sponsored by the Air Force were used in the evaluation. Task I-2 developed a general method for characterizing flight loadings such that the cycle-by-cycle crack-growth analysis could be eliminated. A statistical approach which replaces the actual stress history with a simplified history was developed. To aid in formulation of the procedure, an experimental test program was conducted. From experimental results, significant parameters which control the rate of damage, such as stress levels and ratios, and the load interaction effects, such as tension overload retardation, compressive load acceleration, reduction of retardation by compressive loads, etc, were identified. Task I-3 established guidelines for development of three levels of crack-growth analysis: detail design, individual aircraft tracking, and preliminary design. All technical findings and test data generated in phase I were documented in the Phase I Final Report. (2,3)

Three tasks were conducted in phase II. Task II-1 was the formulation of an advanced life-prediction methodology used for detailed crack-growth analysis. As a result, a two-dimensional (2-D) crack-growth computer program, CRKGRO, which incorporates an improved load interaction model and uses the most efficient damage accumulation scheme, was developed. CRKGRO also provides graphical output options such that users are able to obtain plots, including crack length (a) versus number of flights, growth rate per flight (da/df) versus number of flights, etc. Furthermore, CRKGRO provides the option for users to perform a parametric study. Parameters such as limit stress levels (σ_{lim}) and fracture toughness (K_C) values are currently available to be included in performance of the parametric study of the crack-growth behavior for various types of cracks commonly detected in the airframe structures. Reference 4 presents instructions for executing CRKGRO.

The second task performed in phase II was the formulation of a crack-growth analysis methodology for use in the individual aircraft tracking (IAT) program. A computer routine, FLTGRO, was developed to meet the needs. FLTGRO uses a statistical approach to convert the random cycle-by-cycle flight spectrum to either a one-cycle-per-flight or multisegment-per-flight format, saving costs substantially. The FLTGRO program also provides graphical output options such that the updated crack-growth behavior based on the real-service flight data can be plotted against the crack-growth behavior based on the designed spectrum. The User's Manual of FLTGRO is documented in Reference 5.

Task II-3 was the implementation of a fatigue crack-growth analysis methodology into the Automated Predesign of Aircraft Structures (APAS III) computer program⁽⁶⁾. APAS III is a highly modularized program which is the structural synthesis procedure used within the Structure Technology Evaluation Program (STEP) developed by General Dynamics for the Air Force⁽⁷⁾. A crack-growth analysis module, PREGRO, which is the modified version of FLTGRO, was the final selection incorporated into APAS III. PREGRO realistically accounts for tensile overload retardation and compressive load acceleration effects to fatigue crack growth. Hence, an unnecessary weight penalty or unsafe design can be avoided in the preliminary design stage of any weapon system. To broaden the usage of the APAS III program, a load spectrum for an air-to-air lightweight fighter has been incorporated into APAS such that APAS can be used for the evaluation of fighter-type airplanes in addition to transport-type airplanes.

An experimental verification program was conducted in phase III to verify the crack-growth prediction methods developed in phase II. This program consisted of two major tasks. The first task was a test program which contained two primary test groups: Group I - Fighter Spectrum Loading Test, and Group II - Transport Spectrum Loading Test. The second task was the performance of analytical predictions using the computer codes CRKGRO and FLTGRO developed in phase II. Analytical predictions were then correlated with the test data.

All spectrum tests were conducted at the Structure Test Laboratory of Rockwell/NAAD El Segundo facilities. The test specimens were the standard ASTM center-cracked tension (CCT) panels⁽⁸⁾ machined from a single heat of 2219-T851 aluminum plates. The center notches were installed through the electrical discharge machining process. Test specimens were precracked before the application of spectrum loading. All tests were conducted employing the 500K MTS fatigue testing system. The randomized spectrum loads were controlled by the Datum Servosystem 70, a computer-controlled fatigue test system.

For the Group I tests, four baseline load spectra of the F-15 fighter aircraft furnished by the Air Force were used to generate the fighter baseline

test spectra and their variations. These baseline spectra were the air-to-air (A-A) mission, the air-to-ground (A-G) mission, the instrumentation and navigation (I-N) mission, and the composite mission. All baseline spectra were in the random cycle-by-cycle format. The peak and valley of each cycle were in the form of percentage of design limit stress.

Twenty-one spectrum variation tests were conducted in the Group I test program. All spectra variation were developed from the aforementioned baselines. The variations considered in the tests included stress level, compression load, high load clipping, low load truncation, and mission sequence. In addition to the spectrum variation tests, eight mission-mix variation tests were also conducted in Group I. The A-A, A-G, and I-N missions were used to develop the mixed missions.

For the Group II tests, a typical transport composite mission spectrum furnished by the Air Force in phase I was again used as the baseline. The baseline test was conducted with the initial crack at a slightly different size than that in the phase I test program.⁽³⁾ Seven transport spectrum variations were derived from the composite baseline spectrum. Again, stress level, compressive stress, and low load truncation were the primary variations tested.

Fatigue crack-growth predictions applying the cycle-by-cycle crack-growth analysis methodology were performed through the use of CRKGRO. Analytical predictions were also made by using the FLTGRO program, which employs the spectrum characterization method developed in phase I. Analytical predictions obtained from CRKGRO and FLTGRO were then correlated to the crack-growth test data. To assess the prediction accuracy of each method, the ratio of the predicted crack-growth life to the test crack-growth-life, N_p/N_T was calculated for each test case. Results show that for the 33 fighter spectrum test cases, the average prediction ratio obtained by CRKGRO was $N_p/N_T = 0.88$ with an 0.17 standard deviation. For the eight transport test cases, the average CRKGRO prediction ratio is $N_p/N_T = 1.05$ with an 0.35 standard deviation. When all 41 test cases were combined together, the average CRKGRO prediction ratio was $N_p/N_T = 0.92$ with an 0.22 standard deviation. The average FLTGRO prediction ratio for the fighter spectrum cases was $N_p/N_T = 1.04$ with an 0.26 standard deviation; for the transport cases, the average FLTGRO prediction ratio was 1.50 with an 0.34 standard deviation. The combined FLTGRO prediction ratio was 1.13 with an 0.33 standard deviation. The results of the experimental verification task demonstrated that the predictability of the crack-growth analysis methods developed in this program is well within the required accuracy.

3.0 DEVELOPMENT OF DETAILED CRACK GROWTH ANALYSIS METHODOLOGY

For the performance of detailed damage tolerance and durability analyses as specified in MIL-STD-1530A, a reliable and accurate analytical prediction methodology is needed. In phase I of this research effort⁽¹⁾, guidelines for the development of such a crack growth analysis methodology have been established. The following are some highlights:

1. The crack growth analysis procedure will be developed based on the principles of linear elastic fracture mechanics (LEFM). A mathematical model with the crack growth per cycle, da/dN , as the dependent variable and an appropriate function, $f(K,R)$, as the independent variable will be chosen to represent the crack-growth-rate relationship, where K is the crack-tip stress intensity factor and R is the cyclic stress ratio.
2. A state-of-the-art load interaction model will be incorporated into the crack-growth analysis methodology. The load interaction model chosen will be capable of accounting for the effects of interactions of various types of load cycles, including the tensile overload retardation, faster growing rate due to the existence of the compressive loads, and the reduction of retardation by compressive load immediately following the tensile overload. Furthermore, there will be no excessive data or lengthy computation needed in the analysis.
3. The integration scheme adopted in the detailed crack growth analysis will be efficient, such that there will be no excessive computation cost in the operation.
4. The change of aspect ratio will be accounted for in predicting crack growth lives of part-through cracks or corner cracks at fastener holes.

Efforts denoted in the methodology development phase (phase II of this program) were divided into four steps. The first step was to select the most applicable state-of-the-art crack-growth-rate equation, the most versatile load interaction model, and the most efficient integration scheme. The second step was to organize the framework of the computer software which implements the selected crack growth prediction method. The third step was to formulate the stress intensity factor (K) solutions for the most commonly seen crack configurations and to incorporate these K -factor solutions into the crack library which is a collection of subroutines, each subroutine containing a K -factor solution for a specific crack geometry. The last step was to prepare the user's manual for the computer software.

3.1 SELECTIONS OF FATIGUE CRACK-GROWTH-RATE RELATIONSHIP

For the performance of a detail crack growth analysis using a deterministic approach, the following elements are interrelated:

1. A fatigue crack-growth-rate relationship and the corresponding growth rate constants
2. Initial crack types, sizes, and geometries of the body containing such cracks.
3. Crack-tip stress intensity factor solutions
4. An integration procedure

The fatigue crack-growth-rate data of commonly used metallic structural materials presented in the literature took the following forms:

1. Tabulated form - data were tabulated along with the test variables
2. Graphical display - data were plotted on a chosen coordinate system
3. Mathematical form - data were represented by a mathematical equation

In the performance of fatigue crack growth analysis, the common practice is to perform numerical integration on a given crack-growth-rate equation (sometimes incorrectly called a crack growth law).

In general, the instantaneous rate of change of the crack size per cycle (da/dN) is chosen as the dependent variable in the crack growth equation. However, the independent variable chosen in the literature varies widely from one to another. Prior to the development of the LEFM, the independent variable selected in most crack-growth-rate equations varied from one to another. They were selected to account for parameters which influence the fatigue crack growth behavior. These included the crack size, a ; maximum cyclic stress, σ_{max} ; stress ratio, R ; and other parameters such as environment, Env ; temperature, T ; frequency, f ; and stress concentration factor, k_N . In general form, the fatigue crack-growth-rate equations were expressed as

$$da/dN = f(a, \sigma_{max}, R, T, f, \dots)$$

Numerous crack growth rate equations in this form were proposed in the 1950's and early 1960's. Several of them were briefly described in the phase I report.⁽²⁾ Others can be found from the literature.

The first fatigue-crack-growth-rate equation based on the LEFM concept was proposed by Paris. The famous Paris' fatigue crack-growth-rate equation assumes

that the intensity of the crack-tip stress field (the crack-tip stress intensity factor, K) is the controlling parameter to the cyclic crack growth; i.e.,

$$da/dN = f(K)$$

From data of 7075-T6 and 2024-T3 aluminum alloys, Paris suggested the following equation, which is often referred to as Paris' power law(9).

$$da/dN = C(\Delta K)^n$$

where C and n are experimentally determined constants, and $\Delta K = K_{\max} - K_{\min}$ is the stress intensity factor range.

Paris' rate equation results in a straight-line presentation on a double-logarithm scale with da/dN plotted on the ordinate and ΔK plotted on the abscissa. The exponent n corresponds to the slope of the straight line, and the coefficient C is the growth rate interception corresponding to a unit value of ΔK .

As more test data were generated from fatigue crack growth testing under various loading conditions, it became obvious to many investigators that the simple Paris equation was not adequate in describing the cyclic crack growth characteristics for a given material under all types of loading conditions. Various modifications to Paris rate equation were proposed in the past 20 years. These included the Forman⁽¹⁰⁾, Walker⁽¹¹⁾, Collipriest⁽¹²⁾, Boeing⁽¹³⁾, Grumman⁽¹⁴⁾, three-component⁽¹⁵⁾, modified Walker⁽¹⁶⁾ equations, etc. A review of the state-of-the-art equations was conducted in phase I. Brief descriptions of these modified rate equations were documented in the phase I report⁽²⁾.

In the state-of-the-art methods evaluation task conducted in phase I, important criteria for choosing a constant-amplitude crack-growth-rate equation to be incorporated into the detailed-level crack growth analysis computer module were established, including:

1. It will represent the cyclic crack-growth-rate characteristics in the rate range which is normally of interest to aircraft detailed design analysis.
2. It will be compatible with the selected load interaction model. The load interaction model will account for the retardation effect of the overload contained in the tension (positive stress ratio) cycles and the acceleration effect of the compressive load in the tension-compression (negative stress ratio) cycles.
3. The selected crack-growth-rate equation will be in a relatively simple form such that it can be adopted easily for performing the hand calculations.

Two crack-growth-rate equations which were judged to be the best candidates among all state-of-the art equations for performing the detailed-level crack growth analysis were examined. They were the modified Walker⁽¹⁶⁾ equation (also identified as Rockwell's equation throughout this report) and the three-component ⁽¹⁵⁾ equation.

The Walker equation was formulated based on Walker's effective stress concept, which was developed to account for the stress ratio effects on fatigue crack growth behavior. In the original form, the Walker's effective stress was defined as⁽¹¹⁾

$$\bar{\sigma} = \sigma_{\max}^{1-m} \Delta\sigma^m$$

where m is an empirical constant and $\Delta\sigma = \sigma_{\max} - \sigma_{\min}$ is the stress range.

In terms of the effective stress, the Walker equation can be written as

$$\frac{da}{dN} = f(\bar{\sigma} \sqrt{\pi a}) = f(\bar{\Delta}K)$$

where $\bar{\Delta}K$ is the effective stress intensity range.

Based on Paris' fatigue crack-growth-rate model⁽⁹⁾, the Walker equation can be rewritten in the following form:

$$\begin{aligned} \frac{da}{dN} &= C [\bar{\Delta}K]^n \\ &= C \left[\sigma_{\max}^{1-m} \Delta\sigma^m \sqrt{\pi a} \right]^n \\ &= C \left[(1 - R)^m K_{\max} \right]^n \end{aligned}$$

where K_{\max} is the maximum stress intensity factor and C and n are crack-growth-rate constants.

The crack-growth-rate equation currently employed in the Rockwell in-house-developed fatigue crack growth analysis computer program, EFFGRO⁽¹⁶⁾, is a modified version of the Walker equation. It was formulated in terms of the stress intensity factor range ΔK instead of K_{\max} . In addition, the modified Walker equation adopts the threshold stress intensity factor range concept and the cutoff stress ratio approach. The threshold stress intensity factor range (ΔK_{th}) is defined as the threshold value of ΔK , below which there is not fatigue crack growth. The cutoff stress ratio, R_{cut} , is defined as the cutoff value of the positive stress ratio R , above which no further layering

is shown in the da/dN versus ΔK plot. In terms of ΔK and ΔK_{th} , the modified Walker equation can be expressed as:

for $\Delta K > \Delta K_{th}$

$$\frac{da}{dN} = C \left[\frac{\Delta K}{(1 - \bar{R})^{1-m}} \right]^n, \quad \begin{array}{ll} 0 \leq \bar{R} \leq R_{cut}^+, & \bar{R} = R \\ 0 \leq \bar{R} > R_{cut}^+, & \bar{R} = R_{cut}^+ \end{array}$$

for $\Delta K \leq \Delta K_{th}$

$$\frac{da}{dN} = 0$$

The three-component model was developed by Hudak, et al⁽¹⁵⁾, based on adding the material resistance to fatigue crack growth $((da/dN)^{-1})$, in the three regions of $\log (da/dN)$ versus $\log (\Delta K)$ plot. A mathematical representation of the R -dependence of da/dN using the three-component model takes the following form:

$$\left(\frac{da}{dN} \right)^{-1} = \frac{A_1(R)}{(\Delta K)^{n_1}} + \frac{A_2(R)}{(\Delta K)^{n_2}} - \frac{A_2(R)}{\left[(1 - R) K_c \right]^{n_2}}$$

In the preceding equation, the functions $A_1(R)$ and $A_2(R)$ directly dominate the stress ratio dependencies in regions I and II, respectively. Region I is the slow-growth region, with the growth rate, da/dN , in general, less than 10^{-7} in./cycle, while region II is the intermediate growth region. The crack growth rate in region II is between 10^{-7} and 10^{-3} in./cycle. The onset of instability in region III is described by the term $(1-R) K_c$, where K_c is a fitting parameter.

A study of the predictive accuracies of the three-component model and the modified Walker equation has been conducted using EFFGRO. Experimental crack-growth-rate data for 2219-T851 aluminum alloy at various stress ratios generated by Hudak, et al⁽¹⁵⁾, was used as the material data base because they covered a wide range (from 10^{-9} to 10^{-3} in./cycle at various stress ratios, as shown in Figure 1.

The three-component model predictions employed the rate constants generated by Hudak, et al, for this selected 2219-T851 aluminum data set, as follows:

$$n_1 = 12.5$$

$$n_2 = 3.3$$

$$\begin{cases} A_1(R) = 1.41 \times 10^{14} (1 - R)^{15}, & 0.1 \leq R \leq 0.5; \\ A_1(R) = 4.3 \times 10^9, & R \geq 0.5 \end{cases}$$

$$\begin{cases} A_2(R) = 4 \times 10^8 (1 - R)^{0.92}, & 0.3 \leq R \leq 0.8; \\ A_2(R) = 2.72 \times 10^8, & R = 0.1 \end{cases}$$

$$K_C = 35 \text{ ksi } \sqrt{\text{in.}}$$

The stress ratio (R) dependency of the coefficients $A_1(R)$ and $A_2(R)$ for 2219-T851 aluminum is shown in Figure 2. For values between 0.1 and 0.5, $A_1(R)$ is very sensitive to the stress ratio. For values between 0.5 and 0.8, $A_1(R)$ remains virtually constant. On the contrary, the coefficient $A_2(R)$ varies by a factor of 3 between $R = 0.1$ and 0.3. For R-values between 0.3 and 0.8, the variation in A_2 is shown in Figure 2b.

The modified Walker equation prediction employed growth rate constants (C, n, and m) determined by a computer graphical plotting routine, PLOT RATE(17), from the identical set of 2219-T851 aluminum alloy data. PLOT RATE determines the corresponding rate constants for a specified growth rate equation by curve fitting the crack-growth rate dependent variable da/dN versus any independent variable $f(K,R)$, in a specific form on a double-logarithm scale. The original input data formats to the PLOT RATE program are: (1) crack growth data consist of crack size "a" and corresponding load cycles, and (2) values of da/dN and corresponding K_{max} or $\Delta K = (1-R) K_{max}$. The PLOT RATE program was modified to add digitizing ability such that the crack-growth-rate data presented in $\log (da/dN)$ versus (ΔK) or $\log (K_{max})$ forms can be traced through a subroutine, DTIZ, and then automatically input to PLOT RATE.

For the modified Walker equation, $f(K,R) = (1-R)^m K_{max}$. Figures 3 and 4 show this set of crack-growth-rate data plotted in da/dN versus $(1-R)^m K_{max}$ format for $M=0.4$ and 0.6 . When $m=0.6$, the stress ratio layering effects for 2219-T851 aluminum reduced to minimum. Therefore, the Walker stress ratio collapsing factor $m=0.6$ was chosen. The corresponding C and n values for $m=0.6$ are automatically determined by PLOT RATE through a least-square fitting procedure as:

$$C = 2.004 \times 10^{-10} \quad (\text{in ksi unit})$$

$$n = 4.36$$

Other parameters used in the modified Walker equation for predictions are

$$\Delta K_{th} = (1-R)\Delta K_{th_0}$$

where

$$\Delta K_{th_0} = 2.5 \text{ ksi } \sqrt{\text{in.}}$$

$$R_{cut}^+ = 0.75$$

To investigate the applicable range of these two rate equations, a center-through crack contained in a 6-inch-wide panel subjected to constant-amplitude loads with the maximum stress at a moderate level ($\sigma_{max} = 20$ ksi) case was considered. The initial crack size chosen for the study was $C_i = 0.005$ inch in order to cover the growth behavior in the slow growth region ($da/dN < 10^{-7}$ in./cyc). Crack growth behaviors predicted by EFFGRO using the modified Walker equation and the total range growth rate constants above were plotted as shown in Figures 5 and 6 for $R = 0.1$ and 0.3 , respectively. For comparisons, parallel runs were made by EFFGRO using the three-component model and the corresponding rate constants. Results of the three-component model predictions were plotted against the modified Walker equation predictions shown in Figures 5 and 6. At $R = 0.1$, the crack-growth life from $C_i = 0.005$ to $C_f = 0.8$ inch predicted by the modified Walker equation was $\Delta N = 110 \times 4,000 = 440,000$ cycles. Compared with $\Delta N = 1,268,000$ cycles predicted by the three-component model, a factor of 3 shorter in life prediction resulted. At $R = 0.3$, for the same crack growth interval (0.005 to 0.8 inch), the crack growth life predicted by the modified Walker equation differs only 9 percent to that predicted by the three-component model.

In general, for damage-tolerance analysis of airframe structures, the growth rate range is between 10^{-7} to 10^{-3} inch per cycle. Hence, to assess the ability of the modified Walker equation in performing damage-tolerance

analysis, only those data points in Figure 1 with $da/dN \geq 10^{-7}$ in./cycle above input to PLOT RATE by using the interactive system through DTIZ. Fatigue crack-growth-rate data for $da/dN \geq 10^{-7}$ in./cycle plotted in da/dN versus ΔK format by PLOT RATE are shown in Figure 7. The stress ratio (R) effect is still clearly shown. Again, various values of m were selected using PLOT RATE to plot the da/dN against the independent variable of the modified Walker equation, $f(K,R) = (1-R)^m K_{max}$, on a double-logarithm scale. Results showed that $m = 0.6$ was still the best choice. The corresponding growth rate constants determined by PLOT RATE are shown in Figure 8 as:

$$C = 7.212 \times 10^{-10} \quad (\text{in ksi units})$$

$$n = 3.84$$

Fatigue crack growth behaviors of the same center-through crack under the identical loading conditions were repredicted by EFFGRO using the modified Walker equation with the previously listed rate constants. For the $\sigma_{max} = 20$ ksi, $R = 0.1$ case, the initial crack size was selected to be $C_i = 0.013$ in. The initial crack growth rate at this size is 1.2×10^{-7} in./cycle. For the $\sigma_{max} = 20$ ksi, $R = 0.3$ case, a 0.016 initial crack size was selected. Crack growth behavior predicted by the modified Walker equation using the new set of rate constants for $da/dN \geq 10^{-7}$ in./cycle is shown in Figures 9 and 10. For comparison, the three-component model predictions were reanalyzed by EFFGRO. The same wide-range rate constants were used in the predictions. The predicted growth behavior was plotted against the modified Walker equation predictions shown in Figures 9 and 10. Results show good agreement between the three-component model and the modified Walker equation predictions for crack-growth-rate above 10^{-7} in./cycle.

It was decided to adopt the modified Walker (Rockwell) equation as the fatigue-crack-growth-rate equation in the to be developed computer program due to its simplicity, which was one of the major criteria used in selection of the rate equation.

3.2 LOAD INTERACTION MODEL SELECTIONS

The service loadings of aircraft are variable amplitude in nature. Various load interaction effects on the crack growth behavior under variable amplitude loading have been observed and studied by many investigators. The general effects can be summarized as follows:

1. Tensile overloads introduce significant retardation of the crack growth. The retarded growth sometimes does not immediately follow the overload cycles. Some data indicate that if the overload is sufficiently high with respect to the following load levels, the crack may even stop growing.
2. Compressive loads in tension-compression or compression-tension cycles (negative stress-ratio cycles) tend to accelerate the crack growth rate.
3. Tensile underloads in a low-high sequence of loading tend to accelerate the crack growth rate immediately following the low-high transition.
4. A block of overload cycles with the same amplitude tend to retard the crack growth more than a single overload cycle.

Various mathematical models have been proposed by numerous investigators to account for the load interaction effects on fatigue crack growth behaviour under variable amplitude loadings. Most widely used are the Wheeler retardation model⁽¹⁸⁾, Willenborg retardation model⁽¹⁹⁾, Vroman retardation model⁽²⁰⁾, Elber closure model⁽²¹⁾ and their modified versions; i.e., the generalized closure model developed by Bell, et al⁽²²⁾, the contact stress model formulated by Dill, et al⁽²³⁾, and the Vroman/Chang model proposed by Chang⁽²⁴⁾. A review of these models was conducted in phase I.

Guidelines for choosing a load interaction model used in the detailed crack growth analysis program were also established as a result of the state-of-the-art methods review. The following items summarize the guidelines presented in the phase I technical report⁽²⁾.

1. The load interaction model will be able to account for the retardation effect due to existence of tensile overload cycles, the

acceleration effect caused by compressive loads and the coupling effects such as reducing retardation by compressive load cycles immediately following the overloads.

2. The model will be compatible with the constant-amplitude fatigue crack-growth-rate equation used in the computer program.
3. The model will be simple and contain a limited amount of empirical constants such that no excessive test data need to be generated.
4. The model will be easily implemented in the computer program. Furthermore, there will be no lengthy calculation involved in applying the load interaction model.

Rigorously speaking, none of the existing models reported in the literature meet all the requirements listed above. For example, the crack closure model proposed by Bell, et al⁽²²⁾, has been shown in the literature consistently providing fairly good predictions for a variety of loading conditions. However, their closure model is strictly an empirical model. Variable-amplitude test data, in addition to constant-amplitude data, are required for each material where predictions are required. Consequently, if the crack closure model is used on production-base detailed crack growth analysis rather than a specific research project, conducting an extensive test program will be necessary to generate the required data base for several candidate materials.

The contact stress model, on the other hand, is based on the analysis of crack surface contact stresses. The contact stresses behind the crack tip are found by treating the potential interference as a wedge between the surfaces and performing an elastic-plastic analysis of the stresses caused by this wedge. Dill, et al⁽²³⁾, employed a finite-element model consisting of 25 constant stress elements to idealize the wedge. Bueckner's weight function approach⁽²⁵⁾ was used to develop an influence coefficient matrix for the displacement stress relationship between elements. The analysis was interactive so that a solution was determined wherein the maximum contact stress was limited to the yield strength of the material. In its basic form, this spectrum crack growth prediction method is not cost effective for performing crack growth analysis in the detailed design stage of a weapon system development. Some techniques have been developed to accelerate the analysis for spectrum predictions.

The effective stress model developed by Willenborg, et al⁽¹⁹⁾, assumes that the overload retardation effect on crack growth is caused by variations in the local stress field as the crack grows through the compressive residual

stress zone produced by the overload. The "effective stress," which is defined as $(\sigma)_{\text{eff}} = \sigma^{\infty} - \sigma_{\text{RED}}$, is then employed to calculate the effective stress intensity factor range, $(\Delta K)_{\text{eff}}$, and the effective stress ratio, R_{eff} . It can be shown that the value of $(\Delta K)_{\text{eff}}$ is the same as that of ΔK^{∞} ; thus, the Willenborg model actually predicts retardation by depressing the effective stress ratio, $R_{\text{eff}} = (\sigma_{\text{min}}^{\infty} - \sigma_{\text{RED}}) / (\sigma_{\text{max}}^{\infty} - \sigma_{\text{RED}})$, below that remotely applied, while keeping the effective stress intensity factor range unchanged. The Willenborg model predicts that maximum retardation will occur immediately after application of the overload and that the growth rate will return to its constant-amplitude counterpart when the current interaction zone reaches to the end of the overload interaction zone. It also can be shown that the Willenborg model predicts zero crack growth rate for the case when the overload ratio is two (the so-called overload shutoff ratio). Test results obtained by several investigators show that the actual overload shutoff ratio can be greater than two. Gallagher, et al⁽²⁶⁾, has proposed a generalized Willenborg model to correct prediction of the overload-to-maximum-load ratio required to arrest the crack growth. The generalized Willenborg model has been demonstrated to provide satisfactory predictions on the retardation effect on the crack growth behavior under variable-amplitude loading containing overload cycles^(27,28). However, the current generalized Willenborg model does not account for acceleration effects on crack growth due to either compression loadings in the tension-compression load cycles or underloads (small tension-tension load cycles) in low-high sequence loadings.

The Vroman model resembles the Willenborg model in the sense that it also uses the "residual stress" concept in predicting overload retardation effects to the crack growth. The original Vroman model⁽²⁰⁾, which only accounts for overload retardation effect, was developed independently during the same period as the Willenborg model (1970-71). Yet, the original Vroman model is based on the mathematical formulation of the effective stress intensity factor range, ΔK_{eff} , such that the numerical value of ΔK_{eff} is always less than $\Delta K = K_{\text{max}}^{\infty} - K_{\text{min}}^{\infty}$ when the overload is existing; hence, the corresponding value of the fatigue crack-growth rate is smaller than its constant-amplitude counterpart, resulting in crack-growth-rate retardation. The original Vroman retardation model had a 0.333 constant which was arbitrarily selected and later found to be adequate to correlate the crack-growth test data using the B-1 strategical bomber spectrum⁽²⁹⁾. Chang, et al⁽³⁰⁾, later suggested that this constant is a material and spectrum-dependent constant. They proposed that for a specific material, it should be empirically determined, based on specific spectrum test data.

The Vroman model was also modified to account for the underload acceleration (crack-tip sharpening) effect by Chang, et al⁽³¹⁾. This was done by adding a term to the original ΔK calculation such that, if there

existed a number of underload cycles, the value of the current effective stress intensity factor range is larger than its constant-amplitude counterpart, resulting in crack-growth-rate acceleration. To be compatible with the residual stress-concept formulation for the overload retardation case, the acceleration term was formulated by the so-called "residual displacement" concept. The relationship between the crack-opening displacement and the stress intensity factor proposed by Wells⁽³²⁾ was used in the formulation. Chang⁽³³⁾ also proposed to form the crack-growth-rate equation for the negative stress ratio cases as $da/dN = C[(1-R)q_{K_{max}}]^n$, where $q(R)$ is the acceleration index which is determined from test data generated for a specific value of the negative stress ratio R . This interaction model was identified as the Vroman/Chang model⁽²⁴⁾.

The Vroman/Chang load interaction model still has many deficiencies. First of all, this load interaction model is not able to account for the retardation effect due to the existence of a large number of overload cycles. Consequently, the prediction is conservative for this type of loading. Secondly, it cannot predict the delayed retardation phenomena or the effective zone of the underload acceleration. Thirdly, it does not account for negation of the retardation caused by compression loading. Another drawback of this model is the fact that it also relies on certain test data in order to determine its empirical constants, even though the amount of tests needed to be conducted for one specific material and a specific spectrum is rather limited.

Candidate models to be implemented into the detailed crack growth analysis computer program have been evaluated. The approach was to investigate whether it was feasible to modify an existing model such that it could meet most of the requirements listed previously. Two existing models were selected as candidates, the generalized Willenborg model and the Vroman/Chang model. In order to obtain a one-to-one comparison, it was decided to employ only one existing computer program to perform the crack growth predictions. This implied that the generalized Willenborg model and the Vroman/Chang model should be implemented into the same computer program. Rockwell's in-house-developed computer software, EFFGRO⁽¹⁶⁾ was chosen to carry out this task. This was because the linear approximation damage accumulation scheme currently employed in EFFGRO is more attractive than other accumulative schemes commonly used. Ten test cases from the experimental development program conducted in phase I were arbitrarily selected for the correlation. Table 1 shows loading profiles of these 10 cases. In order to verify the accuracy of prediction, crack lives of these 10 cases were also predicted by using the Air Force's CRACKS program⁽³⁴⁾ with the generalized Willenborg model. Both EFFGRO and

CRACKS predictions were obtained using the following rate equation and the corresponding crack-growth-rate constants for 2219-T851 aluminum alloy. This set of crack-growth-rate constants was obtained by processing the PLOT RATE computer program⁽¹⁷⁾ through the constant-amplitude crack growth baseline test data generated in phase I.

For $\Delta K > \Delta K_{th}$

$$\frac{da}{dN} = C \left[\frac{\Delta K_{eff}}{(1-R_{eff})^{1-m}} \right]^n, \quad R \geq 0$$

where

$$C = 8.367 \times 10^{-10}$$

$$n = 3.64$$

$$m = 0.6$$

For $\Delta K \leq \Delta K_{th}$

$$\frac{da}{dN} = 0$$

where

$$\Delta K_{th} = \Delta K_o, \quad \Delta K_o = 1.5 \text{ Ksi } \sqrt{\text{in.}}$$

Comparisons of the crack life predictions obtained by EFFGRO and CRACKS are summarized in Table 1, together with the test results. The ratio of the predicted life to the test life, $R = N_{pred}/N_{test}$ for each test case is also presented in the table. It can be seen that the crack lives predicted by EFFGRO are very close to those predicted by CRACKS. In several cases, such as M-12, M-53, M-45, M-51, the two sets of predictions are almost identical.

Because the generalized Willenborg model is widely used in the aircraft industry, it was decided to modify this model to account for the compressive stress effects to the crack growth.

The generalized Willenborg model has been demonstrated to be adequate in predicting the tensile overload retardation effects for flight spectrum loadings (27,28). Because the generalized Willenborg model predicts retardation by reducing the effective stress intensity factors for a retarded cycle, negative effective stress ratios ($R_{eff} < 0$) frequently result for a cracked structure subjected to a flight spectrum loading. This can be shown by investigating the generalized Willenborg model in the following mathematical form:

$$\begin{cases} (K_{max})_{eff} = K_{\infty max} - \phi \left[K_{max}^{OL} \left(1 - \frac{\Delta a}{Z_{OL}} \right)^{1/2} - K_{\infty max} \right] \\ (K_{min})_{eff} = K_{\infty min} - \phi \left[K_{max}^{OL} \left(1 - \frac{\Delta a}{Z_{OL}} \right)^{1/2} - K_{\infty max} \right] \end{cases}$$

and

$$\phi = \frac{1 - \left(\frac{(K_{max})_{TH}}{K_{\infty max}} \right)}{R_{SO} - 1}$$

Where K_{∞} is the applied stress intensity factor, K_{max}^{OL} is the stress intensity factor corresponding to the maximum overload, Δa is the growth following overload, Z_{OL} is the overload interaction zone size, $(K_{max})_{TH}$ is the threshold stress intensity value, and R_{SO} is the overload shutoff ratio.

The effective stress ratio is defined as

$$R_{\text{eff}} = (K_{\text{min}})_{\text{eff}} / (K_{\text{max}})_{\text{eff}}$$

Hence, if $(K_{\text{min}})_{\text{eff}}$ is negative, the effective stress ratio will be negative. There are two possibilities that $(K_{\text{min}})_{\text{eff}}$ is negative. One is that the applied minimum cyclic stress is negative, such as the compression tension load cycle in a random flight spectrum. The second possibility is that the reduction term in the $(K_{\text{min}})_{\text{eff}}$ equation is mathematically greater than $(K_{\infty})_{\text{min}}$.

Extensive experimental data generated in recent years have shown that crack growth rates at negative stress ratios are generally higher than their $R = 0$ counterparts. Hence, it is important that the effects of the negative stress ratios be properly accounted for in the crack-growth predictions using the Willenborg retardation model. To properly account for such negative stress ratio effects, the Chang acceleration scheme was adapted in the methodology. Chang (33), proposed to employ the crack-growth-rate equation for the negative stress ratio cases as

$$\frac{da}{dN} = C \left[(1 - R)^{q_R} K_{\text{max}} \right]^n, \quad R < 0$$

where q_R is the acceleration index which is determined from test data generated for a specific value of the negative stress ratio R and its $R = 0$ counterpart.

For example, if experimental data of 2219-T851 aluminum showed that the crack growth rate at $R = -0.3$ is 20-percent faster than that at $R = 0$, the acceleration index $q_{-0.3}$ can be then calculated as follows:

$$\frac{da}{dN}_{(R=-0.3)} = 1.2 \frac{da}{dN}_{(R=0)}$$

or

$$C \left[(1 + 0.3)^q K_{\max} \right]^n = 1.2 C (K_{\max})^n$$

It implies

$$q_{(R = -0.3)} = \frac{1}{n} \left[\frac{\log (1.2)}{\log (1.3)} \right] = 0.19 \text{ for } n = 3.64$$

To adapt the Chang acceleration scheme in the Willenborg model, the growth rate equation for negative effective stress ratio cases becomes

$$\frac{da}{dN} = C \left[(1 - R_{\text{eff}})^{q_{R_{\text{eff}}}} (K_{\max})_{\text{eff}} \right]^n, R_{\text{eff}} < 0$$

This acceleration scheme for negative effective stress ratio was incorporated into EFGRO in conjunction with the Willenborg retardation model and is identified as the Willenborg/Chang model. Test data for the variable-amplitude loadings containing compression-tension cycles generated in phase I were recorrelated by EFGRO predictions using the Willenborg/Chang model. Results of the predictions were also compared with those predicted previously without accounting for the negative effective stress ratio acceleration effects. Improvement in predictions were clearly shown. A typical comparison is presented in Figure 11. Crack-growth test data were also presented (shown in the figure by the broken line). They show that when the negative effective stress ratio was set to zero, the Willenborg model predicted life was 19,514 cycles. Compared to the test life, which was 17,200 cycles, a 13-percent over-estimation resulted. Using the Willenborg/Chang model, the-predicted-life-to-the-test-life ratio becomes 0.94.

Experimental data have shown that application of a compression spike following one or more tensile overload applications may negate or reduce the effect of the overload retardation on subsequent crack-growth rates. Without accounting for this load interaction effect, unconservative predictions will result. In the generalized Willenborg model, the amount of crack growth affected by

an overload is determined by the overload interaction zone size, Z_{OL} . Increasing the interaction zone size will retard the crack growth more. On the contrary, decreasing Z_{OL} will reduce the retardation.

One approach is decreasing the overload interaction zone size when the overload is followed by a compressive load is to employ the effective stress ratio of this specific tension-compression load cycle in the overload interaction zone size calculation. The effective overload interaction zone size is defined in terms of the effective stress ratio (R_{eff}) as:

$$(Z_{OL})_{eff} = (1 + R_{eff}) (Z_{OL}), \quad R_{eff} < 0$$

For the plane stress condition,

$$Z_{OL} = \frac{1}{2\pi} \left(\frac{K_{\infty \max}}{\sigma_{ty}} \right)^2$$

The effective overload interaction zone size was incorporated into the Willenborg/Chang model to account for the reduction of retardation effect caused by a compressive spike load immediately following the overload.

Test data of the entire series of the variable-amplitude load testing conducted in phase I were correlated again with analytical predictions using EFGRO with the previously described methodology. Basic crack-growth-rate constants of 2219-T851 aluminum alloy used in the correlations were those used previously in the phase I report⁽²⁾:

$$C = 8.367 \times 10^{-10} \text{ (in ksi units)} \quad \Delta K_{th} = 2.5(1-R) \text{ ksi } \sqrt{\text{in.}}$$

$$n = 3.64$$

$$R_{cut}^+ = 0.75$$

$$m = 0.6$$

$$R_{cut}^- = -0.99$$

The value of the Chang acceleration index q was selected to be 0.3, which is an average value assumed to be applicable for all negative stress ratios for 2219-T851 aluminum. The overload shutoff ratio selected for 2219-T851 aluminum was $R_{SO} = 3.0$.

Table 2 summarizes the crack growth data correlations for tests M-1 through M-60, including the life predictions by the currently developed improved methodology and the ratios of the prediction to the test lives. For the sake of comparison, lives predicted in phase I by using EFFGRO with the Vroman/Chang model and CRACKS with the Willenborg model were also included in the table. Results show that the average prediction ratio for the Willenborg/Chang model was 0.959 with a 0.385 standard deviation for the 60 test cases correlated. Compared to the generalized Willenborg model prediction (average prediction ratio = 1.43, with a 0.954 standard deviation), the improvement in the prediction accuracy is clearly seen.

3.3 SELECTION OF THE DAMAGE ACCUMULATION SCHEME

Commonly practiced fatigue crack growth analytical prediction methods are primarily based on a damage accumulation scheme which interrelates the following elements:

1. A fatigue crack-growth-rate relationship and the corresponding growth rate constants, fracture properties, and other related material properties
2. Initial crack types, sizes, and geometries of the cracked bodies
3. Crack-tip stress intensity factor solutions
4. Loading spectra descriptions
5. Integration procedures

Because the detailed level crack growth analysis is kept on a cycle-by-cycle calculation basis, the growth-rate model of a crack subjected to cyclic loading will be in the following form:

$$da/dN = F(a, \sigma_{\max}, R, \beta(a), \dots)$$

Where a is the crack size, σ_{\max} is the maximum applied cyclic stress, R is the cyclic stress ratio, and $\beta(a)$ is the geometric functions.

The preceding first-order differential equation can be solved in numerous ways, depending on the specific application. In general, two categories of analytical predictions are required. Category I is the estimation of the elapsed time (number of cycles) which is required to grow a crack from an initial size, a_0 , to any final size, a_f , subjected to cyclic loadings. Category II is the prediction of the incremental growth of a known size crack within a specific period of time (number of cycles). In mathematical forms,

Category I

$$N = \sum_{i=1}^{N-1} \Delta N_i = \sum_{i=1}^{N-1} \left[\frac{a_{i+1} - a_i}{F(a, \sigma_{\max}, R, \beta(a), \dots)} \right]$$

Category II

$$\Delta a = a_f - a_0 = \sum_{i=1}^N \left. \frac{da}{dN} \right|_i$$

A review of commonly employed techniques in obtaining the solutions for the two categories was conducted in phase I of this program. These included the Runge-Kutta integration technique⁽³⁵⁾, Taylor series approximation method⁽³⁶⁾ and linear approximation method⁽³⁷⁾. A brief summary of these techniques was presented in the phase I technical report⁽²⁾.

One obvious requirement which will be imposed on any crack growth prediction methodology is the predictive accuracy. Among the previously mentioned techniques, the Runge-Kutta integration method provides the most accurate prediction in general.

The Runge-Kutta integration technique calculates the increment of crack size Δa as follows:

$$\Delta a = a_{N+1} - a_N = \frac{1}{6} (k_0 + 2k_1 + 2k_2 + k_3)$$

where a_N is the current crack size and the Runge coefficients are defined as:

$$k_0 = \Delta N \cdot \left. \frac{da}{dN} \right|_{a_N}$$

$$k_1 = \Delta N \cdot \left. \frac{da}{dN} \right|_{a_N + k_0/2}$$

$$k_2 = \Delta N \cdot \left. \frac{da}{dN} \right|_{a_N + k_1/2}$$

$$k_3 = \Delta N \cdot \left. \frac{da}{dN} \right|_{a_N + k_2}$$

Figure 12 illustrates the geometrical interpretation of the values k_0 through k_3 . All four k -values represent the slopes at various points. Value k_0 is the slope at the starting point; k_3 is the slope at the righthand point whose ordinate is $a_N + k_2 \Delta N$; k_2 is one of the two slopes considered at midpoint with the ordinate $a_N + 1/2 k_1 \Delta N$; and, finally, k_1 is the second slope at midpoint whose ordinate is $a_N + 1/2 k_0 \Delta N$.

The Runge-Kutta integration technique is currently used in the CRACKS program. Because this integration technique involves calculating the crack growth rate, da/dN , four times for each load cycle, substantial computation time will be consumed by using this accumulation technique in the computer program. This is especially true when the complex flight spectrum loading is applied.

The linear-approximation method currently employed in many crack growth analysis computer programs is a very efficient damage accumulation scheme. Because it is so efficient, the computer routine first to adopt this method was named EFFGRO.⁽³⁷⁾ The linear-approximation method assumes that the growth rate is constant throughout a load step in a spectrum so that the crack size is in a linear relationship with the number of load cycles. The following paragraphs briefly describe this damage accumulation procedure currently existing in EFFGRO.

The load spectrum in the actual integration portion of the EFFGRO program is:

<u>Step</u>	<u>Max Stress</u>	<u>Min Stress</u>	<u>No. of Cyc/ Block (Flight)</u>
1	σ_{\max_1}	σ_{\min_1}	N_1
2	σ_{\max_2}	σ_{\min_2}	N_2
3	σ_{\max_3}	σ_{\min_3}	N_3
\vdots	\vdots	\vdots	\vdots
i	σ_{\max_i}	σ_{\min_i}	N_i

The damage-accumulation scheme proceeds by considering a load step (i) and using σ_{\max_i} and σ_{\min_i} to calculate da/dN .

The value of $(\delta a)/(da/dN)$ is then compared to N_i , where "a" is the crack size. If $(\delta a)/(da/dN)$ is greater than N_i , then the crack growth for that particular load step is $\Delta a = N_i \times (da/dN)$, "a" is increased by Δa , and the program proceeds to the next load step.

If $(\delta a)/(da/dN)$ is less than or equal to N_i , then the number of cycles to grow (δa) is $(\delta a)/(da/dN)$. this value is subtracted from N_i , the crack size "a" is increased by (δa) , and the load step is reconsidered. This process continues with $(\delta a)/(da/dN)$ being compared to the remaining cycles in the step. When all load steps in the block (or flight) are exhausted, the program proceeds to the first step of the next block (or flight).

A preliminary evaluation on the efficiency of two commonly used integration schemes has been conducted. They were the Runge-Kutta integration technique and the Vroman linear approximation method. Crack-growth analyses for a center-through crack contained in the 2219-T851 aluminum plate subjected to various types of loading cases were used for the evaluation. Parallel runs were made with CRACKS and the modified EFGRO programs, using the generalized Willenborg retardation model. Computer runs from CRACKS represented the results using the Runge-Kutta technique, while the runs from EFGRO provided predictions using the linear approximation method. The approach taken in rating the efficiency of these two integration schemes was to compare their computer costs; i.e., the computing billing units (CBU's) charged for comparable runs. This approach, of course, can only provide relative comparisons. Yet, from the results summarized in Table 3, it clearly indicates that in general, the Vroman linear approximation scheme is more efficient than the Runge-Kutta method.

Efforts have also been devoted to investigating the sensitivity of the crack incremental interval (δa) used in the Vroman linear approximation method to the predictive accuracy. Selected center-through crack growth data generated from the phase I methodology development test program⁽²⁾ and the B-1 fracture mechanics program⁽³⁸⁾, were used as an experimental data base. These included two center-through cracks under constant-amplitude load at stress levels $\sigma_{\max} = 8$ and 40 ksi (test cases M-1 and M-7) and a part-through crack under constant-amplitude load (test case B-434).

Five different incremental intervals selected in the investigation were:

$$\delta a = 0.001a, 0.005a, 0.01a, 0.05a, 0.1a$$

The EFGRO program was modified slightly to incorporate these flexible interval options. Crack growth behavior predictions for the previously listed test cases were then performed by running EFGRO with these five different incremental intervals. Results of the predicted cycles for each test case with various δa are presented in Table 4, together with the test data. CBU charges are also presented in the table for reference in the machine cost. It shows that to increase the incremental interval from $\delta a = 0.001a$ to $0.05a$, the predictive accuracy only was reduced an insignificant amount (5 percent at the most), while the computer cost was cut down by a factor of five.

Increasing δa further to $0.1a$ did not result in a big savings of computer cost but reduced the predictive accuracy by almost 10 percent for most cases investigated. Hence, it seems that $\delta a = 0.05a$ is an optimum interval for use in the Vroman linear approximation method.

3.4 TWO-DIMENSIONAL (2-D) CRACK GROWTH APPROACH EVALUATION

It is a well-known fact that part-through cracks, including corner cracks at fastener holes, change shapes (aspect ratios) under cyclic loading, either constant-amplitude or variable-amplitude. One common approach is to assume that the growth of such a part-through crack is uniform in the depth (along the thickness) and length (along the surface) directions. The stress intensity factor at the maximum depth, K_A , is used as the controlling parameter in calculating the crack growth rate, da/dN . This approach is identified as the 1-D crack growth analysis. For part-through cracks under uniform tensile load with initial aspect ratios in the stable shape region; i.e., $a/2c$ is approximately 0.5, the 1-D crack-growth-analysis approach provides adequate predictions⁽³⁹⁾. For other cases, inaccurate predictions will result.

To account for the shape-change effects of the part-through crack, the 2-D crack growth analysis approach is apparently a better choice. The 2-D crack-growth-analysis option is currently available in the EFFGRO program. The methodology used in EFFGRO is to assume that the crack growth in the two principal directions of a part-through crack is a function of the stress intensity factors in these directions only. For constant-amplitude loadings, the crack growth rates at the depth and the length directions are:

$$da/dN = C_A \left[\frac{\Delta K_A}{(1-R)^{1-m_A}} \right]^{n_A}, \quad R \geq 0$$

$$dc/dN = C_C \left[\frac{\Delta K_C}{(1-R)^{1-m_C}} \right]^{n_C}, \quad R \geq 0$$

Where C_A , n_A , m_A and C_C , n_C , m_C are the material crack growth rate constants along the depth and the length directions, respectively; R is the stress ratio.

Stress intensity factors at the maximum depth and crack tip along the surface contained on current EFFGRO can be expressed as:

$$\begin{aligned} K_A &= F\left(\frac{a}{t}, \frac{a}{c}, \frac{c}{w}\right) \sigma \sqrt{\frac{\pi a}{Q}} \\ K_C &= 1.12 \sigma \left(\frac{a}{c}\right) \sqrt{\frac{\pi c}{Q}}, \quad \text{For } \frac{a}{2c} \leq 0.5 \\ &= 1.12 \sigma \sqrt{\frac{\pi c}{Q}}, \quad \frac{a}{2c} > 0.5 \end{aligned}$$

where $F(a/t, a/c, c/w)$ is the geometrical correction factor for the effects of the front surface, back face, and finite width to the stress intensity factor. The parameter Q is given by

$$Q = \phi^2 - 0.212 (\sigma/\sigma_{ty})^2$$

where

$$\phi = [1 + 1.45 (a/c)^{1.64}]^{1/2} \quad \text{for } a/2c \leq 0.5$$

$$\phi = [1 + 1.45 (c/a)^{1.64}]^{1/2} \quad \text{for } a/2c > 0.5$$

Currently, for a surface flaw, the geometrical correction factor $F(a/t, a/c, c/w)$ used in the EFFGRO program is the multiplication of three discrete correction factors as

$$F(a/t, a/c, c/w) = M_F \times M_B \times M_W$$

where M_F , M_B , and M_W are the front face, back face, and width correction factor for the stress intensity, respectively.

Values of M_F and M_W used in EFFGRO, are as follows:

$$M_F = 1 + 0.12 (1 - a/2c)^2$$

$$M_W = [1 - 0.025 (2c/W)^2 + 0.06 (2c/W)^4] \sqrt{\sec \pi c/W}$$

where W is the width of the structure.

The back-face correction factor is stored in the 2-D EFFGRO crack library in the following tabulated form.

a/2c	a/t								
	0.1	0.2	0.3	0.4	0.5	0.6	0.7	0.8	0.9
0.05	1.0	1.02	1.04	1.05	1.08	1.13	1.2	1.36	1.76
0.1	1.0	1.0	1.02	1.03	1.06	1.1	1.16	1.27	1.53
0.2	1.0	1.0	1.02	1.01	1.04	1.07	1.13	1.20	1.37
0.3	1.0	1.0	1.0	1.01	1.02	1.05	1.09	1.16	1.28
0.4	1.0	1.0	1.0	1.01	1.02	1.04	1.07	1.13	1.24
0.5	1.0	1.0	1.0	1.0	1.01	1.02	1.05	1.10	1.19

A study on predictive accuracies for a surface flaw fatigue-life predictions by the 1-D and 2-D crack-growth-analysis approaches has been conducted. Constant-amplitude test data documented in Reference 13 formed the primary experimental data base for the evaluation and comparison of the two approaches. The EFFGRO program was used throughout the study because EFFGRO provides both the 1-D and 2-D analysis option.

For the 1-D analysis option, the initial aspect ratio of the surface flaw is assumed to be unchanged. For the 2-D analysis, two types of assumptions were made. In type I, the crack growth rate was assumed to be independent of crack growth direction; i. e., $da/dN = dc/dN$. In type II, the crack growth was to be dependent on crack growth directions; i.e., $da/dN \neq dc/dN$. For lacking of basic fatigue crack-growth-rate data, two cases were arbitrarily assumed in type II analysis; the first case assumed $da/dN = 2 dc/dN$, and the second case assumed $da/dN = 2/3 dc/dN$. A summary of the assumptions for various types of analyses is shown in table 5.

The crack-growth-rate constants and corresponding parameters used in the 1-D and 2-D analyses were least-square fitted by PLOT RATE. Baseline fatigue crack growth data points at various stress ratios presented in da/dN versus K_{max} format were digitized into PLOT RATE through the DTIZ routine described in Appendix A of Reference 40. The best collapsed growth rate data in da/dN versus $(1-R)^{m} K_{max}$ for 2219-T851 aluminum, 9Ni-4Co-0.2C steel, and Ti-6Al-4V beta annealed are shown in Figures 13 through 15, respectively. Table 6 summarizes the rate constants and other fracture properties used in the analysis.

Crack growth predictions of all the four analysis types listed in Table 5 were evaluated against the experimental data for each test case. Comparisons of analytical results to the experimental data for each case evaluated were shown in Tables 7 through 9 for 2219-T851 aluminum, 9Ni-4Co-0.2c steel, and Ti-6Al-4V beta annealed, respectively. Results showed that utilizing the 2-D crack-growth analysis approach, the prediction accuracy is generally improved for all cases. The improvement in the prediction of the final aspect ratio ($a/2c$) of each surface flaw can be clearly seen in these tables. From the results of this study, it was decided to adopt the 2-D analysis as the primary approach for part-through crack-growth predictions.

The computation cost of the 2-D crack-growth approach is a major concern. A study was made to determine the most cost-effective format used for calculation of stress intensity factors. In general, three different formats are being used by the researchers and investigators in presenting the stress intensity factor coefficients for part-through cracks. The first one is to use numerical tables. Typical examples are the single and double cracks emanating at a circular hole contained in an infinitely wide plate subjected to uniaxial or biaxial stresses⁽⁴¹⁾. Graphical display is

another format which has been commonly used. Stress intensity factors handbooks usually adopt this format. The third format is to express the coefficients in an equation form as a function of the appropriate parameters, such as the crack shape (a/c) crack-size-to-plate-width ratio (a/W), crack-size-to-plate-thickness ratio (a/t), crack-size-to-hole-radius ratio (a/R), etc.

A surface flaw test case was selected for the study. This test was one of the 300 tests conducted by Rockwell in the B-1 strategic bomber research⁽³⁸⁾, development, testing, and evaluation (RDT&E) phase. It was a relatively shallow surface crack with an initial aspect ratio $a/2c = 1/3$ and initial crack depth $a_i = 0.06$ inch. The test material was HP9Ni-4Co-0.2C steel alloy with yield strength $\sigma_{ty} = 180$ ksi and ultimate tensile strength $\sigma_{tu} = 200$ ksi. The test specimen was a typical dog-bone type. The surface flaw was introduced by the electrical discharge machining (EDM) process in the center of the test area which had a 4- by 0.5-inch cross section.

The stress intensity factor coefficients for a surface crack are the combination of front face, back face, and width correction factors. To assess the effect of the presentation format on the computation cost between the tabulation and closed-form equation, the back-face correction factors for various aspect ratios ($a/2C$) and crack-size-to-thickness ratios (a/t) were input into the computer program in tabulated and equation forms. The tabulated back-face correction factors used in the study are as previously shown. The tabulated values were derived from the results reported by Shah and Kobayashi⁽⁴²⁾. The closed-form equation for a part-through crack derived by Newman and Raju⁽⁴³⁾, based on their 3-D finite-element results, was used in the study. In the equation form, the combined correction factor for a shallow surface crack ($a/c \leq 1$) is expressed as:

$$F = \left[M_1 + M_2 \left(\frac{a}{t} \right)^2 + M_3 \left(\frac{a}{t} \right)^4 \right] f_\phi g f_w$$

where

$$M_1 = 1.13 - 0.09 \left(\frac{a}{c} \right)$$

$$M_2 = 0.54 + 0.89 / \left(0.2 + \frac{a}{c} \right)$$

$$M_3 = 0.5 - 1 / \left(0.65 + \frac{a}{c} \right) + 14 \left(1 - \frac{a}{c} \right)^{24}$$

$$f_\phi = \left[\left(\frac{a}{c} \right)^2 \cos^2 \phi + \sin^2 \phi \right]^{1/4}$$

$$g = 1 + \left[0.1 + 0.35 \left(\frac{a}{t} \right)^2 \right] (1 - \sin^2 \phi)^2$$

$$f_w = \left[\sec \left(\frac{\pi c}{2b} \sqrt{\frac{a}{t}} \right) \right]^{1/2}$$

At the maximum depth points, $\phi = \pi/2$, F_A takes the following form:

$$F_A = \left[1.13 - 0.09 \left(\frac{a}{c} \right) + \left(-0.54 + 0.89 / \left(0.2 + \left(\frac{a}{c} \right) \right) \right) \left(\frac{a}{t} \right)^2 + \left(0.5 - 1 / \left(0.65 + \frac{a}{c} \right) + 14 \left(1 - \frac{a}{c} \right)^{24} \right) \left(\frac{a}{t} \right)^4 \right]$$

At the maximum length point, $\phi = 0$, F_B can be written as:

$$F_B = \left(1 + \left[0.1 + 0.35 \left(\frac{a}{t} \right)^2 \right] \right) \left(\sqrt{\frac{a}{c}} \right) F_A$$

The result of the study showed that by using the equation form for stress intensity factor calculation in the computer program, a factor of five reduction in computer cost can be achieved, compared to the use of the tabulated form.

From the results of the previously described study, it was decided to adopt the equation format in formulating stress intensity factors for all known part-through crack cases stored in CRKGRO.

3.5 CYCLE COUNTING TECHNIQUE

One of the requirements for accurate predictions of crack-growth behavior under spectrum loadings is a correct representation of loading cycles. A load spectrum used in a spectrum test may not be directly applicable to analytical predictions. This results from the observation that the crack-growth behavior is influenced not only by a load step currently being applied, but also by the total range between previous and current load levels. Hence, to perform analytical predictions on crack-growth behavior under random cycle-by-cycle spectrum loadings, it is essential to have a cycle-counting method such that the growth-rate constants determined from the constant-amplitude loading tests (loadings with well-defined cycles having identical maximum load levels and ranges) can be directly employed in the spectrum loading situation. There have been many cycle-counting methods proposed throughout the last two decades. In his early research work, Dowling investigated eight counting methods which were used to predict fatigue failure of test specimens subjected to spectrum loadings, including the peak, mean crossing peak, level crossing, fatigue meter, range, range mean, rain-flow and range-pair methods(44). Dowling pointed out that all of the previously listed counting methods, except range-pair and rain-flow, have serious flaws. He also concluded that the rain-flow and range-pair cycle-counting methods are considered equivalent for most practical situations. For repeated block loadings, the counting results of these two methods will always be identical. Hence, it was decided in this program that only the ability of predictions with or without range-pair countings would be studied.

The essence of the range-pair counting techniques can be illustrated by considering the load trace as shown in Figure 16. The criteria for counting a cycle are as follows:

1. If $\sigma_2 > \sigma_1$ (Figure 16(a)), then a cycle of amplitude $|\sigma_2 - \sigma_3|/2$ and the mean of $|\sigma_2 + \sigma_3|/2$ is counted if $\sigma_2 \leq \sigma_4$ and $\sigma_3 \geq \sigma_1$.
2. If $\sigma_2 < \sigma_1$ (Figure 16(b)), the same cycle is counted if $\sigma_2 \geq \sigma_4$ and $\sigma_3 \leq \sigma_1$.

Starting at the beginning of a load trace, four consecutive peaks and valleys are considered. If the second and third peak or valley meet the preceding conditions, one cycle is defined, and those two points are deleted from the load trace. The fourth peak or valley now becomes the second, and the next consecutive peak and valley of the load trace are added, to again form a four-point set. This counting continues until the four points being considered cannot define a cycle. When this occurs, the first point will be omitted from consideration and put into a residue trace, and the next peak is added to the load trace. This process continues, adding points to the residue trace as necessary, until there are only two or three points left. These points are added to the residue trace, which is then treated in the same manner as the original trace. The results of this process leave a residue trace as shown in Figure 17. This residue trace will not be range-pair counted.

Instead, these remaining cycles are to be counted such that the highest peak is paired with the lowest valley to form a cycle. Moving away from this cycle in both directions, each successful peak and valley are paired together. If there is an extra peak or valley left on either side, it will be omitted. A peak on one side of the maximum excursion cycle will not be paired with a valley on the other side. Because of the load interaction effects to the crack-growth behavior, the sequence of the load cycles is very important. Hence, the cycles are ordered based on the same order of the peaks as in the original load trace. The load cycles resulting from this counting procedure will thus form the proper load cycles to be used in crack-growth analysis.

The previously described range-pair counting procedure was coded by Streitmatter⁽⁴⁵⁾ in subroutine CYCCNT and subsequently incorporated into the EFFGRO program in the early development phase of the B-1 Strategic Bomber. Subroutine CYCCNT was linked to EFFGRO to perform analytical predictions on some of the random cycle-by-cycle spectrum loading test cases conducted in phase I in order to assess the impact of the cycle-counting effect. The A-G random spectrum was arbitrarily selected in the assessment.

Four sets of analytical predictions were obtained from EFFGRO runs:

1. Spectra not range-pair counted, load interaction effects not accounted for
2. Spectra not range-pair counted, load interaction effects accounted for
3. Spectra range-pair counted, load interaction effects not accounted for
4. Spectra range-pair counted, load interaction effects accounted for

The following were the value of the rate constants and other parameters used in the analysis:

$$C = 5.066 \times 10^{-10} \text{ (in ksi units)}$$

$$n = 3.83$$

$$m = 0.6$$

$$q = 0.3$$

$$\sigma_{ty} = 48 \text{ ksi}$$

$$R_{so} = 3.0$$

$$R_{cut}^{+} = 0.75$$

$$R_{cut}^{-} = -0.99$$

$$\Delta K_{th} = 2.5(1 - |R|)$$

$$K_C = 65 \text{ ksi} \sqrt{\text{in.}}$$

Analytical predictions were correlated with the test data. Again, the ratio of the predicted life to the test life for each case has been calculated. Results were summarized as shown in Table 10. It can be seen that without range-pair counting, the predictions were, in general, unsafe (overestimated life). The fourth set of predictions (spectra range-pair counted, load interaction effects accounted for) correlated the best with test data. From this study, it was decided that all random cycle-by-cycle spectra will be range-pair counted prior to performing analyses.

3.6 COMPUTER PROGRAM INPUTS AND OUTPUTS FORMAT DEVELOPMENT

After the completion of the previously described studies, it has been decided to adopt EFFGRO as the baseline program for the detailed level crack-growth predictions. The decision was made based on the fact that not only the damage accumulation scheme used in EFFGRO is one of the most efficient schemes in growing cracks, but also because the 2-D EFFGRO is a program capable of accounting for the aspect-ratio change effect to the crack growth behavior of part-through cracks by growing the crack in both the length and depth directions.

The detail crack-growth program was named "CRKGRO." The development of CRKGRO was first the conversion of the main program and all necessary subroutines used in the EFFGRO to be executed on the CDC computer system. The input format of the CDC version EFFGRO was then modified using the CRACKS input format as the base. This is because CRACKS currently is being widely used in the Air Force as well as in the aircraft industry. To keep the input format as close as possible to that of CRACKS will avoid disturbance to the users who are already familiar with CRACKS. A slight change in CRACKS input format was deemed necessary because the additional information is required by CRKGRO to execute the two-direction growth of a part-through crack. An one-direction (1D) growth option is provided by CRKGRO. The 1-D growth is based on the maximum depth point.

The spectrum manipulation of CRACKS input in the form of maximum/minimum stress, stress ratio, delta stress, and mean and alternating stress has been retained in the CRKGRO to assure that there will be no major disturbance for those who are used to run CRACKS. Table 11 is the printout of the first part of the preliminary CRKGRO input echo, which contains the material crack-growth-rate constants and other related material properties, configuration of the crack, geometrical dimensions of the cracked body, and other pertinent information. The input echo of the spectrum in the minimum/maximum stress format is shown in Table 12.

The output format of the CRKGRO program was also developed following closely that of the EFFGRO. The standard printout includes the first load block with all calculated values for each parameter, such as $DADN$ (da/dN), $DELTA K$ (ΔK_A), $SIGMAX$ (σ_{MAX}), R , $A(a)$, $C(c)$, $A/2C$ ($a/2C$), etc, for each loading step. Table 13 presents a typical printout. The extra printout option provides all values of these parameters for each step in every n^{th} block, for whatever the option is called.

In the printout, milestones reached are framed or underlined by asterisks, to flag their occurrence. These include the transition from a part-through crack to a through crack, instability reached, etc. At the end of each analysis, crack lengths and crack depths for every 10th block (or flights) are printed out in a tabulated form. A sample is shown in Table 14.

3.7 CRACK TIP STRESS INTENSITY-FACTOR LIBRARY

A collection of stress-intensity-factor solutions for various through- and part-through-crack configurations has been incorporated into CRKGRO through a CRACK LIBRARY module which consists of separate subroutines, each containing one set of stress-intensity-factor solutions. In the previous version of EFFGRO, the crack-growth computations were performed in subroutines GROW, PTC, and TC. Subroutine GROW performed the load level and life cycle iterations and made calls to PTC and TC, which computed the stress intensity factor for given geometries and grew the crack for a part-through or through crack, respectively. The stress-intensity-factor solutions were fragmented to reduce repetition because certain correction functions were the same for different crack geometries. This method of determining the stress intensity factor for a specific crack made modifications and additions difficult.

A CRACK LIBRARY methodology was selected where a specific stress-intensity-factor solution for a specific crack configuration is separate from other solutions. Any part of the solution can be modified without affecting other solutions. Each K-solution is a subroutine KXXXX, where XXXX is the crack code assigned to a certain stress intensity solution. For example, K1010 is the subroutine for a centered surface flaw and K2010 is the subroutine for a centered through crack. Each part-through crack subroutine has two sets of solutions - one for two-direction crack growth, while the other set is for one-direction crack growth option. For the 2D crack growth option, two solutions were formulated, one for the maximum depth point and one for the extreme point along the length direction; i.e., K_A and K_B . Stress-intensity-factor solutions for a shallow crack ($A/C \leq 1$) and for a deep crack ($A/C > 1$) are included in the same subroutine. All geometric correction functions are in the form of polynomials instead of numerical tables, in order to reduce computation costs.

Subroutines PTC and TC have been merged into the GROW subroutine to improve efficiency and reduce computer costs. The stress intensity solution is assigned to the corresponding crack geometry once, and it is only assigned again if breakthrough occurs when a part-through crack transitions into a through crack. CCRIT module original contained in EFFGRO which computes the critical crack size has also been modified to use the CRACK LIBRARY module, as shown in the flow chart of CRKGRO in Figure 18. This module provides the critical crack-size information when the total growth history is not required for a specific analysis. If an analyst, for example, has a two-lifetime criteria to meet, the critical crack may not be attained during the growth history, but the critical crack size is still required in the analysis. The stress-intensity-factor solutions contained in the CRKGRO CRACK LIBRARY for specific crack geometries are given in Appendix A of Reference 4.

3.8 PLOTTING MODULE DEVELOPMENT

The plotting capability of CRKGRO is a comprehensive means of viewing crack growth history without analyzing discrete crack sizes for each flight. For a transport airplane, the life can be in the range of tens of thousands of flights. Plotting every data point would obscure the value and readability of the data and waste computer time. The CRKGRO plotting module was designed to select a few data points which are representative of the overall crack growth history and plot a combination of parameters such as crack sizes, number of flights, growth rates, and the maximum stress intensity factor per flight. Options are included for linear, semilogarithmic, and logarithmic plots of all appropriate parameters.

The flow chart of CRKGRO in Figure 18 illustrates the operations of the plot module. The plot module consists of two subroutines: PTPARM and PLOT. Subroutine PTPARM has four user-dependent plot options: (1) crack sizes versus flights, (2) crack-growth rates versus flights, (3) growth rates versus crack sizes, and (4) growth rates versus the maximum stress intensity factor per flight. If the analysis is for a part-through crack, and if the 2-D option is executed, any plot request involving crack size will yield two plots, one plot for crack length and one for crack depth. For a plot request involving crack-growth rate, the growth rate is computed by the linear interpolation method. PTPARM reads the crack-growth rate data for every flight from a temporary file and selects 30 representative points to be plotted.

Subroutine PLOT does the actual CRT plotting. It constructs the grid and determines the scaling factors according to user input requests. The options available for grid generation are linear, semilog, or log-log plots. Typical plot output for a multimission analysis is shown in Figures 19 through 22. Selection of the first plot option produces a plot of crack length versus life in flights as shown in Figure 19. A discrete set of data points was selected to yield a readable plot and maintain the crack-growth history. Use of the semilog feature is demonstrated in Figure 20 for a plot of dc/dF versus life in flights and in Figure 21, where dc/dF is plotted versus crack length. Crack-growth rate is plotted in Figure 22 on a semilog scale versus the maximum stress intensity factor per flight.

4.0 DEVELOPMENT OF LIFE-PREDICTION METHODOLOGY FOR INDIVIDUAL AIRPLANE TRACKING

Current military standard, MIL-STD-1530A, "Aircraft Structural Integrity Program, Airplane Requirements," (1) states that two major activities designed to focus attention on each potential crack problem shall be included in the force management task. They are the Force Structural Maintenance (FSM) Plan and the Individual Airplane Tracking (IAT) Program. In addition, force management activities also include the loads/environmental spectral survey (L/ESS), updating the design analysis, developing inspection and repair criteria, and forming a structural strength survey.

The objective of the IAT program is to predict the potential crack growth in critical areas of each airframe, keyed to crack-growth limits of damage tolerance limits, inspection times, and economic repair times. In the IAT program, an individual airplane tracking analysis method which establishes and adjusts inspection and repair intervals for each critical area of the airframe, based on the individual airplane usage data, should be developed suited for a particular aircraft system. The damage tolerance and durability analyses and associated test data should be used to establish the analysis method. This tracking analysis should provide the capability to predict crack-growth rates, time to reach the critical crack sizes, and the crack size as a function of total flight time and aircraft usage data.

According to the survey conducted by the University of Dayton/Lockheed/Vought team, there are about 11 IAT methods being used in the IAT programs of 25 aircraft systems in the Air Force inventory. Among them, five methods are based on crack-growth analysis (46). The common practice is to employ a cycle-by-cycle crack-growth computer program to compute the crack growth for a flight or a number of flights.

From the economical point of view, the use of a cycle-by-cycle crack-growth computer code to compute the crack growth in the IAT program is definitely not cost effective. This is not only because the cycle-by-cycle crack-growth analysis consumes too much computation time, resulting in excessive computer cost, but also because there is no need for an accurate representation of the crack-growth behavior on the stress-level-by-stress-level basis for performing individual airplane tracking. Furthermore, it is highly desirable to operate the crack-growth analysis code on a variety of computer systems. It is even more desirable that such codes can be operated on the onboard type of minicomputers. Capacities of such computer systems prevent the use of the sophisticated cycle-by-cycle crack growth method.

One of the primary objectives of phase I of this program was to identify the significant parameters which control damage on a flight-by-flight basis and to develop methodology for characterizing flight loadings, which would eliminate the necessity for performing cycle-by-cycle analysis while producing equivalent crack-growth behavior. Two methods were developed to meet this objective in phase I. They were identified as Method I and Method II in the phase I final report (2). Method I can be used to develop equivalent load spectra in terms of constant-amplitude stress histories (one cycle per flight). Method II can be used to characterize each mission segment. A flight is assumed to consist of constant-amplitude mission segments.

4.1 FLIGHT-BY-FLIGHT CRACK-GROWTH METHOD

Introduction of the flight-by-flight crack-growth concept into the IAT program seems to be a natural extension from the cycle-by-cycle crack-growth approach which is currently being widely used. Gallagher (47) has shown that two multimission military transport-wing stress spectra exhibit crack-growth behavior which can be treated as constant amplitude on the growth-per-flight basis. In phase I of this program, an analytical procedure identified as Method I was developed to implement this flight-by-flight crack-growth rate (da/dF) concept. The following are brief descriptions of the necessary steps required:

1. Generate sample stress histories for all missions and mission segments considered in certain combinations, and repeat the procedure N_A times to produce N_A consecutive sample flight spectra (defined as a unitblock).
2. Use a cycle-by-cycle crack-growth analysis computer program to evaluate the crack growth Δa (due to the unitblock flight spectra under a prescribed number of different values of initial crack size a_0) and then calculate $da/dF = \Delta a/N_A$.
3. Establish the following relationship on the basis of the foregoing numerical results:

$$da/dF = C(\bar{K})^\lambda$$

where \bar{K} is a measure of the stress intensity factor representing the overall effect of the unitblock on the crack growth. In a mathematical form, \bar{K} is written as

$$\bar{K} = (\Delta\sigma^b)^{1/b} \Psi(a)$$

where $(\overline{\Delta\sigma^b})^{1/b}$ represents the statistical average of the bth power of the stress range $\Delta\sigma$ in the stress history and $\Psi(a)$ is a function of crack size and other geometries; i.e., for a center-through crack in a plate.

$$\Psi(a) = \sqrt{\pi a} (\sqrt{\sec(\pi a/W)})$$

4. Plot da/dF against \bar{K} for a number of different values of crack size a on a double logarithm scale, and then determine the two parameters C and λ . Each of the flight spectra representing a particular combination of the stress parameters with the rate of crack-growth evaluated is then replaced by a constant-amplitude stress spectrum with the equivalent rate of crack growth.
5. Repeat the same procedures for other combinations of stress $(\overline{\Delta\sigma^b})^{1/b}$ parameters, resulting in corresponding values of C , λ , and $(\overline{\Delta\sigma^b})^{1/b}$ and also in corresponding equivalent constant-amplitude stress spectra. Thus, obtain a number of sets of parameters

$$[C_1, \lambda_1, (\overline{\Delta\sigma^b})_1^{1/b}], [C_2, \lambda_2, (\overline{\Delta\sigma^b})_2^{1/b}], \dots$$

and a number of growth rates applicable to each of the particular stress parameter combination.

$$(da/dF)_1 = C_1 (\bar{K}_1)^{\lambda_1}$$

$$(da/dF)_2 = C_2 (\bar{K}_2)^{\lambda_2}$$

⋮

$$(da/dF)_N = C_N (\bar{K}_N)^{\lambda_N}$$

where N is the total number of stress-parameter combinations to be considered. Hence, the problem of mission mix and mission sequence can be solved by choosing those growth-rate equations pertinent to the missions in the mix and applying them in the sequence corresponding to the mix.

6. The crack-growth life (F) in flights is obtained by numerical integration of

$$\int_{a_0}^a \Psi(\xi)^{-\lambda} d\xi = C (\overline{\Delta\sigma^b})^{\lambda/b} (F)$$

To investigate the feasibility of using Method I in converting the random cycle-by-cycle spectrum to the equivalent constant-amplitude loading for the performance of IAT crack-growth analysis, a random load spectrum representing the air-to-ground mission of a typical fighter (U.S. Air Force F-15 aircraft) was used. This random load spectrum was generated in terms of peaks and valleys using the SPECGR1 program developed by McDonnell Douglas Aircraft Company (48). A unitblock was constructed by selecting 50 flights, each containing 52 peaks and valleys. The unitblock spectrum table of this typical fighter air-to-ground mission is shown in Reference 3.

A 2219-T851 aluminum plate containing a center-through crack was chosen in the study. The computer program CYCGRO, developed in phase I on the basis of the EFFGRO program, was used to generate the equivalent crack-growth-rate parameters C , $(\Delta\sigma^b)^{1/b}$ and λ .

The modified Walker rate equation, in conjunction with the Vroman/Chang load interaction model, was selected in order to account for the overload retardation and compression load acceleration effects in the study. The following were the corresponding parameters input to CYCGRO (refer to Table 15):

$$C_w = 8.367 \times 10^{-10}, n = 3.64, m = 0.6, A = 0.333, q = 0.3, b = 2$$

$$\sigma_{lim} = 30 \text{ ksi}, \Delta K_{th} = 1.5 \text{ ksi}\sqrt{\text{in}}, K_c = 66 \text{ ksi}\sqrt{\text{in}}, \sigma_y = 48 \text{ ksi}$$

$$R_{cut}^+ = 0.99, R_{cut}^- = -0.99$$

The parameters calculated by CYCGRO for this particular fighter air-to-ground mission are shown in Table 16. For $K > \Delta K_{th}$, the following were the calculated values:

$$SIGMA = (\Delta\sigma^b)^{1/b} = 10.308$$

$$LAMBDA = \lambda = 3.628$$

$$C = 0.23861 \times 10^{-7}$$

$$PRODUCT = C(\Delta\sigma^b)^{\lambda/b} = 0.11298 \times 10^{-3}$$

The crack-growth life was calculated by inputting this set of parameters into the computer program Crack Growth Estimation by Polynomial Expansion (CGEPE), which is primarily used to solve the $da/dF = c(\bar{K})^{\lambda}$ in closed form by expanding the function $(\Psi(a))^{-\lambda}$ into the Mth order polynomial:

$$[\Psi(a)]^{-\lambda} = a^{-\lambda/2} \sum_{i=1}^M A_{i-1} a^{i-1}$$

and estimating the coefficients (A_{i-1}) by fitting this polynomial to $[\Psi(a)]^{-\lambda}$ at specified M values of a. The closed form solution for a is:

$$\sum_{i=1}^M \left[(2A_{i-1}) / (2i - \lambda) \right] (a^{2i-\lambda/2} - a_0^{2i-\lambda/2}) = c(\Delta\sigma)^{\lambda/b} \quad (F)$$

The predicted crack-growth behaviors for both the random cycle-by-cycle and equivalent constant-amplitude spectra are plotted against the test data. Figure 23 presents the results. It can be seen that using the equivalent constant-amplitude load to replace the random cycle-by-cycle flight spectrum is an acceptable approach.

4.2 MISSION-MIX LIFE PREDICTION METHODOLOGY

Efforts were also devoted to investigating the feasibility of extending Method I into the study of the mission-mix effect to the crack-growth behavior. Again, random cycle-by-cycle flight spectra of three different missions of the F-15 fighter were employed. In addition to the A-G mission, these included the air-to-air (A-A) and instrumentation-navigation (I-N) missions. For each type of mission, a unitblock consisting of 50 flights was constructed by using SPECUNI, where a unitblock implies a block of flights most representative of the specific missions throughout the lifetime of the aircraft. Each flight in the unitblock corresponds to a duration of one flight segment, each beginning with a valley stress and ending with a peak stress. The ground-air-ground (G-A-G) cycles were inserted at the beginning and end of each flight in such a way that in each flight the first valley was replaced by and the last peak was followed by the ground load. The exception was that for the first flight in the unitblock, the first simulated stress rise was replaced by a stress rise consisting of the ground load and 70 percent of σ_{Lim} . Hence the magnitude of the G-A-G cycles varies in each flight in the unitblock. The durations per flight for each type of missions are:

1. A-A mission - 52 peaks and valleys
2. A-G mission - 38 peaks and valleys
3. I-N mission - 12 peaks and valleys

The ground loads were taken to be -5 percent of σ_{Lim} for the A-A and I-N missions and -10 percent of σ_{Lim} for the A-G mission. The unitblock spectrum tables of each of these three missions are shown in Reference 3. Peaks and valleys of all the stress events are in the form of percentage of design limit stress, σ_{Lim} . To cover a wide stress range, $\sigma_{Lim} = 20, 30, \text{ and } 40 \text{ ksi}$ were selected in the study. A portion of the stress sequence of peaks and valleys of each of these missions at $\sigma_{Lim} = 20 \text{ ksi}$ is given respectively in Figures 24 through 26.

A composite unitblock constructed for the characterization of the flight spectrum loading conducted in phase I was used to represent the mission mix in this study. The composite mission unitblock is in the following mission mix and sequence:

$$\begin{aligned} 1 \text{ unitblock} = & 11 (A-A)_{1-11} + 11 (A-G)_{1-11} + 3 (I-N)_{1-3} + 11 (A-A)_{12-22} \\ & + 11 (A-G)_{12-22} + 3 (I-N)_{4-6} \end{aligned}$$

Crack-growth data of three test cases (M-90, M-91, and M-92) generated from the methodology development test program conducted in phase I were again used as an experimental data base. The test specimens used in the phase I test program were 2219-T851 aluminum center-cracked panels.

The development of a computer routine identified as the Flight-by-Flight Crack Growth (FLTGRO) program was thus initiated in order to handle the mission-mix situation. FLTGRO is capable of automatically calculating a set of spectrum-dependent crack growth per flight (da/dF) rate parameters ($[C_1, \lambda_1, (\Delta\sigma^b)^{1/b}]$, $C_2, \lambda_2, (\Delta\sigma^b)^{1/b}]$), as described in step 5 of Method I. A good portion of the EFFGRO program was taken to form the base of FLTGRO to determine these parameters. The material crack-growth-per-cycle (da/dN) rate constants and other properties inputted into FLTGRO for 2219-T851 aluminum alloy (Table 17) are:

$$\begin{aligned} C_W &= 8.3666 \times 10^{-10} \\ n &= 3.64 \\ m &= 0.6 \\ Q &= 0.3 \\ R_{cut}^+ &= 0.99 \\ \sigma_{ty} &= 45 \text{ ksi} \\ K_{IC} &= 45 \text{ ksi } \sqrt{\text{in.}} \end{aligned}$$

$$K_C = 65 \text{ ksi } \sqrt{\text{in.}}$$

$$\Delta K_{th} = 2.5 (1-R) \text{ ksi } \sqrt{\text{in.}}$$

$$R_{cut} = -0.99$$

$$b = 2$$

The parameters calculated by FLTGRO for the A-A, A-G, and I-N missions applied to 2219-T851 aluminum center-cracked panels at $\sigma_{Lim} = 20, 30, \text{ and } 40 \text{ ksi}$ are summarized in Table 18. Notice that among all nine cases, the value of λ does not vary more than 3 percent except in one case, indicating the severity of mission type can be ranked by the C values. As expected, the C value of the A-A mission is the largest, indicating it is the severest mission among the three mission types.

The fatigue crack-growth calculations were automatically performed by FLTGRO. The Vroman linear-approximation method was modified for damage accumulations on a flight-by-flight basis. The following paragraphs briefly describe the procedure.

For a given flight-by-flight basis spectrum table, a mixed-mission spectrum can be arranged as follows:

<u>Mission Type</u>	<u>Sigma</u>	<u>No. of Flights/Block</u>
1	$\overline{(\Delta\sigma)_1}^{1/b}$	F_1
2	$\overline{(\Delta\sigma)_2}^{1/b}$	F_2
3	$\overline{(\Delta\sigma)_3}^{1/b}$	F_3
.	.	.
.	.	.
.	.	.
i	$\overline{(\Delta\sigma)_i}^{1/b}$	F_i

The damage-accumulation scheme proceeds by considering a mission type (i) and using $\overline{(\Delta\sigma)_i}^{1/b}$, C_i , and λ_i to calculate $(da/dF)_i$.

The value of $(0.01a)/(da/dF)$ is calculated. If $(0.01a)/(da/dF) > F_i$, then $\Delta a = F_i \times (da/dF)$; "a" is increased by Δa , and the program proceeds to the next mission type. If $(0.01a)/(da/dF) \leq F_i$, then the number of flights to grow $(0.01a)$ is $(0.01a)/(da/dF)$. This value is subtracted from F_i , the crack size is increased by $0.01a$, and the mission type is reconsidered until it meets the first condition; i.e., $(0.01a)/(da/dF) > (F_i - F_{i-1})$. When all the mission types in a block are taken into consideration, the program proceeds to the first mission type of the next block.

Crack-growth behavior predicted by FLTGRO for the three test cases (M-90, M-91, and M-92) were tabulized as shown in Tables 19 through 21. Test data were correlated to the predicted growth behaviors. Figures 27 through 29 show the test data correlations for test cases M-90, M-91 and M-92, respectively. From the results, it can be seen that among the three cases studied, the largest ratio of the predicted life to the test life is $R = 1.59$ (M-90, $\sigma_{Lim} = 20$ ksi), indicating FLTGRO is able to provide reasonably accurate predictions. For the sake of comparison, crack-growth behavior predicted by CRKGRO were also plotted against the test data. A summary of the predicted accuracies and the computer cost by employing FLTGRO and CRKGRO is shown in Table 22. It illustrates the efficiency of FLTGRO.

4.3 MULTISEGMENT-PER-FLIGHT METHOD DEVELOPMENT

The one-cycle-per-flight approach may not be appropriate for the highly maneuverable fighter-type aircraft. Hence, a multisegment-per-flight crack-growth methodology was developed. Figure 30 schematically illustrates the conversion of the random flight spectrum to the multisegment-per-flight spectrum

The multisegment-per-flight crack-growth methodology also uses the analytical procedure as the one-cycle-per flight, except the crack-growth rate is on a cycle-per-segment (da/dS) basis rather than a cycle-per-flight (da/dF) basis. The following are brief descriptions of the necessary required steps:

1. Generate sample stress histories for a specific flight segment such as a maneuver segment; repeat the procedure N_A times to produce N_A consecutive sample flight segments (a uniblock).
2. Use a cycle-by-cycle crack-growth computer program to calculate the crack growth Δa due to the unitblock flight segment starting from a prescribed initial crack size a_0 , and then determine $da/ds = \Delta a/n_i$. Repeat the procedure for a prescribed number of different a_0 values.

3. Establish the following relationship on the basis of the aforementioned results:

$$da/ds = c (\bar{K})^\lambda$$

where \bar{K} is the measure of the stress intensity factor representing the overall effect of the unitblock on the crack growth. In the mathematical form, \bar{K} can be represented by

$$\bar{K} = (\overline{\Delta\sigma^b})^{1/b} \Psi(a)$$

The term $(\overline{\Delta\sigma^b})^{1/b}$ is the statistical average of the b-th power of the stress range, $\Delta\sigma$; $\Psi(a)$ is a function of crack size and other geometrical parameters.

4. Plot da/ds against \bar{K} on a double logarithm scale, and then determine the two parameters C and λ . Choose the appropriate value of σ_{\max} or σ_{\min} and then calculate the corresponding $\bar{\sigma}_{\min}$ or $\bar{\sigma}_{\max}$ based on $(\overline{\Delta\sigma^b})^{1/b}$ value, resulting in the corresponding value of C , λ , and $\bar{\sigma}_{\max}$, $\bar{\sigma}_{\min}$ of the equivalent constant-amplitude flight segment.
5. Repeat the same procedures for other flight segments, thus obtaining a number of sets of parameters

$$[C_1, \lambda_1, \bar{\sigma}_{\max_1}, \bar{\sigma}_{\min_1}], [C_2, \lambda_2, \bar{\sigma}_{\max_2}, \bar{\sigma}_{\min_2}], \dots$$

and a number of growth rates applicable to each of the particular flight segments

$$(da/ds)_1 = C_1 (\bar{K}_1)^{\lambda_1}$$

$$(da/ds)_2 = C_2 (\bar{K}_2)^{\lambda_2}$$

.

.

.

$$(da/ds)_i = C_i (\bar{K}_i)^{\lambda_i}$$

where i is the number of flight segments considered in a typical flight.

6. Choose the number of cycles n_i in each segment and then convert the crack-growth-per-segment rate (da/ds) into the crack-growth-per-cycle rate (da/dN), resulting in

$$(da/dN)_i = \left(\frac{1}{N_i} \right) (da/ds) = \left(\frac{1}{N_i} C_i \right) (\bar{K}_i)^{\lambda_i}$$

7. Use a cycle-by-cycle crack-growth analysis computer program to calculate the growth behavior.

It is noted that the preceding described methodology is similar to the equivalent simple spectrum method developed in phase I except for the last few steps. This equivalent simple spectrum method was identified as Method II in the phase I final report (2). In Method II, the load interaction effect is considered to be a step jump. The crack growth for the cycle (or cycles) immediately following the transition from one flight segment to another segment is determined from:

$$(da/dN)_i = C_w \alpha [\Delta\sigma_i \Psi(a)/(1-\bar{R}_{eq})^{1-m}]^{\lambda_w}$$

where \bar{R}_{eq} is the average equivalent stress ratio; C_w , λ_w , and m are material constants; $\Delta\sigma_i = (\overline{\Delta\sigma^b})_i^{1/b}$ is the b -th root of average of the b -th power of the stress range of the i -th flight segment; and $\Psi(a)$ is a function of the crack size and other geometries.

Values of the constant α depend on the characterization of the transition. A high-low step transition, $\alpha < 1$, accounts for the retardation effect. On the contrary, a low-high transition, $\alpha > 1$, accounts for the underload acceleration (sharpening) effect.

The current methodology called out the use of a cycle-by-cycle crack-growth analysis computer program in determining the crack-growth parameter, $(\overline{\Delta\sigma^b})_i^{1/b}$, C_i , and λ_i . Consequently, load interaction effects can be handled in the usual manner as done in the detailed level analysis in the program. To study the feasibility of this methodology, FLTGRO was modified. The major modification involves the segmentation of an input random cycle-by-cycle spectrum and the conversion of the crack-growth-per-cycle rate $(da/dN)_i$. Furthermore, the original cycle-by-cycle crack-growth calculation done by FLTGRO was limited to the one-cycle-per-step format. To take advantage of the multicycle-per-segment spectrum format, this restriction was lifted so that the linear approximation technique can be efficiently used.

The crack-growth behavior under a typical fighter aircraft (F-15) air-to-ground mission was again estimated by using the modified FLTGRO program. The load history of the fighter was in the random cycle-by-cycle format, which was generated in terms of peaks and valleys by using the SPECGRN 1 computer

program. A unitblock was constructed by selecting 50 flights, each containing 19 pairs of peaks and valleys. The unitblock spectrum table of this typical fighter air-to-ground spectrum is shown in Reference 3.

To study the feasibility of the multisegment-per-flight crack-growth methodology, this fighter air-to-ground spectrum was arbitrarily separated into three flight segments. The first segment consists of one pair of peaks and valleys, the second segment consists of eight pairs of peaks and valleys, and 10 pairs of peaks and valleys were contained in the third segment. A 2219-T851 aluminum plate containing a center-through crack was again chosen in the study. The material crack-growth-per-cycle (da/dN) rate constants and other properties inputted into FLTGRO for 2219-T851 aluminum alloy (Table 23) are:

$$C_w = 8.3557 \times 10^{-10} \text{ (Ksi unit)}$$

$$n = 3.64$$

$$m = 0.6$$

$$q = 0.3$$

$$R_{cut}^+ = \pm 0.99$$

$$\sigma_{ty} = 48 \text{ ksi}$$

$$K_{Ic} = 45 \text{ ksi } \sqrt{\text{in}}$$

$$K_{Ic} = 65 \text{ ksi } \sqrt{\text{in}}$$

$$\Delta K_{th} = 1.5 \text{ ksi } \sqrt{\text{in}}$$

$$b = 2$$

The flight-segment-dependent parameters C , λ , and $(\Delta \sigma^b)^{1/b}$ were calculated by FLTGRO for the specific fighter air-to-ground mission at $\sigma_{lim} = 50 \text{ ksi}$ applied on the 2219-T851 aluminum center-cracked panel. For the sake of comparison, solutions for both with or without the load interaction effects were obtained.

The fatigue crack-growth calculations were performed by using FLTGRO through a modified version of the GROFLT subroutine. This modified GROFLT subroutine is able to calculate the crack growth either on a flight-by-flight basis using $da/dF = C (\bar{K})^\lambda$ as the basic rate equation or a cycle-by-cycle basis using $da/dN = C [\Delta K / (1-R)^{1-m}]^n$. For the multisegment-per-flight option, the cycle-by-cycle rate equation is used. The load interaction model developed for the detailed level crack-growth analysis as described in preceding paragraphs was employed in the modified GROFLT subroutine to account for the load interaction effects from one flight segment to another. Flight-segment-dependent parameters C , λ , and $(\Delta\sigma_2)^{1/2}$ for both with or without load interaction effects were input to FLTGRO to calculate the crack growth. In the calculation, the root-mean-square (RMS) value of maximum stresses of a specific segment of the original random flight spectrum was chosen as the maximum stress for the equivalent constant-amplitude segment. The corresponding minimum stress was determined from $\bar{\sigma}_{\min} = \bar{\sigma}_{\max} - \Delta\sigma$.

Crack-growth predictions with or without consideration of the load interaction effects were generated by using the two sets of parameters, thus providing four different predictions. Figure 31 shows the comparison of crack-growth predictions resulting from the following different approaches:

1. Use the load interaction not-accounted-for parameters and grow cracks by not considering the load interaction
2. Use the load interaction not-accounted-for parameters and grow cracks by considering load interaction between flight segments
3. Use the load interaction accounted-for parameters and grow cracks by not considering load interaction between flight segments
4. Use the load interaction accounted-for parameters and grow cracks by considering load interaction between flight segments.

The crack-growth test generated from M-85 test specimen was plotted as shown as the solid line curve in Figure 31. The loading condition of the M-85 test case was the random cycle-by-cycle spectrum load. The limit stress was 30 ksi. For further comparison, the crack-growth prediction obtained by CRKGRO using the original random cycle-by-cycle flight spectrum as the inputted load as well as the crack-growth predictions obtained by FLTGRO using the one-cycle-per-flight approach are also plotted. They are identified as 6 and 5 in Figure 31, respectively. It can be seen that the approach 3 prediction was almost identical to that of the CRKGRO prediction, indicating this approach can provide predictions as reliable as CRKGRO methodology.

4.4 CRACK GROWTH UPDATING SCHEME

The FLTGRO program uses a random access disk file to store crack-growth data for each control points and each type of mission. Each control point requires the following information: (1) material constants, type of crack, crack geometry, and other parameters necessary to grow a crack, (2) mission type and associated growth rate constants, and (3) a base mission mix. For the crack-growth-per-flight (da/df) approach, the growth-rate parameter stored on the tracking operating file are C , λ , $(\Delta\sigma^2)^{1/2}$, the stress ratio, and the maximum spectrum stress. The multisegment-per-flight method stores growth rate parameter for each flight segment; i.e., C , n , the RMS of the maximum stress in a flight segment, the RMS of σ_{min} in a flight segment, and the number of cycles per segment. The base mission mix is a unitblock of m missions and the number of occurrences per mission.

In any time frame of the IAT program, crack growth at a control point can be tracked by executing the FLTGRO program for the missions that have been completed and accessing the data base to obtain the growth rate parameters for each mission. Capability is provided for adding new missions to the data base or to the baseline mission mix. The crack-growth equation coefficients are computed and optionally replaced or appended to the data base. If the missions flown were deviating from the baseline mission mix, the base mix can be updated to reflect the change.

The FLTGRO program produces a plot of crack length versus life in flights for the actual number of missions completed. The baseline mission mix can be optionally plotted on the same graph with the actual crack-growth history or can be displayed individually. The baseline mission is grown to failure to illustrate the life of the control point specimen. Another option is available which appends the base mission crack-growth history to the actual growth history. A combination of all these options in Figure 32 shows the life of a control point if the base mission was flown, in comparison to the actual life and the predicted life if the base mission is appended.

5.0 DEVELOPMENT OF LIFE-PREDICTION METHODOLOGY FOR PRELIMINARY DESIGN

5.1 INTRODUCTION

The governing document specifying overall requirements for achieving structural integrity of Air Force aircraft is MIL-STD-1530A⁽¹⁾. This document defines the applicable specifications, standards, and handbooks to be used on any new system procurement activity. Design to durability and damage tolerance is addressed in military specifications MIL-A-83444⁽⁴⁹⁾ and MIL -A-008866B⁽⁵⁰⁾ as part of the structural integrity requirements. Longer service-life requirements as a means for offsetting rising aircraft acquisition and operating costs have meant a corresponding increased impact of the durability and damage-tolerance requirements on structural design. Therefore, analytical methods are required for evaluating these criteria at the different stages of vehicle development. At the preliminary design (PD) level, methods are required for proper selection of materials and structural design concepts which balance improvements in service life against weight penalties, cost, and system performance.

Detailed crack-growth analysis is performed by computer programs, such as CRACKS⁽³⁴⁾ and EFFGRO⁽¹⁶⁾, and the currently developed code, CRKGRO. These programs perform the crack-growth analysis on a cycle-by-cycle basis, accounting for stress histories and crack geometries. Utility of these programs for PD use is limited, due to computer time/cost considerations. At the PD level, program operation must be suitable for performing a wide range of trade studies which evaluate materials, construction concepts, environment, and load spectra. The approach would be used in an iterative mode which converges on an optimum design solution for each of the trade study points. Utility in this program operating mode requires a more efficient method for predicting crack growth life.

One of the initial applications of crack-growth-prediction methodology to preliminary design-level computer programs has been the approach employed in APAS III⁽⁶⁾. Although the procedure in APAS is considered to be not accurate enough due to not accounting for load interaction effects, it has demonstrated the feasibility of assessing crack-growth criteria at the preliminary design level. The computerized methods provide a means for performing trade studies that can be used for making material and structural design-concept selections on a timely basis. To increase the prediction accuracy, an improved method was deemed necessary to be implemented into the APAS III.

A rapid method developed by Brussat⁽⁵¹⁾ which uses a larger scale time base in the crack-growth-rate law, such as crack growth per period, da/dp was considered to be a candidate. The essence of this method is to generate a set of point values of crack growth per period, r_i , at distinct crack length, a_i , to approximate the periodic rate functional values of $f_p(a_i)$. This set

of $f_p(a_i)$ is then used to construct an interpolation polynomial $P_p(a)$ such that $da/dp = P_p(a)$. Fatigue crack growth can then be determined by integrating $P_p(a)$ instead of a cycle-by-cycle summation. This crack growth analysis methodology has been incorporated into the PRDGRO computer program developed by Chang and Cheng⁽⁵²⁾. It has been demonstrated that an order-of-magnitude saving on the computation time can be achieved in some applications.

Another method which could be used is the flight-by-flight characterization of crack growth behavior developed in phase I and identified as Method I. The CYCGRO program was developed in phase I to implement this approach⁽²⁾. It employs the procedure of EFFGRO to perform a cycle-by-cycle crack growth analysis for a unitblock stress spectrum. This analysis is performed at a number of different initial crack lengths to obtain crack growth rate per flight $(da/dF)_j$ versus a measure of the stress intensity factor \bar{K}_j . A least-squares curve-fitting approach is then used to estimate the equation form for crack growth rate per flight. A computer code, PREGRO, was formulated on the basis of CYCGRO to perform preliminary design-level life predictions. It performs the life-prediction calculations by using a damage accumulation scheme that evaluates the crack growth per flight rate equation.

The primary objective of this task was to select a preliminary design-level crack life prediction method which accounts for load interaction effects and to develop a crack growth analysis module which implements this predicting method. This crack growth module was then incorporated into APAS.

Supplementary effort was also directed toward extending the utility of APAS for conducting rational preliminary design trade studies on different aircraft categories. These tasks consisted of restoration of the full range of stress intensity factor correction functions developed by Poe⁽⁵³⁾ for riveted stiffened panels containing cracks, extension of the crack growth analysis process to include unstiffened plate construction concepts, extension of the load spectrum library to include a typical spectrum for a lightweight air-to-air fighter, and incorporation of an alternate means for specifying load spectrum.

5.2 PRELIMINARY DESIGN LEVEL CRACK-GROWTH ANALYSIS PROGRAM (PRDGRO)

PRDGRO is a FORTRAN IV program developed by Chang and Cheng⁽⁵²⁾ at Rockwell. It is capable of accounting for the load interaction effects in predicting crack growth behavior under flight spectrum loading. As the term "Preliminary Design Crack-Growth" (PRDGRO) indicates, the program was developed to be used in PD analysis. It employs the fatigue crack-growth-rate function-per-spectrum loading concept originated by Brussat⁽⁵¹⁾. Brussat assumed that fatigue crack-growth-rate function-per-spectrum loading can be constructed

by using interpolation polynomial if the loading is periodic. The essential intert of the method is to generate a set of point-wise values of crack growth per period, r_i , at distinct crack lengths, a_i , to approximate the periodic rate functional values, $f_p(a_i)$. This set of $f_p(a_i)$ is then used to construct an interpolation polynomial, $P_p(a)$, such that a crack growth rate per periodic load, $da/dp = P_p(a)$, is determined. The crack growth is then obtained by integration. The following paragraphs describe briefly the methodology used in PRDGRO.

A periodic fatigue loading, $P(t)$, is a function of time which usually consists of an ordered sequence, P_1, P_2, \dots, P_r , of discrete loading cycles. If $(\Delta a)_j$ denotes the crack growth due to the j th loading cycle in this sequence, the crack growth per period, r , is the total sum of $(\Delta a)_j$.

$$r = \sum_{j=1}^T (\Delta a)_j$$

The values of r vary along the crack length, a . For a set of distinct points of a_i , r can be experimentally determined or can be accumulated cycle-by-cycle by using a selected cyclic growth rate equation.

It is evident that r is dependent on the conditions of crack tip geometry and material state at each specified point, a_i . Therefore, the actual crack growth per period at a_i denoted by r_i should depend strongly on initial crack length, a_0 .

In the calculation of r_i , the load interaction effects on acceleration and retardation are accounted for by choosing the Vroman/Chang⁽²⁴⁾ model, based on the effective stress intensity factor range ΔK_{eff} variations, where K is the stress intensity factor which can be expressed as $K = \beta \sqrt{\pi a}$, in general.

It is worthwhile to mention that r is always a smooth, monotonically increasing function of $\beta(a)$, the stress intensity factor correction function which is monotonically related to crack dimensions. The advantage of this relationship between r and β is that once such a relationship has been computed, it applies for any configuration of crack and structure, provided the same loading sequence and the same material and prediction model are used.

Although r_i is dependent on a_0 , an approximation can be made that

$$r_i = f_p(a_i)$$

when $f_p(a_i)$ is the functional value of crack growth per periodic loading p at crack length a_i .

An interpolation polynomial $P_p(a)$ is constructed by choosing a set of n distinct ordered crack length a_1, a_2, \dots, a_n to generate a set of $f_p(a_i)$. The smallest a_n is smaller than a_0 ; the largest a_n is larger than final crack length, a_f . Since r_i is a smooth monotonic function of β , $P_p(a)$ can be obtained using fewer r_i values, such as $da/dP = P_p(a)$, which depicts the crack growth periodic loading rate law. Experience has shown that simple quadratic interpolation polynomials produce reasonable results.

The solution of crack growth life in terms of the number of period P versus crack increment Δa can be obtained by integrating

$$dp = \int [P_p(a)]^{-1} da$$

Since $P_p(a)$ is a nonzero, smooth, continuous function; $[P_p(a)]^{-1}$ is also a non-singular, smooth, continuous function. Simple integration techniques along the independent value a from a_0 to a_f will yield reasonable total crack growth life l_p in terms of number of periods.

In the practical computation of l_p , the integration polynomial constructed is not $P_p(a)$ but $[P_p(a)]^{-1}$ from a set of $1/r_i$ values which are the inverses of r_i .

A flow chart of the basic module computational processes is shown in Figure 33.

5.3 PRELIMINARY DESIGN-LEVEL CRACK GROWTH ANALYSIS PROGRAM (PREGRO)

PREGRO is a crack growth prediction program based on the flight-by-flight characterization of crack growth behavior identified as Method I in the phase I report⁽²⁾. The basic elements of the Method I program (CYCGRO) were incorporated in PREGRO, and a new subroutine was added to grow the crack on a flight-by-flight basis. This technique consists of a three-step procedure performed by PREGRO and subroutines CLAMDA and GROFLT. In the first step, PREGRO performs a cycle-by-cycle analysis of a unitblock flight spectrum to obtain crack growth rate per flight $(\Delta a/\Delta F)_j$ and a measure of the stress intensity factor \bar{K}_j for j values of initial crack size. The second step consists of using a least-square-fit procedure for the $(\Delta a/\Delta F)_j$ versus \bar{K}_j values to characterize an equivalent growth per flight rate equation in subroutine CLAMDA. In the third step, subroutine GROFLT uses the crack growth per flight rate equation to calculate crack growth life. A flow chart illustrating the computational processes in PREGRO is shown in Figure 34.

Two basic rate equations were employed, one for load cycles with positive stress ratios and the other for negative stress ratio load cycles. The

modified Walker equation (16) serves as the basis for predicting crack growth rates for positive stress ratio load steps. The Chang(33) compressive load acceleration model is used for negative stress ratio load cycles. Observation of experimental data has shown that for low stress intensity factor ranges, crack growth rates are reduced, and at a threshold stress intensity factor range, ΔK_{th} , no discernible growth is observed. This characteristic is accounted for by considering zero growth when the stress intensity factor range is equal to or less than the threshold value. The cyclic growth rate equations incorporating the threshold concept then are as follows:

$$\frac{da}{dN} = C \left[\frac{\Delta K}{(1 - R)^{1-m}} \right]^n \quad \text{for } R \geq 0 \text{ and } \Delta K > \Delta K_{th}$$

$$\frac{da}{dN} = C \left[(1 - R)^q K_{max} \right]^n \quad \text{for } R < 0 \text{ and } \Delta K > \Delta K_{th}$$

$$\frac{da}{dN} = 0 \quad \text{for } \Delta K \leq \Delta K_{th}$$

where

C , m , n , and q = empirically derived material constants based on crack growth tests

R = cyclic stress ratio

K_{max} = maximum stress intensity factor

K_{min} = minimum stress intensity factor

$\Delta K = K_{max} - K_{min}$ = stress intensity factor range

ΔK_{th} = threshold intensity factor

The generalized Willenborg⁽²⁶⁾ retardation model, in conjunction with the Chang acceleration scheme, was selected to account for load interaction effects. The first step in the damage accumulation scheme consists of calculating incremental crack growth based on the cycle-by-cycle growth methodology for a unit-block flight spectrum. The unitblock spectrum consists of all peak and valley loadings which occur for a block of flights representative of the missions flown during the aircraft lifetime.

The Vroman linear approximation method⁽³⁷⁾ is employed to perform the damage accumulation due to the unitblock spectrum. The approach is based on the assumption that growth rate is a constant throughout a load step in a spectrum such that the crack size is in a linear relationship with the number of load cycles. A load step consists of one or more cycles of constant-amplitude loadings. A relatively small incremental change in crack length, δa , is used to calculate the growth rate for a given load step. The number of cycles required to grow the crack through the assumed incremental length is then given by:

$$N = \delta a / (da/dN)$$

The value of N is compared to the cycles in that load step, N_i . If N is greater than N_i , crack growth for that particular step is:

$$\Delta a = N_i (da/dN)$$

Crack length is increased by Δa , and the process continues to the next load step. If N is less than or equal to N_i , N is subtracted from N_i , the crack size is increased by δa , and the load step is reconsidered. This process continues with N being compared to the remaining cycles in the step. Computation continues until all load steps in the unitblock are exhausted.

The foregoing cycle-by-cycle crack growth analysis is performed for the unitblock spectrum for a number of different values of crack size. Crack size, a_j , at the end of the unitblock spectrum is calculated from:

$$a_j = a_{0j} + (\Delta a)_j$$

where a_{0j} are the selected values of initial flaw size and $(\Delta a)_j$ are the incremental changes in the crack size resulting from the unitblock spectrum. Values of the initial crack size, a_{0j} , are selected to cover the expected range of crack sizes, starting at the initial flaw size and continuing through that expected at failure. The crack growth resulting from the unitblock spectrum for a period of N_A flights is then defined by the following:

$$(\Delta a / \Delta F)_j = (\Delta a)_j / N_A$$

For each of the assumed initial flaw sizes, the corresponding measure of stress intensity factor is defined by:

$$\bar{K}_j = \sqrt{(\overline{\Delta \sigma}^2) [\psi(a_{0j}) + \psi(a_j)]} / 2$$

where $(\overline{\Delta \sigma}^2)^{1/2}$ is the root-mean-square of the stress range in a unitblock.

The second step in the computational procedure consists of characterizing the complex flight spectra into an equivalent constant-amplitude loading that will produce the same crack growth life. This method was developed in phase I of this program(2). Based on the observation that the crack growth rate per flight, $(\Delta a/\Delta F)_j$, versus the RMS of stress intensity factor range, \bar{K}_j , is a nearly straight line when plotted on the log-log scale, the following relationship is formulated:

$$\frac{da}{dF} = C(\bar{K})^\lambda$$

The power exponent λ and proportionality constant C are calculated in subroutine CLAMDA by applying a least-square-fit procedure to the $\log (\Delta a/\Delta F)_j$ versus $\log (\bar{K}_j)$ data plot.

Crack growth life is then to be calculated as the third step of the damage accumulation scheme. The linear approximation method is employed to calculate life over a prescribed crack length interval in subroutine GROFLT.

5.4 SELECTION OF THE CRACK GROWTH ANALYSIS MODULE

The procedures in APAS III are designed to perform multistation detail sizing of box-beam structural elements. Program options provide the user with the choice of either analyzing the structure, based on input element sizing definitions, or performing a redesign optimization within practical constraints of element sizes. The optimization procedure is an iterative approach, starting with user-defined initial size estimates and progressing until a member of each symmetry grouping has a zero margin of safety or until minimum gage constraints dictate sizing. This process is initiated for static load strength design, followed by the analysis of fatigue life, crack growth, and residual strength criteria. Within this operating framework of APAS III, an approach was taken to compare the capabilities of the different crack growth prediction modules for a common set of variables.

Test cases were representative of typical wing torque box structures for transport and fighter aircraft categories. Common spectrum stress levels were maintained by executing APAS to obtain strength sizing details which were then input data to a second problem case in which only strength and crack growth analysis were performed.

Fracture mechanics material constants were based on existing APAS library properties for 2024-T62 aluminum. The following is the procedure used to derive comparable material properties for use by both proposed crack growth modules: PRDGRO and PREGRO.

The crack-growth-rate equation used in both of the proposed crack-growth modules is the modified Walker equation, which can be expressed as:

$$\frac{da}{dN} = C \left[\frac{\Delta K}{(1 - R)^{1-m}} \right]^n \quad \text{for } \Delta K > \Delta K_{TH}$$

$$\frac{da}{dN} = 0 \quad \text{for } \Delta K \leq \Delta K_{TH}$$

where C, n, and m are crack-growth-rate constants, ΔK is the stress intensity factor range, R is the stress ratio, and ΔK_{th} is the threshold value of ΔK .

Comparison of this equation with the existing crack growth analysis module (PROGRO) in APAS III suggests a similarity in the definition of material constants. The Erdogan rate equation which serves as the basis for the life prediction method in PROGRO is:

$$\frac{da}{dN} = C K_{max}^m \Delta K^P$$

This equation may be written in another form by making the following substitution.

$$K_{max} = \frac{\Delta K}{(1 - R)}$$

and

$$\begin{aligned} \frac{da}{dN} &= C \left(\frac{\Delta K}{1 - R} \right)^m \Delta K^P \\ &= C \left[\frac{\Delta K}{(1 - R)^{\frac{m}{m+P}}} \right]^{m+P} \end{aligned}$$

Comparison of constants in the modified Walker and Erdogan equations indicates that these equations produce identical growth rates for the material constants as defined in the following equations where the subscripts "w" and "e" represent Walker and Erdogan constants, respectively.

$$C_w = C_e$$

$$n_w = m_e + P_e$$

$$m_w = P_e / (m_e + P_e)$$

A tabulation of 2024-T62 aluminum growth-rate equation constants which were used in the evaluation of crack-growth life predictions are shown in the following (notice that they are in psi units):

<u>Erdogan Equation</u>		<u>Walker Equation</u>	
<u>Parameter</u>	<u>Value</u>	<u>Parameter</u>	<u>Value</u>
C_e	2.726×10^{-22}	C_w	2.726×10^{-22}
m_e	1.5	m_w	0.625
p_e	2.5	n	4.0
$(m+p)$	4.0	ΔK_{th}	1,000

5.4.1 TRANSPORT CASE

The transport case was a wing torque box on a typical four-engine jet transport aircraft. The construction of the torque box was 2024-T62 aluminum upper and lower covers with riveted 7075-T6 J-stringers and Ti-6Al-4V ribs, spars, and spar caps. Stringer spacing was set at 6 inches on the upper cover and 7.5 inches on the lower cover. The cross section at wing spanwise station 600 was used for evaluating the effects of strength and stability sizing, crack-growth analysis, and the redesign/optimization solution. Station 600 nodal coordinates, geometry, and cover element section details are shown in Figure 35. Strength sizing results are shown in Table 24, and the corresponding design stresses are presented in Table 25.

The stress spectrum for the transport case was obtained directly from existing programmed procedures in APAS for evaluating a prescribed load profile and occurrence data, together with a set of external load conditions. The resultant spectrum is based on experimental data for the operation of a medium-range transport aircraft. It is organized according to a prescribed sequence and duration of flight segments. Each segment consists of subsegments or steps of minimum and maximum stresses with the corresponding number of cycles that occur in one flight. The ground-air-ground (G-A-G) cycle is obtained by taking the maximum stress excursion between the peak in flight stress and the valley ground condition stress. Due to the selected approach for developing this spectrum, the number of cycles for a load step includes the decimal equivalent of all loads that occur at least once in 10,000 flights. This spectrum format is not compatible with the data format required for analyzing load interaction effects attendant with the crack-growth-rate retardation/acceleration phenomena. For the purposes of expediency in regard to evaluating the different

crack growth modules, an interim procedure was implemented whereby the transport spectrum encompassing a period of one flight included only those load steps which occurred at least once in every two flights. This spectrum for panel 9 in Figure 35 is presented in Table B-1 in Appendix B of Reference 40. The last load step in Table B-1 represents the G-A-G cycle.

Test cases were executed to compare the performance of the existing crack growth module (PROGRO) with the results of each of the proposed modules. The Vroman/Chang⁽²⁴⁾ load interaction model was used to perform the cycle-by-cycle analysis in both proposed modules. Results of the crack growth analysis test cases based on strength designed structure are presented in Figures 36 through 38 in the form of crack length versus flight curves. For those cases where no load interaction effects were considered, there was a variance of 3 percent in predicted life as shown in Figure 36. Figures 37 and 38 show the effect of overload retardation on crack growth life as predicted by PRDGRO and PREGRO; a comparison of these results with the PROGRO prediction is shown in Figure 39.

The design-to crack-growth life requirements was obtained by performing a redesign optimization. In the transport cases, the initial flaw size was 2 inches, and the inspection interval was 20,000 flights. The transport analysis results for station 600 are shown in Tables 26 through 30. Maximum skin and stiffener stresses, critical flaw size, number of safe-life flights, and the weight penalty for each of the cover panels are presented in these tables. A weight penalty of 8.56 percent was predicted by PROGRO for the lower cover panels as shown in Table 26. Corresponding results by PRDGRO and PREGRO, without accounting for retardation effect, were 7.74 and 8.61 percent, respectively. PRDGRO and PREGRO predict reduced weight penalties as a result of accounting for overload retardation effects. The weight penalties were reduced as a result of considering overload retardation effects. The weight penalties were reduced to 4.19 percent using PRDGRO and to 1.99 percent using PREGRO. (Refer to Tables 28 and 30.) Computer execution time and costs were comparable for the transport runs with the various modules. PREGRO execution time was slightly higher than that for PRDGRO.

5.4.2 FIGHTER CASE

The wing for a contemporary lightweight fighter was selected to evaluate program process results for fighter spectrum and design parameters. The torque box construction for this fighter wing was a multirib design with 2024-T62 integral blade-stringer cover panels and transverse-angle stiffened front and rear spars. The cross section at spanwise station 21.64 was used to evaluate the results of the different crack growth prediction modules. Figure 40 presents the section geometry parameters at station 21.64. Strength sizing details and design stresses are presented in Tables 31 and 32.

A typical load spectrum for an air-to-ground fighter was input into APAS in the form of cycle-by-cycle random stress history. This spectrum, created by program SPECN1(48), consisted of generalized peaks and valleys in the form of percentage of local design limit stress. It reflects a unitblock of 50 flights representative of the missions throughout the aircraft lifetime. G-A-G cycles were inserted at the beginning and end of each flight in such a way that in each flight the first valley was replaced by the ground load and the last peak was followed by the ground load. The resultant spectrum for panel 9 in Figure 40 is presented in Table B-II in Appendix B of Reference 40.

Crack growth analyses were again performed by PROGRO, PRDGRO, and PREGRO modules. Material constants used in the analysis were identical to those used in the transport cases. Crack length versus flight curves resulting from the crack growth analysis of structures sized to strength requirements are presented in Figures 41 through 44. Design to crack growth life requirements was based on an arbitrarily selected initial flaw size of 1 inch, with an inspection interval of 4,000 flights. Predicted weight penalty trends for the fighter wing were similar to those for the transport. APAS results for the fighter wing at station 21.64 are presented in Tables 33 through 37. The predicted weight penalty of 18.95 percent by PROGRO (Table 33) is reduced to no penalty by PREGRO as a result of including retardation effects. PREGRO proved to be more efficient than PRDGRO in evaluating the more complex fighter load spectrum. PREGRO required approximately 30 percent less computer central processing unit time. Based on this advantage, PREGRO was selected for incorporation into APAS.

5.5 APAS III PROGRAM REVISION

The APAS III program uses a modular segmented load structure. The modular configuration of this program facilitated those modifications and additions required to integrate the PREGRO crack growth prediction module and the load spectrum processing revisions.

5.5.1 FRACTURE MECHANICS MATERIAL PROPERTY LIBRARY

The composition of the fracture mechanics material property library was revised to provide the material constants required for the crack growth analysis performed by PREGRO. Crack-growth characterization parameters employed by the modified Walker equation, in conjunction with the Willenborg retardation model and the Chang acceleration scheme which were incorporated into a preliminary library, are shown in Table 38.

This program revision was accomplished by modifying the input data processing routine and the labeled common blocks used for data storage and transmission.

5.5.2 LOAD SPECTRUM GENERATION

The load spectrum for fatigue and crack-growth analyses within APAS was based on operation of a medium-range transport aircraft. In order to extend the utility of APAS, a task was conducted to provide program users with the capability for evaluating a broader range of aircraft categories and mission parameters. Toward this objective, a load spectrum based on a typical light-weight fighter was added to the APAS program library. The existing approaches used for the transport spectrum definition and blocking of mission segment steps were maintained to minimize program revision. Options were added which allow the user to modify parts of the programmed transport or fighter spectra or to specify an entirely new spectrum. An alternate means of defining spectrum loads in the form of stress levels and cycles was also implemented.

The flight profile used as the basis for developing a typical fighter service load spectrum is presented in Table 39. This profile presents the segments of an air-to-air combat mission for a typical lightweight fighter. Maneuver loads for the flight segments were obtained from Reference 50, which presents the data in the form of load factor versus cumulative occurrences. In conjunction with the foregoing data, a representative supersonic air-to-air combat spectrum has been added as shown in Table 40. Taxi load factor versus cumulative occurrence data were obtained from Reference 50. Incremental load factor versus frequency of occurrences for the landing segment was derived from the table of landing sink speed versus cumulative occurrences. Sink speed was converted to vehicle load factor by assuming a landing-gear stroke of 12 inches and oleo efficiency factor of 0.8.

The methods used for subdividing fighter mission segments into subsegments which represent discrete magnitudes of incremental loads were based on existing APAS procedures. The range of incremental load factors was divided into 20 discrete subsegments as shown in Table 41.

The approach to spectrum development in APAS is such that the number of cycles for a load step includes the decimal equivalent of all load excursions that occur at least once in 10,000 flights. This spectrum format is not ideally suitable with the basic formulations for predicting load interaction effects attendant with the crack-growth-rate retardation/acceleration phenomena. Therefore, program modifications were incorporated to process only those load steps which occur at least once in each block of flights. In order to ascertain a reasonable block size for crack growth prediction, a study was conducted for various sizes of flight blocks⁽⁵⁴⁾. The local spectrum for panel 9 of the fighter torque box shown in Figure 40 is presented in Tables 42 through 44 for a block of one, 50, and 100 flights.

A tabulation of the aluminum (2219-T851) growth rate equation constants which were used in the test cases were as follows:

<u>Walker Equation</u>		<u>Erdogan Equation</u>	
<u>Parameter</u>	<u>Value</u>	<u>Parameter</u>	<u>Value</u>
C_w	1.0059×10^{-20} (in psi units)	C_e	1.0059×10^{-20} (in psi units)
m_w	0.6	m_e	1.456
-	-	p_e	2.184
n_w	3.64	$(m+p)$	3.64
q	0.3	-	-

The crack-growth analysis was performed for a centered-through crack with an initial crack length (2a) of 1 inch. A constraint of 15,000 flights was imposed for those cases where the analysis was followed by a redesigned optimization of the structural sizing. A summary of the results obtained from the different program configurations is shown in Table 45. For all cases where PREGRO was executed without consideration for load interaction effects, there was a maximum difference of 1.2 percent between the results obtained from PREGRO and PROGRO. This variance is attributed to the difference in integration schemes for crack growth life.

Crack length versus flight curves resulting from the crack growth analysis of structure sized to strength requirements are presented in Figure 45. These curves are based on a load spectrum consisting of load steps which occur at least once in each flight. There is a negligible difference between the life prediction from PROGRO and that from PREGRO without load interaction effects. The increased life due to the load interaction effects are plotted in Figure 45. The results obtained by performing a redesign optimization are presented in Tables 46 through 49. Maximum skin and stiffener stresses, critical initial flaw size, number of safe-life flights, and the weight penalty for each of the cover panels are presented in these tables. A weight penalty of 10.93 percent was predicted by PROGRO for the lower cover panels, as shown in Table 46. The corresponding result from PREGRO without consideration for load interaction effects was 11.06 percent, as shown in Table 47. The result of accounting for retardation and acceleration effects was a 15.94-percent penalty (Table 48), and an 8.36-percent penalty resulted from considering only the retardation effects (Table 49).

In addition to the analysis performed for the load spectrum consisting of a one-flight block, corresponding program runs were made for load spectra based on 50- and 100-flight blocks. Crack length versus flight curves for these cases are shown in Figures 46 and 47. Structural redesign optimization results are presented in Tables 50 through 57.

Crack length versus flight curves predicted by PROGRO for the different spectra flight block sizes is depicted in Figure 48. The curve based on including all fractional cycle steps, the original premise in PROGRO, is also shown in this figure. The predicted life curves approach close agreement for flight block sizes of 50 and 100 flights. The major difference between the curves for 50- and 100-flight blocks and the curve based on all fractional cycle steps is due to the maximum spectra stresses. The high load conditions with low probability of occurrence which were included in the spectrum which considered fractional cycle steps resulted in a shorter critical crack length. Crack length versus flight curves predicted by PREGRO with retardation and acceleration effects for the different spectra flight block sizes are shown in Figure 49. The predicted life for the 50-flight block was 8.7 percent higher than that for the 100-flight block.

A plot of weight penalties from the structural redesign optimization solutions versus spectrum block sizes is shown in Figure 50. The results from PROGRO are compared with those from PREGRO with retardation and acceleration effects. As noted previously, program solutions approach close agreement for flight block sizes greater than 50 flights. For the case of a one-flight block, the accounting for load interaction effects by PREGRO resulted in an increase in structural penalty. For the 50-flight block size case, PREGRO predicted a decrease in structural penalty due to load interaction effects. This difference can be attributed to the omission of significant high load steps in a truncated spectrum for a one-flight block. For the typical air-to-air fighter spectrum stored in APAS, the 100-flight block size seems to be a satisfactory compromise for use by PREGRO.

5.5.3 STIFFENED PANEL CRACK LIBRARY

A complete library of riveted stringer stiffened panel stress intensity correction factors⁽⁵³⁾ has been restored into APAS. Table values and interpolation procedures for subroutine POEDAT were obtained from VDEP II⁽⁵⁵⁾ program listings. In order to validate table data values and table interpolation procedures; a stand-alone graphic plotting program was used to process stress intensity correction factor library for the 75 sets of data covering a range of stiffener spacings, percent stiffening, and broken stiffeners. The results of sample runs showing the relative difference in predicted life based on the generalized stress intensity correction factor versus interpolated data representing the structural model are shown in Figure 51.

5.5.4 CRACK-GROWTH ANALYSIS FOR PLATE CONSTRUCTION CONCEPTS

APAS crack growth prediction capabilities were extended to include the evaluation of plate construction structural concepts. In order to perform this analysis, a new subroutine CRITIC was created to calculate critical

crack length based on design limit load. Procedures in PREGRO are then used to calculate life based on crack growth from the initial flaw size to the critical crack length. The redesign optimization scheme for plate construction concepts is similar to that used for stringer stiffened panel designs. For the plate construction concepts, flaw-growth criteria are satisfied when the desired life is reached at the instant that the crack reaches critical crack length, as opposed to the stiffened panel concept maximum crack length constraint of six stringer bays.

6.0 EXPERIMENTAL VERIFICATION

To verify the two crack growth prediction methodologies developed in phase II, an experimental verification program was conducted in phase III. This program consisted of two major tasks. The first task was an experimental program which consisted of two primary test groups: group I - Fighter Aircraft Spectrum Loading Test and group II - Transport Aircraft Spectrum Loading Test. The second task was the performance of analytical predictions using two computer codes: CRKGRO and FLTGRO. Analytical prediction results were then correlated with the test data. The following paragraphs describe the experimental program and the correlation results in detail.

6.1 EXPERIMENTAL TEST PROGRAM

6.1.1 FIGHTER AND TRANSPORT SPECTRUM DEVELOPMENT

Two groups of tests were conducted in this experimental verification program. For the group I tests, the following four baseline load spectra of the F-15 fighter aircraft furnished by the Air Force were used to generate the fighter baseline test spectra and their variations.

1. Air-to-Air (A-A) mission - 192 flights, 4,992 cycles
2. Air-to-Ground (A-G) mission - 264 flights, 4,997 cycles
3. Instrumentation and Navigation (I-N) mission - 445 flights, 2,672 cycles
4. Composite mission - 206 flights, 4,246 cycles.

All the baseline spectra were in the random cycle-by-cycle format. The peaks and valleys are in the form of percentage of design limit stresses (DLS). For all the baseline spectra, the design limit stresses were arbitrarily set to 30 ksi. The baseline spectra data are included in Volume II of this final report.

Twenty-one spectrum variations were developed from the preceding fighter baselines. Table 58 shows the fighter spectrum variations test matrix, which represented the following five major spectrum variation types:

1. Stress level
2. Compression load
3. High load clipping

4. Low load truncation

5. Mission sequence

In addition to the spectrum variations, eight mission-mix variations were developed in group I as shown in Table 59. Among these eight mission-mix variations, five used the three fighter baseline spectra (A-A, A-G, and I-N missions) developed in phase I. These three baseline spectra were also generated from the F-15 aircraft baseline load data and were also in the random cycle-by-cycle format. Detailed values of the peak and valley of each cycle for these phase I baseline spectra were documented in Volume II of the phase I final report⁽³⁾. To develop the mission-mix variations, each of the three baseline spectra was arbitrarily divided into five parts. Each part consisted of a certain number of flights. The divided parts of these three baseline spectra are shown in Tables 60 through 62. The symbol $[mission\ x]_j$ represents the j th divided part of the x -mission, while $N[mission\ x]_{m-n}$ indicates N -flight of the x -mission consisting of the flights from the m th flight to the n th flight in the baseline. For example, $(A-A)_1$, represents the first divided part of the (A-A) mission, while $11\ (A-A)_{1-11}$ indicates that there are 11 flights of the (A-A) mission, starting from the first flight to the eleventh flight in the (A-A) mission baseline spectrum. Five mission-mix variations (M-301, M-302, M-303, M-304 and M-305) developed from the phase I baselines were constructed as shown in Table 60.

Three additional fighter mission-mix variations were constructed in group I using the phase III baseline spectra, including $(A-A)^{III}$, $(A-G)^{III}$, and $(I-N)^{III}$ missions shown in Volume II of this final report. The mixture of these three mission-mix variations is shown in Table 61, while the divided parts of each baseline spectrum are listed in Table 62.

For the group II tests, the transport composite baseline spectrum originally developed in phase I, which contained 21 flights, was again used as the baseline. For the sake of completeness, this transport composite mission spectrum table is included in Volume II of this final report. Notice that the peak and valley of each cycle were already in the unit of stresses (ksi). A total of seven transport spectrum variations were derived from this composite baseline spectrum as follows:

1. All the tension and compression stresses were increased by 60 percent.
2. All the compressive stresses were set to zero.

3. All the compressive stresses were increased by 25 percent.
4. All the compressive stresses were increased by 50 percent.
5. All the cycles with maximum stresses less than 8 ksi were truncated.
6. The minimum stresses of those cycles with stress ratio $R > 0.75$ were lowered to $\sigma_{\min} = 0.75 \sigma_{\max}$.
7. Deleted all the cycles of a flight, except the ground-air-ground (G-A-G) cycles. The G-A-G cycle of the 21 composite flights is given in Table 63.

6.1.2 MATERIAL AND SPECIMENS

All test specimens were the ASTM standard center-cracked tension (CCT) specimens ⁽⁸⁾ which were machined from a single heat of 2219-T851 aluminum alloy plates procured to specification QQ-A-250/30. The plates were 48 by 144 inches and had a nominal thickness of 1/4 inch. The plate material was purchased from Ti-Con Industries, Huntington Beach, California. A description of the material, including the chemical and physical properties, is listed in Tables 64 and 65.

The test specimen blanks were machined from three plates. Each blank was uniquely serialized to identify the plate from which it came and its location within that plate. The blanks were then finish-machined to the configuration shown in Figure 52. All test section thicknesses were 0.250 inch, and the longitudinal grain was oriented parallel to the loading direction. The center notches were installed by EDM Laboratories, Garden Grove, California, employing the wire electrical discharge machining process. The center notch configuration was selected in order to minimize geometric considerations in calculating the stress-intensity factor.

6.1.3 TESTING PROCEDURES

All tests were conducted in the Rockwell/NAAD Structure Test Laboratory, employing the 500K MTS fatigue testing systems. An MTS load tower (Figure 53) consists of a rigid load frame and incorporates a dual-bridge load cell and hydraulic actuator. Applied loads are controlled through a closed-loop servo-system and load programmer test system, with load cells and servovalves optimized for controllability and cyclic load rate. The randomized tests were controlled by the Datum servosystem 70, a computer-controlled fatigue test system selected for this application because of its capability to handle much longer waveforms than is possible with the integral MTS computer equipment. As used on the random spectrum tests, the Datum system acts as a

waveform generator and provides a command signal output to the MTS servocontroller. The MTS system returns a load cell feedback signal to the Datum system, which was used for desired versus actual load error checking. The only other interfaces between the two systems are discrete signals providing test control, including hold, run, and ramp on servocontroller error detection. A schematic of the interrelationship of the MTS and Datum 70 systems is shown in Figure 54. Loads were transmitted from the test machine heads to the specimens through hydraulically actuated friction grips.

The EDM crack starter slot in each specimen was precracked to produce an initial crack length, $2c$, of approximately 0.30 inch. Precracking was performed under constant-amplitude cycling at an R-factor of zero and with maximum cyclic stresses of 10 ksi. All tests were run in ambient laboratory air at room temperature. The cyclic rate was between 4 and 6 Hz, depending on such factors as load level, load range, and the presence of compression loads. Crack growth was measured by visual optics reading from precision scales attached to each side of the specimen adjacent to the EDM slot. Measurements were made and recorded after approximately each 0.05-inch increment of growth.

6.1.4 EXPERIMENTAL VERIFICATION TEST RESULTS

The majority of these 2219-T851 aluminum CCT specimens were tested to failure, with the crack growth life of each specimen exceeding 1,000 flights, as required. The measured crack growth data of these tests were originally recorded in a laboratory log book in the measured crack growth (Δa) versus total elapsed cycles (N) format. For the purpose of data reduction and presentation, test data were coded into PLOT RATE⁽¹⁷⁾, an automated graphical presentation program, resulting in a computer printout of the raw data for each test as well as other calculated parameters such as (da/dN) , (K_{max}) , and (ΔK) , in a prearranged tabular form. A typical PLOT RATE printout is shown in Volume II. Notice that the original data tabulation form was designed for calculating those parameters from constant-amplitude loading tests. For spectrum tests, only the measured crack sizes and corresponding tests cycles are valid.

6.1.4.1 Fighter Spectrum Test Results

Fatigue crack growth test results of the four fighter baseline spectra (A-A, A-G, I-N, and composite) were processed by PLOT RATE. Test results of these four fighter baseline spectra tests are documented in Volume II. Table 66 shows the crack lives of these four test specimens: F-B-1 (A-A), F-B-2 (A-G), F-B-3 (I-N) and F-B-4 (composite).

For the purpose of comparison, crack growth curves in the half-crack length (c) versus total elapsed cycles (N) format of these four test cases were plotted by PLOT RATE on a single chart. (See Figure 55.) It shows that the A-A mission is apparently the most severe mission among the four fighter baseline spectra tested. The I-N mission is the least severe one. Comparing the crack growth curves of F-B-3 and F-B-1 for cracks with identical crack length, the crack growth life of the 2219-T851 aluminum CCT specimen under the I-N mission type of random spectrum loading with the DLS = 30 ksi, the crack growth life is 2.3 times longer than its A-A mission counterpart.

The composite spectrum consists of 92 flights of A-A missions, 90 flights of A-G missions, and 24 flights I-N missions. Hence, it was expected that the life of F-B-4 would be longer than that of F-B-1 and shorter than that of F-B-3. The fact that the F-B-4 crack curve is between the F-B-1 and F-B-3 growth curves indicates that the test results are in the right trend.

Growth data of the fighter spectrum variation tests are also shown in Volume II. Again, the test data were presented in the typical tabular format done by PLOT RATE. Test numbers, specimen types, and spectrum variations of these test cases were shown in Table 58. Fatigue crack lives of these test cases are summarized in Table 67. It can be seen from the table that all tests, except FB-V-B-3 and FB-V-B-4, were tested to failure. The random flight spectrum applied to FB-V-B-3 was the I-N mission with DLS = 25 ksi. The tested flight spectrum for FB-V-B-4 was the composite spectrum with DLS also at the 25 ksi level. For FB-V-B-3, 40,080 flights (222,331 cycles) of I-N mission were applied to the test specimen with a final crack length of $c_f = 0.83$ in. For FB-V-B-4, 7,736 flights (159,514 cycles) were applied. The crack grew from $c_i = 0.145$ in. to $c_f = 0.61$ in. The shortest life tested was the increase of DLS to the 35 ksi level for A-A mission (FB-V-C-1). The total crack growth life was 1,293 flights (33,616 cycles).

Spectrum variation effects on crack growth for the four fighter baseline spectra can be seen from the combined crack growth curves as shown in Figures 56 through 60. Fatigue crack life comparisons of the test spectrum variations to the baseline spectra are shown in Tables 68 through 71. Ratios of the crack life under spectrum variation to the baseline spectrum of each type of spectrum variation were also shown in these tables. For all spectrum variations tested, the spectrum variation effects to the crack growth seem to be independent of the mission types. The largest effect to the crack growth

is the stress level. At low stress levels (DLS = 25 ksi), the ratio of the spectrum variation life, N_V , to the baseline life, N_B , for the composite spectrum is $N_V/N_B = 3.08$. For the I-N mission, $N_V/N_B = 2.61$. At high stress levels (DLS = 35 ksi), N_V/N_B for the A-A spectrum is 0.46, for the A-G mission is 0.54, for the I-N mission is 0.63, and for the composite mission is 0.45.

Ratios of the crack growth life of the compressive load variation (all compressive loads set to zero) to the baseline spectra varies from 1.2 for the A-A mission to 1.03 for the A-G mission. For the I-N and composite missions, N_V/N_B is 1.15 and 1.16, respectively. Among all the spectrum variations tested, the 45-percent low-load truncation for the composite mission had the least effect to crack growth life. In this test case, FB-V-G-4, the ratio is 1.01. For the high-load clipping variation when high loads clipped at the 85-percent DLS = 30 ksi level, the ratio is 0.69 for the A-A mission and 0.57 for the composite mission.

The eight test specimens, M-301 through M-308, of the fighter mission-mix variation testing were also tested to failure, with the crack growth life of each specimen exceeding 1,000 flights, as required. The measured crack growth data were again processed through the PLOT RATE program and are presented in Volume II of this report.

Five out of the eight mission-mix variation test spectra were developed using the fighter baseline spectra developed in phase I. The rest of the three test spectra were based on the fighter baselines developed in phase III. The mission-mix variation effects on the crack growth lives of these two sets of tests can be seen in the combined crack growth curves shown in Figures 60 and 61. For the first set, the largest crack growth life variation is between M-301 and M-303. The fatigue crack growth life of M-303 was approximately 20-percent longer than that of M-301. This is because the M-303 test spectrum contained more I-N missions than the M-301 test spectrum, resulting in a longer life. The I-N spectrum is much less severe than the A-A and A-G spectra. Table 72 summarizes the results. For the mission-mix variations which used the phase III fighter spectra as the base, those mixed missions containing similar ratios of A-A missions to the total mission (70/206 for M-306 and 92/207 for M-307), the crack growth lives were not noticeably different. The increase of crack growth life due to the reduction of the ratio of the A-A mission can be clearly seen from the M-308 test case. Figure 61 illustrates this effect. The results of comparison of crack growth lives for this set of mission-mix spectrum test to the baseline is shown in Table 73.

6.1.4.2 Transport Spectrum Test Results

The baseline test specimen, T-B-1, was tested using the transport composite spectrum identical to the one used in test M-93 conducted in phase I. The crack growth lives of these two tests varied only approximately 5 percent. This demonstrated the repeatability of two duplicate tests.

Seven transport spectrum variation tests were conducted under the random spectrum, with the variations described in 6.1.1. Test results of these seven tests are shown in the combined crack growth curves (Figure 62). For direct comparison of the spectrum variation effects, the crack growth life of each test, N_V , was divided by the crack growth life of the baseline test, N_B . Results are shown in Table 74. All test results of the transport spectrum tests are documented in Volume II.

6.2 ANALYTICAL PREDICTION AND CRACK GROWTH DATA CORRELATIONS

6.2.1 ANALYTICAL PREDICTIONS

Fatigue crack growth life predictions on all test cases were performed using the crack growth prediction methodologies developed in phases I and II. The CRKGRO program was used to perform the detailed crack growth analysis on a cycle-by-cycle basis, while the FLTGRO program was used to perform the flight-by-flight crack growth analysis on a one-cycle-per-flight basis. The following paragraphs describe the analytical predictions in detail.

6.2.1.1 Cycle-by-Cycle Crack Growth Predictions

Fatigue crack growth predictions applying the cycle-by-cycle crack growth analysis methodology were performed through the use of CRKGRO. The crack-growth-rate constants and other related crack growth parameters used in the predictions were those established in phase II, Development of Predictive Methodology. Thus, this set of prediction represented the truly "blind prediction" results. The following were the values of each constant and parameter for the 2219-T851 aluminum alloy used in the blind predictions:

C	$= 5.066 \times 10^{-10}$ (in ksi unit)	R_{cut}^+	$= 0.75$
n	$= 3.83$	R_{cut}^-	$= -0.75$
m	$= 0.6$	ΔK_{th_o}	$= 2.5 \text{ ksi } \sqrt{\text{in.}}$
q	$= 0.3$	K_c	$= 65 \text{ ksi } \sqrt{\text{in.}}$
A	$= 1.0$	σ_{ty}	$= 48 \text{ ksi}$
R_{so}	$= 3.0$		

All the random flight spectra were range-pair counted before the performance of the crack growth analysis. To reduce the computation cost, spectra longer than 3,000 cycles were counted segmentally at 500 cycles per segment. Both the load-interaction solutions and the without-load-interaction solutions were obtained for all the test cases. The without-load-interaction solutions did not account for the tensile overload retardation effect, the compressive load acceleration (negative stress ratio) effect, as well as the reduction of retardation by compression loads effect to the crack growth.

Results of the analytical predictions for both the fighter and transport spectrum test groups are summarized in Tables 75 and 76. The predicted life, N_p , for each test case is either in number of cycles and number of flights or just in number of flights as appropriate.

6.2.1.2 Flight-By-Flight Crack Growth Predictions

Analytical predictions were also performed by using the FLTGRO program in order to verify the flight-by-flight crack growth analysis methodology which employs the spectrum characterization method developed in phase I. Only the one-cycle-per-flight option of the FLTGRO program was executed. This is because the multisegment-per-flight option usually provides more accurate predictions (56). To verify the flight-by-flight crack growth prediction method, assessing the less accurate prediction results obtained from FLTGRO should give better indications.

To provide a direct comparison to cycle-by-cycle predictions, the crack-growth-rate constants and other parameters inputted into FLTGRO were identical to those inputted in CRKGRO. Again, random flight spectra were range-pair counted prior to the performance of the analysis. Only the load-interaction solution option was executed.

Crack growth predictions obtained from FLTGRO for both the fighter spectrum test cases and the transport spectrum test cases were also listed in Tables 75 and 76. The predicted lives (N_p) were in number of flights.

6.2.2 CRACK GROWTH TEST DATA CORRELATIONS

Analytical predictions obtained from CRKGRO and FLTGRO were correlated to the crack growth test data in order to verify the prediction methods developed in this program. The predicted crack growth behavior obtained from the computer program for each predicted case was plotted against the test data. Typical such plots are shown in Figures 63 through 68. The rest of the plots can be found in References 56 through 58. The test crack growth curves were the graphical outputs of the PLOT RATE program. The analytical prediction curves were plotted by hand. Only the load-interaction solutions were plotted.

The dashed and dotted lines in those figures represent the crack growth behavior predicted by CRKGRO using the cycle-by-cycle crack growth prediction approach, whereas the broken lines represent the crack growth predicted by FLTGRO using the flight-by-flight crack growth analysis method. In these figures, all the lives are in number of cycles. It can be seen that for most cases, the prediction correlated with the test data rather well.

To assess the prediction accuracy of each method, the ratio of the predicted crack growth life to the test crack growth life, N_p/N_t , was calculated for each test case. The results were summarized in Table 75 for the fighter spectrum test group and in Table 76 for the transport spectrum test group. Figure 69 shows the plots of the predicted lives versus the test lives for the 33 fighter test cases. A histogram for the 33 fighter test case correlations is shown in Figure 70.

The average prediction ratios for the fighter spectra and the transport spectra for each set of solutions were calculated together with their standard deviations. Results are shown in each table. For the fighter spectrum test group, the average prediction ratio of the 33 test cases is 0.88, with a 0.17 standard deviation for the load-interaction solutions obtained from CRKGRO, and 0.64, with a 0.15 standard deviation for the without-load-interaction counterparts. The average prediction ratio is 1.04, with a 0.26 standard deviation for the load-interaction solution obtained from FLTGRO. Table 77 presents the average prediction ratio and the corresponding standard deviation for each set of analytical predictions for the fighter spectrum test group and the transport spectrum test group separately.

From the results of the test data correlations, the prediction accuracies for both CRKGRO and FLTGRO load-interaction predictions on the fighter spectrum test cases are well within the acceptable range for the currently required damage-tolerance analysis for fighter aircraft. Yet, from the transport prediction results shown in Table 76, it was felt that the predictions were in general, not too desirable. Hence, refinement efforts in the prediction for the transport cases were conducted.

6.2.3 REFINEMENT OF ANALYTICAL PREDICTIONS

6.2.3.1 New Fatigue Crack-Growth-Rate Equation for Negative Stress Ratios

The fatigue crack-growth-rate equation for negative stress ratios ($R < 0$) used in the blind predictions presented in the preceding section is expressed as follows:

$$da/dN = C [(1-R)^q K_{max}]^n$$

where q is the acceleration index for a specific negative stress ratio and C and n are the crack growth rate constants obtained from the $R \geq 0$ test data.

The value of q is determined by the following relationship proposed by Chang:

$$q = [\ln(r)/\ln(1-R)]/n$$

where r is the ratio of the crack growth rate at a specific negative stress ratio to its $R = 0$ counterpart measured from tests.

For the load-interaction solution, the fatigue crack-growth-rate equation as shown previously is used in conjunction with the Willenborg retardation model in CRKGRO when the calculated effective stress ratio is negative. The stress ratio R is then replaced by the effective stress ratio, R_{eff} , which becomes:

$$da/dN = C [(1-R_{eff})^q K_{max_eff}]^n$$

Because R_{eff} varies from one cycle to another cycle in random spectrum loadings for a given material, a set of q -values is needed in order to accurately determinate the fatigue crack growth rates. To generate a set of q -values for a wide negative stress ratio range requires extensive experimental data. Therefore, to be practical, an "average q -value" approach was employed in the fatigue crack growth correlations conducted previously. This is to apply a single q -value for a certain negative stress ratio range in the Chang equation in obtaining an average negative stress ratio effect to the fatigue crack growth behavior in that specific negative stress ratio range. For 2219-T851 aluminum, the average q -value chosen in the analytical predictions for the negative stress ratio range from $0 > R_{eff} \geq -0.99$ was 0.3.

The Walker equation used in CRKGRO for positive stress ratios is formulated in terms of ΔK as follows:

$$da/dN = C [\Delta K / (1-R)^{1-m}]^n$$

where m is the Walker stress ratio collapsing factor for positive stress ratios.

Converting ΔK to $(1-R)K_{max}$, it becomes:

$$da/dN = C [(1-R)^m K_{max}]^n$$

Notice that the Walker equation and the Chang equation for negative stress ratio are identical in mathematical form. Yet, the exponent in the Walker equation is determined in a different way, as described in Reference 54.

To avoid the confusion in the usage of these two equations, a new fatigue crack-growth-rate equation for negative stress ratios has been formulated by Chang ⁽⁵⁸⁾. This new equation is expressed as:

$$da/dN = C [(1+R^2)^q K_{max}]^n$$

where the constants C and n are the same crack-growth-rate constants obtained from the $R \geq 0$ test data as they were required in the fatigue crack-growth-rate equation.

The value of q in the preceding equation can be determined using a relationship similar to Chang's equation; i.e.,

$$q = [\ln(r)/\ln(1+R^2)]/n$$

where r is the ratio of the crack growth rate at a specified negative stress ratio to its $R = 0$ counterpart obtained from experimental test data.

This new equation has been incorporated into the CRKGRO program. Again, for the spectrum load application, the average q-value approach was adopted. For 2419-T851 aluminum in the negative stress ratio range from $0 \leq R_{eff} \leq -0.75$, $q = 1$ was found to be a good number.

To assess the predictive accuracy for employing this new rate equation in the crack growth analysis, correlations on all the 33 fighter spectrum tests were conducted. This was done by running CRKGRO with the following set of rate constants. Notice that except for the q value, the remainder of the constants and parameters were identical to those used in the "blind predictions".

C	= 5.066×10^{-10} (in ksi unit)	q	= 1.0
n	= 3.83	R_{cut}^+	= 0.75
m	= 0.6	R_{cut}^-	= -0.75
ΔK_{th0}	= 2.5 ksi $\sqrt{\text{in.}}$	K_c	= 65 ksi $\sqrt{\text{in.}}$
R_{so}	= 3.0	σ_{ty}	= 48 ksi

As before, all the random flight spectra were range-pair counted before the performance of the crack growth analysis. Spectra longer than 3,000 cycles were counted sequentially at 500 cycles per segment.

The ratio of the predicted crack growth life to the test crack growth life, N_p/N_T , was calculated for each test case of the fighter spectrum group and presented in Table 78. For comparison, N_p/N_T ratios obtained using the old equation were also presented in this table. Results showed that these two sets of predictions were almost identical. The average ratio for the predictions using the new equation is 0.87 with a 0.17 standard deviation, while the predictions using the old equation are 0.88 with a 0.17 standard deviation. Figure 70 shows the plot of the predicted lives versus the test lives from the 33 test cases.

For further comparison, histograms of these two sets of prediction results were constructed as shown in Figure 71. These two histograms almost completely overlapped, which indicates the similarity of the two negative stress ratio rate equations. The histogram of the result of predictions without considering the load interaction was also plotted in Figure 71 for the sake of comparison.

Analytical predictions on the eight transport spectrum cases were also obtained by rerunning the CRKGRO program with the new rate equation, with $q = 1.0$. As before, all the flight spectra were range-pair counted before performing the crack growth analysis. The ratio of the predicted crack growth life to the test crack growth life was again calculated for each test case of the transport spectrum group. Table 78 summarizes the result of the comparison for the analytical predictions using the new equation and the old equation. The average N_p/N_T ratio was 0.78 with a 0.43 standard deviation.

6.2.3.2 Change of Crack-Growth-Rate Parameters

From the results of the transport spectrum test data correlations shown in Table 79, the predictions seemed somewhat overconservative. Hence, efforts have been devoted to investigating the sensitivities of the crack growth parameters for 2219-T851 aluminum used in the analysis. The negative stress ratio cutoff value, R_{cut}^- was the first to be investigated. In the previous analytical predictions, R_{cut}^- was selected to be -0.75, based on the assumption that for this material under the fully revised cyclic loading condition; i.e., $R = -1$, the overload retardation effect will be reduced to only 25 percent by the compressive load immediately followed. This high percentage reduction was not based on solid test data. Hence, the value is rather questionable. For fighter spectrum cases, because the tension-compression cycles are not the predominant damage cycles, the use of inaccurate R_{cut}^- in the analysis did not affect the predictive accuracies.

Yet, for transport spectrum cases, the G-A-G cycle of each flight contributed 60 percent of the damage as shown in Table 79. Consequently, bigger errors were most likely introduced to the analytical predictions by using the purely assumed R_{cut} value. To investigate this effect, a study of the R_{cut} to the predictive accuracy was thus conducted. Data employed in this sensitivity study were two transport spectrum test data which were related to the increasing of the compressive load levels (tests T-B-V-4 and T-B-V-5) and the fighter composite baseline test F-B-4. Values of the negative stress ratio cutoff used in this study were $R_{cut} = -0.75$, -0.50 , and -0.25 . Results of the study (Table 80) showed that for transport cases, the predicted lives increased by a bigger factor when the value of the R_{cut} changed from -0.75 to -0.25 . In T-B-V-4, for example, the prediction ratios changed from $N_p/N_T = 0.53$ to 1.10 when R_{cut} changed from -0.75 to -0.5 . For the fighter case, the predicted lives virtually did not change.

From this study, it was decided to select $R_{cut} = -0.5$ for use in the second round of predictions for all 33 fighter test cases and the eight transport test cases. The rest of the crack growth constants and parameters were kept unchanged. Analytical predictions were again correlated with test data. The correlation results are summarized in Table 81 for fighter cases and in Table 82 for transport cases. For the 33 fighter spectrum cases, there were only slight changes in the predicted lives. The average prediction of the second round is 0.88 , with a 0.17 standard deviation. Compared to the blind predictions, only 1 percent difference in the average prediction ratio is shown. For the eight transport spectrum cases, the improvement in the life predictions definitely showed up. The average prediction ratio changed from $N_p/N_T = 0.78$, with a 0.43 standard deviation, to $N_p/N_T = 1.05$, with a 0.35 standard deviation. When all 41 test cases are combined, the average CRKGRO prediction ratio is $N_p/N_T = 0.92$ with an 0.22 standard deviation, which is well within the needed prediction accuracy for damage-tolerance analysis. Figure 71 shows the correlation results of all 41 test cases. A histogram of these 41 correlation cases is shown in Figure 72.

7.0 CONCLUSION AND RECOMMENDATION

7.1 CONCLUSIONS

From results of the experimental verification task and other technical evaluations performed in this research program, the following conclusions have been reached:

1. For the performance of analytical predictions of the fatigue crack-growth behavior and life, it is necessary to account for the spectrum loading effects in order to obtain more accurate results.
2. Although the tensile overload retardation is the most significant effect which occurs during flight spectrum loadings, the compressive load acceleration effect is also significant. The compressive load acceleration effect and the tensile overload retardation effect tend to cancel each other in a random cycle-by-cycle spectrum for fighter spectra.
3. If the spectrum loading is in the random cycle-by-cycle format, it is essential to process the random spectrum through a cycle counting algorithm before performance of the crack-growth analysis.
4. The cycle-by-cycle crack-growth analysis methodology implemented in the detailed level crack-growth analysis computer code, CRKGRO, provides very good analytical predictions on crack growth lives under both fighter and transport spectrum loadings. The average predicted-life-to-the-test-life ratio for the 41 test cases was 0.92 with an 0.22 standard deviation.
5. The new rate equation for the negative stress ratios proposed by Chang(58) (i.e., $da/dN = C[(1 + R^2)^q K_{max}]^n$, $R < 0$) correlates the compressive load acceleration effects very well.
6. The spectrum characterization approach identified as Method I in this report is an attractive method used to convert the complicated and lengthy random flight spectrum into the equivalent constant-amplitude loadings. This method can also be used in the ranking of spectrum severity in the spectrum variation study.
7. The flight-by-flight crack-growth analysis methodology implemented into the FLTGRO program for the use of individual aircraft tracking provides very good predictions on most of the test cases conducted in this program. This indicates the potential use of this methodology on fatigue crack life predictions. It is felt that this

methodology eventually can be used for the detailed level crack-growth analysis required in the damage-tolerance control for the benefit of cost savings.

8. An efficient computerized scheme implemented into the current STEP program provides a means for including impact of damage-tolerant requirements early in the preliminary design stage where configuration concept, construction, and material selection trades are made. The approach which accounts for load interaction effects ensures that excessive penalties are not imposed due to the omission of overload retardation effects. Conversely, by accounting for acceleration effects, unrealistic optimism can be avoided.

7.2 RECOMMENDATIONS

Based on results of this program, the following items have been identified as recommended future efforts directed toward validation of the crack-growth prediction methods developed in this program and extension of the use of these methods to the "small cracks" for the durability analysis to meet the requirement of MIL-A-8866B⁽⁵⁰⁾.

1. The load interaction model developed in this program which was subsequently implemented in the crack-growth analysis computer codes, including CRKGRO, FLTGRO, and APAS IV, has been demonstrated, from the results of the experimental verification program, to be a very good engineering model. However, it was verified with only one material; namely, 2219-T851 aluminum. Even though the generalized Willenborg model has been used extensively for various airframe materials throughout the aircraft industry, the coupling effect of the combination of the generalized Willenborg model and the Chang acceleration scheme is worth investigating for other commonly used materials. A test program which consists of the following materials is worth consideration. Identical fighter and transport baseline spectra are recommended for use in the test program. A typical bomber spectrum such as the random flight spectrum of the B-1 strategic bomber is recommended to be added in the test program:
 - a. Aluminum alloy - 7075-T7351 or 7075-T7651
 - b. Titanium alloy - Ti-6Al-4V recrystallized, annealed
 - c. Steel alloy - HP 9Ni-400-C.2C

2. The initial sizes of all CCT test specimens conducted in the experimental verification test program were in the neighborhood of 0.25 inch. This is because, according to the test plan, all test specimens were planned to be tested to failure. Therefore, in order to avoid excessive test time, a through-the-thickness crack with an initial crack size of 0.25 inch was selected. It is anticipated that if the initial flaw inserted into each specimen were a semicircular surface flaw with a length ($2c$) equal to 0.25 inch and a depth (a) equal to a 0.125 inch as specified in MIL-A-83444A⁽⁴⁹⁾ was selected, the experimental verification result would be no surprise. However, if the initial crack size were much smaller (say, $2c$ equal to or less than 0.005 inch), it would have been with less confidence on the outcome of the experimental verification program results. This is due to the fact that the LEFM might not be applicable to characterize the crack behavior in that small crack size range. Particularly, it is because the crack-growth rate equation (the modified Walker equation) used in the CRKGRO program is not directly suitable to represent the crack-growth behavior in such a low $(1-R)^{mK_{max}}$ range. Consequently, it will not provide good analytical predictions for cracks with such a small initial size. A similar research effort such as this program is highly recommended in order to investigate the predictability of the crack-growth methodology presented in this report.

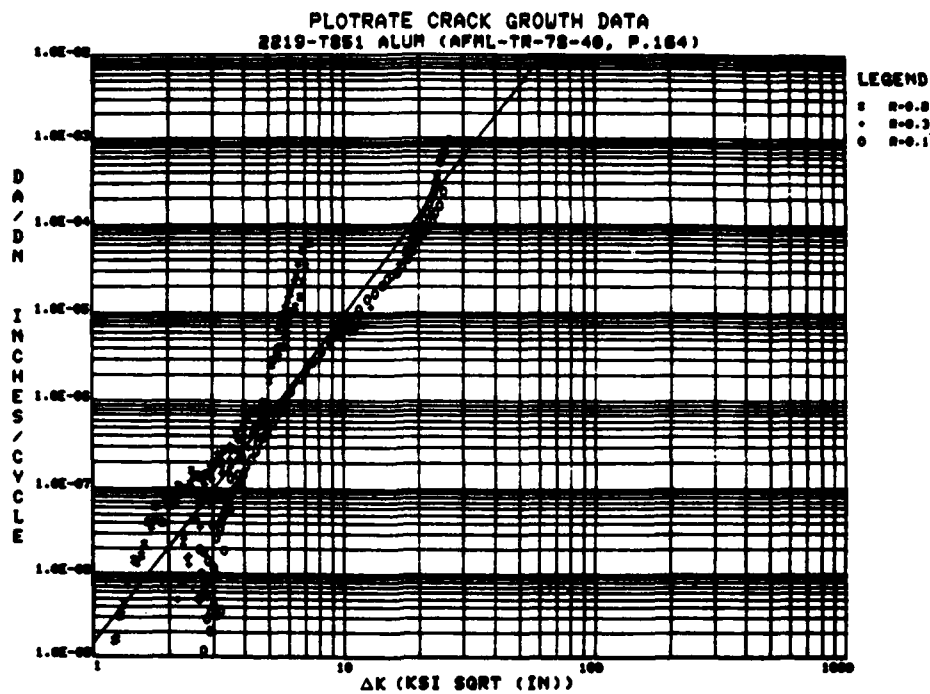


Figure 1. Wide-Range Fatigue Crack-Growth-Rate Data of 2219-T851 Aluminum Alloy at Various Stress Ratios (refer to Reference 15)

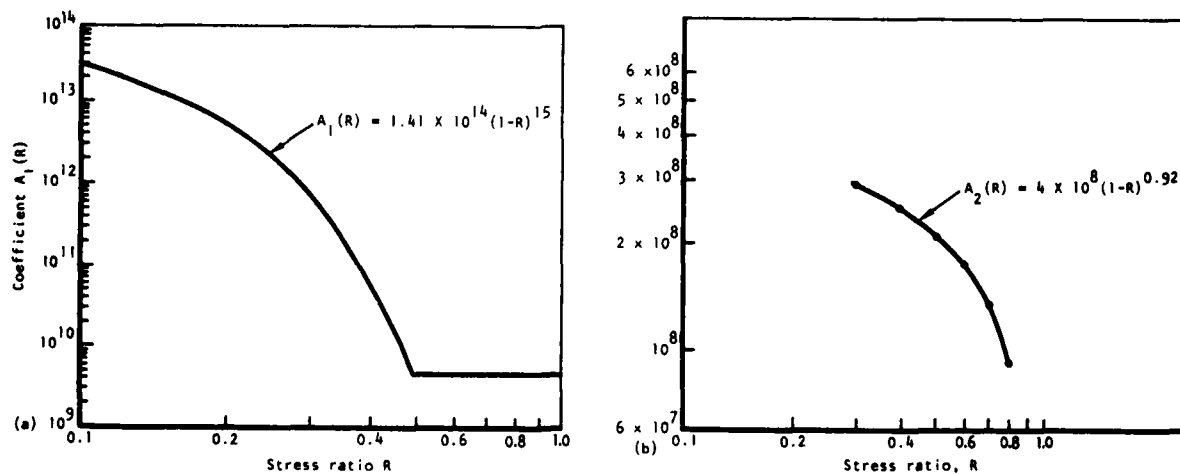


Figure 2. Coefficients $A_1(R)$ and $A_2(R)$ in the Three-Component Model for 2219-T851 Aluminum

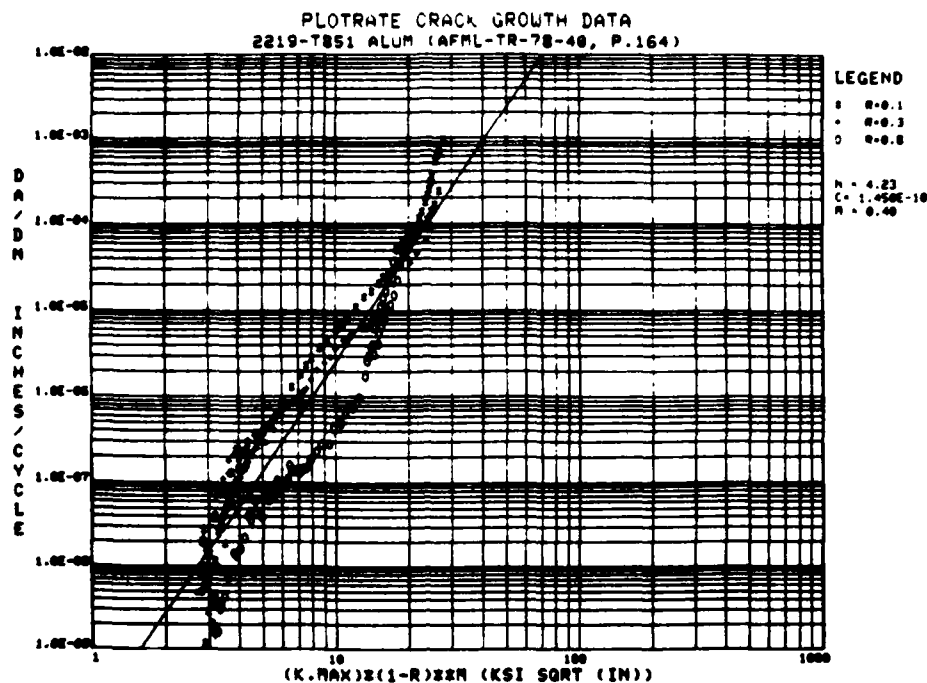


Figure 3. Wide-Range Fatigue Crack-Growth Rate Data of 2219-T851 Aluminum Alloy Plotted in da/dN Versus $(1-R)^m K_{max}$ Format for $m = 0.4$

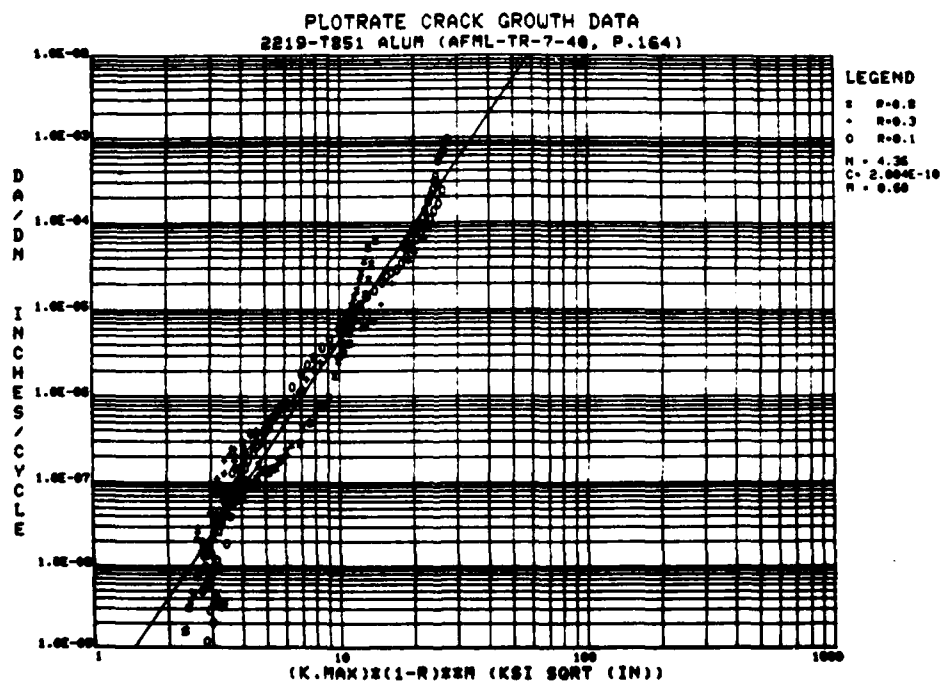


Figure 4. Wide-Range Fatigue Crack-Growth Rate Data of 2219-T851 Aluminum Alloy Plotted in da/dN Versus $(1-R)^m K_{max}$ Format for $m = 0.6$

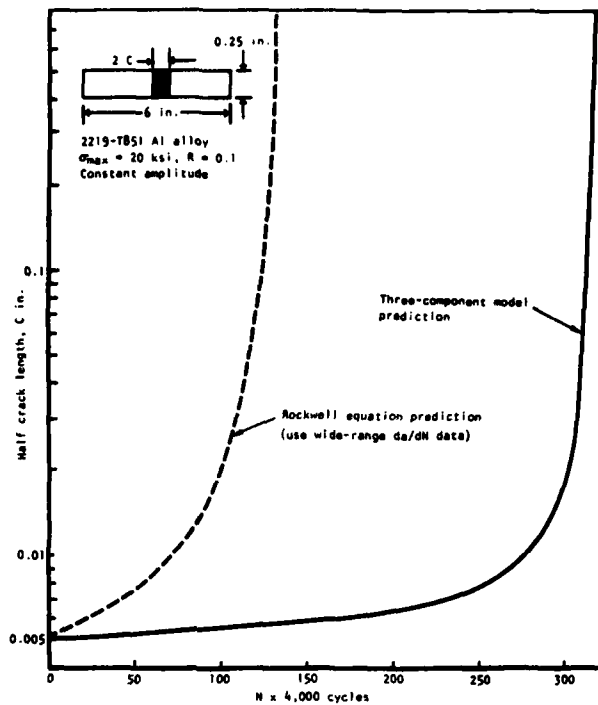


Figure 5. Comparison of Crack-Growth Behavior Predictions for Crack With Small Initial Size ($C_i = 0.005$ inches) Subjected to $\sigma_{max} = 20$ ksi, $R = 0.1$, Constant-Amplitude Loading

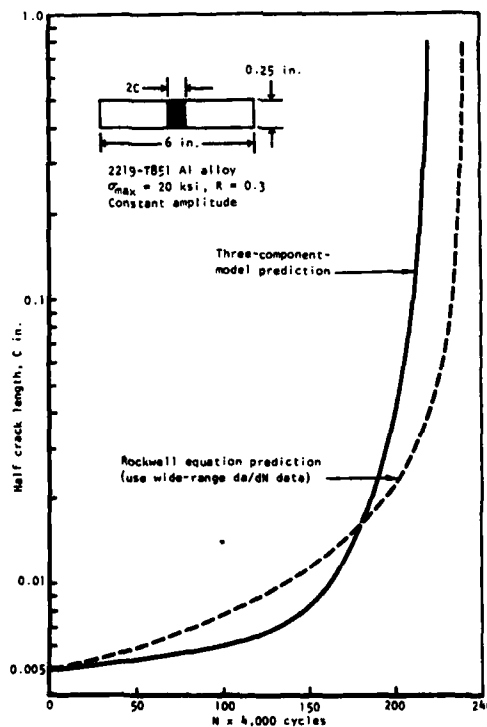


Figure 6. Comparison of Crack-Growth Behavior Predictions for Crack With Small Initial Size ($C_i = 0.005$ inches) Subjected to $\sigma_{max} = 20$ ksi, $R = 0.3$, Constant-Amplitude Loading

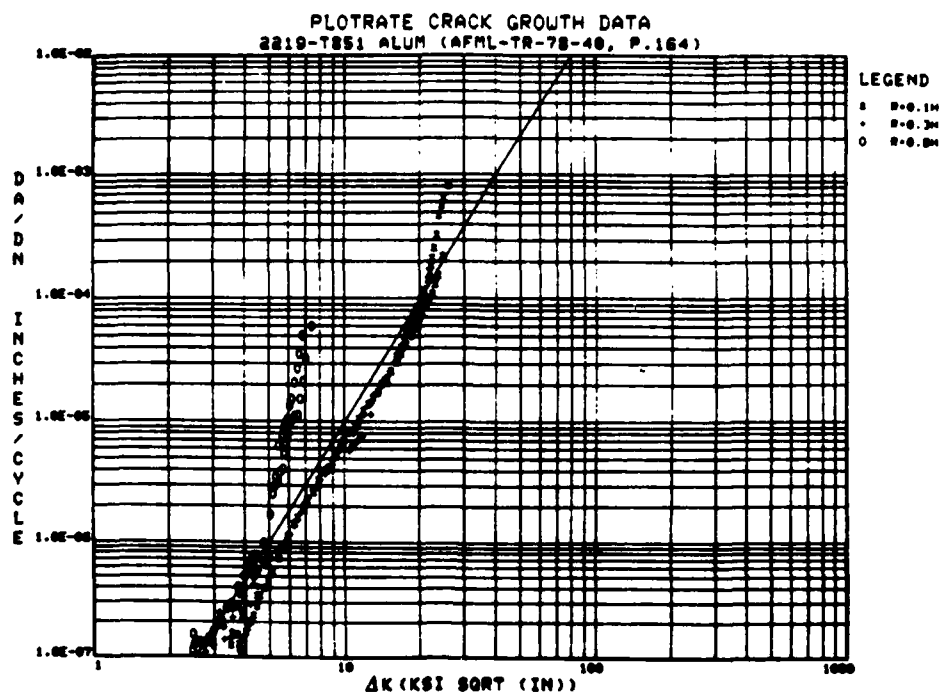


Figure 7. Fatigue Crack-Growth-Rate Data of 2219-T851 Aluminum Alloy ($da/dN \geq 10^{-7}$ inches/cycle) at Various Stress Ratios

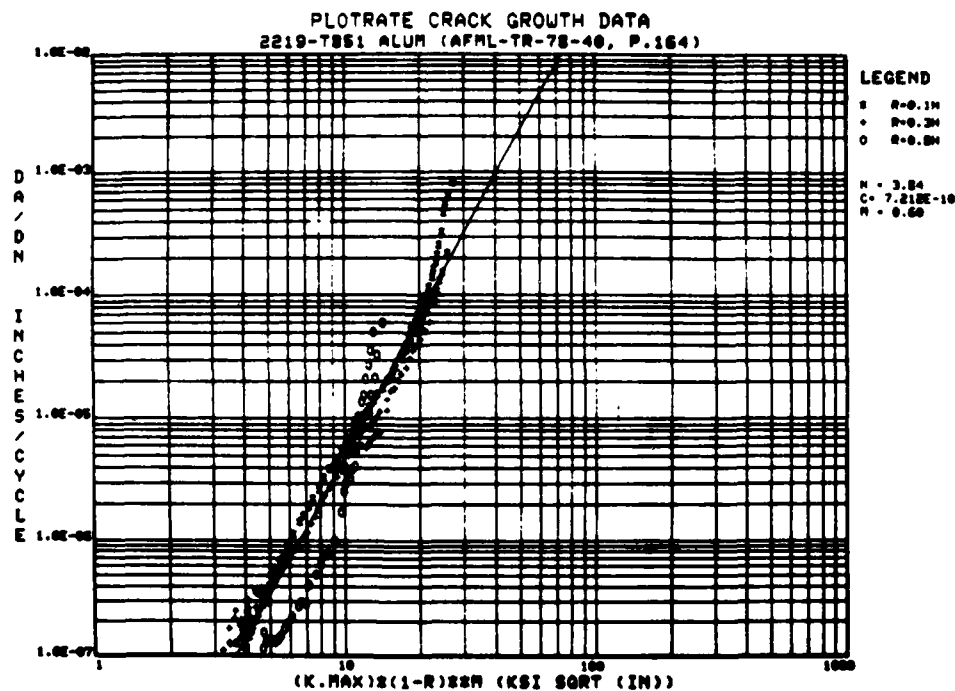


Figure 8. Fatigue Crack-Growth-Rate Data of 2219-T851 Aluminum Alloy ($da/dN \geq 10^{-7}$ inches/cycle) Plotted in da/dN Versus $(1-R)^m K_{max}$ Format for $m = 0.6$

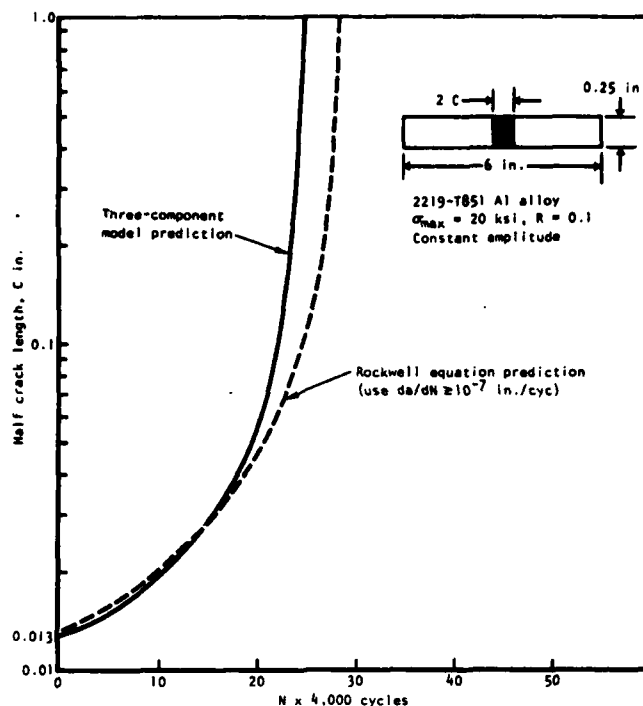


Figure 9. Comparison of Crack-Growth Behavior Predictions for a Through-Crack ($C_i = 0.013$ inches) Subjected to $\sigma_{\max} = 20$ ksi, $R = 0.1$ Constant-Amplitude Loading

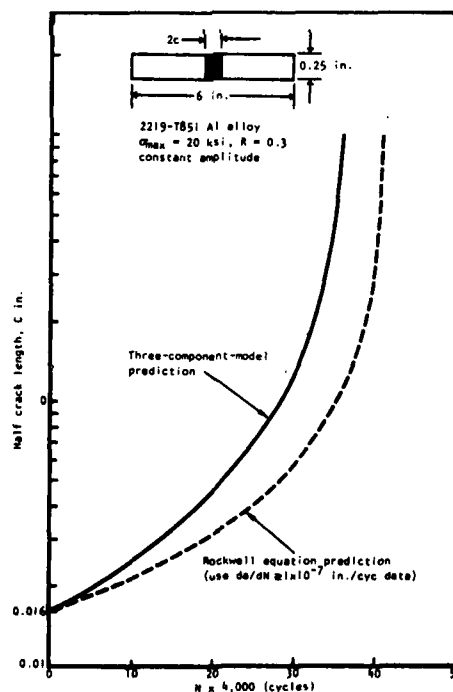


Figure 10. Comparison of Crack-Growth Behavior Predictions for a Through-Crack ($C_i = 0.016$ inches) Subjected to $\sigma_{\max} = 20$ ksi, $R = 0.3$, Constant-Amplitude Loading

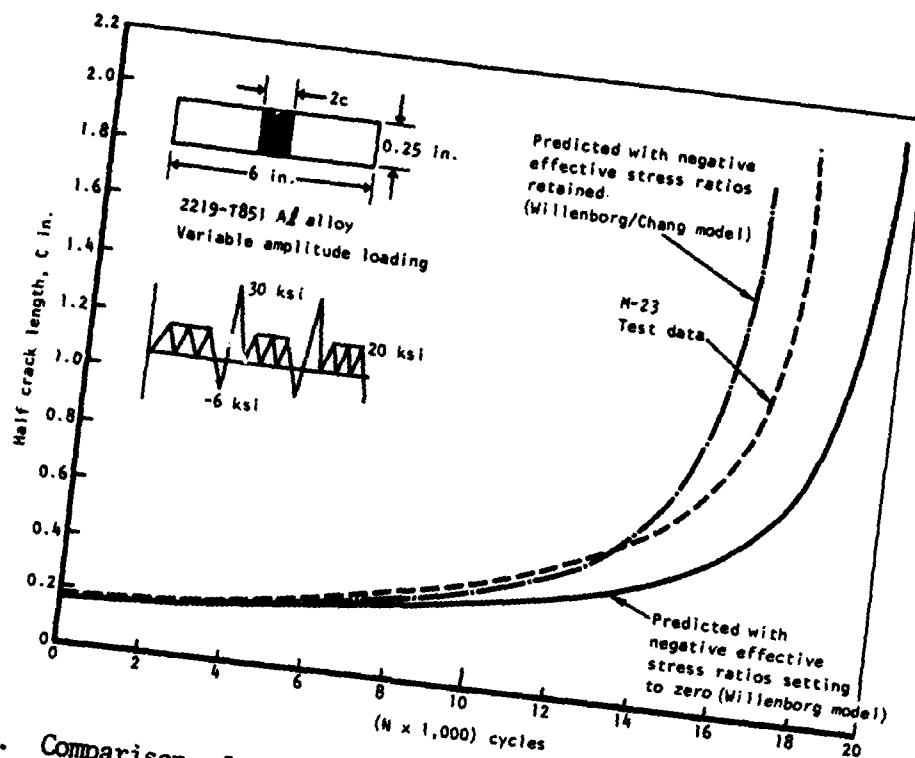


Figure 11. Comparison of Crack-Growth Behaviors Predicted by Willenborg/Chang and Willenborg Models

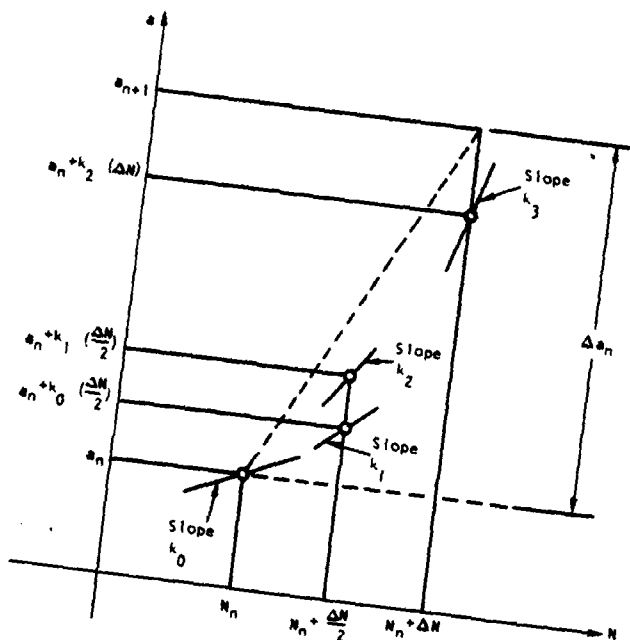


Figure 12. Four Slopes Used in Runge-Kutta Method

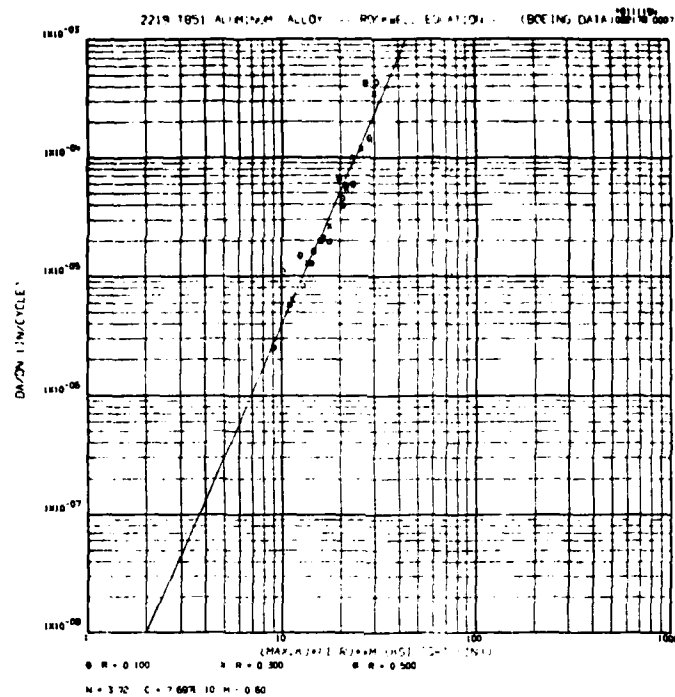


Figure 13. Boeing 2219-T851 Aluminum Baseline Crack-Growth-Rate Data Plotted in da/dN Versus $(1-R)^m K_{max}$ Format

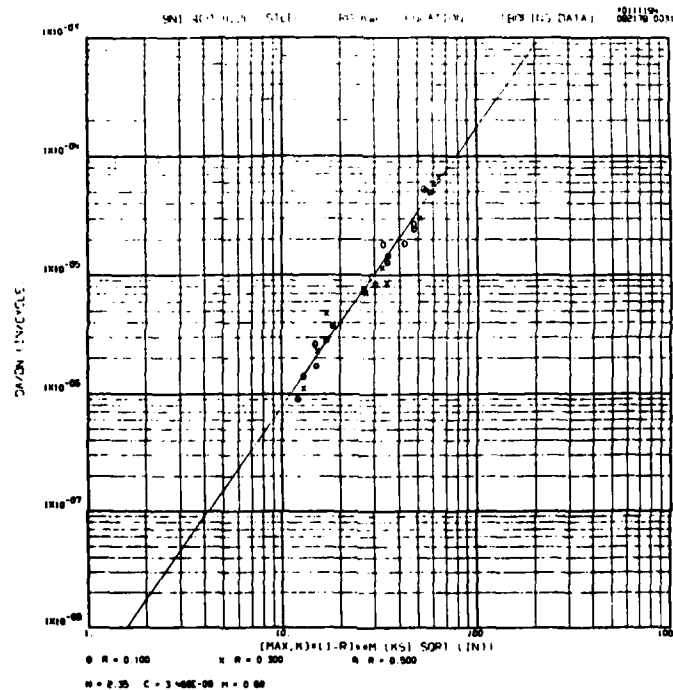


Figure 14. Boeing 9Ni-4Co-0.2C Steel Baseline Crack-Growth-Rate Data Plotted in da/dN Versus $(1-R)^m K_{max}$ Format

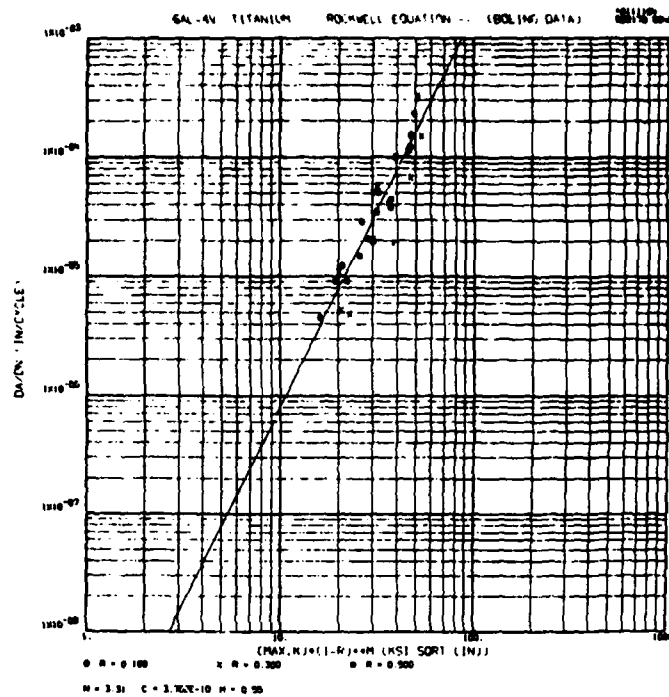


Figure 15. Boeing Ti-6Al-4V Baseline Crack-Growth-Rate Data
Plotted in da/dN Versus $(1-R)^m K_{max}$ Format

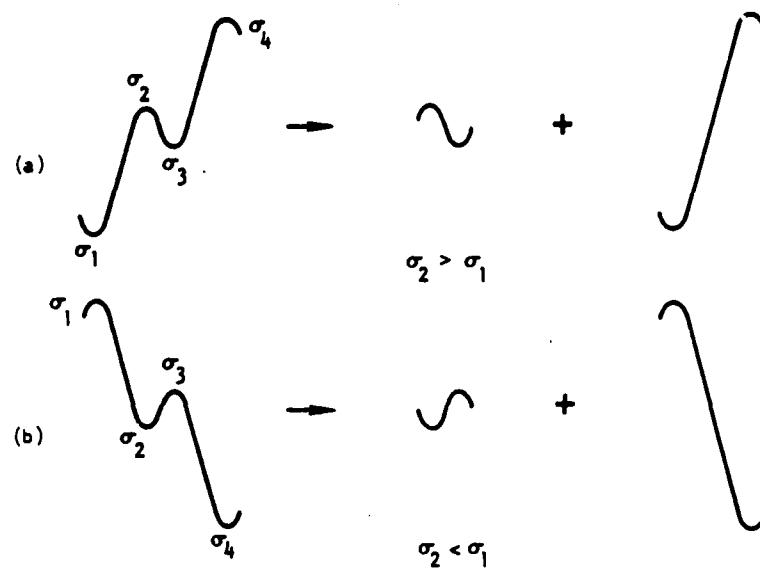
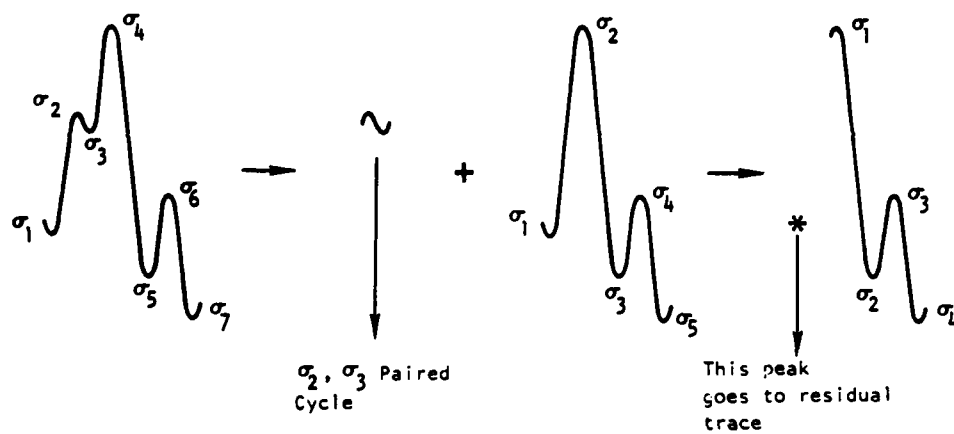
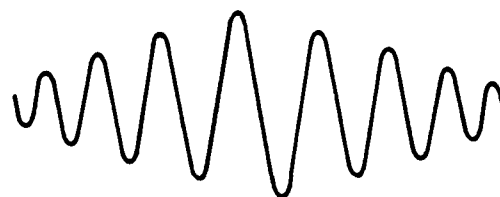


Figure 16. Range-Pair Technique of Counting Spectrum Load Cycles

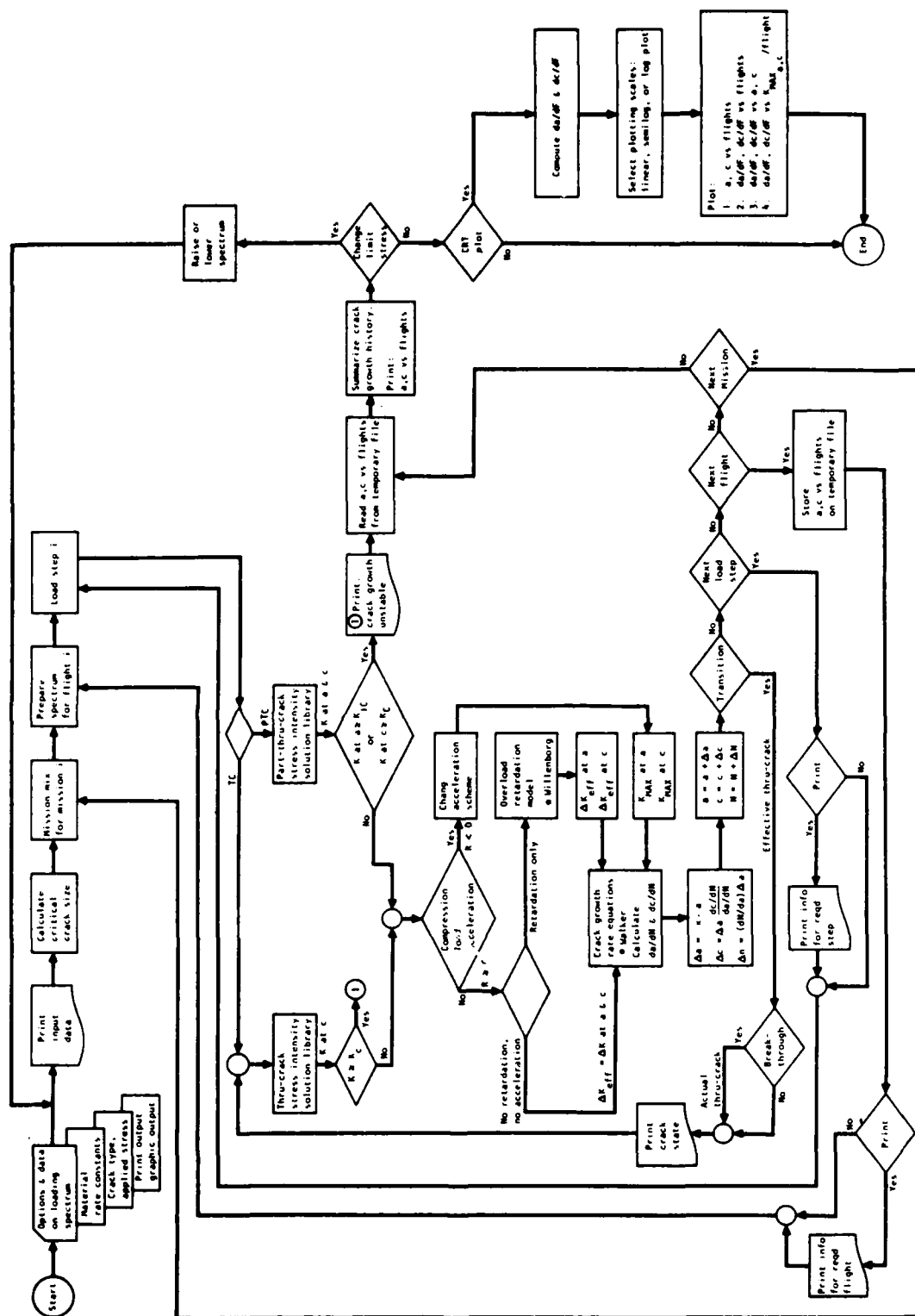


(a) Removal of nondefined cycles



(b) Final residual trace

Figure 17. Range-Pair Counting of Nondefined Load Cycles



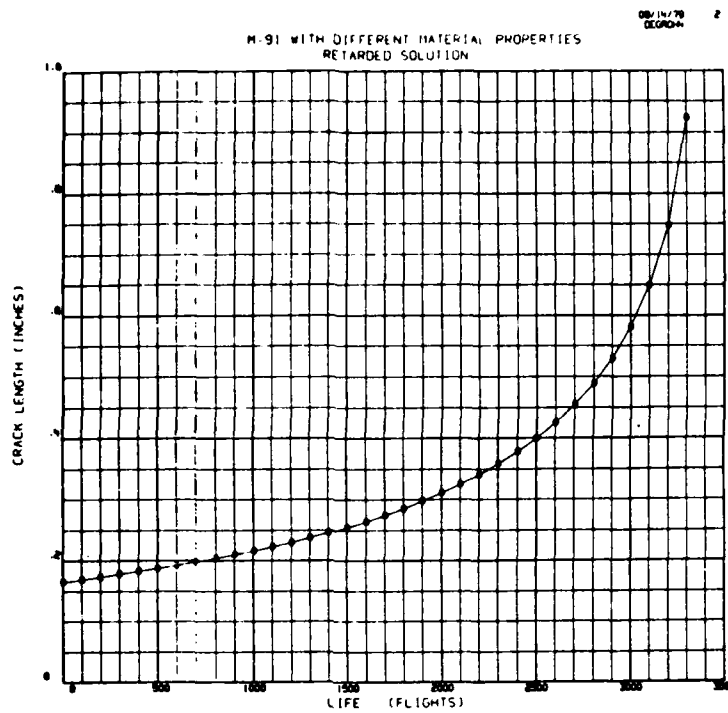


Figure 19. Sample CRKGRO CRT Plot, C Versus N

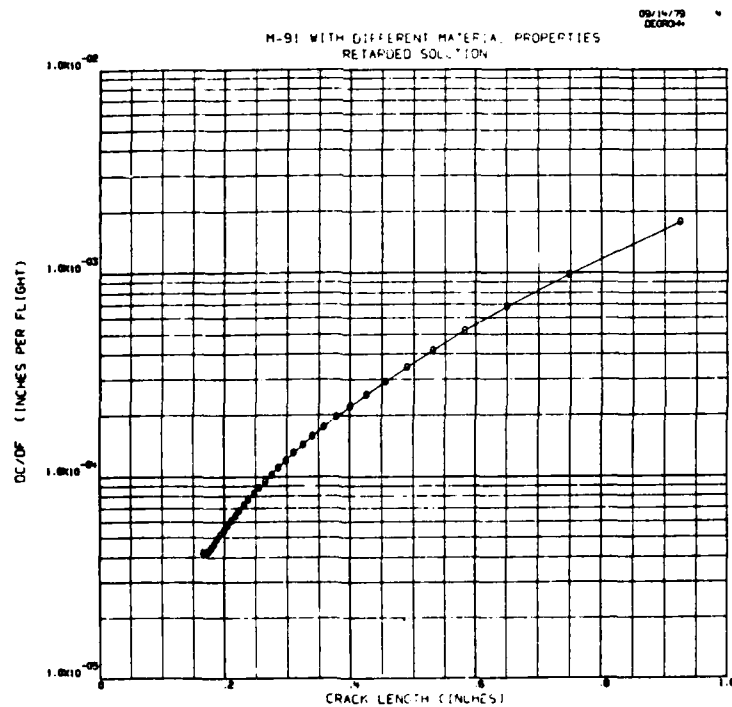


Figure 20. Sample CRKGRO CRT Plot, dc/dF Versus C

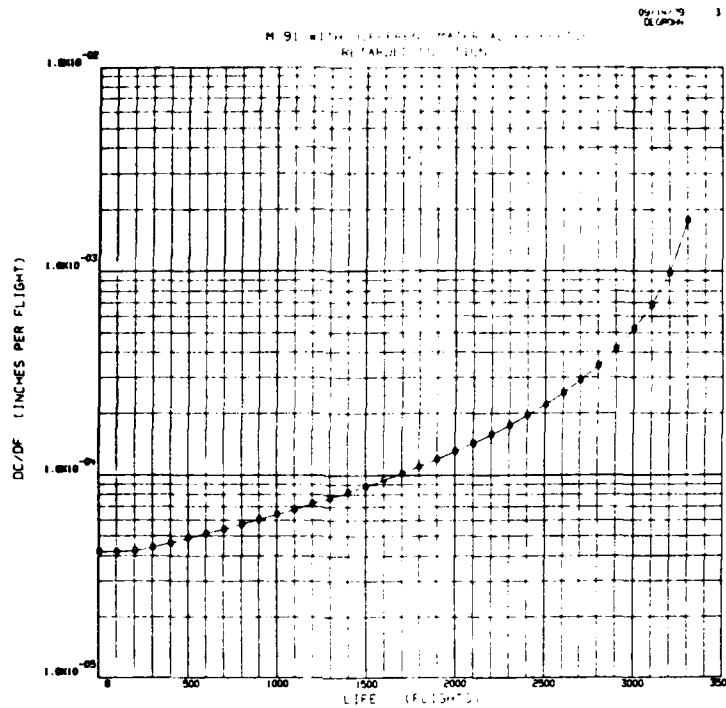


Figure 21. Sample CRKGRO CRT Plot, dc/dF Versus N

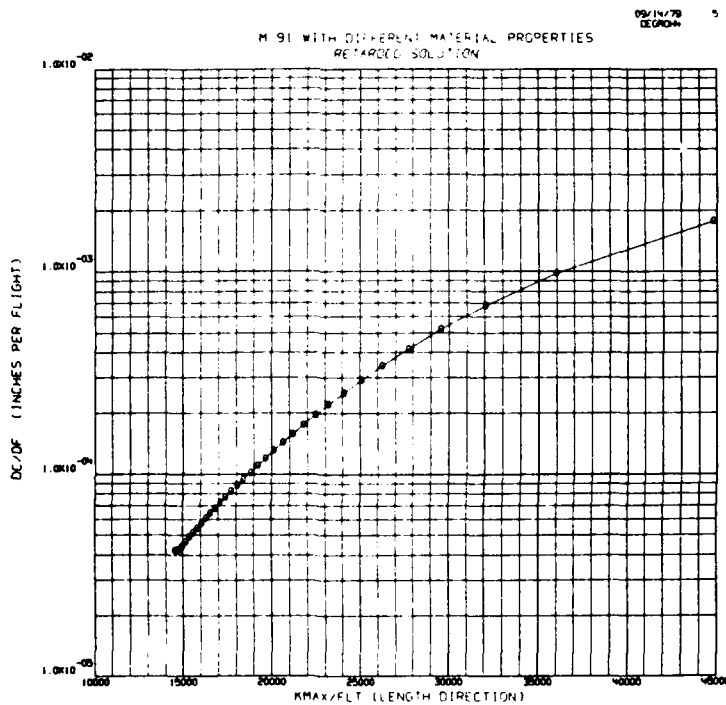


Figure 22. Sample CRKGRO CRT Plot, dc/dF Versus K_{\max}/Flight

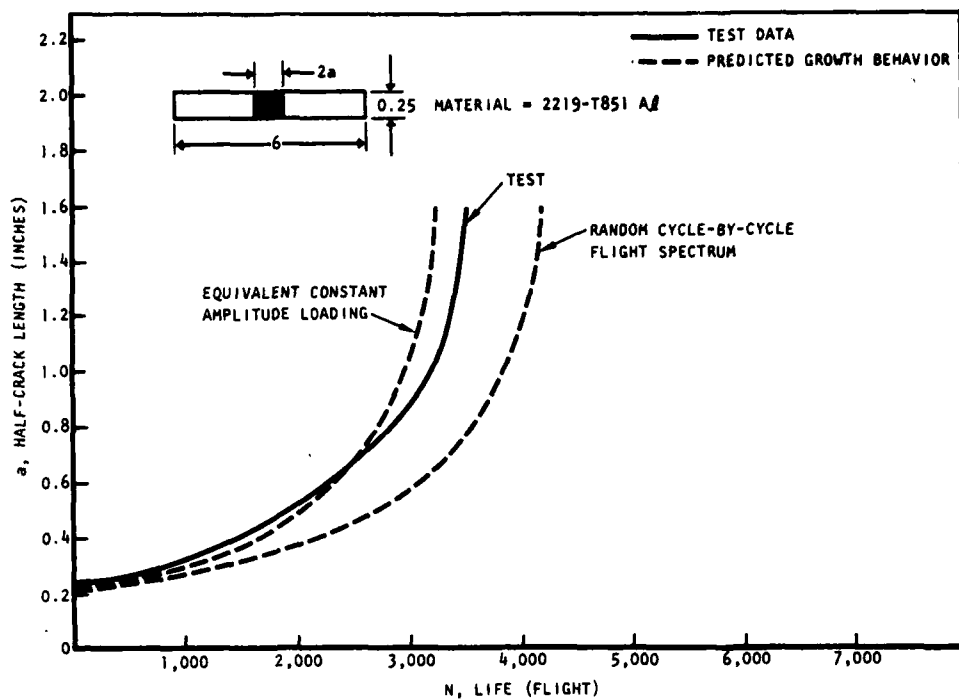


Figure 23. Comparisons of Predicted Crack-Growth Behavior Under Equivalent Constant Amplitude to Random Spectrum Load Test Data

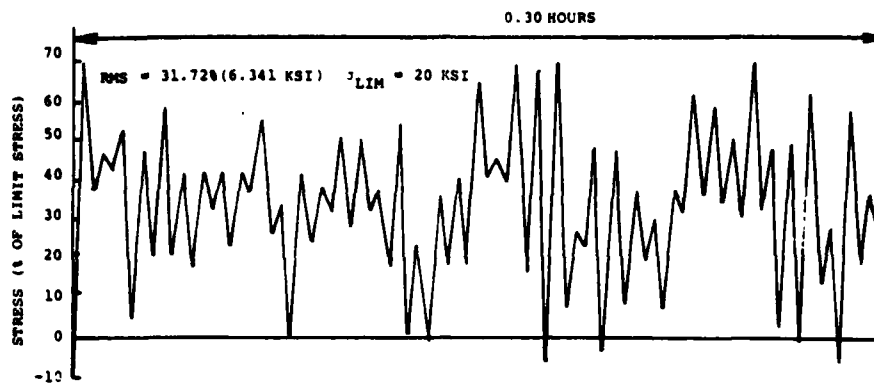


Figure 24. A Sample History of Air-to-Air Maneuver Spectra

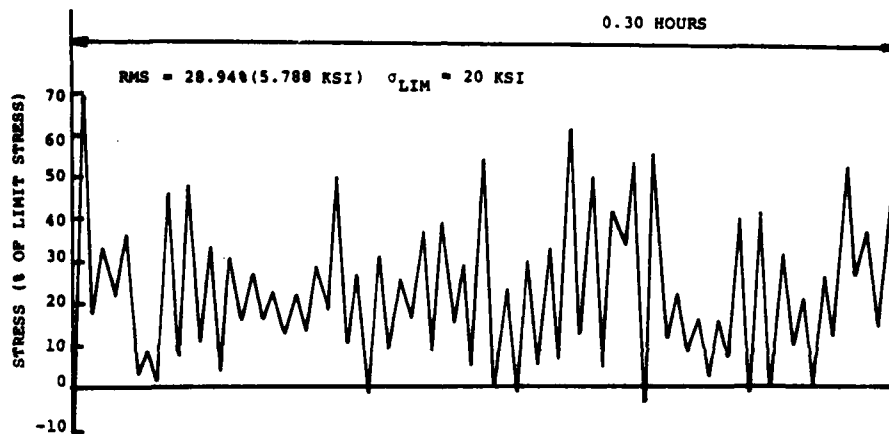


Figure 25. A Sample History of Air-to-Ground Maneuver Spectra

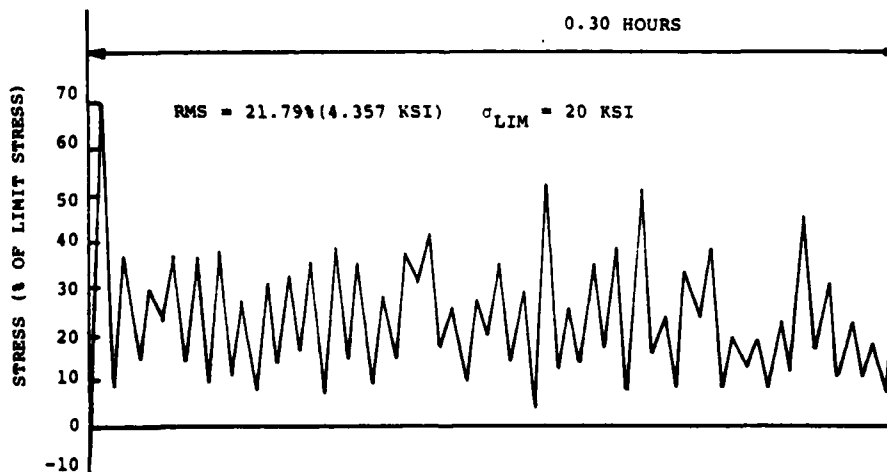


Figure 26. A Sample History of Instrumentation and Navigation Maneuver Spectra

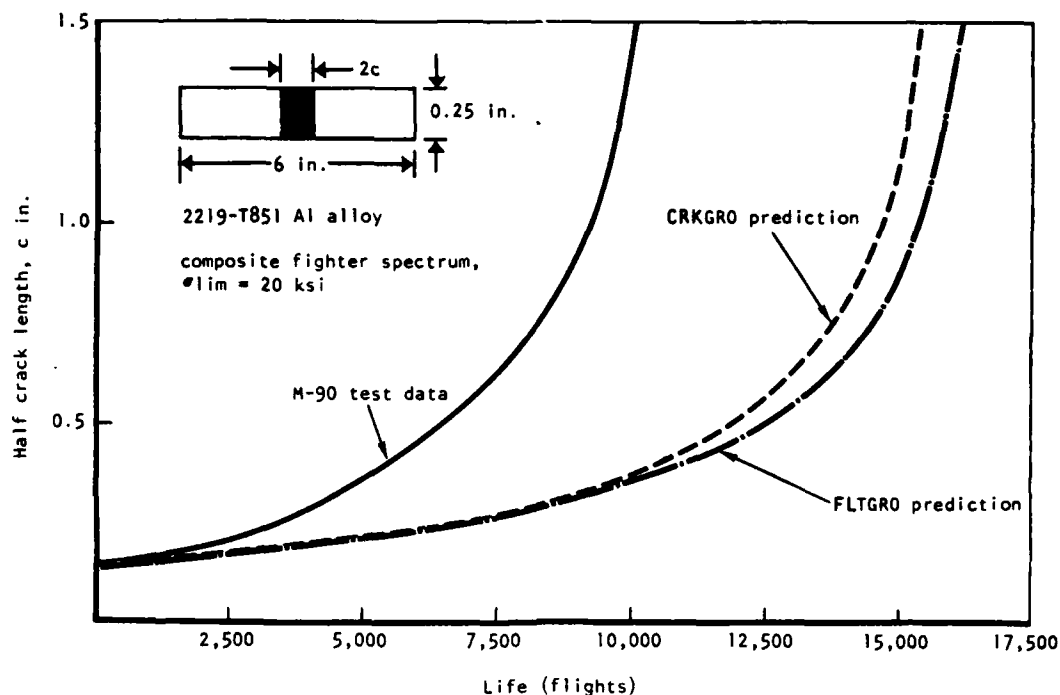


Figure 27. Comparisons of Predicted Crack-Growth Behaviors to Test Data for Center-Through Crack Subjected to A Composite Fighter Spectrum, $\sigma_{lim} = 20$ ksi

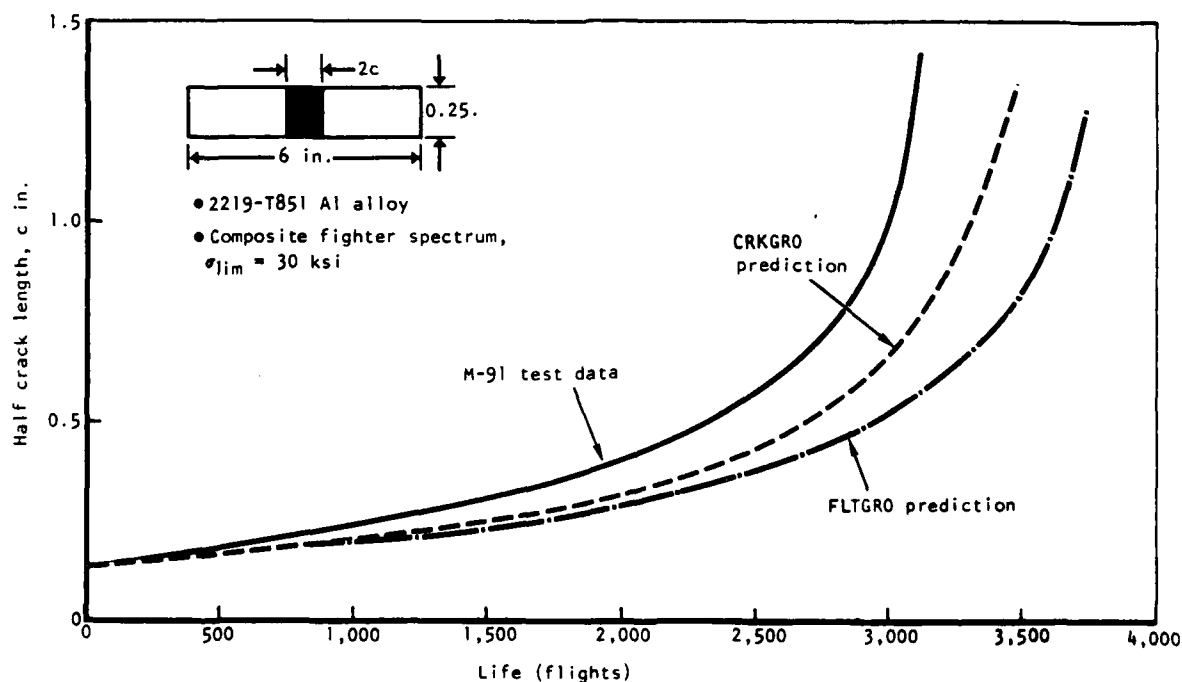


Figure 28. Comparisons of Predicted Crack-Growth Behaviors to Test Data for Center-Through Crack Subjected to A Composite Fighter Spectrum, $\sigma_{lim} = 30$ ksi

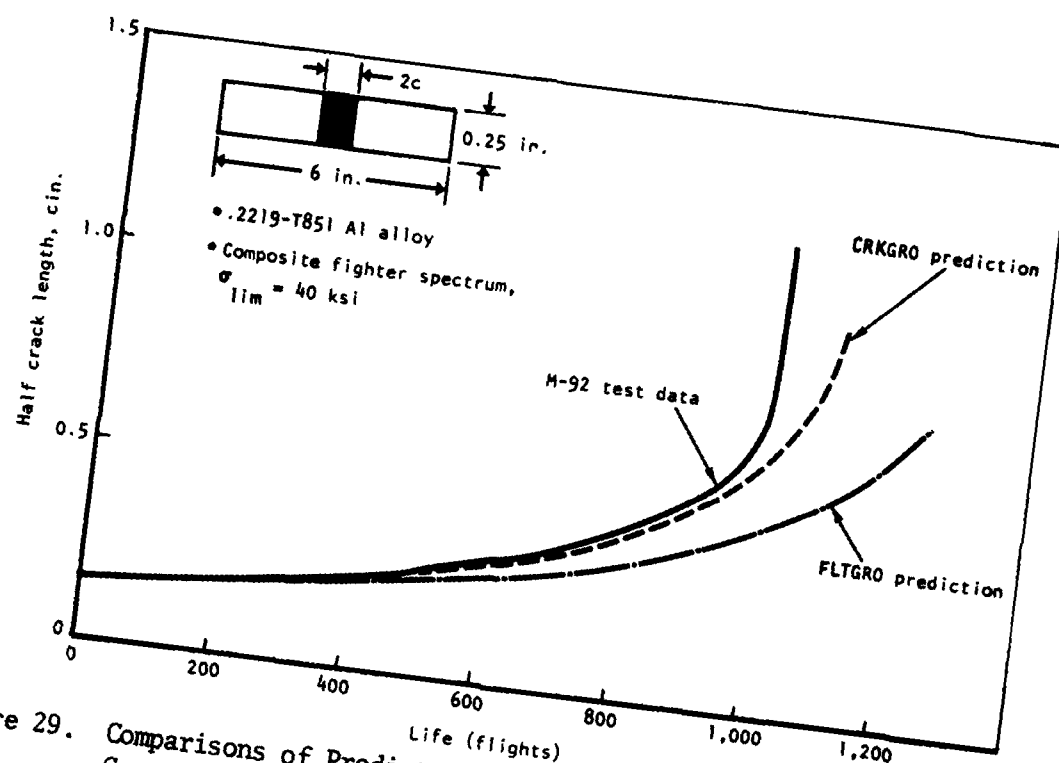


Figure 29. Comparisons of Predicted Crack-Growth Behaviors to Test Data for Center-Through Crack Subjected to a Composite Fighter Spectrum, $\sigma_{lim} = 40$ ksi

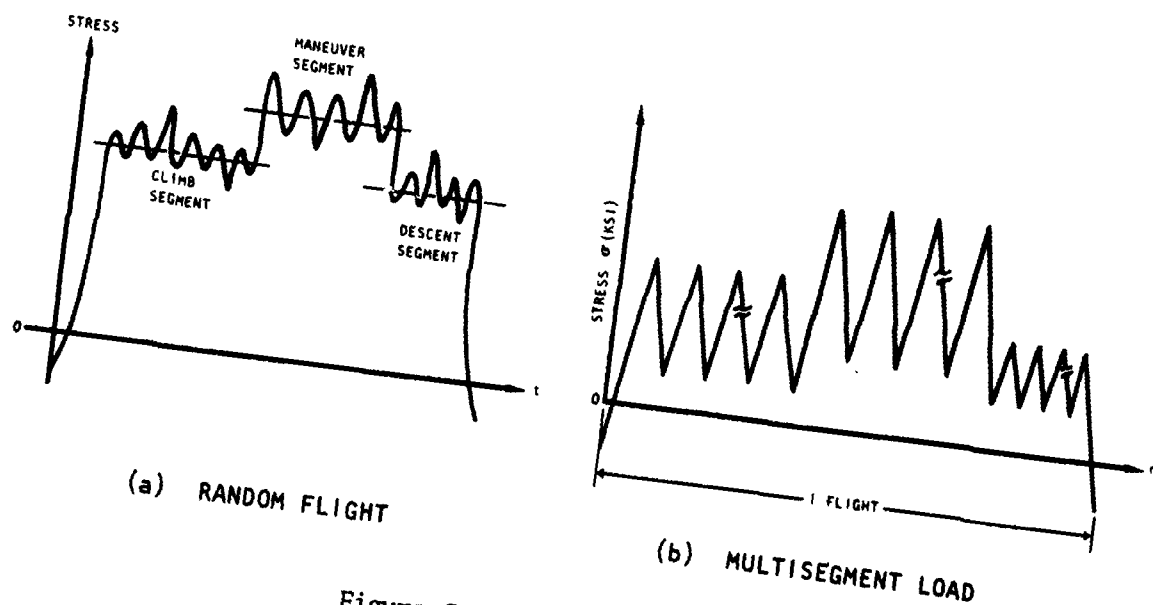


Figure 30. Spectrum Schematic

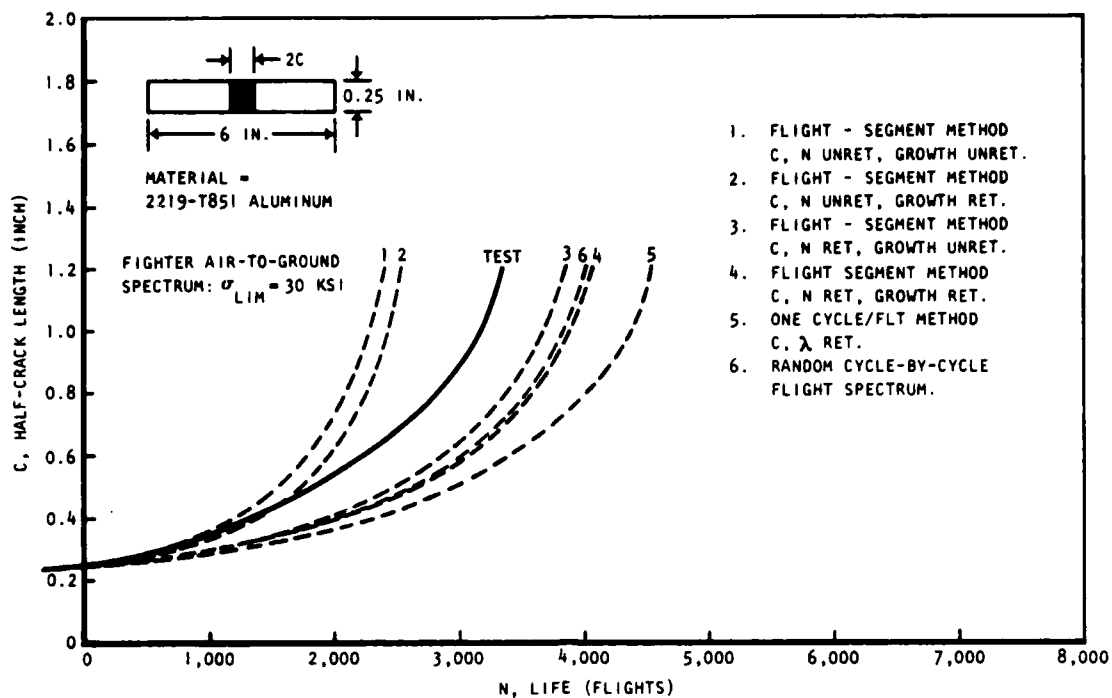


Figure 31. Comparison of Crack-Growth Predictions Using Various Approaches

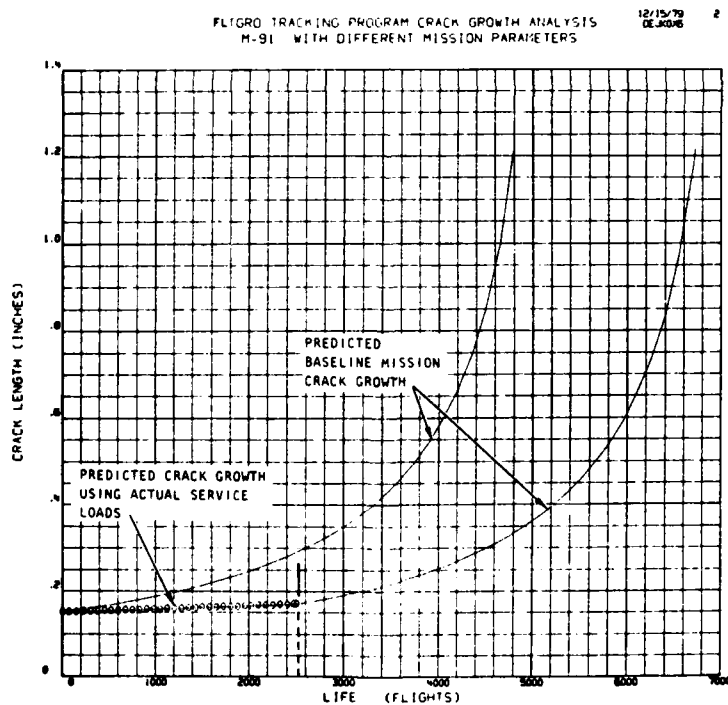


Figure 32. FLTGRO Tracking Program Crack-Growth Analysis M-91 With Different Mission Parameters

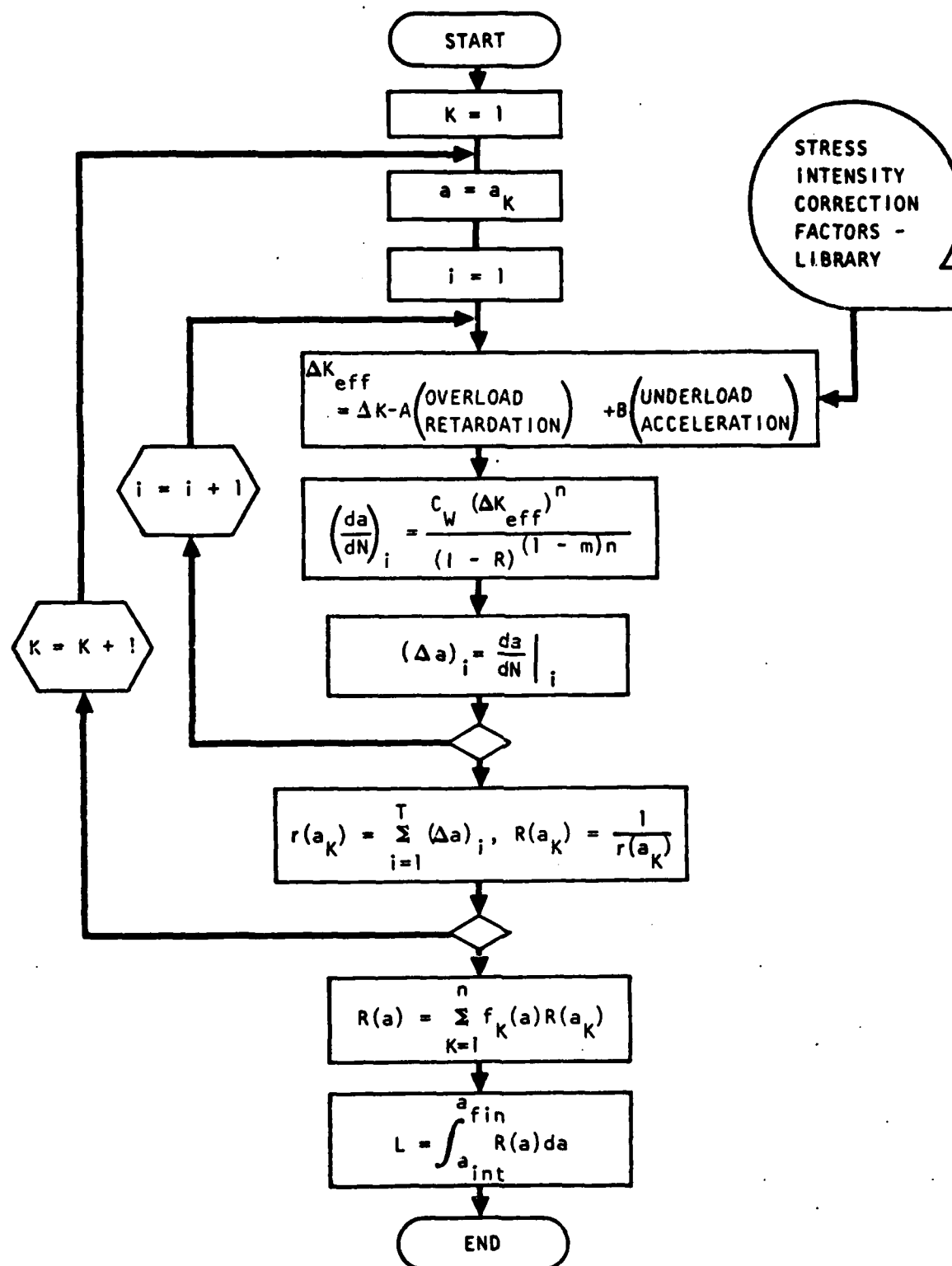


Figure 33. Program Flow Chart of PRDGRO

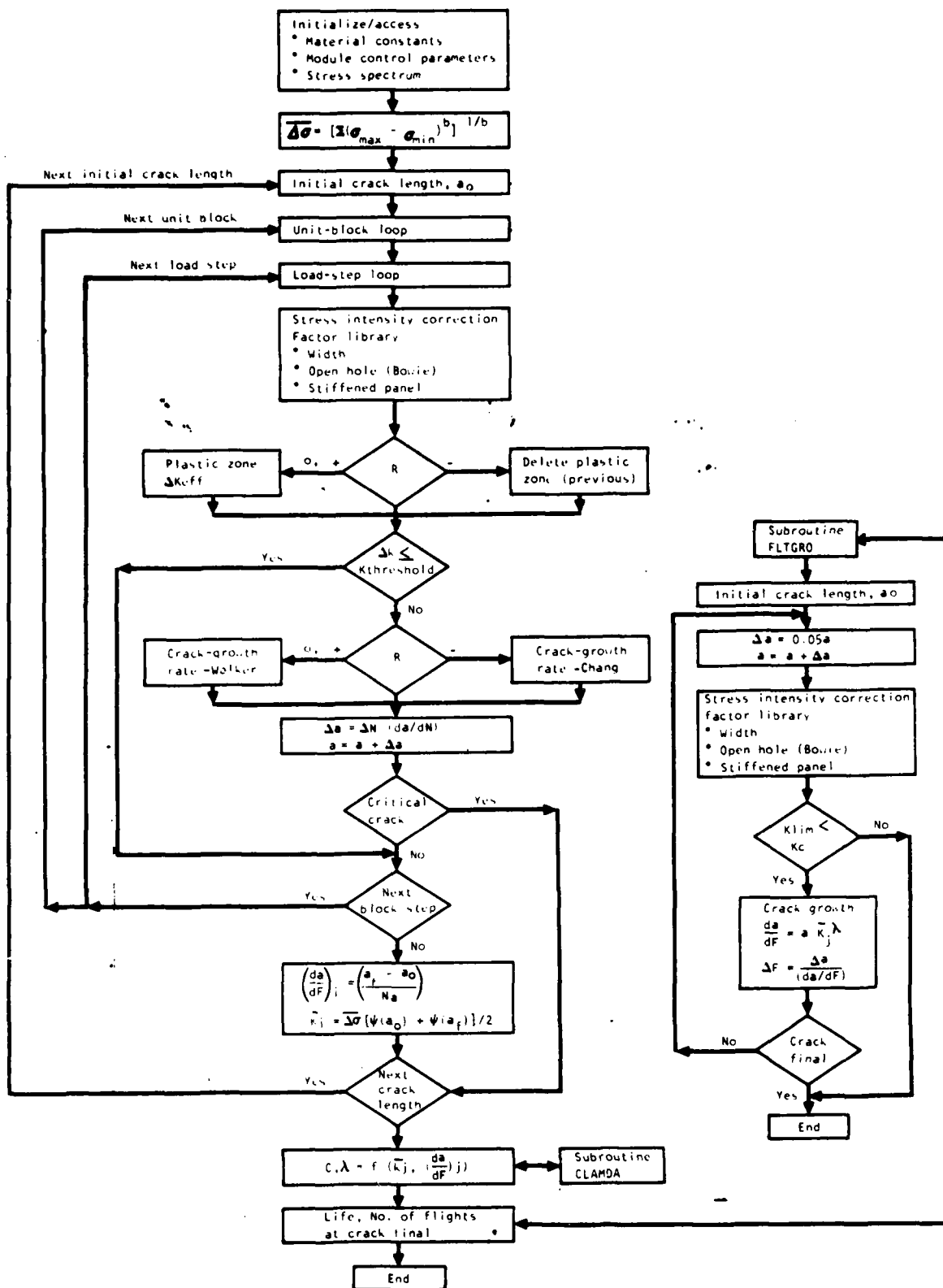


Figure 34. Program Flow Chart of PREGRO

STATION 600.00
SECTION NODAL GEOMETRY

NODE	X	Z	NODE	X	Z	NODE	X	Z
1	32.86	14.34	2	57.51	18.13	3	82.16	19.18
4	126.86	14.65	5	131.48	14.38	6	131.48	-7.19
7	126.86	-7.71	8	82.16	-8.69	9	57.51	-8.99
10	32.86	-8.99						

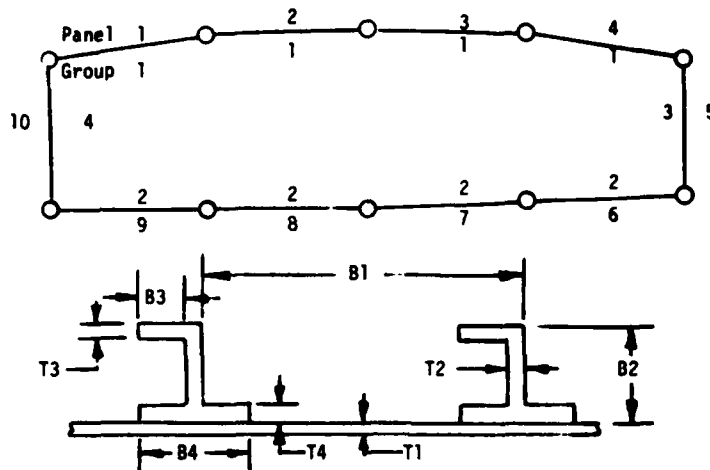


Figure 35. Sample Transport Wing Geometric Parameters

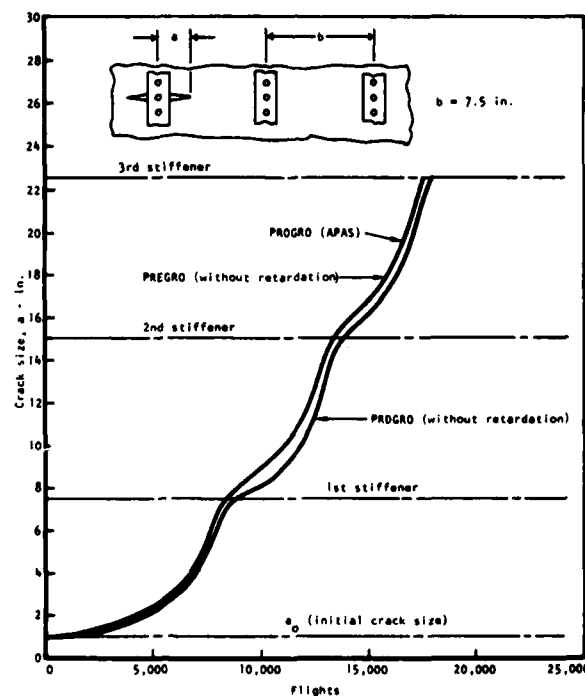


Figure 36. Crack-Growth Prediction for a Transport Spectrum Using the Different Crack-Growth Modules in APAS

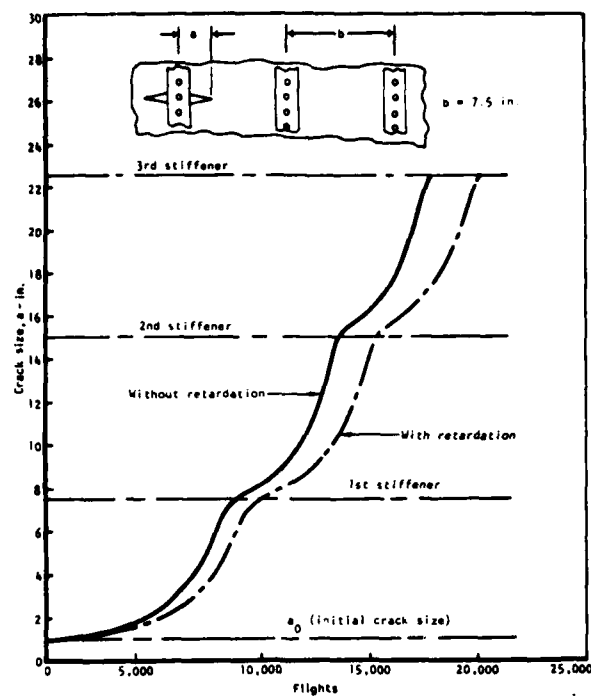


Figure 37. Crack-Growth Prediction for a Transport Spectrum Using PRDGRO

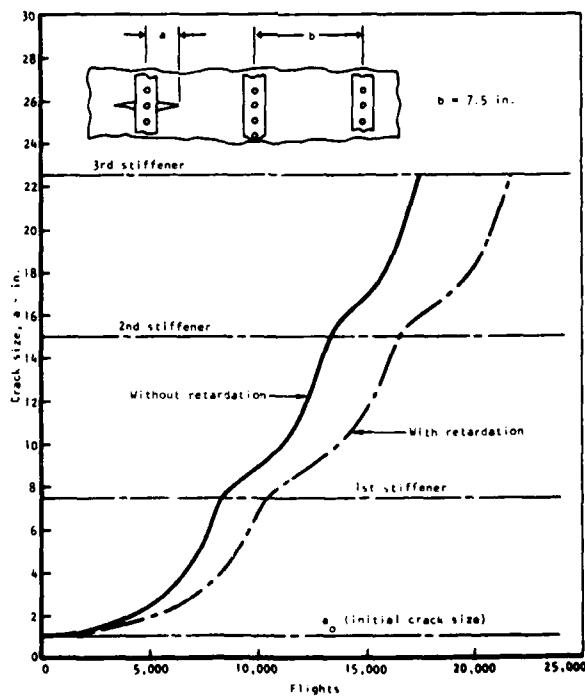


Figure 38. Crack-Growth Prediction for a Transport Spectrum Using PREGRO

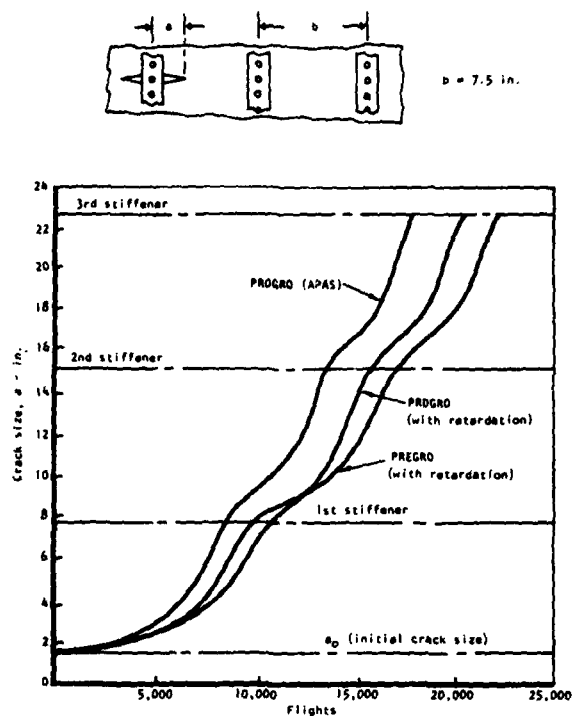


Figure 39. Crack-Growth Prediction for a Transport Spectrum, Including Overload Retardation Effects

STATION 21.64
SECTION NODAL GEOMETRY

NCODE	X	Z	NCODE	X	Z	NCODE	X	Z
1	38.48	3.94	2	61.11	4.43	3	83.74	4.20
4	129.37	3.37	5	129.00	2.11	6	129.00	-0.65
7	106.37	-1.50	8	83.74	-2.27	9	61.11	-2.66
10	38.48	-2.42						

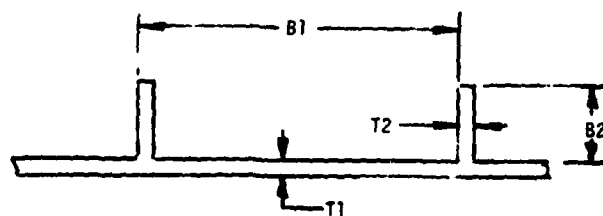
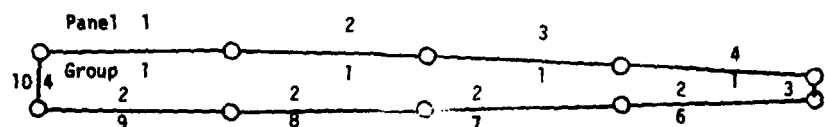


Figure 40. Sample Fighter Wing Geometric Parameters

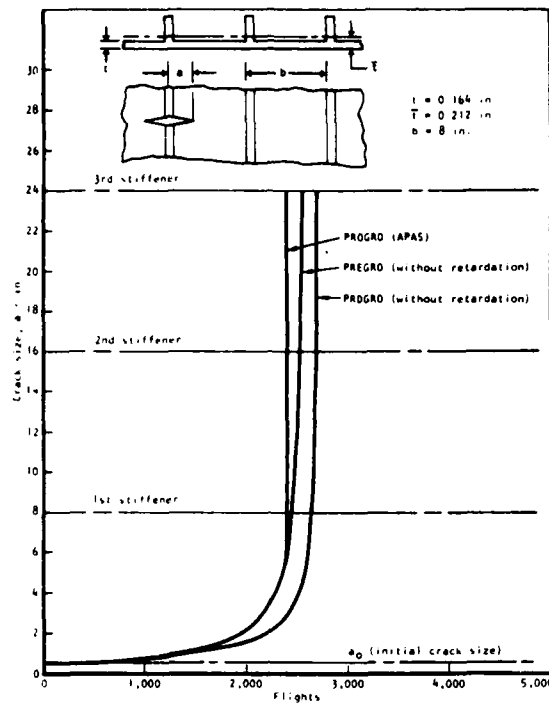


Figure 41. Crack-Growth Prediction for a Fighter Spectrum Using the Different Crack Growth Modules in APAS

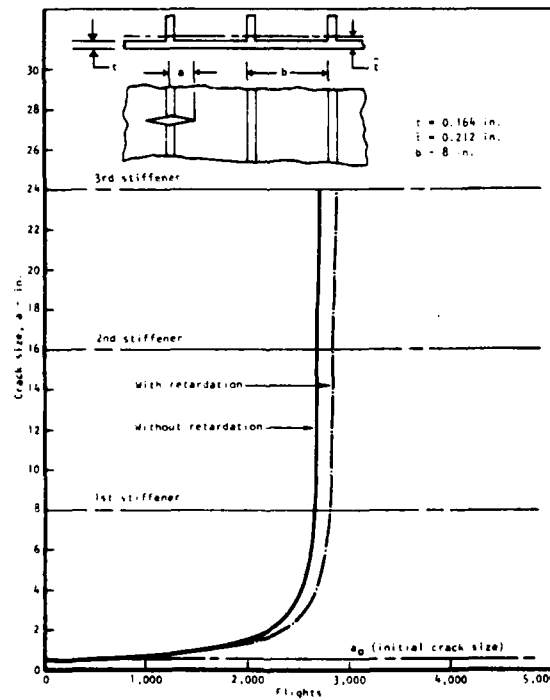


Figure 42. Crack-Growth Prediction for a Fighter Spectrum Using PRDGRO

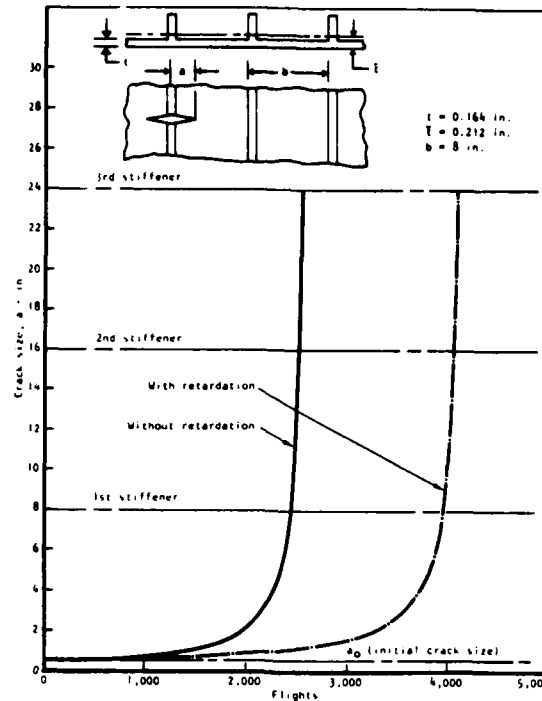


Figure 43. Crack-Growth Prediction for a Fighter Spectrum using PREGRO

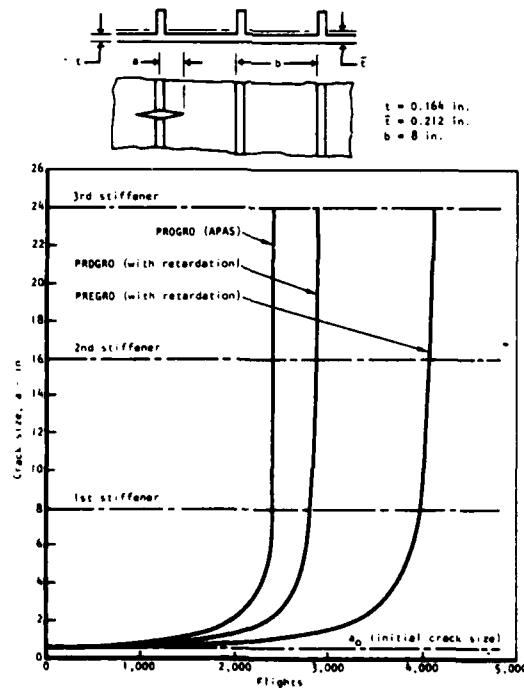


Figure 44. Crack-Growth Prediction for a Fighter Spectrum, Including Overload Retardation Effects

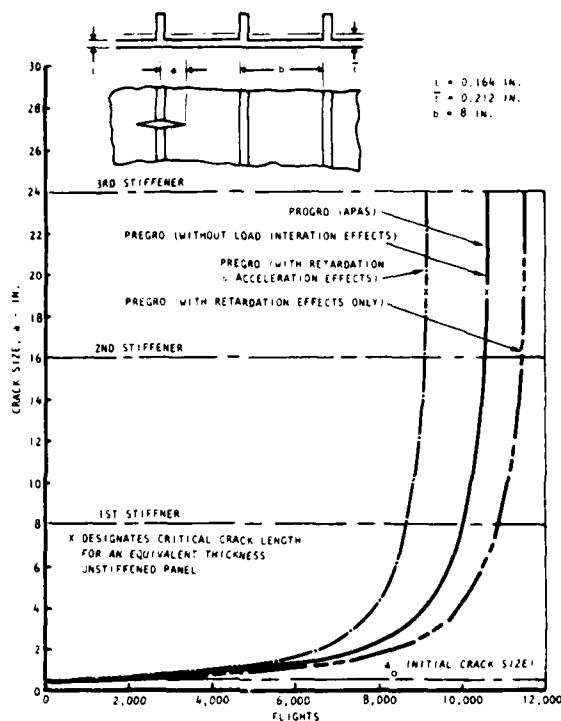


Figure 45. Crack-Growth Prediction Using PROGRO and PREGRO for Library Fighter Spectrum, 1 Flight Block

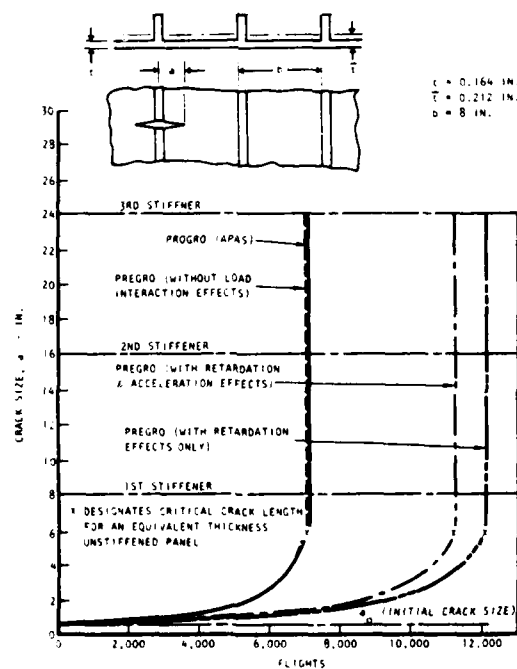


Figure 46. Crack-Growth Prediction Using PROGRO and PREGRO for Library Fighter Spectrum, 50 Flight Blocks

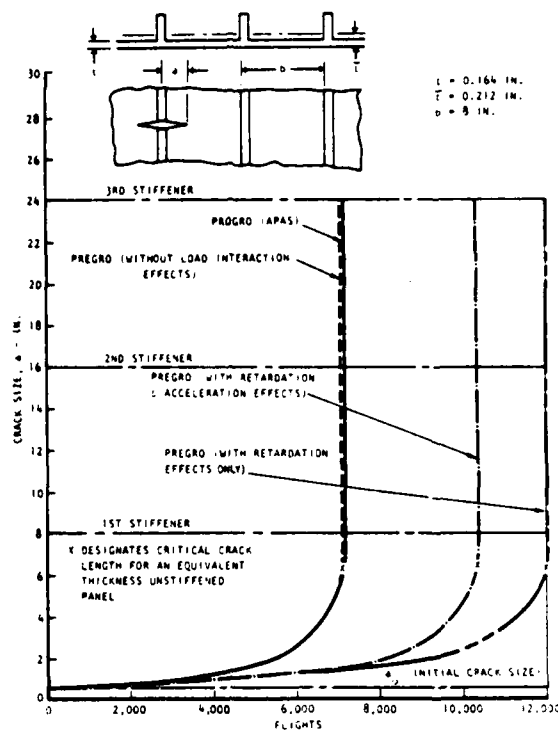


Figure 47. Crack-Growth Prediction Using PROGRO and PREGRO for Library Fighter Spectrum, 100 Flight Blocks

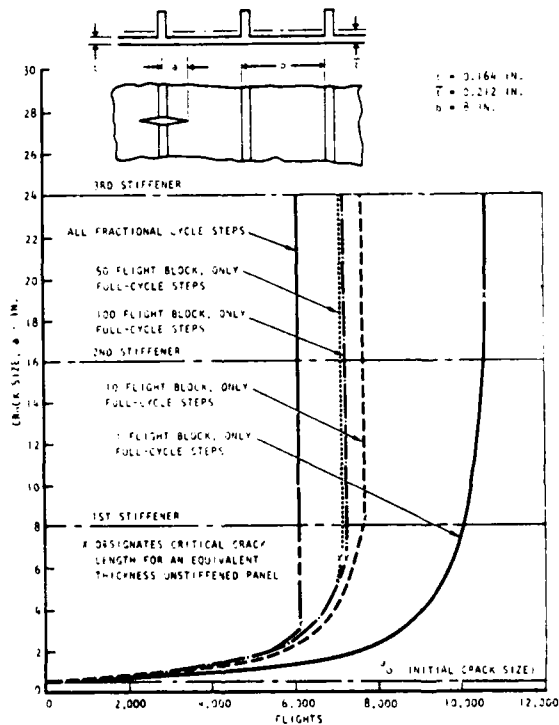


Figure 48. Crack-Growth Prediction Using PROGRO for Library Fighter Spectrum

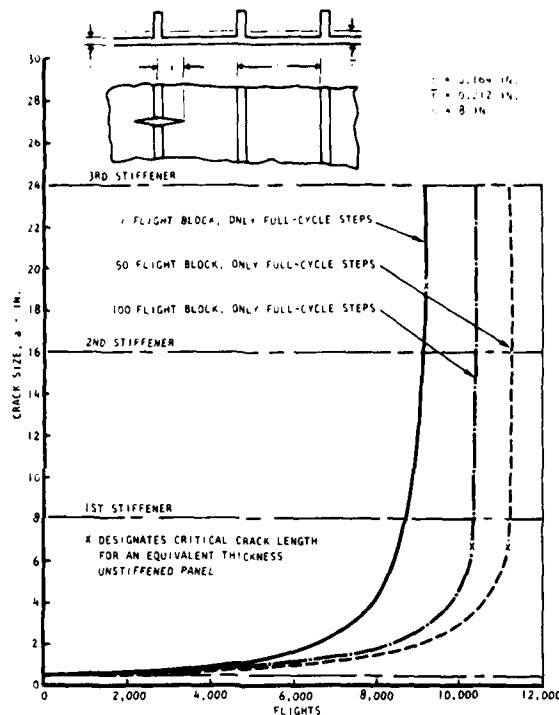


Figure 49. Crack-Growth Prediction Using PREGRO with Retardation and Acceleration Effects for Library Fighter Spectrum

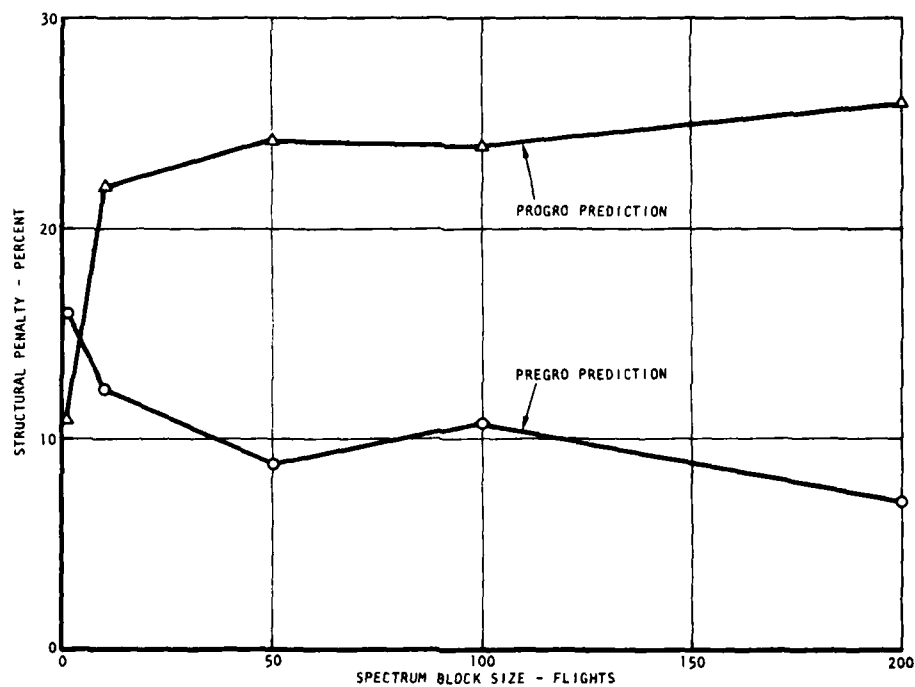


Figure 50. Weight Penalty Versus Load Spectrum Block Size

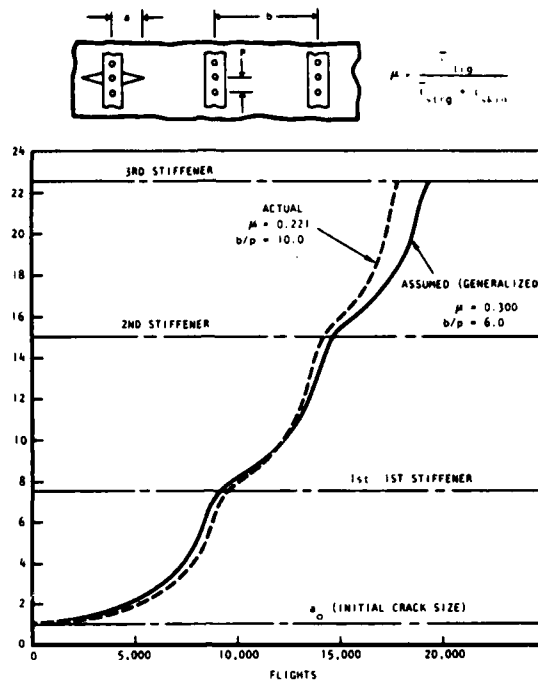


Figure 51. Crack-Growth Prediction Based on Actual and Generalized Stress Intensity Correction Factors

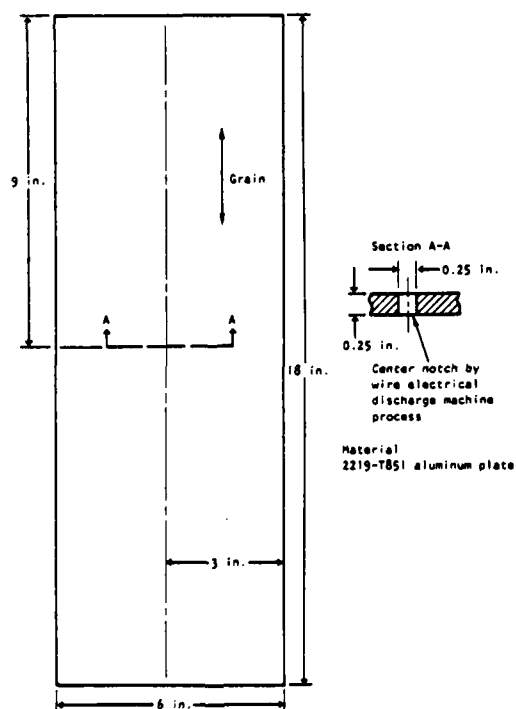


Figure 52. Test Specimen Configuration

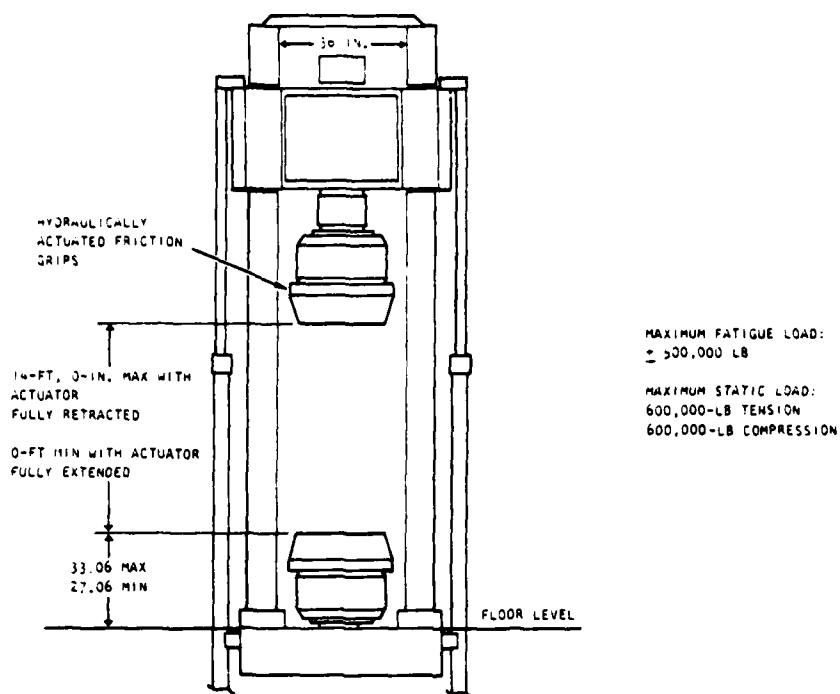


Figure 53. 500 KIP Materials Test System

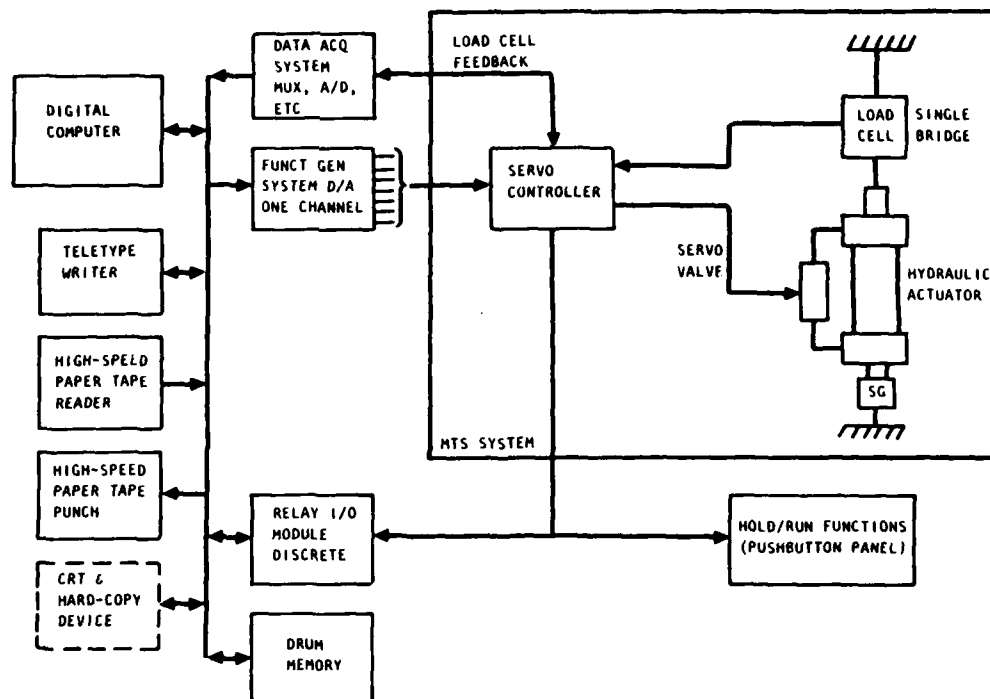


Figure 54. Schematic of MTS/Datum System 70

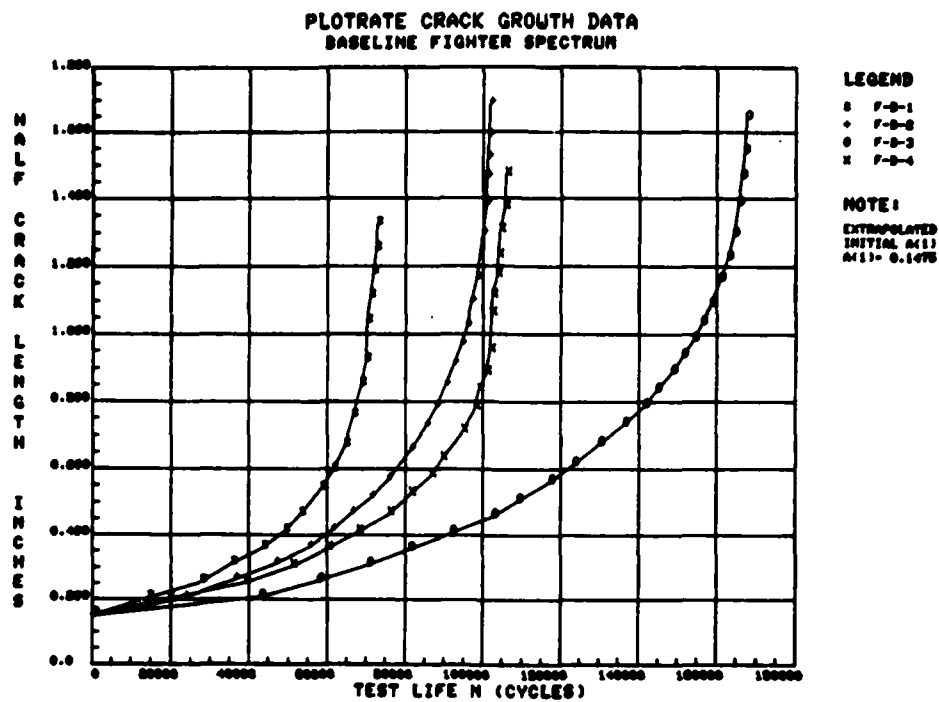


Figure 55. Fighter Baseline Crack-Growth Comparison

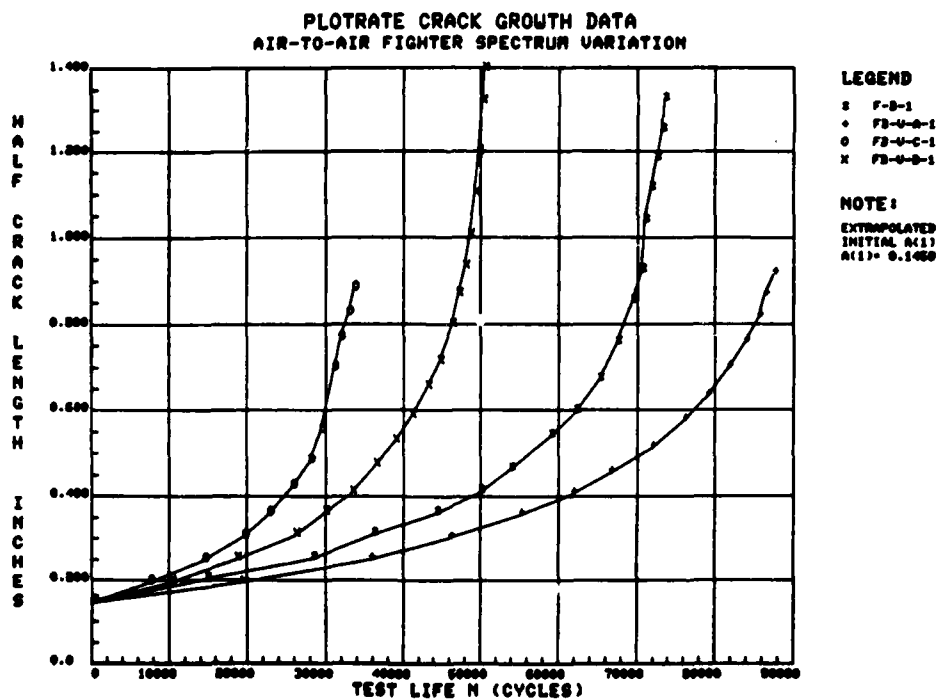


Figure 56. Fighter A-A Mission Spectrum Variation Crack-Growth Comparison

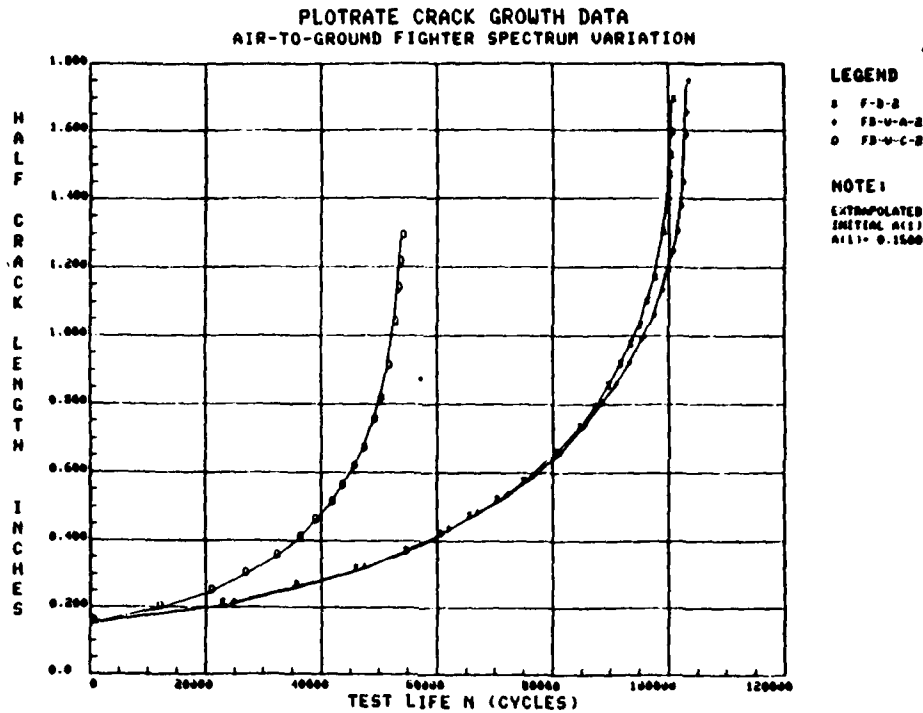


Figure 57. Fighter A-G Mission Spectrum Variation Crack-Growth Comparison

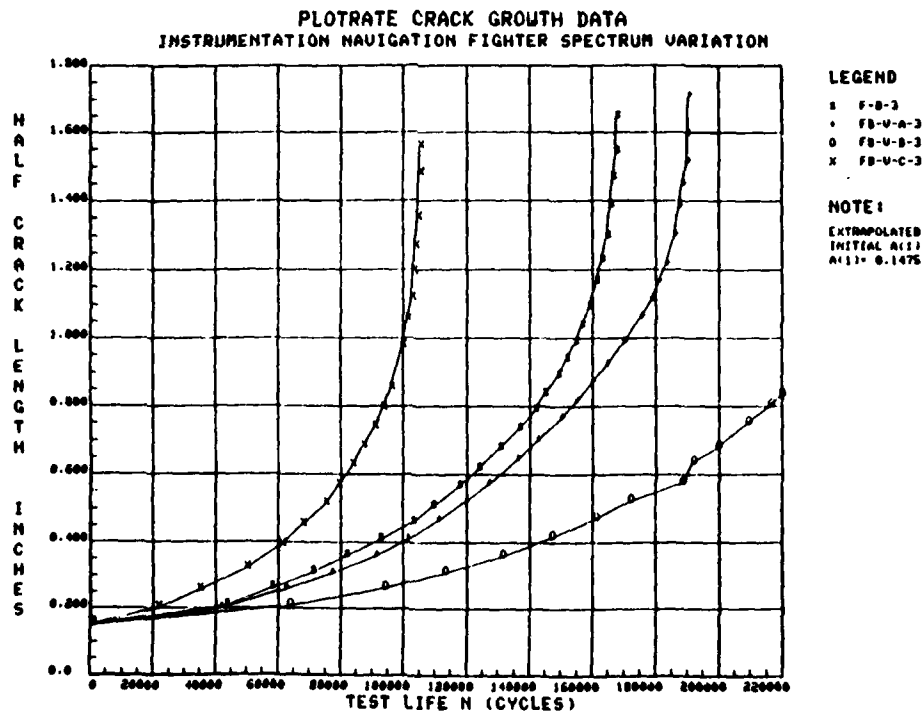


Figure 58. Fighter I-N Mission Spectrum Variation Crack-Growth Comparison

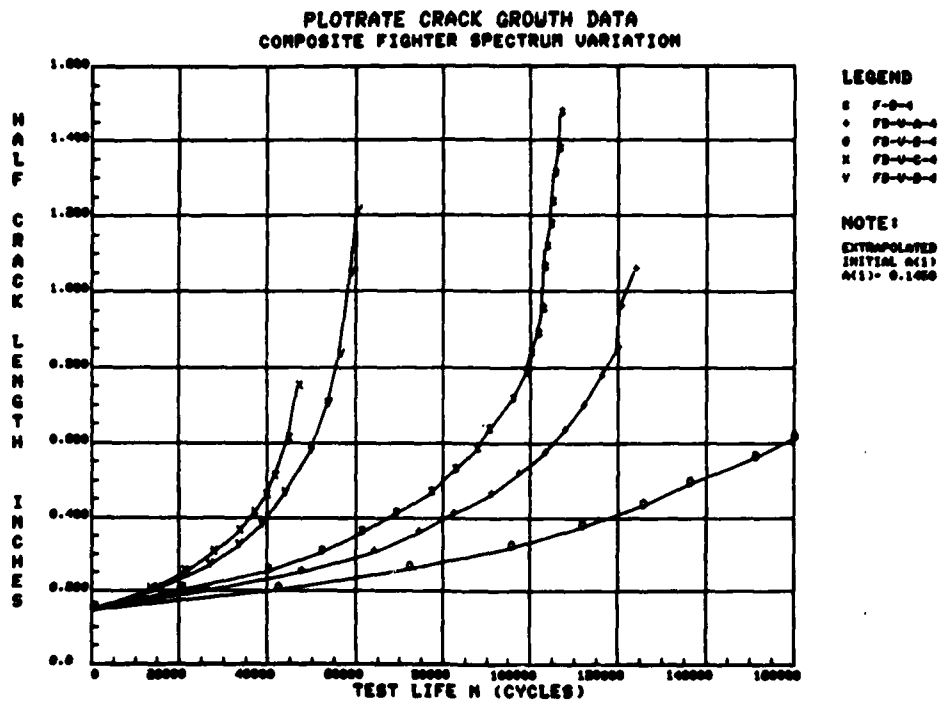


Figure 59. Fighter Composite Spectrum Variation Crack-Growth Comparison

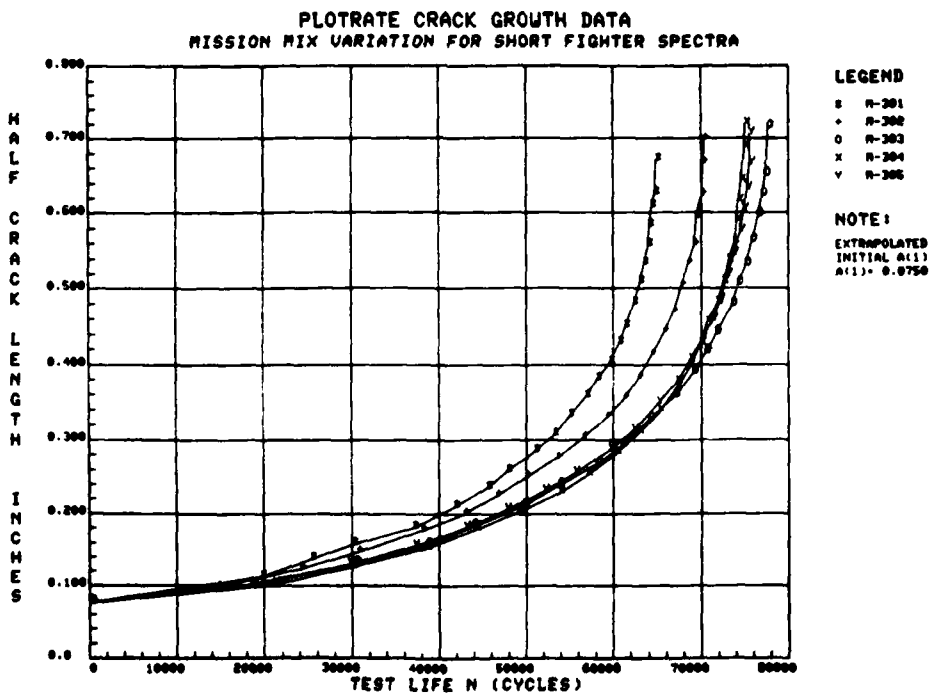


Figure 60. Mission Mix Variation for Short Fighter Spectra

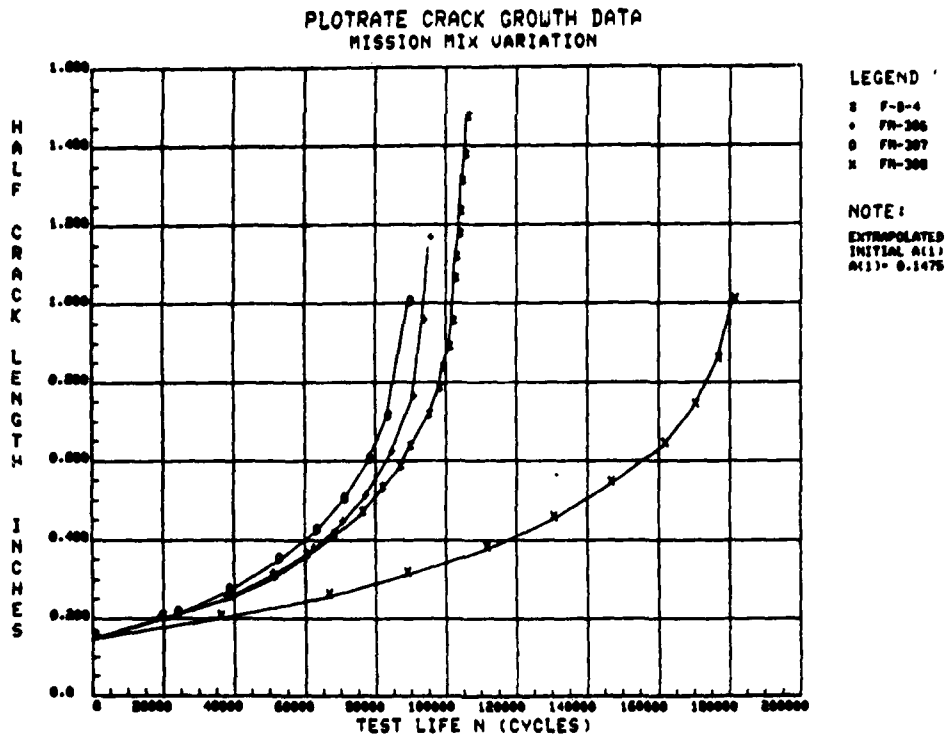


Figure 61. Fighter Composite Mission-Mix Variation Crack-Growth Test Data Comparison

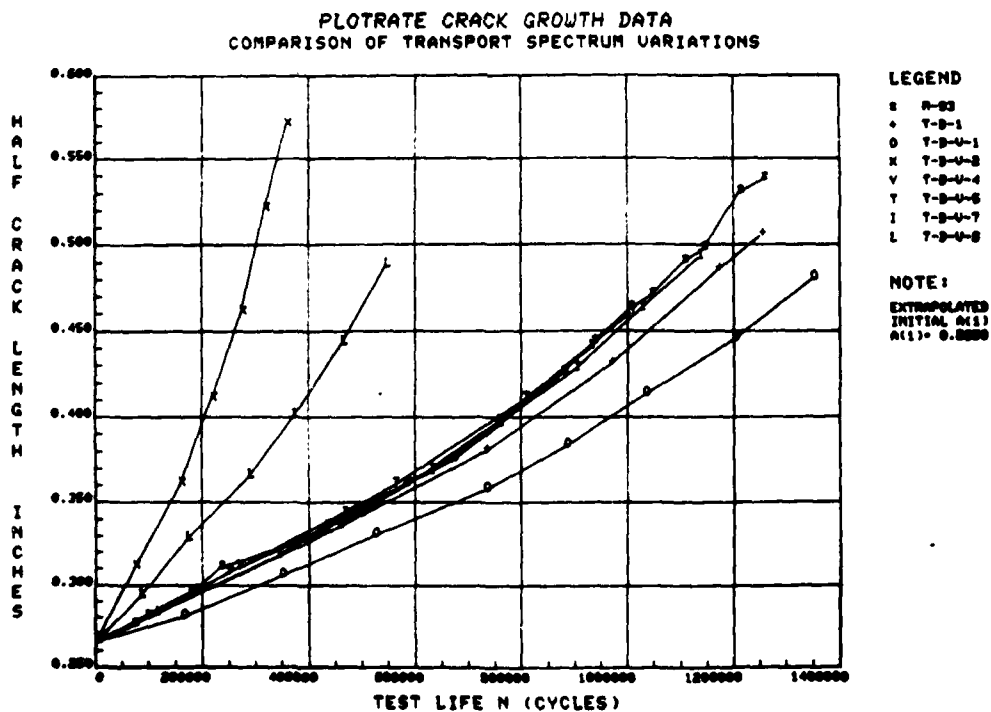


Figure 62. Comparison of Transport Spectrum Variation to Baseline

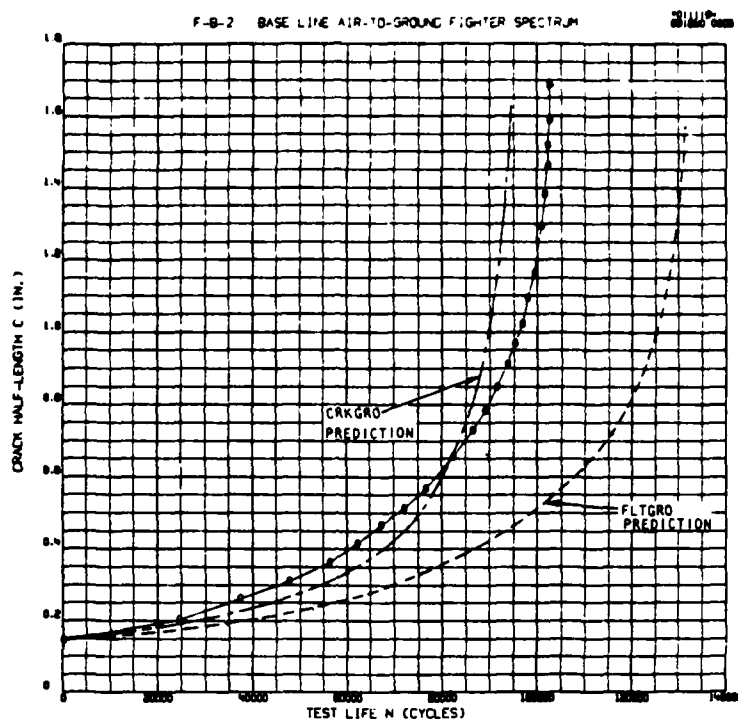


Figure 63. Crack-Growth Correlations, Fighter A-G Baseline

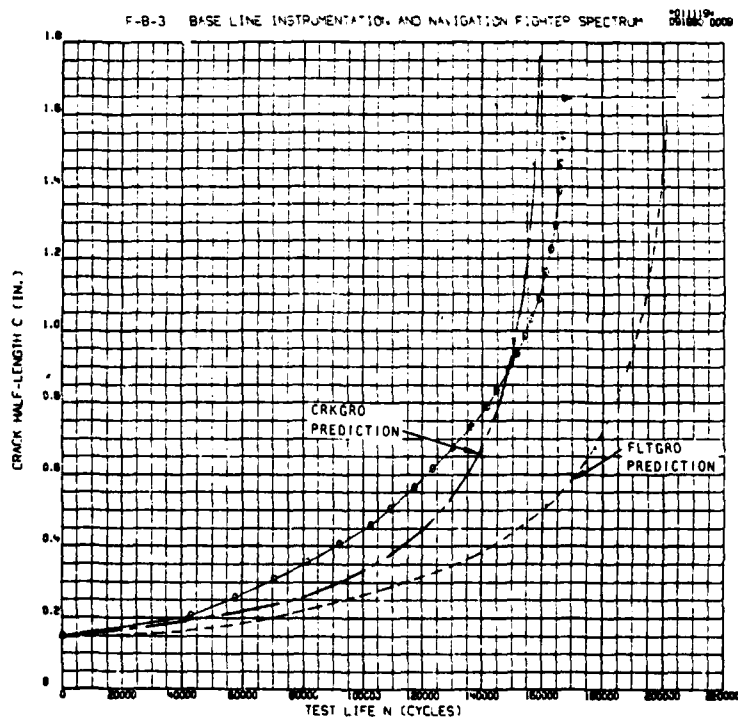


Figure 64. Crack-Growth Correlations, Fighter I-N Baseline

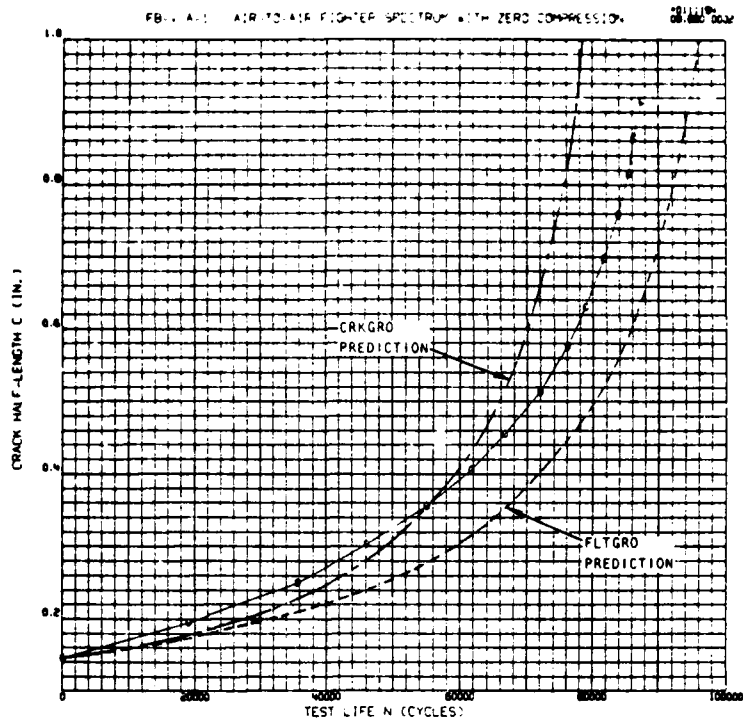


Figure 65. Crack-Growth Correlations, Fighter A-A Mission with Compressive Loads Set to Zero

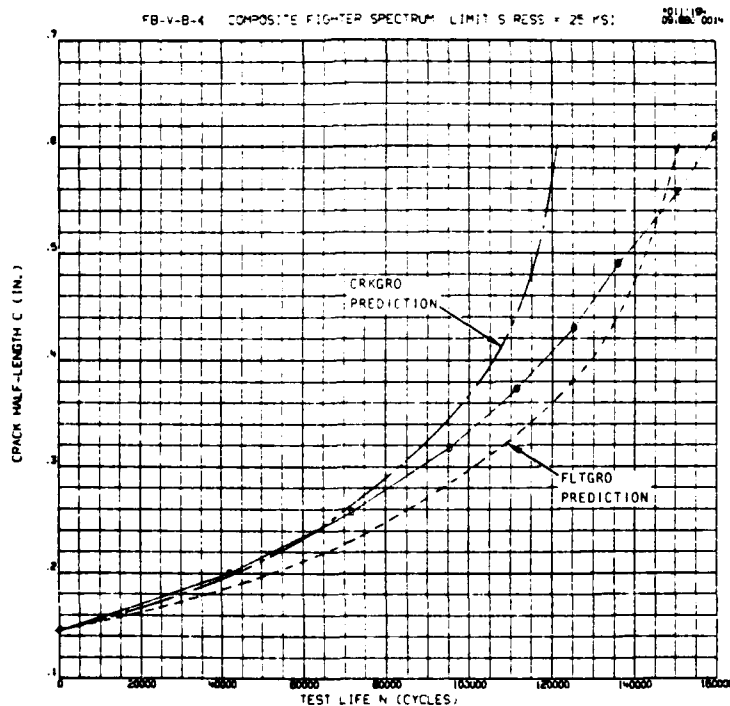


Figure 66. Crack-Growth Correlations, Fighter Composite Spectrum - DLS = 25 ksi

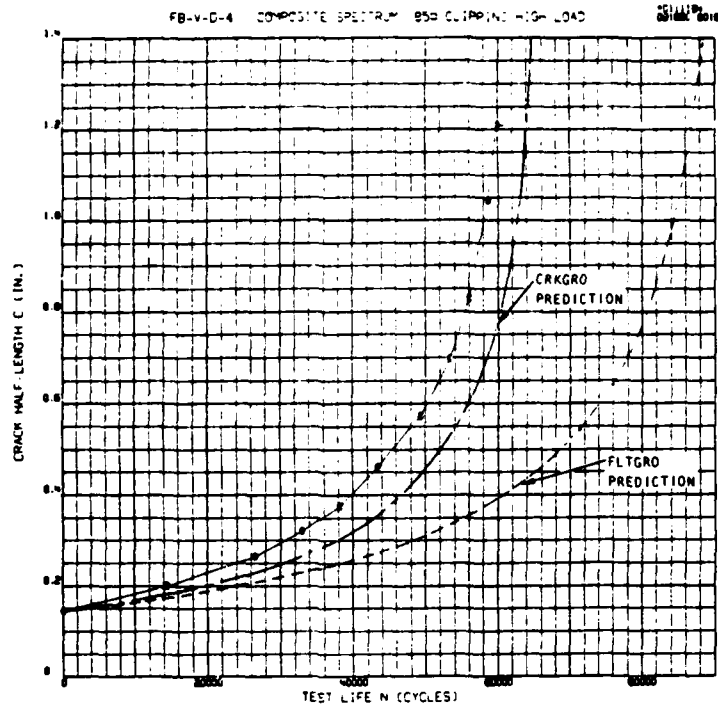


Figure 67. Crack-Growth Correlations, Fighter Composite Spectrum - High Loads Clipped at 85 Percent

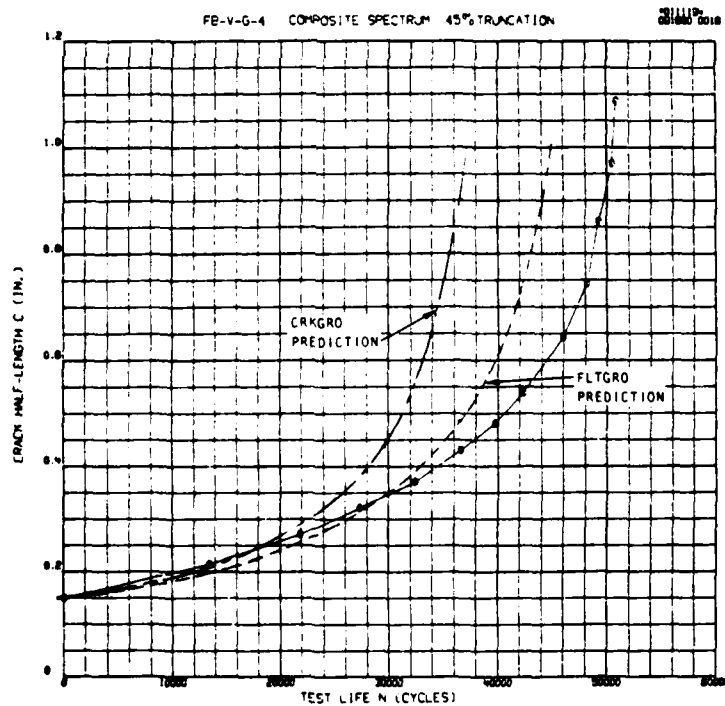


Figure 68. Crack-Growth Correlations, Fighter Composite Spectrum - 45-Percent Low-Load Truncation

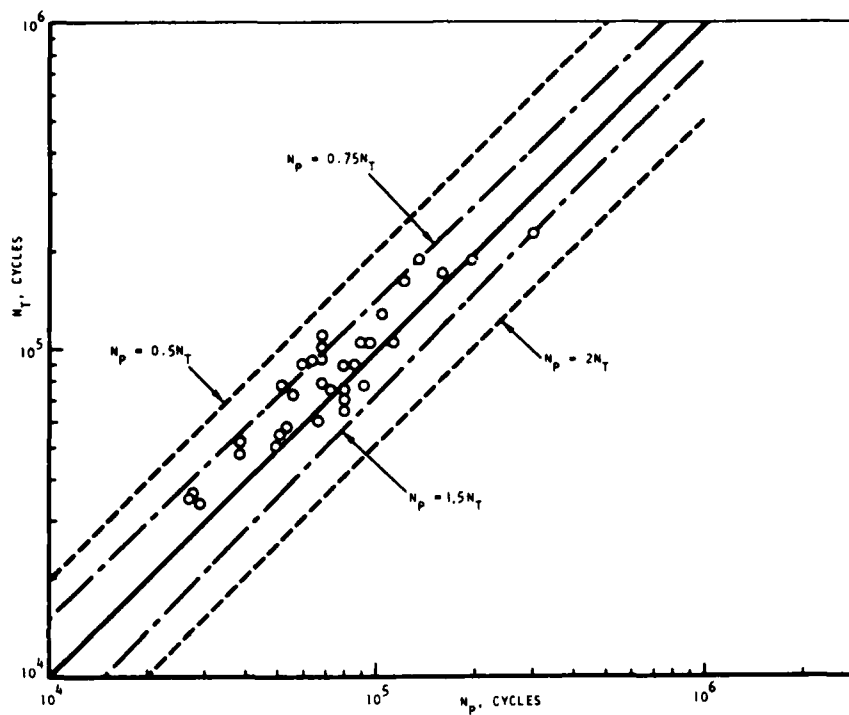


Figure 69. Correlation of Fighter Spectrum Test Results, CRKGRO With Load Interaction Predictions (Old Equation)

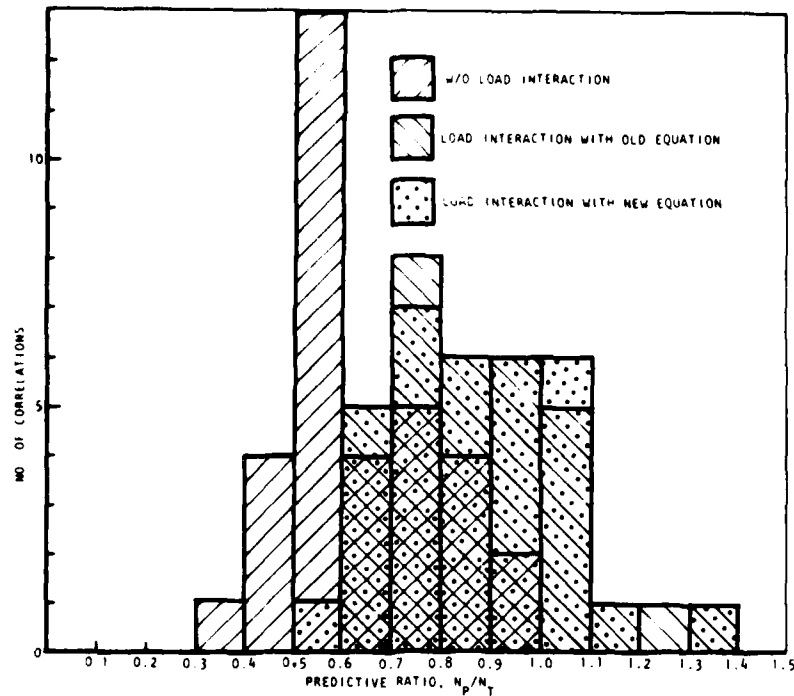


Figure 70. Histogram, CRKGRO Life Predictions Correlated With Fighter Spectrum Test Data

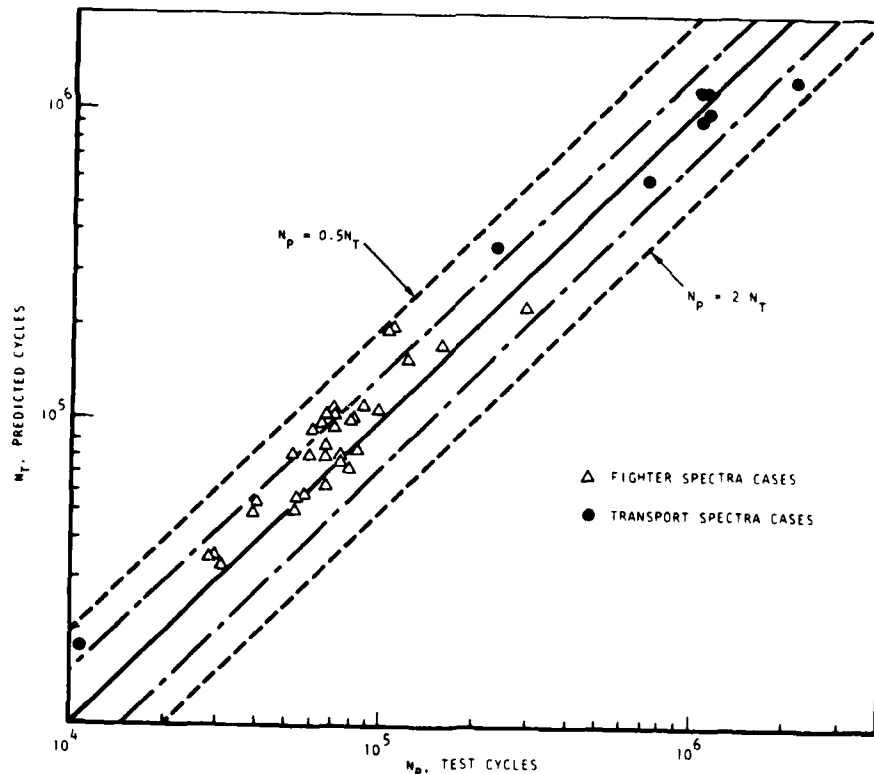


Figure 71. Correlation of Combined Fighter and Transport Spectrum Test Results, CRKGRO With Load Interaction Predictions (New Equation)

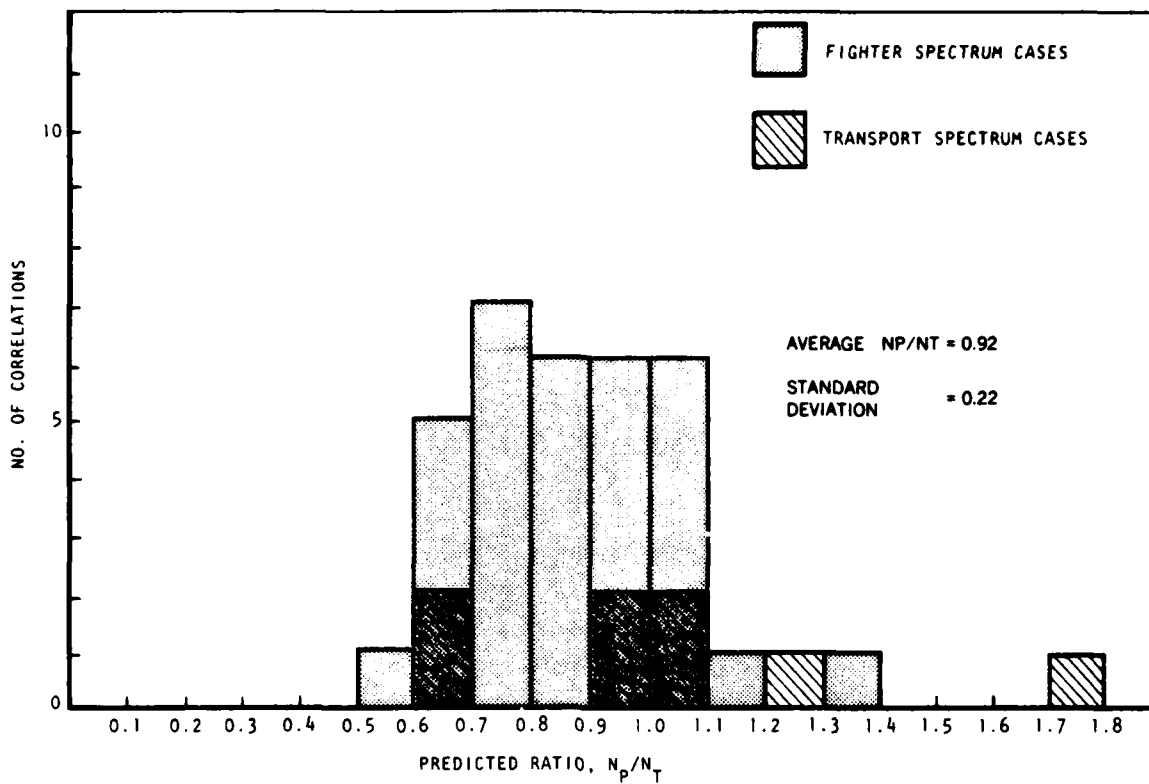


Figure 72. Histogram, CRKGRO Life Predictions Correlated With Combined Fighter and Transport Spectrum Test Data (New Equation)

TABLE 1. SUMMARY - COMPARISONS OF PREDICTED CRACK LIVES OBTAINED FROM EFFGRO AND CRACKS

Test	Test Condition										Test Life N_{test} (cycles)	Analytical Prediction			
	Applied Base Load				Over- load		N_1 (cycles)	N_2 (cycles)	EFFGRO			Cracks			
	Loading Profile	σ_{max} (ksi)	σ_{min} (ksi)	σ_{max} (ksi)	σ_{min} (ksi)	Predicted Life N_{pred} (cycles)			R^*	Predicted Life N_{pred} (cycles)		R^*			
M-12		20	0	30	0	2,500	2,500	14,105	0.85	14,105	0.85				
M-13		20	0	45	0	2,500	2,500	42,516	0.86	40,015	0.81				
M-43		50	0	20	0	500	To failure	10,885	0.61	11,500	0.65				
M-41		40	0	20	0	500	To failure	8,562	0.17	9,250	0.18				
M-45		30	0	20	6	5,370	To failure	17,704	0.75	17,621	0.75				
M-46		10	12	20	6	500	To failure	23,680	0.18	25,501	0.19				
M-51		8	0	20	0	2,500	500	74,625	0.86	74,750	0.86				
M-52		20	0	10	0	500	50	8,210	1.00	8,800	1.07				
M-53		8	2.4	20	2.4	2,500	500	101,761	0.90	102,000	0.9				
M-54		20	6	10	6	500	50	10,970	1.18	12,050	1.29				



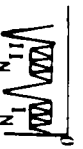
$R^* = N_{pred}/N_{Test}$

TABLE 2. SUMMARY, CRACK GROWTH DATA CORRELATIONS

Test	Test condition					$(C_1 - C_f)$	Analytical predictions					
	Applied base load		Over-/Under-load		N_I (cycle)	N_{II} (cycle)	EFRCO with Vroman/Chang model		Cracks IV with Willenborg model		EFRCO with Willenborg/Chang model	
	σ_{Max} (ksi)	σ_{Min} (ksi)	σ_{Max} (ksi)	σ_{Min} (ksi)			N_{pred} (cycle)	R	N_{pred} (cycle)	R	N_{pred} (cyc)	R
M-1		0					384,500	1.09	387,250	1.09	387,320	1.09
M-2												
M-3		-8					120,000	0.93	>200,000	>2	119,270	0.92
M-4												
M-5		0					825	0.98	940	1.11	828	0.98
M-6												
M-7		28					12,050	0.81	12,250	0.82	12,156	0.82

Note: $R = \frac{N_{pred}}{N_{test}}$

TABLE 2. SUMMARY, CRACK GROWTH DATA CORRELATIONS (Cont)

Test	Test condition						$(C_1 - C_f)$	Analytical predictions						
	Applied base load			Over-/Under-load		N_I (cycle)		N_{II} (cycle)	EFRCO with Vroman/Chang model		CRACKS IV with Willenborg model		EFRCO with Willenborg/Chang model	
									σ_{Max} (ksi)	σ_{Min} (ksi)	σ_{Max} (ksi)	σ_{Min} (ksi)	N_{pred} (cycle)	R
	Loading profile	σ_{Max} (ksi)	σ_{Min} (ksi)	N_{Test} (cycle)										
M-8		40	-4					0.155- C_{CR} 469	784	1.67	1,100	2.35	790	1.68
M-9		8	-0.8					0.153-0.735 175,000	270,700	1.55	305,400	1.74	271,000	1.55
M-10		40	-12					0.160- C_{CR} 251	624	2.48	950	3.78	633	2.52
M-11		20	0	30	0	2,500	To failure	0.148- C_{CR} 15,182	13,180	0.87	14,501	0.96	15,885	1.05
M-12		20	0	30	0	2,500	2,500	0.149- C_{CR} 16,623	13,590	0.82	21,608	1.30	14,105	0.85
M-13		20	0	45	0	2,500	2,500	2,500	0.147-0.84 49,600	32,500	0.66	>250,100	>5	52,520
M-14		20	6	40	6	2,500	2,500	0.155- C_{CR} 225,090	175,000	0.78	>500,200	>2	57,522	0.26
M-15		30	21	40	21	2,500	2,500	0.156- C_{CR} 125,050	117,500	0.94	45,017	0.36	40,017	0.32

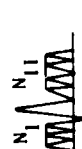

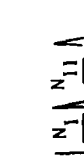
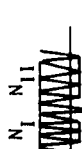
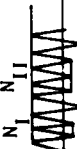
Note: $R = \frac{N_{pred}}{N_{test}}$

TABLE 2. SUMMARY OF CRACK GROWTH DATA CORRELATIONS (Cont)

Test	Test condition						$(C_1 - C_f)$	Analytical predictions						
	Applied base load			Over-/Under-load		N_I (cycle)		N_{II} (cycle)	EFFGRO with Vroman/Chang model		CRACKS IV with Willenborg model		EFFGRO with Willenborg/Chang model	
									σ_{Max} (ksi)	σ_{Min} (ksi)	σ_{Max} (ksi)	σ_{Min} (ksi)	N_{pred} (cycle)	R
	Loading profile	σ_{Max} (ksi)	σ_{Min} (ksi)	σ_{Max} (ksi)	σ_{Min} (ksi)	N_I (cycle)		N_{II} (cycle)	N_{Test} (cycle)	N_{pred} (cycle)	R	N_{pred} (cycle)	R	N_{pred} (cycle)
M-16		20	0	20	-6	2,500	2,500	0.151- C_{CR} 11,370	12,700	1.12	12,820	1.13	12,710	1.12
M-17		20	6	20	-6	2,500	2,500	0.152- C_{CR} 20,810	>23,300	>1	27,510	1.32	23,095	1.11
M-18		40	28	40	-12	2,500	2,500	0.145- C_{CR} 11,600	13,000	1.12	13,005	1.12	13,027	1.12
M-19		20	0	30	-6	2,500	To failure	0.145- C_{CR} 13,460	13,454	1.0	14,751	1.1	13,416	1.0
M-20		20	0	30	-6	2,500	2,500	0.150- C_{CR} 36,083	13,414	0.37	19,757	0.55	13,331	0.37
M-21		20	0	40	-12	2,500	2,500	0.160- C_{CR} 22,850	15,000	0.66	>75,030	>3	14,790	0.65

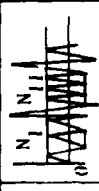


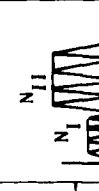
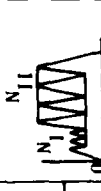
Note: $R = \frac{N_{pred}}{N_{test}}$

TABLE 2. SUMMARY, CRACK GROWTH DATA CORRELATIONS (Cont)

Test	Test condition						(C_1-C_f)	Analytical predictions							
	Applied base load			Over-/Under load		N_{II} (cycle)		Test life N_{Test} (cycle)		iFFQRO with Vroman/Chang model		CRACKS IV with Willenborg model		iFFQRO with Willenborg/Chang model	
										N_{pred} (cycle)	R	N_{pred} (cycle)	R	N_{pred} (cycle)	R
	σ_{Max} (ksi)	σ_{Min} (ksi)	σ_{Max} (ksi)	σ_{Min} (ksi)	N_I (cycle)	N_{pred} (cycle)		R	N_{pred} (cycle)	R	N_{pred} (cycle)	R			
M-22		20	0	30	-6	2,500	0.158- C_{CR} 13,948	12,334	0.88	13,502	0.97	12,576	0.90		
M-23		20	0	30	-6	2,500	0.151- C_{CR} 17,200	13,319	0.77	19,514	1.14	14,098	0.82		
M-24		20	-6	30	-6	2,500	0.220- C_{CR} 10,950	6,430	0.59	12,504	1.14	6,564	0.60		
M-25		20	-6	40	-6	2,500	0.151- C_{CR} 22,512	9,513	0.42	>75,030	>3	12,504	0.56		
M-26		8	-2.4	8	-16	2,500	0.151- C_{CR} 269,840	270,102	1.00	359,500	1.33	270,076	1.0		
M-27		8	-2.4	8	-16	2,500	0.178- C_{CR} 194,723	229,644	1.18	>304,120	>1.5	228,956	1.18		

Note: $R = \frac{N_{pred}}{N_{test}}$

TABLE 2. SUMMARY, CRACK GROWTH DATA CORRELATIONS (Cont)

Test	Test condition							$(C_1 - C_2)$	Analytical predictions					
	Applied base load			Over-/Under-load		N_I (cycle)	N_{II} (cycle)		EFHRO with Vroman/Chang model		CRACKS IV with Willenborg model		EFHRO with Willenborg/Chang model	
									σ_{max} (ksi)	σ_{min} (ksi)	σ_{max} (ksi)	σ_{min} (ksi)	N_{pred} (cycle)	R
	Loading profile	σ_{max} (ksi)	σ_{min} (ksi)	σ_{max} (ksi)	σ_{min} (ksi)	N_I (cycle)	N_{II} (cycle)		Test life N_{Test} (cycle)	N_{pred} (cycle)	R	N_{pred} (cycle)	R	N_{pred} (cycle)
M-28		20	-6	30	-15	2,500	2,500	0.233- C_{CR} 10,003	6,050	0.6	10,003	1.00	6,054	0.61
M-29		20	-6	40	-15	2,500	2,500	0.160- C_{CR} 15,005	8,960	0.6	>75,030	>5	9,907	0.66
M-30		20	-6	40	-15	2,500	2,500	0.145- C_{CR} 20,007	9,912	0.5	>75,030	>3	14,528	0.73
M-31		8	0	20	0	10,000	To failure	0.150- C_{CR} 22,430	22,443	0.92	23,000	0.94	22,436	0.92
M-32		20	0	40	0	5,000	To failure	0.155- C_{CR} 5,275	5,476	1.04	5,500	1.04	5,475	1.04
M-33		8	2.4	20	2.4	10,000	To failure	0.148- C_{CR} 27,000	26,990	1.00	27,000	1.00	26,988	1.0
M-34		20	6	40	12	5,000	To failure	0.150- C_{CR} 6,884	6,584	0.96	7,000	1.02	6,583	0.96

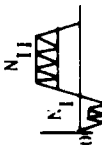
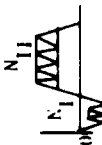
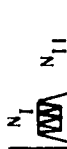

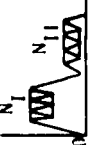
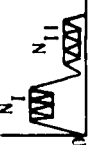
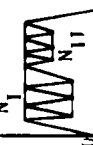
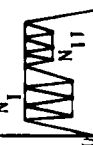
Note: $R = \frac{N_{pred}}{N_{test}}$

TABLE 2. SUMMARY, CRACK GROWTH DATA CORRELATIONS (Cont)

Test	Test condition							$(C_1 - C_2)$	Analytical predictions					
	Applied base load			Over-/Under-load		N_I (cycle)	N_{II} (cycle)		EFGRO with Vromann/Chang model		CRACKS IV with Willenborg model		EFGRO with Willenborg/Chang model	
									N_{pred}	R	N_{pred}	R	N_{pred}	R
	σ_{Max} (ksi)	σ_{Min} (ksi)	σ_{Max} (ksi)	σ_{Min} (ksi)	N_I (cycle)	N_{II} (cycle)	N_{pred} (cycle)		R	N_{pred} (cycle)	R	N_{pred} (cycle)	R	
M-35	8	0	20	14	10,000	To failure	0.143- C_{CR} 178,838	191,845	1.07	192,500	1.08	192,433	1.08	
M-36	20	0	40	28	5,000	To failure	0.150- C_{CR} 9,346	12,051	1.29	12,000	1.28	12,050	1.29	
M-37	8	2.4	20	0	10,000	To failure	0.155- C_{CR} 24,200	21,904	0.91	23,000	0.95	21,903	0.90	
M-38	20	-6	40	0	5,000	To failure	0.150- C_{CR} 5,197	5,376	1.03	5,600	1.08	5,376	1.03	
M-39	0	-6	20	0	5,000	To failure	0.150- C_{CR} 19,300	17,796	0.92	18,000	0.93	17,795	0.92	
M-40	0	-12	40	0	5,000	To failure	0.150- C_{CR} 5,653	5,910	1.04	6,000	1.06	5,910	1.05	

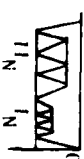

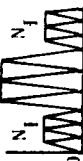
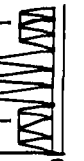
Note: $R = \frac{N_{pred}}{N_{test}}$

TABLE 2. SUMMARY, CRACK GROWTH DATA CORRELATIONS (Cont)

Test	Test condition							$(C_1 - C_f)$	Analytical predictions					
	Applied base load			Over-/Under-load		N_I (cycle)	N_{II} (cycle)		EFFGRO with Vroman/Chang model		CRACKS IV with Willenborg model		EFFGRO with Willenborg/Chang model	
									N_{pred}	R	N_{pred}	R	N_{pred}	R
	Loading profile	σ_{Max} (ksi)	σ_{Min} (ksi)	σ_{Max} (ksi)	σ_{Min} (ksi)	N_{Test} (cycle)	N_{pred}		R	N_{pred}	R	N_{pred}	R	N_{pred}
M-41		-3	-6	20	10	5,000	To failure	0.150- C_{CR} 67,400	0.94	63,150	0.94	63,147	0.94	
M-42		-3	-12	20	10	5,000	To failure	0.155- C_{CR} 57,842	1.06	61,255	1.06	61,251	1.06	
M-43		30	0	20	0	500	To failure	0.158- C_{CR} 17,813	0.6	10,676	0.70	10,885	0.61	
M-44		40	0	20	0	500	To failure	0.153- C_{CR} 50,470	0.15	7,407	0.58	8,731	0.17	
M-45		30	9	20	6	3,370	To failure	0.145- C_{CR} 23,624	0.76	18,030	0.77	17,842	0.76	
M-46		40	12	20	6	500	To failure	0.150- C_{CR} 133,260	0.21	28,453	0.38	25,471	0.19	
M-47		20	6	20	14	500	To failure	0.153-0.697 203,526	0.71	144,590	0.83	147,101	0.72	
M-48		40	12	40	28	500	To failure	0.158 C_{CR} 10,489	0.88	9,256	0.91	9,256	0.88	

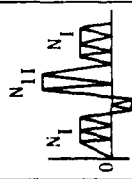
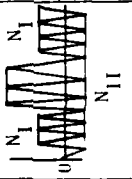
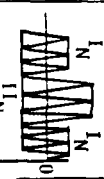
Note: $R = \frac{N_{pred}}{N_{test}}$

TABLE 2. SUMMARY, CRACK GROWTH DATA CORRELATIONS (Cont)

Test	Test condition							(C ₁ -C ₂)	Analytical predictions							
	Applied base load			Over-/Under-load		N _{II} (cycle)	N _I (cycle)		EFHCR0 with Vroman/Chang model		CRACKS IV with Willenborg model		EFHCR0 with Willenborg/Chang model			
									σ _{Max} (ksi)	σ _{Min} (ksi)	σ _{Max} (ksi)	σ _{Min} (ksi)	N _{pred} (cycle)	R	N _{pred} (cycle)	R
M-49		20	14	20	0	500	To failure	27,401	1.07	27,500	1.07	27,400	1.07			
M-50		40	28	40	12	500	To failure	2,332	1.03	2,500	1.10	2,332	1.03			
M-51		8	0	20	0	2,500	500	74,718	0.86	75,000	0.87	74,616	0.86			
M-52		20	0	40	0	500	50	8,217	1.00	10,950	1.33	8,227	1.0			
M-53		8	2.4	20	2.4	2,500	500	104,871	0.92	105,000	0.92	104,587	0.92			
M-54		20	6	40	6	500	50	13,700	1.47	15,350	1.65	12,085	1.50			
M-55		8	0	20	0	2,500	50	502,000	0.91	211,000	0.38	374,500	0.68			
M-56		20	0	40	0	2,500	50	12,904	0.71	10,300	0.57	12,588	0.69			

Note: $R = \frac{N_{pred}}{N_{test}}$

TABLE 2. SUMMARY, CRACK GROWTH DATA CORRELATIONS (Concl)

Test	Test condition							(C_1-C_f)	Analytical predictions											
	Applied base load			Over-/Under-load		N_I (cycle)			N_{II} (cycle)		EFHCRO with Vroman/Chang model		CRACKS IV with Willenborg model		EFHCRO with Willenborg/Chang model					
											σ_{Max} (ksi)	σ_{Min} (ksi)	σ_{Max} (ksi)	σ_{Min} (ksi)	N_{pred} (cycle)	R	N_{pred} (cycle)	R	N_{pred} (cycle)	R
M-57				20	0	0	-12	2,500	50	0.145- C_{CR} 20,760	12,960	0.62	41,600	2.04	18,157	0.87				
M-58				20	-6	40	-6	2,500	500	0.153- C_{CR} 2,774	4,500	1.6	5,750	2.08	4,954	1.79				
M-59				8	-2.4	30	-2.4	5,000	2,500	0.158- C_{CR} 7,402	7,413	1.0	13,750	1.86	7,413	1.0				
M-60				8	-2.4	8	-16	2,500	2,500	0.150-0.6 123,197	170,500	1.38	>250,000	>2	170,800	1.39				

Note: $R = \frac{N_{pred}}{N_{test}}$

TABLE 3. SUMMARY OF COMPUTER COST COMPARISON - RUNGE-KUTTA METHOD VERSUS
LINEAR APPROXIMATION METHOD

Loading type	Cracks		LITCRO		$\frac{CMI(Cracks)}{CMI(LITCRO)}$
	Predicted Life (Cycles)	CMI	Predicted Life (Cycles)	CMI	
Constant Amplitude	1,000,500 2,100,750	0.1552	1,004,270 2,181,850	0.0260	5.2
	1,010,325 150,000	1.0023	1,001,420 150,000	0.0685	14.7
	11,325 21,675	0.0177	11,310 21,650	0.0098	1.8
Single Overload	11,105 14,105	0.0590	11,105 12,860	0.0570	1.05
	10,015 12,505	0.0092	12,515 12,505	0.0067	1.57
	55,010 25,010	0.0255	55,010 25,010	0.0068	5.15
Block Loading	11,500 9,250 17,620 25,500	0.0218	10,885 8,560 17,705 25,680	0.0260	0.84
	10,185 8,000 17,620 25,000	0.0127	10,495 6,850 17,470 22,135	0.0250	0.51
	71,750 8,800 102,000 12,050	0.0308	74,625 8,210 101,760 10,970	0.0177	1.74
	65,750 6,550 95,750 9,900	0.0128	65,625 6,000 95,760 9,850	0.0177	0.72
Random cycle-by-cycle flight spectrum	150,050 90,000	2.0667 0.1098	155,290 90,500	0.1598 0.2267	5.8 2.2

TABLE 4. SUMMARY - INCREMENTAL INTERVAL SIZE-SENSITIVITY STUDY

Test case	Loading condition (ksi)	Crack Type & size (in.)	Test life (cycles)	Predicted lives (cycles)				
				$\delta a = 0.001a$	$\delta a = 0.005a$	$\delta a = 0.01a$	$\delta a = 0.05a$	$\delta a = 0.1a$
M-1	Constant amplitude 8 - 0	TC a = 0.14	353,810	387,850	387,662	387,323	375,787	359,535
M-7	40 - 28	a = 0.155	14,870	12,155	12,144	12,126	12,087	12,031
B-434	14 - 0.7	PTC a = 0.06	205,000	343,010	342,925	342,722	333,374	320,200
		a/2c - 0.5						
Computer cost (billing unit)				0.0568	0.0205	0.0158	0.012	0.012

TABLE 2-V. SUMMARY OF ASSUMPTIONS IN EACH ANALYSIS APPROACH

Analysis type	Assumptions
1-d	The aspect ratio $a/2c$ is constant
2-D type I	$da/dN = dc/dN$
2-D type II-a	$da/dN = 2dc/dN$
2-D type II-b	$da/dN = 2/3 dc/dN$

TABLE 2-VI. MATERIAL'S CRACK GROWTH AND FRACTURE PROPERTIES

Material	C_A	n_A	m_A	K_{Ic} (ksi $\sqrt{in.}$)	K_c (ksi $\sqrt{in.}$)	ΔK_{th_o} (ksi $\sqrt{in.}$)	σ_{ty} (ksi)
2219-T851	7.697×10^{-10}	3.72	0.6	45	76	1.5	51.3
9Ni-4 CO-0.2c steel	3.466×10^{-9}	2.35	.6	154	200	5.5	180
Ti-6Al-4V (β A)	3.762×10^{-10}	3.31	.55	80	160	5	115

TABLE 7. MATERIAL - 2219-T851 ALUMINUM ALLOY

Specimen No.	σ_{max} (ksi)	R	a_1 (in.)	$(a/\Delta a)_1$	Test		Analytical predictions							
							One dimension		$da/dN = dc/dN$		$da/dN = 2 dc/dN$		$da/dN = 2/3 dc/dN$	
					N_f (cyc.)	$(a/\Delta a)_f$	N_{p1} (cyc.)	$(a/\Delta a)$	N_{p2} (cyc.)	$(a/\Delta a)$	N_{p3} (cyc.)	$(a/\Delta a)$	N_{p4} (cyc.)	$(a/\Delta a)$
SIT A1-2	18	0.1	.125 .141 .216	.190 .294 .428	7,500	.267 .365 .426	8,550 11,000 11,510	.191 .294 .428	9,990 12,630 12,080	.259 .358 .448	10,080 13,090 13,350	.265 .373 .488	9,710 12,250 11,170	.254 .340 .418
SIT A1-2	10	.1	.246 .297 .365	.165 .295 .422	13,500	.217 .327 .419	22,400 21,430 19,210	.165 .295 .422	25,480 25,960 20,700	.214 .335 .450	25,560 24,220 21,430	.215 .339 .465	25,410 23,530 20,040	.213 .326 .440
SIT A5-1	50	.5	.114 .148 .210	.171 .305 .437	6,000	.229 .331 .413	4,080 3,570 4,820	.171 .305 .437	4,650 3,870 4,935	.227 .341 .447	4,680 3,950 5,317	.228 .351 .478	4,630 3,800 4,640	.225 .332 .423
SIT A5-2	18	.5	.215 .284 .360	.142 .280 .442	11,000	.183 .310 .411	9,600 7,490 6,140	.142 .280 .442	10,780 8,190 6,380	.181 .309 .453	10,800 8,280 6,540	.182 .314 .462	10,760 8,110 6,230	.182 .307 .447

TABLE 8. MATERIAL - 9Ni-4Co-0.2C STEEL

Specimen No.	σ_{max} (ksi)	R	a_1 (in.)	$(a/2c)_1$	Test		Analytical predictions							
					N_T (cyc)	$(a/2c)_T$	One-dimension		$da/dN = dc/dN$		$da/dN = 2 dc/dN$		$da/dN = 2/3 dc/dN$	
							N_{p1} (cyc)	$(a/2c)_1$	N_{p2} (cyc)	$(a/2c)_2$	N_{p3} (cyc)	$(a/2c)_3$	N_{p4} (cyc)	$(a/2c)_4$
SUT SI-2 (1) (2) (3)	30	0.1	0.148 .196 .245	0.149 .294 .411	8,920	0.194 .339 .437	8,870 7,310 5,420	0.149 .294 .441	9,520 7,710 6,580	0.189 .327 .457	9,550 7,810 6,750	0.191 .336 .470	9,490 7,630 6,430	0.187 .320 .443
SUT SS-2 (1) (2) (3)	45	0.5	.149 .195 .243	.149 .294 .428	7,500	.181 .315 .419	5,700 5,070 3,610	.149 .294 .428	5,990 5,300 3,680	.177 .318 .441	6,020 5,350 3,740	.179 .325 .449	5,990 5,250 3,630	.176 .313 .432

TABLE 9. MATERIAL - Ti-6Al-4V BETA ANNEALED

Specimen No.	σ_{max} (ksi)	R	a_i (in.)	$(a/2c)_i$	Test		Analytical predictions							
					N_T (cyc)	$(a/2c)_F$	One-dimension		$da/dN = dc/dN$		$da/dN = 2 dc/dN$		$da/dN = 2/3 dc/dN$	
							N_{p1} (cyc)	$(a/2c)$	N_{p2} (cyc)	$(a/2c)$	N_{p3} (cyc)	$(a/2c)$		N_{p4} (cyc)
SJT 11-1 (1) (2) (3)	45	0.1	0.072 .101 .152	0.145 .285 .451	8,740	0.327 .424 .436	5,500 6,420 6,810	0.145 .285 .451	7,500 8,250 6,950	0.304 .404 .462	7,660 9,030 8,410	0.310 .455 .531	7,360 7,730 6,190	0.288 .369 .417
SJT 11-2 (1)	27	.1	.174	.138	9,925	.214	7,430	.138	9,130	.219	9,170	.221	9,080	.217
SJT 15-1 (1) (2) (3)	70	.5	.072 .106 .148	.145 .297 .439	6,300	.245 .361 .465	2,645 2,832 4,121	.145 .297 .439	3,250 3,334 4,282	.247 .375 .457	3,280 3,515 5,082	.252 .403 .522	3,222 3,191 3,844	.241 .352 .410
SJT 15-2 (1)	42	.5	.198	.157	8,182	.229	4,074	.157	4,890	.231	4,920	.234	4,870	.229

TABLE 10. COMPARISON OF PREDICATIVE ACCURACIES - CYCLE-COUNTING EFFECT STUDY

Test number	Mission type	δ_{lim} (ksi)	$C_i - C_f$ (in.)	Test life (cycles)	CRKGRO				Predictions			
					Not range-pair counted				Range-pair counted			
					w/o load interaction (1)		w/load interaction (2)		w/o load interaction (3)		w/load interaction (4)	
					Cycles	R	Cycles	R	Cycles	R	Cycles	R
M-84	Fighter A-G	20	0.158 - fail	268,908	359,427	1.34	521,687	1.94	304,209	1.13	369,427	1.37
M-85	Fighter A-G	30	0.144 - fail	95,642	83,057	.87	123,867	1.30	70,274	.73	86,793	.91
M-86	Fighter A-G	40	0.153 - fail	36,367	25,031	.68	37,574	1.02	21,187	.57	26,212	.71
1. Spectra not range-pair counted, load interaction effects not accounted for 2. Spectra not range-pair counted, load interaction effects accounted for 3. Spectra range-pair counted, load interaction effects not accounted for 4. Spectra range-pair counted, load interaction effects accounted for												

TABLE 11. CRKGRO PROGRAM INPUT ECHO, MATERIAL PROPERTIES, AND CRACK GEOMETRIES

```

DETAILED DESIGN CRACK GROWTH ANALYSIS :

IMPSLE-LOAD INTERACTION CCRR. - ROCKWELL TEST 595, HP-9-20
SPECIMEN : HP-9-4-20, STEEL PLATE
CRACK CCF 1:10 SURFACE CRACK, CENTERED
CRACK GROWTH RATE EQUATION : WALMER
      DA/DN = C*(DELTA K/((1-R)**((1-M))))**N

FRACTURE TOUGHNESS
GROWTH RATE EQ. CCNST. = C
GROWTH RATE EQ. EXP. = A
GROWTH RATE EQ. EXP. = M
GROWTH RATE EQ. EXP. = G
      .6000
      .2375

YIELD STRENGTH      180000.0
DELTA K THRESHOLD    5500.00
R CLTCFF = .75      -R CLTCFF = -.99

RETARDATION MODEL : VEGHAN
RET. CCNST. A = .2323

EFFECTIVE PLATE WIDTH = 2.20
INIT. HALF CRACK LENGTH = .0700
INIT. CRACK DEPTH = .0700
INITIAL CYCLE NUMBER = .5000
ASPECT RATIO (A/2C) = 2.4550
PHI SQUARE

MAX. NUMBER OF REPEAT LOAD BLOCK = 1000
THE LOADING (SPECTRUM) HAS 41 STEPS (MAX. 100)
DESIGN LIMIT STRESS = 10000. (PSI)
      **** BLT INSTABILITY WILL BE BASED ON MAX. STRESS ****
  
```

TABLE 12. TYPICAL CRKGRO PROGRAM INPUT ECHO STRESS SPECTRUM

6/11/79

SPECTRLP FOR IPPSLE TEST CASE 599

SPECTRLP FOR SEGMENT 1

RANCM SPECTRLP FOR TEST CASE 599

STEF NC	MAX.STRESS	MIN.STRESS	CYCLES
1	0.0	0.0	1.00
2	147000.0	93000.0	1.00
3	142500.0	97500.0	1.00
4	136500.0	103500.0	1.00
5	137500.0	102500.0	1.00
6	159500.0	-50000.0	1.00
7	49500.0	-55500.0	1.00
8	27500.0	-60000.0	1.00
9	87500.0	22500.0	1.00
10	77500.0	32500.0	1.00
11	57000.0	60000.0	1.00
12	53000.0	90000.0	1.00
13	51000.0	100000.0	1.00
14	45000.0	150000.0	1.00
15	36000.0	210000.0	1.00
16	67000.0	165000.0	1.00
17	57000.0	125000.0	1.00
18	53000.0	125000.0	1.00
19	57000.0	136000.0	1.00
20	51000.0	180000.0	1.00
21	42000.0	260000.0	1.00
22	39000.0	324000.0	1.00
23	100000.0	-27500.0	1.00
24	73500.0	-75000.0	1.00
25	50000.0	-50000.0	1.00
26	142500.0	97500.0	1.00
27	142500.0	97500.0	1.00
28	135000.0	105000.0	1.00
29	135000.0	105000.0	1.00
30	135000.0	105000.0	1.00
31	127500.0	112500.0	1.00
32	127500.0	112500.0	1.00
33	127500.0	112500.0	1.00
34	127500.0	112500.0	1.00
35	127500.0	112500.0	1.00
36	127500.0	112500.0	1.00
37	127500.0	112500.0	1.00
38	127500.0	112500.0	1.00
39	127500.0	112500.0	1.00
40	127500.0	112500.0	1.00
41	127500.0	112500.0	1.00
42	127500.0	112500.0	1.00
43	127500.0	112500.0	1.00
44	127500.0	112500.0	1.00
45	127500.0	112500.0	1.00
46	127500.0	112500.0	1.00
47	127500.0	112500.0	1.00
48	127500.0	112500.0	1.00
49	127500.0	112500.0	1.00
50	127500.0	112500.0	1.00
51	127500.0	112500.0	1.00
52	127500.0	112500.0	1.00
53	127500.0	112500.0	1.00
54	127500.0	112500.0	1.00
55	127500.0	112500.0	1.00
56	127500.0	112500.0	1.00
57	127500.0	112500.0	1.00
58	127500.0	112500.0	1.00
59	127500.0	112500.0	1.00
60	127500.0	112500.0	1.00
61	127500.0	112500.0	1.00
62	127500.0	112500.0	1.00
63	127500.0	112500.0	1.00
64	127500.0	112500.0	1.00
65	127500.0	112500.0	1.00
66	127500.0	112500.0	1.00
67	127500.0	112500.0	1.00
68	127500.0	112500.0	1.00
69	127500.0	112500.0	1.00
70	127500.0	112500.0	1.00
71	127500.0	112500.0	1.00
72	127500.0	112500.0	1.00
73	127500.0	112500.0	1.00
74	127500.0	112500.0	1.00
75	127500.0	112500.0	1.00
76	127500.0	112500.0	1.00
77	127500.0	112500.0	1.00
78	127500.0	112500.0	1.00
79	127500.0	112500.0	1.00
80	127500.0	112500.0	1.00
81	127500.0	112500.0	1.00
82	127500.0	112500.0	1.00
83	127500.0	112500.0	1.00
84	127500.0	112500.0	1.00
85	127500.0	112500.0	1.00
86	127500.0	112500.0	1.00
87	127500.0	112500.0	1.00
88	127500.0	112500.0	1.00
89	127500.0	112500.0	1.00
90	127500.0	112500.0	1.00
91	127500.0	112500.0	1.00
92	127500.0	112500.0	1.00
93	127500.0	112500.0	1.00
94	127500.0	112500.0	1.00
95	127500.0	112500.0	1.00
96	127500.0	112500.0	1.00
97	127500.0	112500.0	1.00
98	127500.0	112500.0	1.00
99	127500.0	112500.0	1.00
100	127500.0	112500.0	1.00

***** LND CF INPUT *****

TABLE 13. TYPICAL CRKGRO PROGRAM OUTPUT

IMPSLE-LCAL INTERACTION CORR. - ROCKWELL TEST 599, HP-5-20 THE CRACK AT THE BEGINNING OF BLOCK 1000 A = .277972 C = .297178												06/11/75:
STEP	CYC.	A	C	(1/2C) (A/T)	DADA DCCN	DELTA DELTC	AKMAX CKMAX	SIGMAX SIGMIN	K F(A/R)	GRAD RES	BFCCR WCRR	
2	1.	.2779	.2972	.4675 .5585	.421E-04 .436E-04	36654.8 37227.8	59782.5 101287.9	147000.0 93000.0	.633 1.000	1.000 0.000	1.022 1.013	
..... AT FRACTURAL (.7, OR .8, OR .9) K SLR C OF 99700. KMAX= 59782.5 A = .277972 IN BLOCK 1000 (STEP 3 CYCLE 0.) C = .297221												
3	1.	.2779	.2973	.4675 .5586	.290E-04 .300E-04	29453.1 29867.5	96546.7 58002.2	142500.0 97500.0	.684 1.000	1.000 0.000	1.022 1.013	
4	1.	.2780	.2973	.4675 .5587	.143E-04 .148E-04	19867.5 21116.8	92255.3 53645.3	136500.0 103500.0	.750 1.000	1.000 0.000	1.022 1.013	
5	7.	.2780	.2973	.4675 .5587	.307E-05 .314E-05	12217.2 12412.2	87592.1 89317.5	136500.0 109500.0	.750 1.000	1.000 0.000	1.022 1.013	
6	1.	.2780	.2973	.4675 .5587	.257E-04 .266E-04	77222.5 78466.7	37665.9 38237.1	57300.0 -60000.0	1.000 1.000	1.000 0.000	1.022 1.013	
7	1.	.2780	.2973	.4675 .5588	.184E-04 .191E-04	68226.2 69354.6	32677.8 33165.6	49500.0 -50000.0	.990 1.000	1.000 0.000	1.022 1.013	
8	1.	.2780	.2973	.4675 .5588	.136E-04 .141E-04	59269.2 61262.2	28695.2 28912.8	43500.0 -46500.0	.990 1.000	1.000 0.000	1.022 1.013	
9	10.	.2781	.2974	.4675 .5589	.441E-05 .456E-05	39515.2 40109.2	17781.8 18049.3	27300.0 -33000.0	.990 1.000	1.000 0.000	1.022 1.013	
10	1.	.2781	.2974	.4675 .5589	.217E-04 .223E-04	40119.2 41574.5	57667.1 58736.6	87000.0 60000.0	.669 1.000	1.000 0.000	1.022 1.013	
11	1.	.2781	.2974	.4675 .5590	.261E-05 .263E-05	14358.1 14411.1	46718.9 47420.7	70500.0 22500.0	.315 1.000	1.000 0.000	1.022 1.013	
12	1.	.2781	.2974	.4675 .5590	0. 0.	-6578.8 -6842.1	37675.8 38245.8	57000.0 36000.0	.632 1.000	1.000 0.000	1.022 1.013	
13	1.	.2781	.2974	.4675 .5590	0. 0.	-7978.1 -8262.4	21747.6 22774.2	33000.0 6000.0	.182 1.000	1.000 0.000	1.022 1.013	
14	1.	.2781	.2974	.4675 .5590	.274E-06 .286E-06	5945.0 5869.8	33682.3 34188.3	51000.0 9000.0	.176 1.000	1.000 0.000	1.022 1.013	
15	10.	.2781	.2974	.4675 .5590	0. 0.	-3285.2 -3539.8	29695.3 30141.4	45000.0 15000.0	.332 1.000	1.000 0.000	1.022 1.013	
16	20.	.2781	.2974	.4675 .5590	0. 0.	-12578.4 -12932.0	25717.5 26103.8	39000.0 21000.0	.538 1.000	1.000 0.000	1.022 1.013	
17	1.	.2781	.2974	.4675 .5590	.177E-05 .183E-05	14252.1 14422.2	43694.5 44254.9	66000.0 10500.0	.159 1.000	1.000 0.000	1.022 1.013	

TABLE 14. CRKGRO PROGRAM OUTPUTS - SUMMARY OF CRACK GROWTH

CRACK GROWTH SUMMARY TABLE FOR EVERY 10-TH BLOCK											
INITIAL CRACK = .0700											
A	C	.0707	.0715	.0722	.0730	.0738	.0747	.0755	.0764	.0772	.0782
A	C	.0709	.0719	.0728	.0738	.0748	.0758	.0769	.0779	.0790	.0801
A	C	.0751	.0800	.0809	.0819	.0829	.0839	.0849	.0859	.0869	.0880
A	C	.0810	.0821	.0833	.0844	.0855	.0867	.0879	.0891	.0903	.0916
A	C	.0851	.0902	.0913	.0924	.0936	.0948	.0960	.0972	.0984	.0997
A	C	.0927	.0940	.0953	.0966	.0979	.0993	.1006	.1020	.1034	.1049
A	C	.1010	.1023	.1036	.1049	.1063	.1076	.1090	.1105	.1119	.1134
A	C	.1062	.1077	.1092	.1107	.1122	.1138	.1154	.1170	.1186	.1203
A	C	.1149	.1164	.1180	.1195	.1211	.1228	.1244	.1261	.1278	.1296
A	C	.1219	.1235	.1253	.1271	.1289	.1307	.1326	.1345	.1364	.1384
A	C	.1313	.1331	.1350	.1368	.1387	.1406	.1426	.1446	.1466	.1487
A	C	.1402	.1422	.1442	.1463	.1484	.1505	.1527	.1549	.1571	.1595
A	C	.1508	.1529	.1551	.1573	.1595	.1618	.1641	.1665	.1689	.1715
A	C	.1617	.1640	.1664	.1688	.1713	.1738	.1764	.1790	.1816	.1844
A	C	.1729	.1765	.1791	.1817	.1844	.1872	.1900	.1929	.1960	.1992
A	C	.1870	.1898	.1926	.1955	.1984	.2014	.2047	.2079	.2113	.2148
A	C	.2123	.2156	.2189	.2224	.2259	.2294	.2331	.2368	.2401	.2446
A	C	.2179	.2214	.2250	.2287	.2324	.2362	.2401	.2441	.2481	.2524
A	C	.2285	.2326	.2368	.2410	.2454	.2498	.2544	.2591	.2639	.2689
A	C	.2362	.2405	.2449	.2494	.2540	.2585	.2633	.2681	.2731	.2783
A	C	.2439	.2491	.2544	.2598	.2654	.2711	.2769	.2827	.2886	.2946
A	C	.2521	.2584	.2648	.2713	.2779	.2847	.2916	.2986	.3057	.3129
A	C	.2628	.2697	.2769	.2844	.2921	.2999	.3078	.3158	.3239	.3322
A	C	.2748	.2827	.2909	.2994	.3081	.3171	.3262	.3356	.3452	.3553
A	C	.2813	.2897	.2984	.3074	.3167	.3263	.3361	.3461	.3565	.3672
A	C	.2926	.3019	.3115	.3214	.3317	.3423	.3531	.3641	.3753	.3869
A	C	.3054	.3159	.3267	.3378	.3492	.3609	.3729	.3851	.3976	.4113
A	C	.3186	.3299	.3416	.3537	.3662	.3791	.3923	.4059	.4199	.4346
CRITICAL CRACK IS IN BLOCK 1226 A = .0445 C = .0483:											

TABLE 15. INPUT ECHO OF CYCGRO PROGRAM FOR DETERMINING $C, \lambda, (\overline{\Delta\sigma^b})^{1/b}$

```

COMPLTER PROGRAM 'CYCGRO'

2219-TR51. CENTERED THRU CRACK
INPUT MATERIAL CONSTANTS AND CONTRCL PARAMETERS

YIELD STRESS ----- SIGMAY= 48000.00 (PSI)
KIC FOR A ----- AKIC = 33000.00 (PSI*SQRT(INCH))
KIC FOR C ----- CKIC = 66000.00 (PSI*SQRT(INCH))
POWER = 0.20000E+01
WALKER'S COEFF ----- C = 0.10055E-19 FOR (PSI)
WALKER'S COEFF ----- C = 0.83667E-09 FOR (KSI)
EXP SMALL N ----- N = 0.36400E+01
DELTA K THRESHOLD --- KTH= 0.15000E+04 (PSI*SQRT(INCH))
EXP SMALL M ----- M = 0.60000E+00
R CUT-OFF --- R-CUT+ = 0.99000E+00

*COMPRESSIVE STRESSES WILL BE LEFT IN THE SPECTRUM*
-R CUTOFF ----- R-CUT- = -0.9900
EXP SMALL Q ----- Q = 0.3000

INIT. HALF CRACK SIZE CO= SPECIFIED LATER.
INITIAL CRACK DEPTH -- AO= 0.0 (INCH)
ASPECT RATIO ----- AO/2CC= 0.0
PHI SQUARED ----- = 0.0
EQUIVALENT THICKNESS - T = 0.25000E+00 (INCH)
HALF WIDTH ----- W/2 = 0.30000E+01 (INCH)

TYPE = 2 (PART THROUGH CRACK=1, THROUGH CRACK=2)
LOCATION= 1 (CENTER CRACK =1, EDGE CRACK =2)
RETARD = 1 (NO RETARDATION=0, WITH RETARDATION=1)

EMP.CONSTANT (MODIFYING KMAX,KMIN,KLIM)= 1.000

```

TABLE 16. PARAMETRICS CALCULATED BY CYCGRO PROGRAM

CALCULATED RESULTS FOR ALL K-VALUES		FOR K > DELKTH	FOR K < DELKTH
POWER = 0.20000E+01		POWER = 0.20000E+01	POWER = 0.20000E+01
SIGMA = 0.10308E+02 LAMBDA = 0.36275E+01 LOG(C) = -0.76223E+01 C = 0.23861E-07 PRODUCT = 0.11298E-03		SIGMA = 0.10308E+02 LAMBDA = 0.36275E+01 LOG(C) = -0.76223E+01 C = 0.23861E-07 PRODUCT = 0.11298E-03	SIGMA = 0.10308E+02 LAMBDA = NO VALUE LOG(C) = NO VALUE C = NO VALUE PRODUCT = NO VALUE

TABLE 17. INPUT ECHO FOR FLTGRO

INDIVIDUAL AIRCRAFT TRACKING CRACK GROWTH ANALYSIS

M = 91 WITH DIFFERENT "MISSION" PARAMETERS

2219-1051, CENTERED THRU CRACK

CRACK GROWTH RATE EQUATION FOR CALCULATING C, LAMBDA, AND SIGMA:

$$DA/DN = CWALK * (DELTA K / (1-K)) ** ((1-M) ** 0.5)$$

CRACK GROWTH RATE EQUATION FOR CALCULATING LIFE:

$$DA/DF = C * (K/AF) ** LAMBDA$$

INPUT MATERIAL CONSTANTS AND CONTROL PARAMETERS

YIELD STRESS ----- SIGMA_YE 400 0.00 (PSI)
 K1C FOR A ----- K1C_A 400 0.00 (PSI*SQRT(INCH))
 K1C FOR C ----- K1C_C 400 0.00 (PSI*SQRT(INCH))
 POWERS = 2.00 0.00
 WALKER'S COEFF ----- C = 1.00E-19 FOR (PSI)
 WALKER'S COEFF ----- C = 1.00E-19 FOR (KSI)
 EXP SMALL TIMES HOLD ----- F THE 1.00E+01
 DELTA K TIMES HOLD ----- F THE 1.00E+01 (PSI*SQRT(INCH))
 EXP SMALL M ----- M = 0.49 0.00
 K CUT-OFF ----- K-CUT = 0.49 0.00

*COMPRESSIVE STRESSORS FULL OF LEFT IN THE SPECTRUM

K CUT-OFF ----- K-CUT = 0.00
 EXP SMALL C ----- C = 0.00

INITIAL HALF CRACK SIZE C0E SPECIFIED LATER.

INITIAL CRACK DEPTH ----- A = 0.00 (INCH)

ASPECT RATIO ----- A/R = 0.00

PHI CRACK THICKNESS ----- PHI = 0.00 (INCH)

EQUIVALENT THICKNESS ----- W = 0.00 (INCH)

HALF WIDTH ----- W/2 = 0.00 (INCH)

TYPE = 1 CRACK LOCATED CRACKED THROUGH CRACKED

LOCATION = 1 (OFFICE CRACK FLY LINE CRACKED)

REPAIR = 1 CRACK REPAIR WITH RETARDATION

INF. CONSTANT (CRACK GROWTH RATE) = 1.00

TABLE 18. SUMMARY OF PARAMETERS DETERMINED BY FLTGRO FOR

A-A, A-G, AND I-N MISSIONS AT $\sigma_{lim} = 20, 30, \text{ AND } 40 \text{ KSI}$

Mission type Parameter	A-A	A-G	I-N
$\sigma_{lim} = 20 \text{ ksi}$ C λ $\frac{1}{(\Delta\sigma)^2} 1/2$	1.273×10^{-9} 3.68 7.3813 ksi	1.0877×10^{-9} 3.7024 6.8728 ksi	9.0216×10^{-10} 3.9185 4.672 ksi
$\sigma_{lim} = 30 \text{ ksi}$ C λ $\frac{1}{(\Delta\sigma)^2} 1/2$	1.4898×10^{-9} 3.597 11.072 ksi	1.2503×10^{-9} 3.6315 10.309 ksi	1.181×10^{-9} 3.761 7.008 ksi
$\sigma_{lim} = 40 \text{ ksi}$ C λ $\frac{1}{(\Delta\sigma)^2} 1/2$	1.5679×10^{-9} 3.5704 14.763 ksi	1.2991×10^{-9} 3.6125 13.746 ksi	1.2984×10^{-9} 3.7195 9.344 ksi

TABLE 3-V. PREDICTED CRACK-GROWTH BEHAVIOR BY FLTGR, M-90

M - 90 WITH DIFFERENT MISSION PARAMETERS

CRACK GROWTH SUMMARY TABLE FOR EVERY 125 FLIGHTS

INITIAL CRACK = .1525

19/24/79

125	.1536	.1548	.1559	.1571	.1583	.1595	.1608	.1620	.1633	.1646
1375	.1659	.1672	.1586	.1699	.1713	.1727	.1742	.1756	.1771	.1786
2625	.1801	.1817	.1832	.1848	.1864	.1881	.1898	.1915	.1932	.1950
3875	.1968	.1986	.2005	.2023	.2043	.2062	.2082	.2102	.2123	.2144
5125	.2166	.2187	.2210	.2232	.2255	.2279	.2303	.2328	.2353	.2378
6375	.2404	.2431	.2458	.2485	.2514	.2543	.2572	.2602	.2633	.2665
7625	.2697	.2730	.2764	.2798	.2834	.2870	.2907	.2945	.2984	.3024
8875	.3065	.3107	.3151	.3195	.3240	.3287	.3335	.3385	.3436	.3488
10125	.3542	.3597	.3655	.3713	.3774	.3837	.3902	.3969	.4038	.4109
11375	.4183	.4260	.4339	.4421	.4507	.4595	.4687	.4783	.4863	.4987
12625	.5095	.5208	.5326	.5450	.5579	.5715	.5858	.6008	.6166	.6332
13875	.6509	.6695	.6894	.7115	.7330	.7570	.7829	.8107	.8408	.8735
15125	.9093	.9485	.9920	1.0406	1.0955	1.1582	1.2314	1.3187	1.4268	1.5688
16375	1.7774									

FINAL CRACK = 1.8713 OCCURRED IN FLIGHT 16409

TABLE 3-VI. PREDICTED CRACK-GROWTH BEHAVIOR BY FLTGR0, M-91

M - 91 WITH DIFFERENT MISSION PARAMETERS												09/24/79
CRACK GROWTH SUMMARY TABLE FOR EVERY 25 FLIGHTS												
INITIAL CRACK = .1500												
25	.1510	.1520	.1529	.1540	.1550	.1560	.1570	.1581	.1592	.1603		
275	.1613	.1625	.1636	.1647	.1659	.1670	.1682	.1694	.1706	.1719		
525	.1731	.1744	.1756	.1769	.1782	.1796	.1809	.1823	.1837	.1851		
775	.1865	.1879	.1894	.1909	.1924	.1939	.1955	.1971	.1987	.2003		
1025	.2019	.2036	.2053	.2070	.2088	.2105	.2123	.2142	.2160	.2179		
1275	.2198	.2216	.2234	.2252	.2270	.2289	.2320	.2342	.2364	.2386		
1525	.2409	.2432	.2455	.2479	.2503	.2528	.2553	.2579	.2605	.2632		
1775	.2659	.2687	.2715	.2744	.2773	.2803	.2833	.2865	.2896	.2929		
2025	.2962	.2996	.3030	.3065	.3101	.3138	.3176	.3214	.3254	.3294		
2275	.3335	.3377	.3420	.3464	.3510	.3556	.3603	.3652	.3702	.3753		
2525	.3606	.3660	.3715	.3770	.3831	.3891	.4053	.4216	.4282	.4349		
2775	.4419	.4491	.4565	.4641	.4720	.4801	.4885	.4972	.5062	.5156		
3025	.5252	.5353	.5457	.5565	.5677	.5794	.5916	.6043	.6176	.6314		
3275	.5459	.5611	.5770	.5937	.7113	.7298	.7494	.7701	.7920	.8153		
3525	.6401	.6667	.6951	.9208	.9509	.9950	1.0343	1.0777	1.1257	1.1795		

FINAL CRACK = 1.2033 OCCURRED IN FLIGHT 3756

TABLE 21. PREDICTED CRACK-GROWTH BEHAVIOR BY FLTGR0, M-92

09/24/79

M - 92 WITH DIFFERENT MISSION PARAMETERS

CRACK GROWTH SUMMARY TABLE FOR EVERY 25 FLIGHTS

INITIAL CRACK = .1570

25	.1527	.1556	.1585	.1615	.1647	.1679	.1713	.1744	.1784	.1821
275	.1860	.1901	.1943	.1987	.2033	.2080	.2130	.2182	.2236	.2293
525	.2352	.2415	.2480	.2548	.2621	.2697	.2777	.2861	.2951	.3045
775	.3146	.3252	.3366	.3487	.3617	.3756	.3905	.4065	.4239	.4426
1025	.4631	.4853	.5098	.5367	.5655	.5957	.6377	.6792	.7276	

FINAL CRACK = .7704 OCCURRED IN FLIGHT 1249

TABLE 22. SUMMARY, COMPARISON OF CRKGRO AND FLTGRO PROGRAM

PREDICTIVE ACCURACIES AND COSTS

Test case	Test life N_T (flight)	CRKGRO program			FLTGRO program		
		Predicted life N_p (flight)	R*	Computer cost (\$)	Predicted life N_p (flight)	R*	Computer cost (\$)
M-90 $\sigma_{lim} = 20$ ksi	10,352	15,561	1.5	22	16,409	1.59	0.96
M-91 $\sigma_{lim} = 30$ ksi	3,111	3,428	1.1	8	3,756	1.21	0.9
M-92 $\sigma_{lim} = 40$ ksi	1,052	1,111	1.06	3.56	1,240	1.18	0.73

$$*R = N_p/N_T$$

TABLE 23. FLTGRO INPUT EGHO

INDIVIDUAL AIRCRAFT TRACKING CRACK GROWTH ANALYSIS FLTGRO

M-83 AIR-TO-GROUND MISSION, 70 KSI

2214-1651, CENTERED THRU CRACK

CRACK GROWTH RATE EQUATION FOR CALCULATING C, LAMBDA, AND SIGMA:

$$DA/DN = C \cdot \Delta K \cdot (\Delta K / (1-R))^{(1-M)} \cdot \lambda$$

INPUT MATERIAL CONSTANTS AND CONTROL PARAMETERS

YIELD STRESS ----- SIGMA Y 42000 (PSI)
 KIC FOR A ----- AKIC 45000 (PSI*SQRT(INCH))
 KIC FOR C ----- CKIC 50000 (PSI*SQRT(INCH))
 POWER E .200 (L+J)
 WALKER'S COEFF ----- C 13.59E-19 FOR (PSI)
 WALKER'S COEFF ----- C 33.57E-09 FOR (KSI)
 EXP SMALL N ----- N 364
 DELTA K THRESHOLD ----- KTH 15000 (PSI*SQRT(INCH))
 EXP SMALL N ----- N 60
 R CUT-OFF ----- R-CUT 0.99

COMPRESSION STRESSES WILL BE LEFT IN THE SPECTRUM

R CUT-OFF ----- R-CUT 0.99
 EXP SMALL N ----- N 364

INITIAL CRACK SIZE C = SELECTED LATER (INCH)
 INITIAL CRACK DEFINITION A =
 ASPECT RATIO A/2C =
 PHI SQUARED ----- PHI 0.25
 EQUIVALENT THICKNESS T = 0.39 (INCH)
 HALF WIDTH ----- W/2 0.39 (INCH)

TYPE = 2 (PART THROUGH CRACK=1, THROUGH CRACK=2)
 LOCATION = 1 (CENTRAL CRACK=2)
 RETARD = 1 (N. RETARDATION=1)

TABLE 24. SAMPLE TRANSPORT DETAILED SIZING DATA

STATION 600.00

PANEL DETAIL GEOMETRIC DATA

PANEL NO.	END NODES	CONST TYPE	MATERIAL SKIN	NO. STIFF	SYMMETRY GROUP	DS	TBAR SKIN	YBAR SKIN	TBAR STIF	YBAR STIF
1	1, 2	5	1	2	1	24.93	.109	.054	.065	.774
2	2, 3	5	1	2	1	24.67	.109	.054	.065	.774
3	3, 4	5	1	2	1	24.65	.109	.054	.065	.774
4	4, 5	5	1	2	1	25.02	.109	.054	.065	.774
5	5, 6	21	3	0	3	21.58	.087	0.000	0.000	0.000
6	6, 7	5	1	2	2	24.65	.109	.055	.031	.720
7	7, 8	5	1	2	2	24.66	.109	.055	.031	.720
8	8, 9	5	1	2	2	24.65	.109	.055	.031	.720
9	9, 10	5	1	2	2	24.65	.109	.055	.031	.720
10	10, 1	21	3	0	4	23.37	.097	0.000	0.000	0.000

PANEL NO.	T1	T2	T3	T4	B1	B2	B3	B4
1	.109	.149	.081	.052	6.00	1.50	.74	2.00
2	.109	.149	.081	.052	6.00	1.50	.74	2.00
3	.109	.149	.081	.052	6.00	1.50	.74	2.00
4	.109	.149	.081	.052	6.00	1.50	.74	2.00
5	.070	.076	0.000	0.000	5.50	.66	0.00	0.00
6	.109	.076	.085	.040	7.50	1.50	.44	2.00
7	.109	.076	.085	.040	7.50	1.50	.44	2.00
8	.109	.076	.085	.040	7.50	1.50	.44	2.00
9	.109	.076	.085	.040	7.50	1.50	.44	2.00
10	.075	.090	0.000	0.000	5.50	.66	0.00	0.00

SPAR-CAP DETAIL GEOMETRIC DATA

ELEMENT NO.	NODE	CONST TYPE	MATERIAL NUMBER	SYMMETRY GROUP	ANGLE (DEG)	AREA	YBAR
1	1	2	3	1	0.00	.224	.283
2	5	2	3	1	0.00	.224	.283
3	6	2	3	2	180.00	.180	.277
4	10	2	3	2	180.00	.180	.277

ELEMENT NO.	T1	T2	T3	T4	B1	B2	B3	B4
1	.050	.050	.050	0.000	1.50	1.50	1.50	0.00
2	.050	.050	.050	0.000	1.50	1.50	1.50	0.00
3	.040	.040	.040	0.000	1.50	1.50	1.50	0.00
4	.040	.040	.040	0.000	1.50	1.50	1.50	0.00

TABLE 25. SAMPLE TRANSPORT-DESIGN STRESSES
STATION 600.00

ELEMENT APPLIED STRESSES

CONDITION		1	2	3	4
ELEMENT ID(TYPE)					
PANEL 1 (5)	SX	-24410.	9864.	10392.	-3531.
	SY	0.	0.	0.	0.
	SXY	7358.	-5916.	-5365.	-1533.
	SXST	-24650.	9961.	10494.	-3565.
PANEL 2 (5)	SX	-28322.	12052.	11956.	-3847.
	SY	0.	0.	0.	0.
	SXY	2874.	-3980.	-2346.	-2087.
	SXST	-28600.	12173.	12074.	-3885.
PANEL 3 (5)	SX	-27625.	12226.	11557.	-3561.
	SY	0.	0.	0.	0.
	SXY	-1849.	-1816.	762.	-2627.
	SXST	-27896.	12346.	11671.	-3596.
PANEL 4 (5)	SX	-21197.	3898.	8716.	-2524.
	SY	0.	0.	0.	0.
	SXY	-6143.	271.	3521.	-3075.
	SXST	-21405.	9995.	8802.	-2549.
PANEL 5 (21)	SX	11416.	-3605.	-5438.	2037.
	SY	0.	0.	0.	0.
	SXY	-12419.	2038.	7203.	-4997.
	SXST				
PANEL 6 (5)	SX	30455.	-12659.	-13291.	4233.
	SY	0.	0.	0.	0.
	SXY	-4894.	56.	2503.	-2805.
	SXST	30754.	-12783.	-13421.	4274.
PANEL 7 (5)	SX	30814.	-13294.	-13342.	4084.
	SY	0.	0.	0.	0.
	SXY	-796.	-1727.	-248.	-2307.
	SXST	31116.	-13425.	-13472.	4124.
PANEL 8 (5)	SX	30931.	-13824.	-13289.	3904.
	SY	0.	0.	0.	0.
	SXY	3410.	-3654.	-3016.	-1823.
	SXST	31234.	-13959.	-13419.	3942.
PANEL 9 (5)	SX	29990.	-13892.	-12786.	3586.
	SY	0.	0.	0.	0.
	SXY	7581.	-5661.	-5708.	-1380.
	SXST	30284.	-14028.	-12911.	3621.
PANEL 10 (21)	SX	6557.	-4486.	-2727.	175.
	SY	0.	0.	0.	0.
	SXY	15784.	-10687.	-11288.	-1564.
	SXST				
SPAR-CAP 1 (2)	SX	-31985.	12345.	13694.	-4867.
SPAR-CAP 2 (2)	SX	-24091.	11901.	9690.	-2608.
SPAR-CAP 3 (2)	SX	46946.	-19120.	-20576.	6684.
SPAR-CAP 4 (2)	SX	45121.	-21327.	-19158.	522.

TABLE 26. FLAW GROWTH ANALYSIS RESULTS USING PROGRO - TRANSPORT SPECTRUM

STATION 600.00

INITIAL CRACK SIZE • 2A 2.10 INCHES
INSPECTION INTERVAL 20000 FLIGHTS

PANEL NO.	SYMMETRY GROUP	MAXIMUM SPECTRUM STRESS (PSI)	MAXIMUM SPECTRUM STRESS STIFF. (PSI)	CRITICAL INITIAL FLAW SIZE (2A, IN.)	SAFE LIFE (FLIGHTS)	WEIGHT PENALTY (PERCENT)
1	1	5935.	6672.	29.516	2355+16	0.0
2	1	7701.	7858.	27.215	2375+16	0.0
3	1	7525.	7650.	27.750	2375+16	0.0
4	1	5738.	5794.	32.284	4445+16	0.0
5	1	10112.	10237.	2.179	2357+16	0.0
6	1	10131.	10239.	2.179	2357+16	0.0
7	1	10144.	10242.	2.179	2357+16	0.0
8	1	10159.	10241.	2.179	2357+16	0.0
9	1	10159.	10241.	2.179	2357+16	0.0
10	1	10159.	10241.	2.179	2357+16	0.0
11	1	10159.	10241.	2.179	2357+16	0.0
12	1	10159.	10241.	2.179	2357+16	0.0
13	1	10159.	10241.	2.179	2357+16	0.0
14	1	10159.	10241.	2.179	2357+16	0.0
15	1	10159.	10241.	2.179	2357+16	0.0
16	1	10159.	10241.	2.179	2357+16	0.0
17	1	10159.	10241.	2.179	2357+16	0.0
18	1	10159.	10241.	2.179	2357+16	0.0
19	1	10159.	10241.	2.179	2357+16	0.0
20	1	10159.	10241.	2.179	2357+16	0.0
21	1	10159.	10241.	2.179	2357+16	0.0
22	1	10159.	10241.	2.179	2357+16	0.0
23	1	10159.	10241.	2.179	2357+16	0.0
24	1	10159.	10241.	2.179	2357+16	0.0
25	1	10159.	10241.	2.179	2357+16	0.0
26	1	10159.	10241.	2.179	2357+16	0.0
27	1	10159.	10241.	2.179	2357+16	0.0
28	1	10159.	10241.	2.179	2357+16	0.0
29	1	10159.	10241.	2.179	2357+16	0.0
30	1	10159.	10241.	2.179	2357+16	0.0
31	1	10159.	10241.	2.179	2357+16	0.0
32	1	10159.	10241.	2.179	2357+16	0.0
33	1	10159.	10241.	2.179	2357+16	0.0
34	1	10159.	10241.	2.179	2357+16	0.0
35	1	10159.	10241.	2.179	2357+16	0.0
36	1	10159.	10241.	2.179	2357+16	0.0
37	1	10159.	10241.	2.179	2357+16	0.0
38	1	10159.	10241.	2.179	2357+16	0.0
39	1	10159.	10241.	2.179	2357+16	0.0
40	1	10159.	10241.	2.179	2357+16	0.0
41	1	10159.	10241.	2.179	2357+16	0.0
42	1	10159.	10241.	2.179	2357+16	0.0
43	1	10159.	10241.	2.179	2357+16	0.0
44	1	10159.	10241.	2.179	2357+16	0.0
45	1	10159.	10241.	2.179	2357+16	0.0
46	1	10159.	10241.	2.179	2357+16	0.0
47	1	10159.	10241.	2.179	2357+16	0.0
48	1	10159.	10241.	2.179	2357+16	0.0
49	1	10159.	10241.	2.179	2357+16	0.0
50	1	10159.	10241.	2.179	2357+16	0.0
51	1	10159.	10241.	2.179	2357+16	0.0
52	1	10159.	10241.	2.179	2357+16	0.0
53	1	10159.	10241.	2.179	2357+16	0.0
54	1	10159.	10241.	2.179	2357+16	0.0
55	1	10159.	10241.	2.179	2357+16	0.0
56	1	10159.	10241.	2.179	2357+16	0.0
57	1	10159.	10241.	2.179	2357+16	0.0
58	1	10159.	10241.	2.179	2357+16	0.0
59	1	10159.	10241.	2.179	2357+16	0.0
60	1	10159.	10241.	2.179	2357+16	0.0
61	1	10159.	10241.	2.179	2357+16	0.0
62	1	10159.	10241.	2.179	2357+16	0.0
63	1	10159.	10241.	2.179	2357+16	0.0
64	1	10159.	10241.	2.179	2357+16	0.0
65	1	10159.	10241.	2.179	2357+16	0.0
66	1	10159.	10241.	2.179	2357+16	0.0
67	1	10159.	10241.	2.179	2357+16	0.0
68	1	10159.	10241.	2.179	2357+16	0.0
69	1	10159.	10241.	2.179	2357+16	0.0
70	1	10159.	10241.	2.179	2357+16	0.0
71	1	10159.	10241.	2.179	2357+16	0.0
72	1	10159.	10241.	2.179	2357+16	0.0
73	1	10159.	10241.	2.179	2357+16	0.0
74	1	10159.	10241.	2.179	2357+16	0.0
75	1	10159.	10241.	2.179	2357+16	0.0
76	1	10159.	10241.	2.179	2357+16	0.0
77	1	10159.	10241.	2.179	2357+16	0.0
78	1	10159.	10241.	2.179	2357+16	0.0
79	1	10159.	10241.	2.179	2357+16	0.0
80	1	10159.	10241.	2.179	2357+16	0.0
81	1	10159.	10241.	2.179	2357+16	0.0
82	1	10159.	10241.	2.179	2357+16	0.0
83	1	10159.	10241.	2.179	2357+16	0.0
84	1	10159.	10241.	2.179	2357+16	0.0
85	1	10159.	10241.	2.179	2357+16	0.0
86	1	10159.	10241.	2.179	2357+16	0.0
87	1	10159.	10241.	2.179	2357+16	0.0
88	1	10159.	10241.	2.179	2357+16	0.0
89	1	10159.	10241.	2.179	2357+16	0.0
90	1	10159.	10241.	2.179	2357+16	0.0
91	1	10159.	10241.	2.179	2357+16	0.0
92	1	10159.	10241.	2.179	2357+16	0.0
93	1	10159.	10241.	2.179	2357+16	0.0
94	1	10159.	10241.	2.179	2357+16	0.0
95	1	10159.	10241.	2.179	2357+16	0.0
96	1	10159.	10241.	2.179	2357+16	0.0
97	1	10159.	10241.	2.179	2357+16	0.0
98	1	10159.	10241.	2.179	2357+16	0.0
99	1	10159.	10241.	2.179	2357+16	0.0
100	1	10159.	10241.	2.179	2357+16	0.0

TABLE 27. FLAW GROWTH ANALYSIS RESULTS USING PRDGRO
WITHOUT RETARDATION - TRANSPORT SPECTRUM

INITIAL CRACK SIZE, 2A 2.000 INCHES
INSPECTION INTERVAL 2000. FLIGHTS

PANEL NO.	SYMMETRY GROUP	MAXIMUM SPECTRUM STRESS SKIN (PSI)	MAXIMUM SPECTRUM STRESS STIFF. (PSI)	CRITICAL INITIAL FLAW SIZE (2A, IN.)	SAFE LIFE (FLIGHTS)	WEIGHT PENALTY (PERCENT)
1	1	5832.	5847.	29.531	.245E+06	.00
2	1	7732.	7853.	27.217	.142E+06	.00
3	1	7526.	7611.	27.785	.161E+06	.00
4	1	5733.	5784.	32.320	.476E+06	.00
5	3	12134.	12317.	2.175	.215E+05	7.74
6	2	12213.	12333.	2.000	.210E+05	7.74
7	2	12134.	12243.	2.034	.211E+05	7.74
8	2	11517.	11721.	2.964	.234E+05	7.74
9	4	1.	1.	0.000	.	.00

TABLE 28. FLAW GROWTH ANALYSIS RESULTS USING PRDGRO
WITH RETARDATION - TRANSPORT SPECTRUM

INITIAL CRACK SIZE, 2A 2.000 INCHES
INSPECTION INTERVAL 2000. FLIGHTS

PANEL NO.	SYMMETRY GROUP	MAXIMUM SPECTRUM STRESS SKIN (PSI)	MAXIMUM SPECTRUM STRESS STIFF. (PSI)	CRITICAL INITIAL FLAW SIZE (2A, IN.)	SAFE LIFE (FLIGHTS)	WEIGHT PENALTY (PERCENT)
1	1	5788.	5855.	29.615	.245E+06	.00
2	1	7793.	7852.	27.257	.142E+06	.00
3	1	7524.	7612.	27.816	.162E+06	.00
4	1	5711.	5768.	32.418	.488E+06	.00
5	3	12533.	12642.	2.164	.215E+05	4.19
6	2	12573.	12696.	2.110	.199E+05	4.19
7	2	12421.	12614.	2.014	.212E+05	4.19
8	2	11911.	12087.	2.920	.233E+05	4.19
9	4	1.	1.	0.000	.	.00

TABLE 29. FLAW GROWTH ANALYSIS RESULTS USING PREGRO
WITHOUT RETARDATION - TRANSPORT SPECTRUM

INITIAL CRACK SIZE, CA 2.000 INCHES
INSPECTION INTERVAL 20000 FLIGHTS

PANEL NO.	SYMMETRY GROUP	MAXIMUM SPECTRUM STRESS SKIN (PSI)	MAXIMUM SPECTRUM STRESS STIFF. (PSI)	CRITICAL INITIAL FLAW SIZE (2A, IN.)	SAFE LIFE (FLIGHTS)	WEIGHT PENALTY (PERCENT)
1	1	5500.	5872.	29.614	.234E+06	.00
2	1	7721.	7858.	27.212	.137E+06	.00
3	1	7525.	7644.	27.737	.157E+06	.00
4	1	5735.	5795.	32.488	.464E+06	.00
5	2	12113.	12232.	2.177	.215E+06	1.00
6	2	12125.	12244.	2.130	.212E+06	8.61
7	2	12133.	12157.	2.136	.211E+06	8.61
8	2	11623.	11639.	2.444	.217E+06	5.61
9	4	11623.	11639.	2.444	.217E+06	5.61

TABLE 30. FLAW GROWTH ANALYSIS RESULTS USING PREGRO
WITH RETARDATION - TRANSPORT SPECTRUM

INITIAL CRACK SIZE, CA 2.000 INCHES
INSPECTION INTERVAL 20000 FLIGHTS

PANEL NO.	SYMMETRY GROUP	MAXIMUM SPECTRUM STRESS SKIN (PSI)	MAXIMUM SPECTRUM STRESS STIFF. (PSI)	CRITICAL INITIAL FLAW SIZE (2A, IN.)	SAFE LIFE (FLIGHTS)	WEIGHT PENALTY (PERCENT)
1	1	5721.	5846.	29.729	.241E+06	.00
2	1	7721.	7858.	27.247	.138E+06	.00
3	1	7525.	7644.	27.835	.158E+06	.00
4	1	5735.	5751.	32.587	.444E+06	.00
5	2	12113.	12116.	2.172	.215E+06	1.00
6	2	12125.	12125.	2.130	.212E+06	1.00
7	2	12133.	12140.	2.141	.211E+06	1.00
8	2	11623.	11633.	2.441	.217E+06	1.00
9	4	11623.	11613.	2.441	.217E+06	1.00

TABLE 31. SAMPLE FIGHTER-DETAIL-SIZING DATA

STATION 21.64

PANEL DETAIL GEOMETRIC DATA

PANEL NO.	END NODES	CONST TYPE	MATERIAL SKIN	NO. STIFF	SYMMETRY GROUP	DS	TBAR SKIN	YBAR SKIN	TBAR STIF	YBAR STIF
1	1, 2	1	1	0	1	22.63	.254	.195	0.000	0.000
2	2, 3	1	1	0	1	22.63	.254	.195	0.000	0.000
3	3, 4	1	1	0	1	22.65	.254	.195	0.000	0.000
4	4, 5	1	1	0	1	22.66	.254	.195	0.000	0.000
5	5, 6	21	1	0	2	2.76	.273	0.000	0.000	0.000
6	6, 7	1	1	0	2	22.65	.212	.153	0.000	0.000
7	7, 8	1	1	0	2	22.64	.212	.153	0.000	0.000
8	8, 9	1	1	0	2	22.63	.212	.153	0.000	0.000
9	9, 10	1	1	0	2	22.63	.212	.153	0.000	0.000
10	10, 1	21	1	0	4	6.36	.200	0.000	0.000	0.000

PANEL NO	T1	T2	T3	T4	B1	B2	B3	B4
1	.229	.145	0.000	0.000	8.00	1.39	0.00	0.00
2	.229	.145	0.000	0.000	8.00	1.39	0.00	0.00
3	.229	.145	0.000	0.000	8.00	1.39	0.00	0.00
4	.229	.145	0.000	0.000	8.00	1.39	0.00	0.00
5	.198	.186	0.000	0.000	5.00	1.00	0.00	0.00
6	.192	.164	0.000	0.000	8.00	1.00	0.00	0.00
7	.192	.164	0.000	0.000	8.00	1.00	0.00	0.00
8	.192	.164	0.000	0.000	8.00	1.00	0.00	0.00
9	.192	.164	0.000	0.000	8.00	1.00	0.00	0.00
10	.135	.163	0.000	0.000	5.00	1.00	0.00	0.00

SPAR-CAP DETAIL GEOMETRIC DATA

ELEMENT NO.	NODE	CONST TYPE	MATERIAL NUMBER	SYMMETRY GROUP	ANGLE (DEG)	AREA	YBAR
1	1	2	1	1	0.00	.405	.169
2	5	2	1	1	0.00	.405	.169
3	6	2	1	2	180.00	.370	.146
4	10	2	1	2	180.00	.370	.146

ELEMENT NO.	T1	T2	T3	T4	B1	B2	B3	B4
1	.172	.176	.057	0.000	1.00	1.00	1.00	0.00
2	.172	.176	.057	0.000	1.00	1.00	1.00	0.00
3	.176	.153	.040	0.000	1.00	1.00	1.00	0.00
4	.176	.153	.040	0.000	1.00	1.00	1.00	0.00

TABLE 32. SAMPLE FIGHTER-DESIGN STRESSES

STATION 21.64

ELEMENT APPLIED STRESSES

CONDITION			1	2	3	4
ELEMENT ID (TYPE)						
PANEL	1 (1)	SX	-22386.	11503.	-11387.	-5195.
		SY	0.	0.	0.	0.
		SXY	8760.	-4532.	-5684.	5427.
PANEL	2 (1)	SX	-23654.	12154.	-12031.	-5485.
		SY	0.	0.	0.	0.
		SXY	-1867.	225.	-7894.	4160.
PANEL	3 (1)	SX	-19902.	10226.	-10123.	-4615.
		SY	0.	0.	0.	0.
		SXY	-11906.	4702.	-9974.	2967.
PANEL	4 (1)	SX	-12496.	6421.	-6356.	-2900.
		SY	0.	0.	0.	0.
		SXY	-19133.	7931.	-11474.	2106.
PANEL	5 (21)	SX	2038.	-1047.	1037.	473.
		SY	0.	0.	0.	0.
		SXY	-24639.	10297.	-13769.	2124.
PANEL	6 (1)	SX	15515.	-7972.	7892.	3601.
		SY	0.	0.	0.	0.
		SXY	-22197.	9181.	-13567.	2593.
PANEL	7 (1)	SX	21801.	-11202.	11089.	5055.
		SY	0.	0.	0.	0.
		SXY	-13791.	5425.	-11822.	3594.
PANEL	8 (1)	SX	26390.	-13560.	13423.	6124.
		SY	0.	0.	0.	0.
		SXY	-2660.	451.	-9512.	4919.
PANEL	9 (1)	SX	27252.	-14003.	13861.	6324.
		SY	0.	0.	0.	0.
		SXY	9880.	-5152.	-6909.	6412.
PANEL	10 (21)	SX	3048.	-1566.	1550.	707.
		SY	0.	0.	0.	0.
		SXY	24104.	-11818.	-7730.	10311.
SPAR-CAP	1 (2)	SX	-19175.	9853.	-9753.	-4450.
SPAR-CAP	2 (2)	SX	-6898.	3545.	-3509.	-1601.
SPAR-CAP	3 (2)	SX	11148.	-5728.	5670.	2587.
SPAR-CAP	4 (2)	SX	25444.	-13074.	12942.	5905.

TABLE 33. FLAW GROWTH ANALYSIS RESULTS
USING PROGRO - FIGHTER SPECTRUM

INITIAL CRACK SIZE • 24 1.00 INCHES
INSPECTION INTERVAL 4000 FLIGHTS

PANEL NO.	SYMMETRY GROUP	MAXIMUM SPECTRUM STRESS SKIN (PSI)	MAXIMUM SPECTRUM STRESS STIFF. (PSI)	CRITICAL INITIAL FLAW SIZE (2A, IN.)	SAFE LIFE (FLIGHTS)	WEIGHT PENALTY (PERCENT)
1	1	3349.	7349.	47.632	.241E+16	.00
2	1	3491.	7481.	47.571	.217E+16	.00
3	1	2923.	2923.	47.786	.416E+16	.00
4	1	1863.	1863.	47.665	.252E+16	.00
5	1	1863.	1863.	47.665	.252E+16	.00
6	1	1863.	1863.	47.665	.252E+16	.00
7	1	1863.	1863.	47.665	.252E+16	.00
8	1	1863.	1863.	47.665	.252E+16	.00
9	1	1863.	1863.	47.665	.252E+16	.00
10	1	1863.	1863.	47.665	.252E+16	.00
11	1	1863.	1863.	47.665	.252E+16	.00
12	1	1863.	1863.	47.665	.252E+16	.00
13	1	1863.	1863.	47.665	.252E+16	.00
14	1	1863.	1863.	47.665	.252E+16	.00
15	1	1863.	1863.	47.665	.252E+16	.00
16	1	1863.	1863.	47.665	.252E+16	.00
17	1	1863.	1863.	47.665	.252E+16	.00
18	1	1863.	1863.	47.665	.252E+16	.00
19	1	1863.	1863.	47.665	.252E+16	.00
20	1	1863.	1863.	47.665	.252E+16	.00
21	1	1863.	1863.	47.665	.252E+16	.00
22	1	1863.	1863.	47.665	.252E+16	.00
23	1	1863.	1863.	47.665	.252E+16	.00
24	1	1863.	1863.	47.665	.252E+16	.00
25	1	1863.	1863.	47.665	.252E+16	.00
26	1	1863.	1863.	47.665	.252E+16	.00
27	1	1863.	1863.	47.665	.252E+16	.00
28	1	1863.	1863.	47.665	.252E+16	.00
29	1	1863.	1863.	47.665	.252E+16	.00
30	1	1863.	1863.	47.665	.252E+16	.00
31	1	1863.	1863.	47.665	.252E+16	.00
32	1	1863.	1863.	47.665	.252E+16	.00
33	1	1863.	1863.	47.665	.252E+16	.00
34	1	1863.	1863.	47.665	.252E+16	.00
35	1	1863.	1863.	47.665	.252E+16	.00
36	1	1863.	1863.	47.665	.252E+16	.00
37	1	1863.	1863.	47.665	.252E+16	.00
38	1	1863.	1863.	47.665	.252E+16	.00
39	1	1863.	1863.	47.665	.252E+16	.00
40	1	1863.	1863.	47.665	.252E+16	.00
41	1	1863.	1863.	47.665	.252E+16	.00
42	1	1863.	1863.	47.665	.252E+16	.00
43	1	1863.	1863.	47.665	.252E+16	.00
44	1	1863.	1863.	47.665	.252E+16	.00
45	1	1863.	1863.	47.665	.252E+16	.00
46	1	1863.	1863.	47.665	.252E+16	.00
47	1	1863.	1863.	47.665	.252E+16	.00
48	1	1863.	1863.	47.665	.252E+16	.00
49	1	1863.	1863.	47.665	.252E+16	.00
50	1	1863.	1863.	47.665	.252E+16	.00
51	1	1863.	1863.	47.665	.252E+16	.00
52	1	1863.	1863.	47.665	.252E+16	.00
53	1	1863.	1863.	47.665	.252E+16	.00
54	1	1863.	1863.	47.665	.252E+16	.00
55	1	1863.	1863.	47.665	.252E+16	.00
56	1	1863.	1863.	47.665	.252E+16	.00
57	1	1863.	1863.	47.665	.252E+16	.00
58	1	1863.	1863.	47.665	.252E+16	.00
59	1	1863.	1863.	47.665	.252E+16	.00
60	1	1863.	1863.	47.665	.252E+16	.00
61	1	1863.	1863.	47.665	.252E+16	.00
62	1	1863.	1863.	47.665	.252E+16	.00
63	1	1863.	1863.	47.665	.252E+16	.00
64	1	1863.	1863.	47.665	.252E+16	.00
65	1	1863.	1863.	47.665	.252E+16	.00
66	1	1863.	1863.	47.665	.252E+16	.00
67	1	1863.	1863.	47.665	.252E+16	.00
68	1	1863.	1863.	47.665	.252E+16	.00
69	1	1863.	1863.	47.665	.252E+16	.00
70	1	1863.	1863.	47.665	.252E+16	.00
71	1	1863.	1863.	47.665	.252E+16	.00
72	1	1863.	1863.	47.665	.252E+16	.00
73	1	1863.	1863.	47.665	.252E+16	.00
74	1	1863.	1863.	47.665	.252E+16	.00
75	1	1863.	1863.	47.665	.252E+16	.00
76	1	1863.	1863.	47.665	.252E+16	.00
77	1	1863.	1863.	47.665	.252E+16	.00
78	1	1863.	1863.	47.665	.252E+16	.00
79	1	1863.	1863.	47.665	.252E+16	.00
80	1	1863.	1863.	47.665	.252E+16	.00
81	1	1863.	1863.	47.665	.252E+16	.00
82	1	1863.	1863.	47.665	.252E+16	.00
83	1	1863.	1863.	47.665	.252E+16	.00
84	1	1863.	1863.	47.665	.252E+16	.00
85	1	1863.	1863.	47.665	.252E+16	.00
86	1	1863.	1863.	47.665	.252E+16	.00
87	1	1863.	1863.	47.665	.252E+16	.00
88	1	1863.	1863.	47.665	.252E+16	.00
89	1	1863.	1863.	47.665	.252E+16	.00
90	1	1863.	1863.	47.665	.252E+16	.00
91	1	1863.	1863.	47.665	.252E+16	.00
92	1	1863.	1863.	47.665	.252E+16	.00
93	1	1863.	1863.	47.665	.252E+16	.00
94	1	1863.	1863.	47.665	.252E+16	.00
95	1	1863.	1863.	47.665	.252E+16	.00
96	1	1863.	1863.	47.665	.252E+16	.00
97	1	1863.	1863.	47.665	.252E+16	.00
98	1	1863.	1863.	47.665	.252E+16	.00
99	1	1863.	1863.	47.665	.252E+16	.00
100	1	1863.	1863.	47.665	.252E+16	.00

TABLE 34. FLAW GROWTH ANALYSIS RESULTS USING PRDGRO
WITHOUT RETARDATION - FIGHTER SPECTRUM

INITIAL CRACK SIZE: 2A 1.10 INCHES
INSPECTION INTERVAL 4000 FLIGHTS

PANEL NO.	SYMMETRY GROUP	MAXIMUM SPECTRUM STRESS (PSI)	MAXIMUM SPECTRUM STRESS STIFF. (PSI)	CRITICAL INITIAL FLAW SIZE (2A.IN.)	SAFE LIFE (FLIGHTS)	WEIGHT PENALTY (PERCENT)
1	1	3370.	3335.	47.575	.275E+02	.00
		3401.	3481.	47.575	.274E+02	.00
		2920.	2925.	47.786	.471E+02	.00
		1856.	1856.	47.965	.290E+02	.00
		1130.	1130.	7.671	.406E+05	13.37
		10813.	10813.	2.619	.111E+05	13.37
		10911.	10911.	1.245	.461E+04	13.37
		1938.	1938.	1.057	.415E+04	13.37
	2	3370.	3335.	47.575	.275E+02	.00
		3401.	3481.	47.575	.274E+02	.00
		2920.	2925.	47.786	.471E+02	.00
		1856.	1856.	47.965	.290E+02	.00
		1130.	1130.	7.671	.406E+05	13.37
		10813.	10813.	2.619	.111E+05	13.37
		10911.	10911.	1.245	.461E+04	13.37
		1938.	1938.	1.057	.415E+04	13.37

TABLE 35. FLAW GROWTH ANALYSIS RESULTS USING PRDGRO
WITH RETARDATION - FIGHTER SPECTRUM

INITIAL CRACK SIZE: 2A 1.10 INCHES
INSPECTION INTERVAL 4000 FLIGHTS

PANEL NO.	SYMMETRY GROUP	MAXIMUM SPECTRUM STRESS (PSI)	MAXIMUM SPECTRUM STRESS STIFF. (PSI)	CRITICAL INITIAL FLAW SIZE (2A.IN.)	SAFE LIFE (FLIGHTS)	WEIGHT PENALTY (PERCENT)
1	1	3370.	3335.	47.575	.275E+02	.00
		3401.	3481.	47.575	.274E+02	.00
		2920.	2925.	47.786	.471E+02	.00
		1856.	1856.	47.965	.290E+02	.00
		1130.	1130.	7.671	.406E+05	13.37
		10813.	10813.	2.619	.111E+05	13.37
		10911.	10911.	1.245	.461E+04	13.37
		1938.	1938.	1.057	.415E+04	13.37
	2	3370.	3335.	47.575	.275E+02	.00
		3401.	3481.	47.575	.274E+02	.00
		2920.	2925.	47.786	.471E+02	.00
		1856.	1856.	47.965	.290E+02	.00
		1130.	1130.	7.671	.406E+05	13.37
		10813.	10813.	2.619	.111E+05	13.37
		10911.	10911.	1.245	.461E+04	13.37
		1938.	1938.	1.057	.415E+04	13.37

TABLE 36. FLAW GROWTH ANALYSIS RESULTS USING PREGRO
WITHOUT RETARDATION - FIGHTER SPECTRUM

INITIAL CRACK SIZE, 2A 1.00 INCHES
INSPECTION INTERVAL 4000 FLIGHTS

PANEL NO.	SYMMETRY GROUP	MAXIMUM SPECTRUM STRESS (PSI)	MAXIMUM SPECTRUM STRESS STIFF. (PSI)	CRITICAL INITIAL FLAW SIZE (2A, IN.)	SAFE LIFE (FLIGHTS)	WEIGHT PENALTY (PERCENT)
1	1	3343.	3343.	47.613	.243E+08	.00
2	1	3405.	3405.	47.543	.235E+08	.00
3	1	2927.	2927.	47.772	.413E+08	.00
4	1	1859.	1859.	47.863	.254E+08	.00
5	1	1114.	1114.	7.251	.367E+05	16.98
6	1	1564.	1564.	2.629	.325E+04	16.98
7	1	1381.	1381.	1.117	.432E+04	16.98
8	1	1924.	1924.	1.000	.393E+04	16.98
9	1	1114.	1114.	7.251	.367E+05	16.98
10	1	1564.	1564.	2.629	.325E+04	16.98
11	1	1381.	1381.	1.117	.432E+04	16.98
12	1	1924.	1924.	1.000	.393E+04	16.98
13	1	1114.	1114.	7.251	.367E+05	16.98
14	1	1564.	1564.	2.629	.325E+04	16.98
15	1	1381.	1381.	1.117	.432E+04	16.98
16	1	1924.	1924.	1.000	.393E+04	16.98
17	1	1114.	1114.	7.251	.367E+05	16.98
18	1	1564.	1564.	2.629	.325E+04	16.98
19	1	1381.	1381.	1.117	.432E+04	16.98
20	1	1924.	1924.	1.000	.393E+04	16.98
21	1	1114.	1114.	7.251	.367E+05	16.98
22	1	1564.	1564.	2.629	.325E+04	16.98
23	1	1381.	1381.	1.117	.432E+04	16.98
24	1	1924.	1924.	1.000	.393E+04	16.98
25	1	1114.	1114.	7.251	.367E+05	16.98
26	1	1564.	1564.	2.629	.325E+04	16.98
27	1	1381.	1381.	1.117	.432E+04	16.98
28	1	1924.	1924.	1.000	.393E+04	16.98
29	1	1114.	1114.	7.251	.367E+05	16.98
30	1	1564.	1564.	2.629	.325E+04	16.98
31	1	1381.	1381.	1.117	.432E+04	16.98
32	1	1924.	1924.	1.000	.393E+04	16.98
33	1	1114.	1114.	7.251	.367E+05	16.98
34	1	1564.	1564.	2.629	.325E+04	16.98
35	1	1381.	1381.	1.117	.432E+04	16.98
36	1	1924.	1924.	1.000	.393E+04	16.98
37	1	1114.	1114.	7.251	.367E+05	16.98
38	1	1564.	1564.	2.629	.325E+04	16.98
39	1	1381.	1381.	1.117	.432E+04	16.98
40	1	1924.	1924.	1.000	.393E+04	16.98
41	1	1114.	1114.	7.251	.367E+05	16.98
42	1	1564.	1564.	2.629	.325E+04	16.98
43	1	1381.	1381.	1.117	.432E+04	16.98
44	1	1924.	1924.	1.000	.393E+04	16.98
45	1	1114.	1114.	7.251	.367E+05	16.98
46	1	1564.	1564.	2.629	.325E+04	16.98
47	1	1381.	1381.	1.117	.432E+04	16.98
48	1	1924.	1924.	1.000	.393E+04	16.98
49	1	1114.	1114.	7.251	.367E+05	16.98
50	1	1564.	1564.	2.629	.325E+04	16.98
51	1	1381.	1381.	1.117	.432E+04	16.98
52	1	1924.	1924.	1.000	.393E+04	16.98
53	1	1114.	1114.	7.251	.367E+05	16.98
54	1	1564.	1564.	2.629	.325E+04	16.98
55	1	1381.	1381.	1.117	.432E+04	16.98
56	1	1924.	1924.	1.000	.393E+04	16.98
57	1	1114.	1114.	7.251	.367E+05	16.98
58	1	1564.	1564.	2.629	.325E+04	16.98
59	1	1381.	1381.	1.117	.432E+04	16.98
60	1	1924.	1924.	1.000	.393E+04	16.98
61	1	1114.	1114.	7.251	.367E+05	16.98
62	1	1564.	1564.	2.629	.325E+04	16.98
63	1	1381.	1381.	1.117	.432E+04	16.98
64	1	1924.	1924.	1.000	.393E+04	16.98
65	1	1114.	1114.	7.251	.367E+05	16.98
66	1	1564.	1564.	2.629	.325E+04	16.98
67	1	1381.	1381.	1.117	.432E+04	16.98
68	1	1924.	1924.	1.000	.393E+04	16.98
69	1	1114.	1114.	7.251	.367E+05	16.98
70	1	1564.	1564.	2.629	.325E+04	16.98
71	1	1381.	1381.	1.117	.432E+04	16.98
72	1	1924.	1924.	1.000	.393E+04	16.98
73	1	1114.	1114.	7.251	.367E+05	16.98
74	1	1564.	1564.	2.629	.325E+04	16.98
75	1	1381.	1381.	1.117	.432E+04	16.98
76	1	1924.	1924.	1.000	.393E+04	16.98
77	1	1114.	1114.	7.251	.367E+05	16.98
78	1	1564.	1564.	2.629	.325E+04	16.98
79	1	1381.	1381.	1.117	.432E+04	16.98
80	1	1924.	1924.	1.000	.393E+04	16.98
81	1	1114.	1114.	7.251	.367E+05	16.98
82	1	1564.	1564.	2.629	.325E+04	16.98
83	1	1381.	1381.	1.117	.432E+04	16.98
84	1	1924.	1924.	1.000	.393E+04	16.98
85	1	1114.	1114.	7.251	.367E+05	16.98
86	1	1564.	1564.	2.629	.325E+04	16.98
87	1	1381.	1381.	1.117	.432E+04	16.98
88	1	1924.	1924.	1.000	.393E+04	16.98
89	1	1114.	1114.	7.251	.367E+05	16.98
90	1	1564.	1564.	2.629	.325E+04	16.98
91	1	1381.	1381.	1.117	.432E+04	16.98
92	1	1924.	1924.	1.000	.393E+04	16.98
93	1	1114.	1114.	7.251	.367E+05	16.98
94	1	1564.	1564.	2.629	.325E+04	16.98
95	1	1381.	1381.	1.117	.432E+04	16.98
96	1	1924.	1924.	1.000	.393E+04	16.98
97	1	1114.	1114.	7.251	.367E+05	16.98
98	1	1564.	1564.	2.629	.325E+04	16.98
99	1	1381.	1381.	1.117	.432E+04	16.98
100	1	1924.	1924.	1.000	.393E+04	16.98

TABLE 37. FLAW GROWTH ANALYSIS RESULTS USING PREGRO
WITH RETARDATION - FIGHTER SPECTRUM

INITIAL CRACK SIZE, 2A 1.00 INCHES
INSPECTION INTERVAL 4000 FLIGHTS

PANEL NO.	SYMMETRY GROUP	MAXIMUM SPECTRUM STRESS (PSI)	MAXIMUM SPECTRUM STRESS STIFF. (PSI)	CRITICAL INITIAL FLAW SIZE (2A, IN.)	SAFE LIFE (FLIGHTS)	WEIGHT PENALTY (PERCENT)
1	1	3291.	3291.	47.772	.415E+08	.00
2	1	3477.	3477.	47.715	.335E+08	.00
3	1	2926.	2926.	47.855	.520E+08	.00
4	1	1847.	1847.	47.878	.430E+08	.00
5	1	1114.	1114.	7.251	.367E+05	16.98
6	1	1224.	1224.	7.810	.415E+05	16.98
7	1	1721.	1721.	2.609	.115E+04	16.98
8	1	1522.	1522.	1.206	.405E+04	16.98
9	1	2152.	2152.	1.027	.417E+04	16.98
10	1	1114.	1114.	7.251	.367E+05	16.98
11	1	1224.	1224.	7.810	.415E+05	16.98
12	1	1721.	1721.	2.609	.115E+04	16.98
13	1	1522.	1522.	1.206	.405E+04	16.98
14	1	2152.	2152.	1.027	.417E+04	16.98
15	1	1114.	1114.	7.251	.367E+05	16.98
16	1	1224.	1224.	7.810	.415E+05	16.98
17	1	1721.	1721.	2.609	.115E+04	16.98
18	1	1522.	1522.	1.206	.405E+04	16.98
19	1	2152.	2152.	1.027	.417E+04	16.98
20	1	1114.	1114.	7.251	.367E+05	16.98
21	1	1224.	1224.	7.810	.415E+05	16.98
22	1	1721.	1721.	2.609	.115E+04	16.98
23	1	1522.	1522.	1.206	.405E+04	16.98
24	1	2152.	2152.	1.027	.417E+04	16.98
25	1	1114.	1114.	7.251	.367E+05	16.98
26	1	1224.	1224.	7.810	.415E+05	16.98
27	1	1721.	1721.	2.609	.115E+04	16.98
28	1	1522.	1522.	1.206	.405E+04	16.98
29	1	2152.	2152.	1.027	.417E+04	16.98
30	1	1114.	1114.	7.251	.367E+05	16.98
31	1	1224.	1224.	7.810	.415E+05	16.98
32	1	1721.	1721.	2.609	.115E+04	16.98
33	1	1522.	1522.	1.206	.405E+04	16.98
34	1	2152.	2152.	1.027	.417E+04	16.98
35	1	1114.	1114.	7.251	.367E+05	16.98
36	1	1224.	1224.	7.810	.415E+05	16.98
37	1	1721.	1721.	2.609	.115E+04	16.98
38	1	1522.	1522.	1.206	.405E+04	16.98
39	1	2152.	2152.	1.027	.417E+04	16.98
40	1	1114.	1114.	7.251	.367E+05	16.98
41	1	1224.	1224.	7.810	.415E+05	16.98
42	1	1721.	1721.	2.609	.115E+04	16.98
43	1	1522.	1522.	1.206	.405E+04	16.98
44	1	2152.	2152.	1.027	.417E+04	16.98
45	1	1114.	1114.	7.251	.367E+05	16.98
46	1	1224.	1224.	7.810	.415E+05	16.98
47	1	1721.	1721.	2.609	.115E+04	16.98
48	1	1522.	1522.	1.206	.405E+04	16.98
49	1	2152.	2152.	1.027	.417E+04	16.98
50	1	1114.	1114.	7.251	.367E+05	16.98
51	1	1224.	1224.	7.810	.415E+05	16.98
52	1	1721.	1721.	2.609	.115E+04	16.98
53	1	1522.	1522.	1.206	.405E+04	16.98
54	1	2152.	2152.	1.027	.417E+04	16.98
55	1	1114.	1114.	7.251	.367E+05	16.98
56	1	1224.	1224.	7.810	.415E+05	16.98
57	1	1721.	1721.	2.609	.115E+04	16.98
58	1	1522.	1522.	1.206	.405E+04	16.98
59	1	2152.	2152.	1.027	.417E+04	16.98
60	1	1114.	1114.	7.251	.367E+05	16.98
61	1	1224.	1224.	7.810	.415E+05	16.98
62	1	1721.	1721.	2.609	.115E+04	16.98
63	1	1522.	1522.	1.206	.405E+04	16.98
64	1	2152.	2152.	1.027	.417E+04	16.98
65	1	1114.	1114.	7.251	.367E+05	16.98
66	1	1224.	1224.	7.810	.415E+05	16.98
67	1	1721.	1721.	2.609	.115E+04	16.98
68	1	1522.	1522.	1.206	.405E+04	16.98
69	1	2152.	2152.	1.027	.417E+04	16.98
70	1	1114.	1114.	7.251	.367E+05	16.98
71	1	1224.	1224.	7.810	.415E+05	16.98
72	1	1721.	1721.	2.609	.115E+04	16.98
73	1	1522.	1522.	1.206	.405E+04	16.98
74	1	2152.	2152.	1.027	.417E+04	16.98
75	1	1114.	1114.	7.251	.367E+05	16.98
76	1	1224.	1224.	7.810	.415E+05	16.98
77	1	1721.	1721.	2.609	.115E+04	16.98
78	1	1522.	1522.	1.206	.405E+04	16.98
79	1	2152.	2152.	1.027	.417E+04	16.98
80	1	1114.	1114.	7.251	.367E+05	16.98
81	1	1224.	1224.	7.810	.415E+05	16.98
82	1	1721.	1721.	2.609	.115E+04	16.98
83	1	1522.	1522.	1.206	.405E+04	16.98
84	1	2152.	2152.	1.027	.417E+04	16.98
85	1	1114.	1114.	7.251	.367E+05	16.98
86	1	1224.	1224.	7.810	.415E+05	16.98
87	1	1721.	1721.	2.609	.115E+04	16.98
88	1	1522.	1522.	1.206	.405E+04	16.98
89	1	2152.	2152.	1.027	.417E+04	16.98
90	1	1114.	1114.	7.251	.367E+05	16.98
91	1	1224.	1224.	7.810	.415E+05	16.98
92	1	1721.	1721.	2.609	.115E+04	16.98
93	1	1522.	1522.	1.206	.405E+04	16.98
94	1	2152.	2152.	1.027	.417E+04	16.98
95	1	1114.	1114.	7.251	.367E+05	16.98
96	1	1224.	1224.	7.810	.415E+05	16.98
97	1	1721.	1721.	2.609	.115E+04	16.98
98	1	1522.	1522.	1.206	.405E+04	16.98
99	1	2152.	2152.	1.027	.417E+04	16.98
100	1	1114.	1114.	7.251	.367E+05	16.98

TABLE 38. PRELIMINARY FRACTURE MECHANICS MATERIAL PROPERTY LIBRARY DATA

Material (Basis) Properties	Aluminum (2219-T851)	Titanium (6Al-4V RA)	Steel (Inco 718)
C - growth-rate equation coefficient (psi units)	1.0059E-20	1.107E-23	1.99E-24
m - growth-rate equation (1-R) exponent	0.6	0.5	0.32
n - growth-rate equation exponent	3.64	4.07	4.01
q - acceleration model exponent	0.3	0.3	0.3
k_c - plane stress fracture toughness, psi $\sqrt{\text{in.}}$	92,000	140,000	170,000
k_{Ic} - plane strain fracture toughness, psi $\sqrt{\text{in.}}$	45,000	70,000	85,000
ΔK_{th0} - threshold value of Δk at R = 0, psi $\sqrt{\text{in.}}$	2,500	4,500	5,500
Shutoff ratio	3.0	3.0	3.5
RCUT - positive stress ratio cutoff	0.75	0.65	0.75
RCUTN - negative stress ratio cutoff	-0.99	-0.20	-0.30

TABLE 39. TYPICAL LIGHTWEIGHT FIGHTER AIR-TO-AIR COMBAT MISSION

Segment	Gross Weight (lb)	Altitude (1,000 ft)	Mach No.	Distance (n mi)	Time (min)
1. Taxi	12,855	SL	-	-	-
2. Climb	12,855 - 12,480	0 - 46	0.72 - 0.85	42.6	5.364
3. Cruise	12,480 - 12,175	46	0.85	112.3	13.820
4. Combat	12,175 - 12,005	30	0.90	-	0.620
5. Accelerate	12,005 - 11,740	30	0.9 - 1.4	8.15	0.707
6. Combat	11,740 - 10,260	30	1.4	-	1.125
7. Cruise	10,260 - 9,920	50	0.85	154.9	19.290
8. Loiter	9,920 - 9,625	10	0.33	-	15.0
9. Landing	9,625	SL	-	-	-

TABLE 40. CUMULATIVE OCCURRENCES PER 1,000 FLIGHT HOURS
OF SUPERSONIC AIR-TO-AIR COMBAT

Load Factor N_z	Cumulative Occurrences
10.0	0
9.0	0
8.0	16
7.0	90
6.0	500
5.0	2,900
4.0	17,000
3.0	90,000
2.0	250,000
1.5	320,000
0.0	16,000
-1.0	45
-2.0	0.1
-3.0	0
-4.0	0

TABLE 41. TYPICAL AIR-TO-AIR FIGHTER FATIGUE SPECTRUM - CYCLES PER 1,000 FLIGHTS

Subs. cat.	1	2	3	4	5	6	7	8	9	10	11	12	13	14	15	16	17	18	19	20
Load type*	Δ 1.0	Δ 1.3	Δ 1.6	Δ 2.0	Δ 2.5	Δ 3.0	Δ 3.5	Δ 4.0	Δ 4.5	Δ 5.0	Δ 5.5	Δ 6.0	Δ 6.5	Δ 7.0	Δ 7.5	Δ 8.0	Δ 8.5	Δ 9.0	Δ 9.5	Δ 10.0
1				250,000		135,000	85,000	55,000	12,500	5,150	840	210								
2												1,857	65.5							
3												2,556.7	985.8	250.5	4.6					
4	1.1	0.6	11.8		112.5							1,705	1,381.7	682	191.2	50.2	12.2	5.6	0.9	0.2
5	1.1											150.8	50.4	11.8	0.2					
6	1.1	0.4	0.6		294.5							2,462.5	2,500.3	605.8	105	18.6	5.2	0.7		
7	1.1											5,508.7	1,576	521.5	6.4					
8	1.1											6,500	1,265	165.5	18.5	1.5				
9	5.2			325		180	107	64	52	18	17.2	9	0.9							

* 1. Landing

2. Taxi

3. Landing impact

TABLE 42. APAS-GENERATED AIR-TO-AIR FIGHTER SPECTRUM
EXCLUDING FRACTIONAL CYCLES, 1-FLIGHT BLOCK

PROGRAM GENERATED SPECTRUM			
STEP	STRESS-KAY	STRESS-IN	CYCLES
1	0.000	-6366.032	223.000
2	0.000	-5571.271	135.000
3	0.000	-5574.511	79.000
4	0.000	-7277.751	35.000
5	0.000	-7500.990	12.000
6	0.000	-7884.230	3.000
7	0.000	-8127.469	1.000
8	6046.031	3023.016	2.000
9	6046.031	3023.016	3.000
10	9069.047	3023.016	1.000
11	6046.031	3023.016	2.000
12	9069.047	3023.016	1.000
13	12092.063	3023.016	1.000
14	6046.031	3023.016	3.000
15	9069.047	3023.016	2.000
16	12092.063	3023.016	1.000
17	6046.031	3023.016	4.000
18	9069.047	3023.016	1.000
19	6046.031	3023.016	6.000
20	9069.047	3023.016	1.000
21	12092.063	-8127.469	1.000

TABLE 43. APAS-GENERATED AIR-TO-AIR FIGHTER SPECTRUM
EXCLUDING FRACTIONAL CYCLES, 50-FLIGHT BLOCK

PROGRAM GENERATED SPECTRUM			
STEP	STRESS-MAX	STRESS-MIN	CYCLES
1	0.000	-5349.032	11450.000
2	0.000	-5571.271	8750.000
3	0.000	-4574.511	3425.000
4	0.000	-7277.701	1750.000
5	0.000	-7380.990	615.000
6	0.000	-7584.230	157.000
7	0.000	-8187.469	42.000
8	0.000	-9097.188	13.000
9	6046.031	3023.016	43.000
10	6046.031	3023.016	3.000
11	6046.031	3023.016	128.000
12	9069.047	3023.016	47.000
13	12092.063	3023.016	12.000
14	3023.016	-3023.016	1.000
15	3023.016	0.000	22.000
16	6046.031	3023.016	95.000
17	9069.047	3023.016	68.000
18	12092.063	3023.016	34.000
19	15115.079	3023.016	13.000
20	18138.094	3023.016	3.000
21	21161.110	3023.016	1.000
22	6046.031	3023.016	7.000
23	9069.047	3023.016	3.000
24	12092.063	3023.016	1.000
25	3023.016	0.000	15.000
26	6046.031	3023.016	149.000
27	9069.047	3023.016	115.000
28	12092.063	3023.016	32.000
29	15115.079	3023.016	5.000
30	18138.094	3023.016	1.000
31	6046.031	3023.016	178.000
32	9069.047	3023.016	69.000
33	12092.063	3023.016	16.000
34	6046.031	3023.016	115.000
35	9069.047	3023.016	63.000
36	12092.063	3023.016	5.000
37	15115.079	3023.016	1.000
38	3023.016	2720.714	16.000
39	3023.016	2418.413	4.000
40	3023.016	2116.111	5.000
41	3023.016	1813.809	3.000
42	3023.016	1511.507	2.000
43	3023.016	1209.205	1.000
44	3023.016	906.903	1.000
45	18138.094	-906.903	1.000
46	15115.079	-1709.7.188	2.000
47	15115.079	-3097.188	2.000
48	15115.079	-8187.469	3.000
49	12092.063	-9097.188	4.000
50	12092.063	-8187.469	4.000
51	12092.063	-8187.469	5.000
52	12092.063	-7584.230	5.000
53	12092.063	-7584.230	15.000

TABLE 44. APAS-GENERATED AIR-TO-AIR FIGHTER SPECTRUM
EXCLUDING FRACTIONAL CYCLES, 100 FLIGHT BLOCK

PROGRAM GENERATED SPECTRUM			
STEP	STRESS-1A4	STRESS-1B	CYCLES
1	0.000	-6344.032	22000.000
2	0.000	-6371.071	13500.000
3	0.000	-6374.511	7850.000
4	0.000	-7277.751	3500.000
5	0.000	-7330.350	1250.000
6	0.000	-7384.230	315.000
7	0.000	-8187.469	84.000
8	0.000	-8097.128	21.000
9	6044.031	3023.016	186.000
10	6069.047	3023.016	6.000
11	6044.031	3023.016	254.000
12	6069.047	3023.016	99.000
13	12092.063	3023.016	23.000
14	6023.016	-3023.016	1.000
15	6023.016	0.000	44.000
16	6046.031	3023.016	170.000
17	6069.047	3023.016	138.000
18	12092.063	3023.016	69.000
19	15115.073	3023.016	19.000
20	15138.094	3023.016	5.000
21	21161.112	3023.016	1.000
22	6046.031	3023.016	13.000
23	6069.047	3023.016	5.000
24	12092.063	3023.016	1.000
25	3023.016	-3023.016	1.000
26	6023.016	0.000	29.000
27	6046.031	3023.016	296.000
28	6069.047	3023.016	231.000
29	12092.063	3023.016	60.000
30	15115.073	3023.016	10.000
31	15138.094	3023.016	2.000
32	6046.031	3023.016	357.000
33	6069.047	3023.016	138.000
34	12092.063	3023.016	52.000
35	15115.073	3023.016	1.000
36	6046.031	3023.016	630.000
37	6069.047	3023.016	124.000
38	12092.063	3023.016	17.000
39	15115.073	3023.016	2.000
40	3023.016	2720.714	32.000
41	3023.016	2418.413	13.000
42	3023.016	2115.111	11.000
43	3023.016	1513.099	1.000
44	3023.016	1511.098	3.000
45	3023.016	1209.086	2.000
46	3023.016	906.905	2.000
47	3023.016	0.000	1.000
48	15138.094	-3023.016	1.000
49	15138.094	-3023.016	2.000
50	15115.073	-3023.016	1.000
51	15115.073	-3023.016	1.000
52	15115.073	-3023.016	1.000
53	15115.073	-3023.016	1.000
54	12092.063	-3023.016	2.000
55	12092.063	-3023.016	1.000
56	12092.063	-3023.016	1.000
57	12092.063	-3023.016	2.000
58	12092.063	-3023.016	2.000

TABLE 45. APAS PROGRAM RESULTS - AIR-TO-AIR FIGHTER SPECTRUM

Program Configuration		1 Flight Block		50 Flight Block		100 Flight Block		All Fractional Cycles	
Module	Constraints	Analysis/opt % penalty	Analysis, flights	Analysis/opt % penalty	Analysis, flights	Analysis/opt % penalty	Analysis flights	Analysis/opt % penalty	Analysis flights
PROGRO	None	10.93	10,616	24.19	7,120	23.84	7,187	28.60	6113
PRECRO	Without retardation, Without acceleration	11.06	10,588	24.43	7,057	24.09	7,121	-	-
PRECRO	With retardation, With acceleration	15.94	9,200	8.77	11,235	10.70	10,339	-	-
PRECRO	With retardation, Without acceleration	8.36	11,508	6.29	12,203	6.58	12,022	-	-

* Analysis/optimization penalty based on:
initial crack length, $2a = 1$ inch
15,000 flights

TABLE 46. FLAW-GROWTH-ANALYSIS RESULTS USING PROGRO -
LIBRARY FIGHTER SPECTRUM, 1-FLIGHT BLOCK

FLAW GROWTH ANALYSIS RESULTS

		INITIAL CRACK SIZE, 2A		1.000 INCHES		
		INSPECTION INTERVAL		15000. FLIGHTS		
PANEL NO.	SYMMETRY GROUP	MAXIMUM SPECTRUM STRESS SKIN (PSI)	MAXIMUM SPECTRUM STRESS STIFF. (PSI)	CRITICAL INITIAL FLAW SIZE (2A, IN.)	SAFE LIFE (FLIGHTS)	WEIGHT PENALTY (PERCENT)
1	1	6759.	6759.	2.547	.310E+05	.00
2	1	7074.	7074.	2.893	.262E+05	.00
3	1	5951.	5951.	3.958	.493E+05	.00
4	1	3781.	3781.	17.040	.257E+06	.00
5	3	0.	0.	0.000	0.	0.00
6	2	6279.	6279.	4.089	.117E+06	10.93
7	2	8859.	8859.	2.717	.332E+05	10.93
8	2	10730.	10730.	1.167	.165E+05	10.93
9	2	11024.	11024.	1.000	.150E+05	10.93
10	4	0.	0.	0.000	0.	0.00

TABLE 47. FLAW-GROWTH-ANALYSIS RESULTS USING PREGRO WITHOUT LOAD INTERACTION EFFECTS - LIBRARY FIGHTER SPECTRUM, ONE FLIGHT BLOCK

FLAW GROWTH ANALYSIS RESULTS

		INITIAL CRACK SIZE, 2A		1.000 INCHES		
		INSPECTION INTERVAL		15000. FLIGHTS		
PANEL NO.	SYMMETRY GROUP	MAXIMUM SPECTRUM STRESS SKIN (PSI)	MAXIMUM SPECTRUM STRESS STIFF. (PSI)	CRITICAL INITIAL FLAW SIZE (2A, IN.)	SAFE LIFE (FLIGHTS)	WEIGHT PENALTY (PERCENT)
1	1	6759.	6759.	2.824	.345E+05	.00
2	1	7078.	7078.	2.598	.288E+05	.00
3	1	5950.	5950.	4.409	.554E+05	.00
4	1	3781.	3781.	17.271	.229E+06	.00
5	3	0.	0.	0.000	0.	0.00
6	2	6054.	6054.	3.275	.117E+06	11.36
7	2	8851.	8851.	2.722	.333E+05	11.36
8	2	10720.	10720.	1.171	.166E+05	11.36
9	2	11012.	11012.	1.000	.150E+05	11.36
10	4	0.	0.	0.000	0.	0.00

TABLE 48. FLAW-GROWTH-ANALYSIS RESULTS USING PREGRO WITH RETARDATION
AND ACCELERATION EFFECTS - LIBRARY FIGHTER SPECTRUM, 1 FLIGHT BLOCK

FLAW GROWTH ANALYSIS RESULTS

		INITIAL CRACK SIZE, 2A		1.000 INCHES		
		INSPECTION INTERVAL		15000. FLIGHTS		
PANEL NO.	SYMMETRY GROUP	MAXIMUM SPECTRUM STRESS (PSI)	MAXIMUM SPECTRUM STRESS STIFF. (PSI)	CRITICAL INITIAL FLAW SIZE (2A, IN.)	SAFE LIFE (FLIGHTS)	WEIGHT PENALTY (PERCENT)
1	1	6770.	6770.	2.491	.303E+05	.00
2	1	7052.	7052.	2.070	.260E+05	.00
3	1	5937.	5937.	3.935	.463E+05	.00
4	1	3789.	3789.	16.672	.243E+06	.00
5	3	0.	0.	0.000	0.	0.00
6	2	6024.	6024.	5.097	.117E+06	15.94
7	2	6532.	6532.	2.704	.380E+05	15.94
8	2	10335.	10335.	1.159	.164E+05	15.94
9	2	10897.	10897.	1.003	.180E+05	15.94
10	4	0.	0.	0.000	0.	0.00

TABLE 49. FLAW-GROWTH-ANALYSIS RESULTS USING PREGRO WITH RETARDATION
EFFECTS - LIBRARY FIGHTER SPECTRUM, 1 FLIGHT BLOCK

FLAW GROWTH ANALYSIS RESULTS

		INITIAL CRACK SIZE, 2A		1.000 INCHES		
		INSPECTION INTERVAL		15000. FLIGHTS		
PANEL NO.	SYMMETRY GROUP	MAXIMUM SPECTRUM STRESS (PSI)	MAXIMUM SPECTRUM STRESS STIFF. (PSI)	CRITICAL INITIAL FLAW SIZE (2A, IN.)	SAFE LIFE (FLIGHTS)	WEIGHT PENALTY (PERCENT)
1	1	6753.	6753.	2.811	.744E+05	.00
2	1	7083.	7083.	2.386	.291E+05	.00
3	1	5959.	5959.	4.350	.551E+05	.00
4	1	3775.	3775.	12.327	.290E+06	.00
5	3	0.	0.	0.000	0.	0.00
6	2	6405.	6405.	8.137	.117E+06	8.36
7	2	9039.	9039.	2.737	.334E+05	8.36
8	2	10946.	10946.	1.178	.165E+05	8.36
9	2	11260.	11260.	1.000	.150E+05	8.36
10	4	0.	0.	0.000	0.	0.00

TABLE 50. FLAW-GROWTH ANALYSIS RESULTS USING PROGRO -
LIBRARY FIGHTER SPECTRUM, 50 FLIGHT BLOCKS

FLAW GROWTH ANALYSIS RESULTS

INITIAL CRACK SIZE, 2A		1.000 INCHES				
INSPECTION INTERVAL		15000. FLIGHTS				
PANEL NO.	SYMMETRY GROUP	MAXIMUM SPECTRUM STRESS (PSI)	MAXIMUM SPECTRUM STRESS STIFF. (PSI)	CRITICAL INITIAL FLAW SIZE (2A, IN.)	SAFE LIFE (FLIGHTS)	WEIGHT PENALTY (PERCENT)
1	1	7542.	7542.	2.479	.302E+05	.00
2	1	7818.	7818.	2.117	.265E+05	.00
3	1	6574.	6574.	3.999	.497E+05	.00
4	1	4224.	4224.	16.671	.249E+06	.00
5	3	0.	0.	0.000	0.	0.00
6	2	9909.	9909.	9.475	.123E+06	24.19
7	2	14088.	14088.	2.651	.377E+05	24.19
8	2	17077.	17077.	1.125	.162E+05	24.19
9	2	17427.	17427.	1.001	.150E+05	24.19
10	4	0.	0.	0.000	0.	0.00

TABLE 51. FLAW-GROWTH-ANALYSIS RESULTS USING PREGRO WITHOUT LOAD INTERACTION EFFECTS - LIBRARY FIGHTER SPECTRUM, 50 FLIGHT BLOCKS

FLAW GROWTH ANALYSIS RESULTS

INITIAL CRACK SIZE, 2A		1.000 INCHES				
INSPECTION INTERVAL		15000. FLIGHTS				
PANEL NO.	SYMMETRY GROUP	MAXIMUM SPECTRUM STRESS (PSI)	MAXIMUM SPECTRUM STRESS STIFF. (PSI)	CRITICAL INITIAL FLAW SIZE (2A, IN.)	SAFE LIFE (FLIGHTS)	WEIGHT PENALTY (PERCENT)
1	1	7542.	7542.	2.745	.366E+05	.00
2	1	7817.	7817.	2.402	.310E+05	.00
3	1	6577.	6577.	4.443	.698E+05	.00
4	1	4224.	4224.	17.673	.279E+06	.00
5	3	0.	0.	0.000	0.	0.00
6	2	9903.	9903.	9.486	.124E+06	24.43
7	2	14186.	14186.	2.655	.378E+05	24.43
8	2	17044.	17044.	1.100	.150E+05	24.43
9	2	17394.	17394.	1.000	.139E+05	24.43
10	4	0.	0.	0.000	0.	0.00

TABLE 52. FLAW-GROWTH-ANALYSIS RESULTS USING PREGRO WITH RETARDATION AND ACCELERATION EFFECTS - LIBRARY FIGHTER SPECTRUM, 50 FLIGHT BLOCKS

FLAW GROWTH ANALYSIS RESULTS

		INITIAL CRACK SIZE, 2A		1.000 INCHES		
		INSPECTION INTERVAL		15000. FLIGHTS		
PANEL NO.	SYMMETRY GROUP	MAXIMUM SPECTRUM STRESS (SKI) (PSI)	MAXIMUM SPECTRUM STRESS (STIFF) (PSI)	CRITICAL INITIAL FLAW SIZE (2A, IN.)	SAFE LIFE (FLIGHTS)	WEIGHT PENALTY (PERCENT)
1	1	7504.	7504.	2.493	.303E+05	.00
2	1	7863.	7863.	2.011	.255E+05	.00
3	1	6619.	6619.	3.849	.482E+05	.00
4	1	4197.	4197.	16.702	.253E+06	.00
5	3	?	?	0.000	0.	0.00
6	2	11171.	11171.	9.252	.122E+06	8.77
7	2	15767.	15767.	2.622	.342E+05	8.77
8	2	19095.	19095.	1.157	.166E+05	8.77
9	2	19638.	19638.	1.000	.159E+05	8.77
10	4	?	?	0.000	0.	0.00

TABLE 53. FLAW-GROWTH-ANALYSIS RESULTS USING PREGRO WITH RETARDATION EFFECTS - LIBRARY FIGHTER SPECTRUM, 50 FLIGHT BLOCKS

FLAW GROWTH ANALYSIS RESULTS

		INITIAL CRACK SIZE, 2A		1.000 INCHES		
		INSPECTION INTERVAL		15000. FLIGHTS		
PANEL NO.	SYMMETRY GROUP	MAXIMUM SPECTRUM STRESS (SKI) (PSI)	MAXIMUM SPECTRUM STRESS (STIFF) (PSI)	CRITICAL INITIAL FLAW SIZE (2A, IN.)	SAFE LIFE (FLIGHTS)	WEIGHT PENALTY (PERCENT)
1	1	7498.	7498.	2.817	.347E+05	.00
2	1	7873.	7873.	2.375	.240E+05	.00
3	1	6629.	6629.	4.373	.549E+05	.00
4	1	4192.	4192.	18.373	.240E+06	.00
5	3	?	?	0.000	0.	0.00
6	2	11417.	11407.	9.314	.121E+06	6.29
7	2	16031.	16021.	2.663	.344E+05	6.29
8	2	19474.	19474.	1.163	.157E+05	6.29
9	2	20051.	20050.	1.000	.150E+05	6.29
10	4	?	?	0.000	0.	0.00

TABLE 54. FLAW-GROWTH-ANALYSIS RESULTS USING PREGRO -
LIBRARY FIGHTER SPECTRUM, 100 FLIGHT BLOCKS

FLAW GROWTH ANALYSIS RESULTS

INITIAL CRACK SIZE, 2A				1.000 INCHES		
INSPECTION INTERVAL				15000. FLIGHTS		
PANEL NO.	SYMMETRY GROUP	MAXIMUM SPECTRUM STRESS (PSI)	MAXIMUM SPECTRUM STRESS STIFF. (PSI)	CRITICAL INITIAL FLAW SIZE (2A, IN.)	SAFE LIFE (FLIGHTS)	WEIGHT PENALTY (PERCENT)
1	1	7541.	7541.	2.477	.392E+06	.00
2	1	7513.	7513.	2.117	.264E+06	.00
3	1	6575.	6575.	3.994	.497E+05	.00
4	1	4223.	4223.	15.667	.249E+06	.00
5	3	0.	0.	0.000	0.	0.00
6	2	9935.	9935.	2.475	.123E+06	23.84
7	2	14122.	14122.	2.652	.774E+05	23.84
8	2	17111.	17111.	1.126	.162E+05	23.84
9	2	17471.	17471.	1.061	.158E+05	23.84
10	4	0.	0.	0.000	0.	0.00

TABLE 55. FLAW-GROWTH-ANALYSIS RESULTS USING PREGRO WITHOUT LOAD INTERACTION EFFECTS - LIBRARY FIGHTER SPECTRUM, 100 FLIGHT BLOCKS

FLAW GROWTH ANALYSIS RESULTS

INITIAL CRACK SIZE, 2A				1.000 INCHES		
INSPECTION INTERVAL				15000. FLIGHTS		
PANEL NO.	SYMMETRY GROUP	MAXIMUM SPECTRUM STRESS (PSI)	MAXIMUM SPECTRUM STRESS STIFF. (PSI)	CRITICAL INITIAL FLAW SIZE (2A, IN.)	SAFE LIFE (FLIGHTS)	WEIGHT PENALTY (PERCENT)
1	1	7541.	7541.	2.747	.330E+06	.00
2	1	7513.	7513.	2.423	.230E+06	.00
3	1	6574.	6574.	4.445	.630E+05	.00
4	1	4223.	4223.	17.874	.278E+06	.00
5	3	0.	0.	0.000	0.	0.00
6	2	9915.	9915.	2.475	.124E+06	24.09
7	2	14097.	14097.	2.568	.230E+05	24.09
8	2	17002.	17002.	1.130	.152E+05	24.09
9	2	17473.	17473.	1.090	.147E+05	24.09
10	4	0.	0.	0.000	0.	0.00

TABLE 56. FLAW-GROWTH-ANALYSIS RESULTS USING PREGRO WITH RETARDATION AND ACCELERATION EFFECTS - LIBRARY FIGHTER SPECTRUM, 100 FLIGHT BLOCKS

FLAW GROWTH ANALYSIS RESULTS

INITIAL CRACK SIZE, 2A		1.000 INCHES				
INSPECTION INTERVAL		15000. FLIGHTS				
PANEL NO.	SYMMETRY GROUP	MAXIMUM SPECTRUM STRESS SKIN (PSI)	MAXIMUM SPECTRUM STRESS STIFF. (PSI)	CRITICAL INITIAL FLAW SIZE (2A, I ₁)	SAFE LIFE (FLIGHTS)	WEIGHT PENALTY (PERCENT)
1	1	7532.	7509.	2.486	.303E+06	.00
2	1	7661.	7661.	2.022	.256E+06	.00
3	1	6613.	6613.	3.367	.484E+05	.00
4	1	4200.	4200.	10.661	.252E+06	.00
5	3	0.	0.	0.000	0.	0.00
6	3	11894.	11994.	2.055	.128E+06	10.70
7	2	15532.	15532.	2.636	.354E+05	10.70
8	2	13611.	13611.	1.158	.167E+05	10.70
9	2	13323.	13323.	1.000	.150E+05	10.70
10	4	0.	0.	0.000	0.	0.00

TABLE 57. FLAW-GROWTH-ANALYSIS RESULTS USING PREGRO WITH RETARDATION EFFECTS - LIBRARY FIGHTER SPECTRUM, 100 FLIGHT BLOCKS

FLAW GROWTH ANALYSIS RESULTS

INITIAL CRACK SIZE, 2A		1.000 INCHES				
INSPECTION INTERVAL		15000. FLIGHTS				
PANEL NO.	SYMMETRY GROUP	MAXIMUM SPECTRUM STRESS SKIN (PSI)	MAXIMUM SPECTRUM STRESS STIFF. (PSI)	CRITICAL INITIAL FLAW SIZE (2A, I ₁)	SAFE LIFE (FLIGHTS)	WEIGHT PENALTY (PERCENT)
1	1	7407.	7407.	2.412	.347E+06	.00
2	1	7677.	7677.	2.372	.280E+06	.00
3	1	6627.	6627.	4.367	.546E+05	.00
4	1	4132.	4132.	10.334	.230E+06	.00
5	3	0.	0.	0.000	0.	0.00
6	3	11372.	11372.	2.214	.123E+06	6.58
7	2	15044.	15044.	2.633	.347E+05	6.58
8	2	13428.	13428.	1.166	.167E+05	6.58
9	2	13001.	13001.	1.000	.150E+05	6.58
10	4	0.	0.	0.000	0.	0.00

TABLE 58. FIGHTER SPECTRUM VARIATION TEST PROGRAM

Test No.	Spectrum Type	Variations
F-B-V-A-1	A-A	Compressive loads set to zero
F-B-V-A-2	A-G	Compressive loads set to zero
F-B-V-A-3	I-N	Compressive loads set to zero
F-B-V-A-4	Composite	Compressive loads set to zero
F-B-V-B-3	I-N	Decreasing DLS to 25 ksi
F-B-V-B-4	Composite	Decreasing DLS to 25 ksi
F-B-V-C-1	A-A	Increasing DLS to 35 ksi
F-B-V-C-2	A-G	Increasing DLS to 35 ksi
F-B-V-C-3	I-N	Increasing DLS to 35 ksi
F-B-V-C-4	Composite	Increasing DLS to 35 ksi
F-B-V-D-1	A-A	Clipping high loads at 85%
F-B-V-D-4	Composite	Clipping high loads at 85%
F-B-V-E-1	A-A	Clipping high loads at 95%
F-B-V-E-4	Composite	Clipping high loads at 95%
F-B-V-F-4	Composite	Truncating 35% low loads
F-B-V-G-4	Composite	Truncating 45% low loads
F-B-V-H-4	Composite	Truncating 55% low loads
F-B-V-I-4	Composite	Mission sequence variation I
F-B-V-J-4	Composite	Mission sequence variation II
F-B-V-K-4	Composite	Comp load increased 25%
F-B-V-L-4	Composite	Comp load increased 50%

TABLE 59. FIGHTER SPECTRUM MISSION-MIX TEST PROGRAM

Test No.	Spectrum type	Mission-Mix Variations
M-301	Mission mix (short missions)	$(A-A)^I : (A-G)^I : (I-N)^I = 20:21:17^b$
M-302	Mission mix (short missions)	$(A-A)^I : (A-G)^I : (I-N)^I = 20:20:18$
M-303	Mission mix (short missions)	$(A-A)^I : (A-G)^I : (I-N)^I = 18:19:29$
M-304	Mission mix (short missions)	$(A-A)^I : (A-G)^I : (I-N)^I = 20:21:18$
M-305	Mission mix (short missions)	$(A-A)^I : (A-G)^I : (I-N)^I = 20:20:18$
M-306	Mission mix	$(A-A)^{III^C} : (A-G)^{III} : (I-N)^{III} = 70:68:68$
M-307	Mission mix	$(A-A)^{III} : (A-G)^{III} : (I-N)^{III} = 92:24:91$
M-308	Mission mix	$(A-A)^{III} : (A-G)^{III} : (I-N)^{III} = 24:90:92$
^a (A-A) ^I represents the (A-A) mission generated in phase I in reference 2. ^b Numerical values are based on number of flights in the mixed mission. ^c (A-A) ^{III} represents the (A-A) mission generated in phase III.		

TABLE 60. DIVIDED UNITBLOCK FOR (A-A)^I, (A-G)^I AND (I-N)^I MISSIONS

$(A-A)_1^I = 11(A-A)_{1-11}^I$	$(A-G)_1^I = 11(A-G)_{1-11}^I$	$(I-N)_1^I = 3(I-N)_{1-3}^I$
$(A-A)_2^I = 12(A-A)_{12-25}^I$	$(A-G)_2^I = 11(A-G)_{12-24}^I$	$(I-N)_2^I = 3(I-N)_{4-6}^I$
$(A-A)_3^I = 9(A-A)_{26-34}^I$	$(A-G)_3^I = 10(A-G)_{25-34}^I$	$(I-N)_3^I = 14(I-N)_{7-20}^I$
$(A-A)_4^I = 9(A-A)_{35-43}^I$	$(A-G)_4^I = 9(A-G)_{36-43}^I$	$(I-N)_4^I = 15(I-N)_{21-35}^I$
$(A-A)_5^I = 9(A-A)_{44-52}^I$	$(A-G)_5^I = 9(A-G)_{44-52}^I$	$(I-N)_5^I = 15(I-N)_{36-50}^I$

TABLE 61. GROUP III-a MISSION MIX VARIATION FOR FIGHTER SPECTRA

Test No.	Mission-mix variations
M-301	$(A-A)_1^I + (A-G)_1^I + (I-N)_1^I + (A-A)_3^I + (A-G)_3^I + (I-N)_3^I$
M-302	$(A-A)_1^I + (A-G)_1^I + (I-N)_1^I + (A-A)_4^I + (A-G)_4^I + (I-N)_4^I$
M-303	$(A-A)_3^I + (A-G)_4^I + (I-N)_3^I + (A-A)_4^I + (A-G)_3^I + (I-N)_4^I$
M-304	$(A-A)_1^I + (A-G)_2^I + (I-N)_3^I + (A-A)_5^I + (A-G)_5^I + (I-N)_5^I$
M-305	$(A-A)_1^I + (A-G)_1^I + (I-N)_1^I + (A-A)_5^I + (A-G)_5^I + (I-N)_5^I$
M-306	$(A-A)_3^{III} + (A-G)_3^{III} + (I-N)_3^{III} + (A-A)_4^{III} + (A-G)_4^{III} + (A-G)_4^{III}$
M-307	$(A-A)_1^{III} + (A-G)_5^{III} + (I-N)_5^{III} + (A-A)_2^{III} + (A-G)_6^{III} + (I-N)_6^{III}$
M-308	$(A-A)_5^{III} + (A-G)_1^{III} + (I-N)_7^{III} + (A-A)_6^{III} + (A-G)_2^{III} + (I-N)_8^{III}$

TABLE 62. DIVIDED UNITBLOCKS OF (A-A) ^{III} (A-G) ^{III} and (I-N) ^{III} MISSIONS

(A-A) Mission	(A-G) Mission	(I-N) Mission
(A-A) ₁ ^{III} = 46(A-A) ₁₋₄₆	(A-G) ₁ ^{III} = 45(A-G) ₁₋₄₅	(I-N) ₁ ^{III} = 12(I-N) ₁₋₁₂
(A-A) ₂ ^{III} = 46(A-A) ₄₇₋₉₂	(A-G) ₂ ^{III} = 45(A-G) ₄₆₋₉₀	(I-N) ₂ ^{III} = 12(I-N) ₁₃₋₂₄
(A-A) ₃ ^{III} = 35(A-A) ₁₋₃₅	(A-G) ₃ ^{III} = 34(A-G) ₁₋₃₄	(I-N) ₃ ^{III} = 34(I-N) ₁₋₃₄
(A-A) ₄ ^{III} = 35(A-A) ₃₆₋₇₀	(A-G) ₄ ^{III} = 34(A-G) ₃₅₋₆₈	(I-N) ₄ ^{III} = 34(I-N) ₃₅₋₆₈
(A-A) ₅ ^{III} = 12(A-A) ₁₋₁₂	(A-G) ₅ ^{III} = 12(A-G) ₁₋₁₂	(I-N) ₅ ^{III} = 45(I-N) ₁₋₄₅
(A-A) ₆ ^{III} = 12(A-A) ₁₃₋₂₄	(A-G) ₆ ^{III} = 12(A-G) ₁₃₋₂₄	(I-N) ₆ ^{III} = 45(I-N) ₄₆₋₉₀
		(I-N) ₇ ^{III} = 46(I-N) ₁₋₄₆
		(I-N) ₈ ^{III} = 46(I-N) ₄₇₋₉₂

TABLE 63. TRANSPORT COMPOSITE BASELINE SPECTRUM G-A-G

Type of Flight	σ_{\min} , ksi	σ_{\max} , ksi
Assault	-6.4	12.7
Assault	-6.4	12.9
Training	-8.9	12.7
Training	-8.9	10.4
Assault	-6.4	10.3
Assault	-6.4	12.7
Assault	-6.4	12.9
Training	-8.9	12.7
Training	-8.9	10.4
Assault	-6.4	10.3
Assault	-6.4	12.7
Assault	-6.4	12.9
Training	-8.9	12.7
Training	-8.9	10.4
Assault	-6.4	10.3
Assault	-6.4	12.7
Assault	-6.4	12.9
Training	-8.9	12.7
Training	-8.9	10.4
Logistics	-11.5	10.3
Assault	-6.4	14.0

TABLE 64. 2219-T851 ALUMINUM CHEMICAL CONTENTS

Chemical Properties

Heat No.	Al	Mg	Mn	Zn	Z4	Si	Fe	Cu	Ni
7430252D		0.02	0.20 .40	0.02 .10		0.05 .15	0.10 .25	5.8 6.8	
	Cr	Ti	Th	Ca	c	S	P	Others	
	0.10	0.20 .30						Each 0.05 max Total 0.15 max	

TABLE 65. 2219-T851 ALUMINUM PHYSICAL PROPERTIES

Heat No.	Yield Strength	Tensile Strength	Percent Elongation
7430252D	46,000 min (psi)	62,000 min (psi)	8 min
NOTES: 1. 2219-T851 aluminum QQ-A-250/30, 1/4- x 48- x 144-inch plates 2. Mill source: Reynolds Aluminum Co			

TABLE 66. SUMMARY OF TEST RESULTS FOR FIGHTER BASELINE SPECTRA

Test No.	Baseline Spectra	Crack Growth (C_i to C_f) (in.)	Test Life, N_B	
			Cycles	Flights
F-B-1	Air-to-air	0.145 to failure	73,552	2,829
F-B-2	Air-to-ground	.145 to failure	102,677	5,405
F-B-3	Instrumentation & Navigation	.148 to failure	167,721	30,142
F-B-4	Composite	.145 to failure	106,705	5,171

TABLE 67. SUMMARY OF TEST RESULTS FOR FIGHTER SPECTRUM VARIATIONS

Test No.	Spectrum Variations	Crack Growth (C_i to C_f) (in.)	Test Life, N_V	
			Cycles	Flights
FB-V-A-1	Comp loads set to zero	0.145 to failure	88,528	3,405
FB-V-A-2	Comp loads set to zero	.150 to failure	103,161	5,429
FB-V-A-3	Comp loads set to zero	.145 to failure	193,202	34,720
FB-V-A-4	Comp loads set to zero	.145 to failure	123,689	5,995
FB-V-B-3	DLS = 25 ksi	.145 to .83	222,331	40,080
FB-V-B-4	DLS = 25 ksi	.145 to .61	159,514	7,736
FB-V-C-1	DLS = 35 ksi	.145 to failure	33,616	1,295
FB-V-C-2	DLS = 35 ksi	.145 to failure	55,045	2,897
FB-V-C-3	DLS = 35 ksi	.145 to failure	106,164	19,075
FB-V-C-4	DLS = 35 ksi	.145 to failure	47,683	2,505
FB-V-D-1	High load clipping at 85%	.145 to failure	50,414	1,939
FB-V-D-4	High load clipping at 85%	.145 to failure	60,480	2,924
FB-V-F-4	35% truncation	.150 to failure	75,723	4,864
FB-V-G-4	45% truncation	.148 to failure	52,293	5,171
FB-V-H-4	55% truncation	.145 to failure	35,414	6,833
FB-V-E-4	High load clipping at 95%	.145 to failure	79,490	3,847
FB-V-I-4	Mission sequence A	.145 to failure	102,459	4,965
FB-V-J-4	Mission sequence B	.145 to failure	90,576	4,392
FB-V-K-4	Comp load increased 25%	.145 to failure	98,635	4,775
FB-V-L-4	comp load increased 50%	.145 to failure	89,721	4,347

TABLE 68. COMPARISON OF CRACK LIVES FOR A-A MISSION
SPECTRUM VARIATIONS TO A-A BASELINE SPECTRUM

Test No.	Spectrum Variation	Crack Growth (C_i to C_f) (in.)	Test Life, N_V	
			Cycles	N_V/N_B
FB-V-A-1	Comp loads set to zero	0.145 to failure	3,405	1.2
FB-V-C-1	DLS = 35 ksi	.145 to failure	1,293	0.46
FB-V-D-1	High loads clipped at 85%	.145 to failure	1,939	0.69

TABLE 69. COMPARISON OF CRACK LIVES FOR A-G MISSION
SPECTRUM VARIATIONS TO A-G BASELINE SPECTRUM

Test No.	Spectrum Variation	Crack Growth (C_i to C_f) (in.)	Test Life, N_V	
			Cycles	N_V/N_B
FB-V-A-2	Comp loads set to zero	0.150 to failure	5,429	1.03
FB-V-C-2	DLS = 35 ksi	.145 to failure	2,397	0.54

TABLE 70. COMPARISON OF CRACK LIVES FOR I-N MISSION
SPECTRUM VARIATIONS TO I-N BASELINE SPECTRUM

Test No.	Spectrum Variation	Crack Growth (C_i to C_f) (in.)	Test Life, N_V	
			Cycles	N_V/N_B
FB-V-A-3	Comp loads set to zero	0.148 to failure	34,719	1.15
FB-V-B-3	DLS = 25 ksi	.148 to .83	40,078	2.61
FB-V-C-3	DLS = 35 ksi	.148 to failure	19,072	0.63

TABLE 71. COMPARISON OF CRACK LIVES FOR COMPOSITE MISSION
SPECTRUM VARIATIONS TO COMPOSITE BASELINE SPECTRUM

Test No.	Spectrum Variations	Crack Growth (C_i to C_f) (in.)	Test Life, N_V	
			Flights (Cycles)	N_V/N_B
FB-V-A-4	Comp loads set to zero	0.145 to failure	5,995 (123,689)	1.16
FB-V-B-4	DLS = 25 ksi	.145 to .61	7,736 (159,514)	3.08
FB-V-C-4	DLS = 35 ksi	.145 to failure	2,303 (47,683)	.45
FB-V-D-4	High loads clipped at 85% DLS	.145 to failure	2,924 (60,480)	.57
FB-V-F-4	Low-load truncation at 35% DLS	.150 to failure	4,864 (75,723)	.94*
FB-V-G-4	Low-load truncation at 45% DLS	.148 to failure	5,171 (52,293)	1.01*
FB-V-H-4	Low-load truncation at 55% DLS	.145 to failure	6,833 (35,414)	1.32*
FB-V-E-4	High loads clipped at 95% DLS	.145 to failure	3,847 (79,490)	0.74
FB-V-I-4	Mission sequence A	.145 to failure	4,965 (102,459)	0.96
FB-V-J-4	Mission sequence B	.145 to failure	4,392 (90,576)	0.85
FB-V-K-4	Comp load increased 25%	.145 to failure	4,775 (98,635)	0.92
FB-V-L-4	Comp load increased 50%	.145 to failure	4,347 (89,721)	0.84
*Based on flights				

TABLE 72. COMPARISON OF MISSION-MIX CRACK GROWTH LIVES TO THE BASELINE

Test No.	Mission-Mix Variation	Crack Growth ($C_i - C_f$), in.	Test Life N_M	
			Flights (Cycles)	N_M/N_A^a
M-301	(A-A):(A-G):(I-N) = 20:21:1	0.34 to Failure	3,895 (3,100)	0.99
M-302	(A-A):(A-G):(I-N) = 20:20:18	0.145 to Failure	4,127 (3,600)	1.16
M-303	(A-A):(A-G):(I-N) = 18:19:29	0.145 to Failure	5,258	1.7
M-304	(A-A):(A-G):(I-N) = 20:20:29	0.150 to Failure	4,839	1.5
M-305	(A-A):(A-G):(I-N) = 20:20:18	0.150 to Failure	4,390	1.4
^a The baseline spectrum (M-91, Fighter Composite Spectrum, $\sigma_{lim} = 30$ ksi) had the following mixture: (A-A):(A-G):(I-N) = 23:22:6				

TABLE 5-XVI. SUMMARY OF TEST RESULTS FOR MISSION MIX VARIATIONS - GROUP A

Test No.	Mission Mix Variation	Crack Growth ($C_i - C_f$), in.	Test Life, N_M	
			Flights (cycles)	N_M/N_B^b
M-306	(A-A):(A-G):(I-N) = 70:68:68 ^a	0.145 to failure	5,667 (96,867)	0.91 ^c
M-307	(A-A):(A-G):(I-N) = 92:24:91	0.148 to failure	5,583 (92,031)	.87
M-308	(A-A):(A-G):(I-N) = 24:90:92	0.148 to failure	13,296 (186,390)	1.77
^a Numerical values are No. of flights.				
^b F-B-4, the baseline composite mission was compared.				
^c Based on cycles.				

TABLE 74. SUMMARY OF TRANSPORT SPECTRUM VARIATION TEST RESULTS

Test No.	Spectrum variation	Crack growth (C_i to C_f) in.	Test life, N_f	
			Flights (cycles)	N_f/N_B^a
T-B-V-1	Comp loads set to zero	0.26 to 0.48	10,972 (1,457,138)	1.17
T-B-V-2	Increase stress level by 1.6 factor	0.26 to 0.57	2,751 (365,314)	0.25
T-B-V-4	Increase comp stress level by 50%	0.26 to 0.44	7,364 (377,930)	0.95
T-B-V-5	Increase comp stress level by 25%	0.26 to 0.46	8,013 (1,064,251)	0.95
T-B-V-7	Truncate low load at 8 ksi	0.27 to 0.49	9,969 (1,134,538)	0.98
T-B-V-8	Lower σ_{min} to $0.75\sigma_{max}$	0.26 to 0.49	4,317 (573,279)	0.47
T-B-V-9	Delete all cycles except G-A-G	0.26 to 0.51	16,536 (16,536)	1.11 ^b
^a $N_B = 9,674$ flights (1,284,856 cycles) from $C_i = 0.26$ in. to $C_f = 0.51$ in. ^b Calculated based on number of flights				

TABLE 75. FIGHTER BASELINE AND SPECTRUM VARIATION TESTS
COMPARISON OF PREDICTION ACCURACIES, CRKGRO VERSUS FLTFRO

Test No.	Mission Type	Test Life N_T , Flt (cyc) (C_i-C_f), in.	CRKGRO Prediction				FLTGRO Predictions	
			w/o Load Interaction		Load Interaction		N_p	N_p/N_T
			N_p	N_p/N_T	N_p	N_p/N_T		
F-B-1	A-A baseline	2,829 (73,552) (0.145 to failure)	1,573 (41,189)	0.56	2,153 (55,164)	0.75	2,681	0.95
F-B-2	A-G baseline	5,403 (102,677) (0.148 to failure)	3,034 (74,954)	.73	4,949 (94,463)	.92	6,967	1.29
F-B-3	I-N baseline	30,142 (167,721) (0.145 to failure)	19,595 (109,019)	.65	28,584 (159,335)	.95	36,308	1.20
F-B-4	Composite baseline	5,174 (106,705) (0.148 to failure)	2,490 (51,218)	.48	3,317 (68,291)	.64	3,779	.73
FB-V-A-1	A-A zero comp	3,405 (88,528) (0.145 to failure)	1,573 (40,723)	.46	3,021 (78,790)	.89	3,695	1.08
FB-V-A-2	A-G zero comp	5,429 (103,161) (0.15 to failure)	3,796 (72,213)	.70	5,826 (110,382)	1.07	8,024	1.48
FB-V-A-3	I-N zero comp	34,720 (193,202) (0.145 to failure)	19,944 (110,125)	.57	34,955 (195,134)	1.01	42,023	1.21
FB-V-A-4	Composite zero comp	5,995 (123,689) (0.145 to failure)	2,491 (51,949)	.42	4,965 (102,662)	.83	5,442	.91
FB-V-B-3	I-N DLS = 25 ksi	40,080 (222,331) (0.145 to 0.83)	36,875 (204,544)	.92	54,186 (300,147)	1.35	68,182	1.70
FB-V-B-4	Composite DLS = 25 ksi	7,736 (159,514) (0.145 to 0.61)	4,302 (89,328)	.56	5,909 (121,231)	.76	7,416	.96
FB-V-C-1	A-A DLS = 35 ksi	1,293 (33,616) (0.145 to failure)	878 (22,859)	.68	1,101 (28,574)	.85	1,442	1.11
FB-V-C-2	A-G DLS = 35 ksi	2,867 (55,045) (0.145 to failure)	2,176 (41,284)	.75	2,706 (51,192)	.93	3,951	1.36
FB-V-C-3	I-N DLS = 35 ksi	19,073 (106,164) (0.145 to failure)	10,955 (60,513)	.57	16,000 (89,178)	.84	20,834	1.09
FB-V-C-4	Composite DLS = 35 ksi	2,303 (47,683) (0.145 to failure)	1,273 (26,226)	.55	1,855 (38,146)	.80	2,073	.90

**TABLE 75. FIGHTER BASELINE AND SPECTRUM VARIATION TESTS
COMPARISON OF PREDICTION ACCURACIES, CRKGRO VERSUS FLTGRO (CONT)**

Test No.	Mission Type	Test Life N _T , Flt (cyc) (C _L -C _F), in.	CRKGRO Prediction				FLTGRO Predictions	
			w/o Load Interaction		Load Interaction		N _p	N _p /N _T
			N _p	N _p /N _T	N _p	N _p /N _T		
FB-V-D-1	A-A 85% DLS clipping	1,939 (50,414) (0.145 to failure)	1,653 (42,852)	0.85	1,922 (49,910)	0.99	3,827	1.47
FB-V-D-4	Composite 85% DLS clipping	2,924 (60,480) (0.145 to failure)	2,516 (52,013)	.86	3,134 (64,714)	1.07	4,331	1.48
FB-V-I-1	A-A 95% DLS clipping	2,133 (55,467) (0.145 to failure)	1,618 (42,069)	.76	1,990 (51,739)	.93	2,800	1.31
FB-V-I-4	Composite 95% DLS clipping	3,847 (79,490) (0.145 to failure)	2,493 (51,506)	.65	3,298 (67,979)	.86	4,527	1.12
FB-V-I-4	Composite 35% DLS truncation	4,864 (75,723) (0.145 to failure)	2,493 (58,619)	.51	3,137 (51,492)	.68	3,818	.78
FB-V-G-4	Composite 45% DLS truncation	5,171 (52,293) (0.148 to failure)	2,905 (29,284)	.56	3,729 (37,651)	.72	4,464	.86
FB-V-H-4	Composite 55% DLS truncation	6,833 (55,414) (0.145 to failure)	3,953 (20,540)	.58	5,171 (26,915)	.76	6,000	.88
FB-V-I-4	Composite mission sequence (A)	4,965 (102,459) (0.145 to failure)	2,491 (51,445)	.50	3,333 (68,911)	.67	3,911	.79
FB-V-J-4	Composite mission sequence (B)	4,392 (90,576) (0.145 to failure)	2,518 (51,349)	.57	3,362 (69,344)	.77	4,178	.95
FB-V-K-4	Composite comp load increased 25%	4,775 (98,635) (0.145 to failure)	2,491 (51,445)	.52	3,111 (64,243)	.65	3,561	.75
FB-V-L-4	Composite comp load increased 50%	4,347 (89,721) (0.145 to failure)	2,491 (51,445)	.57	2,905 (59,997)	.67	3,569	.78

TABLE 75. FIGHTER BASELINE AND SPECTRUM VARIATION TESTS
COMPARISON OF PREDICTION ACCURACIES, CRKGRO VERSUS FLTGRO (CONCL)

Test No.	Mission Type	Test Life N_T , Flt (cyc) ($C_i - C_f$), in.	CRKGRO Predictions				FLTGRO Predictions	
			w/o Load Interaction		Load Interaction		N_p	N_p/N_T
			N_p	N_p/N_T	N_p	N_p/N_T		
M-301	Mission mix variation A-1	3,895 (68,833) (0.135 to failure)	3,580	0.92	4,765	1.22	4,384	1.13
M-302	Mission mix variation A-2	4,127 (71,925) (0.145 to failure)	3,459	.84	4,417	1.07	4,151	1.01
M-303	Mission mix variation A-3	5,258 (79,574) (0.145 to failure)	4,348	.83	5,941	1.13	5,139	.98
M-304	Mission mix variation A-4	4,839 (75,084) (0.150 to failure)	3,664	.76	5,107	1.05	4,494	.93
M-305	Mission mix variation A-5	4,390 (75,641) (0.150 to failure)	3,131	.71	4,178	.95	3,779	.86
M-306	Mission mix variation B-1	5,667 (96,867) (0.145 to failure)	3,111 (53,354)	.55	4,843 (82,785)	.85	5,280	.93
M-307	Mission mix variation B-2	5,583 (92,031) (0.148 to failure)	2,905 (47,985)	.52	3,935 (64,925)	.71	4,434	.79
M-308	Mission mix variation B-3	13,296 (186,390) (0.148 to failure)	4,641 (65,087)	.35	9,382 (131,556)	.71	7,620	.57
Average prediction ratio				0.64		0.88		1.04
Standard deviation				0.15		0.17		0.26

TABLE 76. COMPARISON OF PREDICTION ACCURACY FOR TRANSPORT SPECTRA CASES -
CRKGRO VERSUS FLTGRO

Test No.	Mission Type	Test Life Np, flt (cyc) (C _i - C _f), in.	CRKGRO prediction				FLTGRO Predictions	
			Load Interaction		W/O load interaction		Np	Np /N _T
			Np	Np/N _T	Np	Np/N _T		
T-B-1	Composite baseline	9,675(1,284,857) 0.26 - 0.505	11,827(1,570,754)	1.22	16,110(2,139,375)	1.67	15,061	1.56
T-P-V-1	Zero-out compression	10,972(1,457,138) 0.255 - 0.48	18,219(2,419,688)	1.66	16,476(2,188,212)	1.50	18,783	1.71
T-B-V-2	Increasing stress level by 1.6 factor	2,751(365,314) 0.26-0.568	2,189(289,490)	0.79	2,952(392,086)	1.07	2,696	0.98
T-B-V-4	Increasing comp load by 50%	7,364(977,990) 0.258-0.44	9,424(1,251,648)	1.28	13,844(1,838,498)	1.88	12,640	1.72
T-B-V-5	Increasing comp load by 25%	8,013(1,064,251) 0.255-0.458	10,555(1,401,826)	1.32	15,003(1992,440)	1.87	13,833	1.73
T-B-V-7	Truncating low load cycles below 8 ksi	9,969 0.265-0.493	11,631	1.17	15,921	1.60	14,993	1.50
T-B-V-8	Lowering min stresses to 0.75 σ_{max}	4,317(573,280) 0.255-0.488	5,694(756,159)	1.32	6,481(960,690)	1.50	7,891	1.83
T-B-V-9	G-A-G cycles only	16,535(16,535) 0.26-0.505	15,869(15,869)	0.96	27,357(27,357)	1.65	16,031	0.97
Average prediction ratio Standard deviation				1.22 0.26		1.59 0.26		1.50 0.34

TABLE 77. SUMMARY OF CORRELATION RESULTS

	Analytical prediction methodology	Average N_p/N_T	Standard deviation
Fighter spectra test group	CRKGRO load interaction	0.88	0.17
	CRKGRO without load interaction	0.64	0.15
	FLTGRO load interaction	1.04	0.26
Transport spectra test group	CRKGRO load interaction	1.22	0.26
	CRKGRO without load interaction	1.59	0.26
	FLTGRO load interaction	1.50	0.34

TABLE 78. COMPARISON OF PREDICTION ACCURACY FOR FIGHTER SPECTRA
CASES - NEW VERSUS OLD EQUATIONS

Test No.	Mission Type	Test Life N_T , Flt (cyc) (C_i-C_f), in.	CRKGRO Prediction			
			New Equation		Old Equation	
			N_p	N_p/N_T	N_p	N_p/N_T
F-B-1	A-A baseline	2,829 (73,552) (0.145 to failure)	2,225 (57,861)	0.79	2,153 (55,164)	0.75
F-B-2	A-G baseline	5,403 (102,677) (0.148 to failure)	5,073 (96,395)	.94	4,949 (94,463)	.92
F-B-3	I-N baseline	30,142 (167,721) (0.145 to failure)	27,775 (154,437)	.92	28,584 (159,335)	.95
F-B-4	Composite baseline	5,174 (106,705) (0.148 to failure)	3,317 (68,490)	.64	3,317 (68,291)	.64
FB-V-A-1	A-A zero comp	3,405 (88,528) (0.145 to failure)	3,021 (78,790)	.89	3,021 (78,790)	.89
FB-V-A-2	A-G zero comp	5,429 (103,161) (0.15 to failure)	5,826 (110,382)	1.07	5,826 (110,382)	1.07
FB-V-A-3	I-N zero comp	34,720 (193,202) (0.145 to failure)	34,955 (195,134)	1.01	34,955 (195,134)	1.01
FB-V-A-4	Composite zero comp	5,995 (123,689) (0.145 to failure)	4,965 (102,662)	.83	4,965 (102,662)	.83
FB-V-B-3	I-N DLS = 25 ksi	40,080 (222,331) (0.145 to 0.83)	52,552 (292,421)	1.31	54,186 (300,147)	1.35
FB-V-B-4	Composite DLS = 25 ksi	7,736 (159,514) (0.145 to 0.61)	5,913 (122,100)	.77	5,909 (121,231)	.76
FB-V-C-1	A-A DLS = 35 ksi	1,293 (33,616) (0.145 to failure)	1,173 (30,507)	.91	1,101 (28,574)	.85
FB-V-C-2	A-G DLS = 35 ksi	2,867 (55,045) (0.145 to failure)	2,774 (52,706)	.96	2,706 (51,192)	.93
FB-V-C-3	I-N DLS = 35 ksi	19,073 (106,164) (0.145 to failure)	15,520 (86,401)	.81	16,000 (89,178)	.84
FB-V-C-4	Composite DLS = 35 ksi	2,303 (47,683) (0.145 to failure)	1,856 (38,257)	.80	1,855 (38,146)	.80

TABLE 78. COMPARISON OF PREDICTION ACCURACY FOR FIGHTER SPECTRA
CASES - NEW VERSUS OLD EQUATIONS (CONT)

Test No.	Mission Type	Test Life N_T , Flt (cyc) ($C_i - C_f$), in.	CRKGRO Prediction			
			New Equation		Old Equation	
			N_p	N_p/N_T	N_p	N_p/N_T
FB-V-D-1	A-A 85% DLS clipping	1,939 (50,414) (0.145 to failure)	1,982 (51,532)	1.02	1,922 (49,910)	0.99
FB-V-D-4	Composite 85% DLS clipping	2,924 (60,480) (0.145 to failure)	3,209 (66,229)	1.10	3,134 (64,714)	1.07
FB-V-E-1	A-A 95% DLS clipping	2,133 (55,467) (0.145 to failure)	2,061 (53,583)	.97	1,990 (51,739)	.93
FB-V-E-4	Composite 95% DLS clipping	3,847 (79,490) (0.145 to failure)	3,314 (68,399)	.86	3,298 (67,979)	.86
FB-V-F-4	Composite 35% DLS truncation	4,864 (75,723) (0.145 to failure)	(51,666)	.68	3,137 (51,492)	.68
FB-V-G-4	Composite 45% DLS truncation	5,171 (52,293) (0.148 to failure)	(39,773)	.76	3,729 (37,651)	.72
FB-V-H-4	Composite 55% DLS truncation	6,833 (35,414) (0.145 to failure)	(27,805)	.79	5,171 (26,915)	.76
FB-V-I-4	Composite mission sequence (A)	4,965 (102,459) (0.145 to failure)	3,317 (68,489)	.67	3,333 (68,911)	.67
FB-V-J-4	Composite mission sequence (B)	4,392 (90,576) (0.145 to failure)	3,362 (69,344)	.77	3,362 (69,344)	.77
FB-V-K-4	Composite comp load increased 25%	4,775 (98,635) (0.145 to failure)	3,109 (64,183)	.65	3,111 (64,243)	.65
FB-V-L-4	Composite comp load increased 50%	4,347 (89,721) (0.145 to failure)	2,903 (59,937)	.67	2,905 (59,997)	.67

TABLE 78. COMPARISON OF PREDICTION ACCURACY FOR FIGHTER SPECTRA
CASES - NEW VERSUS OLD EQUATIONS (CONCL)

Test No.	Spectrum Type	Test Life N_T , Flt (cyc) ($C_i - C_f$), in.	CRKGRO Predictions			
			New Equation		Old Equation	
			N_p	N_p/N_T	N_p	N_p/N_T
M-301	Mission mix variation A-1	3,895 (68,833) (0.135 to failure)	4,443	1.14	4,765	1.22
M-302	Mission mix variation A-2	4,127 (71,925) (0.145 to failure)	4,234	1.03	4,417	1.07
M-303	Mission mix variation A-3	5,258 (79,574) (0.145 to failure)	5,511	1.05	5,941	1.13
M-304	Mission mix variation A-4	4,839 (75,084) (0.150 to failure)	4,701	.97	5,107	1.05
M-305	Mission mix variation A-5	4,390 (75,641) (0.150 to failure)	3,895	.89	4,178	.95
M-306	Mission mix variation B-1	5,667 (96,867) (0.145 to failure)	4,637 (79,263)	.82	4,843 (82,785)	.85
M-307	Mission mix variation B-2	5,583 (92,031) (0.148 to failure)	3,935 (64,925)	.71	3,935 (64,925)	.71
M-308	Mission mix variation B-3	13,296 (186,390) (0.148 to failure)	7,528 (105,582)	.57	9,382 (131,556)	.71
Average prediction ratio				.87		.88
Standard deviation				.17		.17

TABLE 79. COMPARISON OF PREDICTION ACCURACY FOR TRANSPORT SPECTRA CASES -
NEW VERSUS OLD EQUATIONS

Test No.	Mission Type	Test Life N_T , flt (cyc) ($C_i - C_f$), in.	CRKGRO prediction			
			New equation		Old equation	
			N_p	N_p/N_T	N_p	N_p/N_T
T-B-1	Composite baseline	9,675(1,284,857) 0.26 - 0.505	6,725(893,016)	0.70	11,827(1,570,754)	1.22
T-B-V-1	Zero-out compression	10,972(1,457,138) 0.255 - 0.48	19,239(2,555,089)	1.75	18,219(2,419,688)	1.66
T-B-V-2	Increasing stress level by 1.6 factor	2,751(365,314) 0.26-0.568	1,235(163,985)	0.45	2,189(289,490)	0.79
T-B-V-4	Increasing comp load by 50%	7,364(977,990) 0.258-0.44	3,921(520,677)	0.53	9,424(1,251,648)	1.28
T-B-V-5	Increasing comp load by 25%	8,013(1,064,251) 0.255-0.458	5,141(682,739)	0.64	10,555(1,401,826)	1.32
T-B-V-7	Truncating low load cycles below 8 ksi	9,969 0.265-0.493	6,542	0.66	11,681	1.17
T-B-V-8	Lowering min stresses to $0.75 \sigma_{max}$	4,317(573,280) 0.255-0.488	4,367(579,935)	1.01	5,694(756,159)	1.32
T-B-V-9	G-A-G cycles only	16,535(16,535) 0.26-0.505	7,673(7,673)	0.46	15,869(15,869)	0.96
Average prediction ratio Standard deviation				0.78 0.43		1.22 0.26

TABLE 80. RESULTS OF SENSITIVITY STUDY ON R_{cut}^- VALUES TO
PREDICTION RATIO, N_P/N_T

Test No. R_{cut}^-	-0.75	-0.50	-0.25
T-B-V-4	$N_P/N_T = 0.53$	$N_P/N_T = 1.10$	$N_P/N_T = 1.73$
T-B-V-5	$N_P/N_T = 0.64$	$N_P/N_T = 1.09$	$N_P/N_T = 1.72$
F-B-4	$N_P/N_T = 0.64$	$N_P/N_T = 0.66$	$N_P/N_T = 0.68$
F-B-V-B-3	$N_P/N_T = 1.31$	$N_P/N_T = 1.35$	$N_P/N_T = 1.36$

TABLE 81. COMPARISON OF PREDICTION ACCURACY FOR FIGHTER SPECTRUM CASES -
WITH VARYING NEGATIVE STRESS RATIO CUTOFF VALUES

Test No.	Mission Type	Test Life N_T , Flt (cyc) (C_i-C_f), in.	CRKGRO Prediction			
			Load interaction $R^+ = 0.75$ $R^- = -0.75$		Load interaction $R^+ = 0.75$ $R^- = -0.5$	
			N_p	N_p/N_T	N_p	N_p/N_T
F-B-1	A-A baseline	2,829 (73,552) (0.145 to failure)	2,225 (57,861)	0.79	2,243 (58,324)	0.79
F-B-2	A-G baseline	5,403 (102,677) (0.148 to failure)	5,073 (96,395)	.94	5,112 (97,121)	.95
F-B-3	I-N baseline	30,142 (167,721) (0.145 to failure)	27,775 (154,457)	.92	28,480 (158,491)	.94
F-B-4	Composite baseline	5,174 (106,705) (0.145 to failure)	5,517 (68,490)	.64	3,423 (70,682)	.66
FB-V-A-1	A-A zero comp	3,405 (88,528) (0.145 to failure)	3,021 (78,790)	.89	3,020 (78,542)	.89
FB-V-A-2	A-G zero comp	5,429 (103,161) (0.15 to failure)	5,826 (110,582)	1.07	6,052 (114,992)	1.11
FB-V-A-3	I-N zero comp	34,720 (193,202) (0.145 to failure)	34,955 (195,134)	1.01	35,680 (198,541)	1.03
FB-V-A-4	Composite zero comp	5,995 (123,689) (0.145 to failure)	4,570 (94,388)	.76	4,965 (102,458)	.83
FB-V-B-3	I-N DLS = 25 ksi	40,080 (222,331) (0.145 to 0.83)	52,552 (292,421)	1.31	53,994 (300,444)	1.35
FB-V-B-4	Composite DLS = 25 ksi	7,736 (159,514) (0.145 to 0.61)	5,913 (122,100)	.77	6,021 (124,354)	.78
FB-V-C-1	A-A DLS = 35 ksi	1,293 (33,616) (0.145 to failure)	1,173 (30,507)	.91	1,173 (30,506)	.91
FB-V-C-2	A-G DLS = 35 ksi	2,867 (55,045) (0.145 to failure)	2,774 (52,706)	.96	2,810 (87,686)	.97
FB-V-C-3	I-N DLS = 35 ksi	19,073 (106,164) (0.145 to failure)	15,520 (86,401)	.81	15,734 (87,686)	.83
FB-V-C-4	Composite DLS = 35 ksi	2,303 (47,683) (0.145 to failure)	1,856 (38,257)	.80	1,873 (38,707)	.81
FB-V-D-1	A-A 85% DLS clipping	1,939 (50,414) (0.145 to failure)	1,982 (51,532)	1.02	1,984 (51,591)	1.02
FB-V-D-4	Composite 85% DLS clipping	2,924 (60,480) (0.145 to failure)	3,209 (66,229)	1.10	3,221 (66,528)	1.1
FB-V-E-1	A-A 95% DLS clipping	2,133 (55,467) (0.145 to failure)	2,051 (53,333)	.96	2,051 (53,333)	.96
FB-V-E-4	Composite 95% DLS clipping	3,847 (79,190) (0.145 to failure)	3,314 (68,399)	.86	3,317 (68,491)	.86

TABLE 81. COMPARISON OF PREDICTION ACCURACY FOR FIGHTER SPECTRUM CASES -
WITH VARYING NEGATIVE STRESS RATIO CUTOFF VALUES (CONCL)

Test No.	Mission Type	Test Life N_T , Flt (cyc) (C_i-C_f), in.	CRKGRO Prediction			
			Load interaction $R^+ = 0.75$ $R^- = -0.75$		Load interaction $R^+ = 0.75$ $R^- = -0.50$	
			N_p	N_p/N_T	N_p	N_p/N_T
FB-V-F-4	Composite 35% DLS truncation	4,864 (75,723) (0.145 to failure)	(51,666)	0.68	(52,051)	0.69
FB-V-G-4	Composite 45% DLS truncation	5,171 (52,293) (0.148 to failure)	(39,773)	.76	(39,835)	.76
FB-V-H-4	Composite 55% DLS truncation	6,833 (35,414) (0.145 to failure)	(27,805)	.79	(27,830)	.79
FB-V-I-4	Composite mission sequence (A)	4,965 (102,459) (0.145 to failure)	3,317 (68,489)	.67	3,423 (70,682)	.69
FB-V-J-4	Composite mission sequence (B)	4,392 (90,576) (0.145 to failure)	3,362 (69,344)	.77	3,379 (69,767)	.77
FB-V-K-4	Composite comp load increased 25%	4,775 (98,635) (0.145 to failure)	3,128 (64,666)	.66	3,163 (65,391)	.66
FB-V-L-4	Composite comp load increased 50%	4,347 (89,721) (0.145 to failure)	3,092 (63,733)	.71	3,111 (64,244)	.72
M-301	Mission mix variation A-1	3,895 (68,833) (0.135 to failure)	4,475	1.15	4,526 (79,994)	1.16
M-302	Mission mix variation A-2	4,127 (71,925) (0.145 to failure)	4,234	1.03	4,243 (73,970)	1.03
M-303	Mission mix variation A-3	5,258 (79,574) (0.145 to failure)	5,511	1.05	5,611 (85,452)	1.07
M-304	Mission mix variation A-4	4,839 (75,084) (0.150 to failure)	4,701	.97	4,770 (74,070)	.99
M-305	Mission mix variation A-5	4,390 (75,641) (0.150 to failure)	3,895	.89	3,946 (68,384)	.90
M-306	Mission mix variation B-1	5,667 (96,867) (0.145 to failure)	4,347 (74,474)	.77	4,553 (77,972)	.80
M-307	Mission mix variation B-2	5,583 (92,031) (0.148 to failure)	3,935 (64,925)	.71	3,952 (65,348)	.71
M-308	Mission mix variation B-3	13,296 (186,390) (0.148 to failure)	7,940 (111,353)	.60	7,940 (111,353)	.60
Average prediction ratio				.87		.88
Standard deviation				.17		.17

TABLE 82. COMPARISON OF PREDICTION ACCURACY FOR TRANSPORT SPECTRA CASES -
WITH VARYING NEGATIVE STRESS RATIO CUTOFF VALUES

Test No.	Mission Type	Test Life N_T , flt (cyc) ($C_i - C_f$), in.	CRKGRO prediction			
			$R_{cut} = -0.75$		$R_{cut} = -0.50$	
			N_p	N_p/N_T	N_p	N_p/N_T
T-B-1	Composite baseline	9,675(1,284,857) 0.26 - 0.505	6,725(893,016)	0.70	9,421(1,251,109)	0.97
T-B-V-1	Zero-out compression	10,972(1,457,138) 0.255 - 0.48	19,239(2,555,089)	1.75	19,239(2,555,089)	1.75
T-B-V-2	Increasing stress level by 1.6 factor	2,751(365,314) 0.26-0.568	1,235(163,985)	0.45	1,730(229,792)	0.63
T-B-V-4	Increasing comp load by 50%	7,364(977,990) 0.258-0.44	3,921(520,677)	0.53	8,086(1,073,380)	1.10
T-B-V-5	Increasing comp load by 25%	8,013(1,064,251) 0.255-0.458	5,141(682,739)	0.64	8,766(1,164,107)	1.09
T-B-V-7	Truncating low load cycles below 8 ksi	9,969 0.265-0.493	6,542	0.66	9,316(1,060,169)	0.93
T-B-V-8	Lowering min stresses to $0.75 \sigma_{max}$	4,317(573,280) 0.255-0.488	4,367(579,935)	1.01	5,360(711,838)	1.24
T-B-V-9	G-A-G cycles only	16,535(16,535) 0.26-0.505	7,673(7,673)	0.46	11,648(11,648)	0.70
Average prediction ratio Standard deviation				0.78 0.43		1.05 0.35

REFERENCES

1. Anon, "Military Standard, Aircraft Structural Integrity Program, Airplane Requirements," MIL-STD-1530A, December 1975
2. Chang, J. B., Stolpestad, J. H., Shinozuka, M., and Vaicaitis, R., "Improved Methods for Predicting Spectrum Loading Effects - Phase I Report, Volume I - Results and Discussion," AFFDL-TR-79-3036, Vol I, Air Force Flight Dynamics Laboratory, Wright-Patterson Air Force Base, Ohio, 1979
3. Chang, J.B., and Stolpestad, J.H., "Improved Methods for Predicting Spectrum Loading Effects - Phase I Report, Volume II - Test Data," AFFDL-TR-79-3036, Vol II, Air Force Flight Dynamics Laboratory, Wright-Patterson Air Force Base, Ohio, 1979
4. Chang, J.B., and Szamosi, M., "A User's Manual for a Detailed Level Fatigue Crack Growth Analysis Computer Code, Volume I - the CRKGRO Program," AFWAL-TR-81-3093, Vol I, Air Force Wright Aeronautical Laboratories, Flight Dynamics Laboratory, Wright-Patterson Air Force Base, Ohio, 1981
5. Chang, J.B., and Szamosi, M., "A User's Manual for a Computer Program to Predict Fatigue Crack Growth on Flight-By-Flight Basis (FLTGRO)" AFWAL-TR-81-3094, Air Force Aeronautical Laboratories, Flight Dynamics Laboratory, Wright-Patterson Air Force Base, Ohio, 1981
6. Kruse, G.S., Tanner, C.J., and Wilson, P.J., "User's Manual for APAS III, Volume 1, "CASD-NAS-76-028, General Dynamics Convair Division, San Diego, California, 1976
7. Oman, B.H., Kruse, G.S., and Reed, T.F., "Structural Technology Evaluation Program (STEP), Vol I - Basic Technical Report," AFFDL-TR-77-110, Air Force Flight Dynamics Laboratory, WPAFB, Ohio, 1978
8. Anon, "Tentative Test Method for Constant Amplitude Fatigue Crack Growth Rate Above 10^{-8} m/cycle," E647-78T, Annual Book of ASTM Standards, Part 10, Metals-Physical Mechanical Corrosion Testing, American Society for Testing and Materials, Philadelphia, Pennsylvania, 1979
9. Paris, P.C., Gomez, M.P., and Anderson, W.E., "A Rational Analytic Theory of Fatigue," The Trend in Engineering, Vol 13, No. 1, 1961
10. Forman, R.G., Hearney, V.E., and Engle, R.M., "Numerical Analysis of Crack Propagation in Cyclic-Loaded Structures," Journal of Basic Engineering, Trans of ASME, Vol 89, 1967

11. Walker, K., "The Effect of Stress Ratio During Crack Propagation and Fatigue for 2024-T3 and 7-75-T6 Aluminum," ASTM STP 462, American Society for Testing and Materials, 1970
12. Collipriest, J.E., Jr., and Ehret, R.M., "Computer Modeling of Part-Through-Crack Growth," SD72-CE-15, Rockwell International, Space Division, 1972
13. Hall, L.R., Shah, R.C., and Engstrom, W.L., "Fracture and Fatigue Crack Growth Behavior of Surface Flaws and Flaws Originating at Fastener Holes," AFFDL-TR-74-47, Air Force Flight Dynamics Laboratory, WPAFB, Ohio, 1974
14. Bell, P.D., and Creager, M., "Crack Growth Analyses for Arbitrary Spectrum Loading," AFFDL-TR-74-129, Air Force Flight Dynamics Laboratory, WPAFB, Ohio, 1974
15. Hudak, S.J., Jr, Saxener, A., Bucci, R.J., and Malcolm, R.C., "Development of Standard Methods of Testing and Analyzing Fatigue Crack Growth Rate Data," AFML-TR-78-40, Air Force Materials Laboratory, WPAFB, Ohio, 1978
16. Chang, J.B., "Improved Methods for Predicting Spectrum Loading Effects - First Quarterly Technical Interim Report," NA-78-491, Rockwell International, North American Aircraft Division, Los Angeles, California 1978
17. Chang, J.B., Klein, E., and Cheng, J.S., "Automated Procedures for Fatigue Crack Growth Test Data Processing and Presentation (PLOT RATE User's Guide)," NA-78-860, Rockwell International, 1979
18. Wheeler, O.E., "Spectrum Loading and Crack Growth," Transaction of the ASME, Journal of Basic Engineering, pp 181-186, March 1972
19. Willenborg, J., Engle, R.M., and Wood, H.A., "A Crack Growth Retardation Model Using an Effective Stress Concept," AFFDL-TR-71-1, January 1971
20. Vroman, G.A., "Analytical Prediction of Crack Growth Retardation Using a Residual Stress Concept," Briefing Charts, Rockwell International, North American Aircraft Division, May 1971
21. Elber, W., "The Significance of Fatigue Crack Closure," ASTM STP 486, Damage Tolerance in Aircraft Structures, American Society for Testing and Materials, 1971, pp 230-242
22. Bell, P.D., and Wolfman, A., "Mathematical Modeling of Crack Growth Interaction Effects," ASTM, STP 595, Fatigue Crack Growth Under Spectrum Loads, American Society for Testing and Materials, 1976

23. Dill, H.D., and Saff, C.R., "Spectrum Crack Growth Prediction Method Based on Crack Surface Displacement and Contract Stress," ASTM STP 595, Fatigue Crack Growth, American Society for Testing and Materials, May 1976
24. Chang, J.B., Engle, R.M., and Stolpestad, J., "Fatigue Crack Growth Behavior and Life Predictions for 2219-T851 Aluminum Subjected to Variable-Amplitude Loadings," presented at the 13th National Symposium on Fracture Mechanics, 16-18 June 1980, Philadelphia, Pennsylvania
25. Bueckner, H.F., "A Novel Principle for the Computation of Stress Intensity Factors," Z. Angew, Match Mech, Vol 50, 1970
26. Gallagher, J.P., "A Generalized Development of Yield-Zone Models," AFFDL-TM-74-28, Air Force Flight Dynamics Laboratory, Wright-Patterson Air Force Base, Ohio, 1974
27. Hsu, T.M., and Lassiter, L.W., "Effect of Compressive Overload on Fatigue Crack Growth," AIAA paper 74-365, April 1974
28. Stevens, R.I., Chen, D.K., and Nom, B.W., "Fatigue Crack Growth With Negative Stress Ratio Following Single Overloads in 2024-T3 and 7075-T6 Aluminum Alloy," ASTM, STP 595, Fatigue Crack Growth Under Spectrum Loads, American Society for Testing and Materials, 1976
29. Chang, J.B., "Advanced Bomber Fracture Mechanics Correlation Studies," presented at the WESTEC Conference, Los Angeles, California, 1975
30. Chang, J.B., Streittmatter, S.P., and Tung, P.P., "Effect of B-1 Bomber Spectra Variation on Crack Growth," NA-75-881, Rockwell International, North American Aircraft Division, 26 March 1976
31. Chang, J.B., and Cheng, J.S., "Cost-Effective Fatigue Crack Growth Analysis for Flight Spectrum Loading," NA-78-629, Rockwell International, North American Aircraft Division, Los Angeles 1978
32. Wells, A.A., "Application of Fracture Mechanics at and Beyond General Yielding," British Welding Research Assoc, Report M13/63, 1963
33. Chang, J.B., "Development of Fatigue Crack Growth Model for Flight Spectrum Containing Compressive Load Cycles," NA-76-858, Rockwell International, Los Angeles, 1977
34. Engle, R.M., "CRACKS, A Fortran IV digital Computer Program for Crack Propagation Analysis," AFFDL-TR-70-107, Air Force Flight Dynamics Laboratory, Wright-Patterson Air Force Base, Ohio, 1970

35. Shan, S.K., Numerical Methods and Computers, Addison-Wesley Publishing Company, Inc, 1965
36. Johnson, W.S., "CGR, An Improved Computerized Model to Predict Fatigue Crack Growth Under Spectrum Loading," NSRDC, Report 4577, 1975
37. Szamosi, M., "Crack Propagation Analysis by Vroman's Model, Program EFFGRO," NA-72-94, Rockwell International, Los Angeles, 1972
38. Stolpestad, J., "Summary Report of the B-1 Fracture Mechanics Analysis Verification Test Program," NA-75-675, Rockwell International, Los Angeles, California, 1975
39. Chang, J.B., Summary, ASTM, STP 687, Part-Through Crack Fatigue Life Prediction, American Society for Testing and Materials, Philadelphia, Pennsylvania, 1979
40. Chang, J.B., "Improved Methods for Predicting Spectrum Loading Effects - Fifth Quarterly Interim Report," NA-78-491-5, Rockwell International, North American Aircraft Division, Los Angeles, California
41. Bowie, O.L., "Analysis of an Infinite Plate Containing Radial Cracks Originating from the Boundary of an Internal Circular Hole," Journal of Mathematics and Physics, Vol 35, pp 60-71, 1956
42. Shah, R.C., and Kobayashi, A.S., "In the Surface Flaw Problem," The Surface Crack: Physical Problem and Computation Solutions, American Society of Mechanical Engineers, New York, 1972
43. Newman, J.C., Jr., and Raju, I.S., "Analysis of Surface Crack in a Finite Plate Under Tension or Bending Loads," NASA-TP-1578, NASA Langley Research Center, Hampton, Virginia, 1979
44. Dowling, N.E., "Fatigue Failure Predictions for Complicated Stress Strain Histories," University of Illinois, Urbana, Illinois, Report 337, 1971
45. Streittmatter, S., "A Method of Counting Spectrum Load Cycles," TFD-72-358, Rockwell International, Los Angeles, 1972
46. Clay, L.E., Sandlin, N.H., Marcock, D.S., Brown, K.E., Johnson, R.L., and David, J.C., "Force Management Method, Task I Report, Current methods," AFFDL-TR-78-183, Air Force Flight Dynamics Laboratory, WPAFB, Ohio, 1978
47. Gallagher, J.P., "Estimating Fatigue Crack Lives for Aircraft: Techniques," Experimental Mechanics, Vol 16, No. 11, pp 425-453, November 1976

48. Dill, H.D., and Young, M.T., "Stress History Simulation," Volume I, A User's Manual for a Computer Program to Generate Stress History Simulation, AFFDL-TR-76-113, Air Force Flight Dynamics Laboratory, Wright-Patterson Air Force Base, Ohio, March 1977
49. Anon, Military Specification, "Airplane Damage Tolerance Requirements," MIL-A-83444, July 1974
50. Anon, Military Specification, "Airplane Strength and Rigidity Reliability Requirements, Repeated Loads, and Fatigue," MIL-A-8866B, June 1975
51. Brussat, T.R., "Rapid Calculation of Fatigue Crack by Integration," Fracture Toughness and Slow-Stable Cracking, ASTM STP559, 1974
52. Chang, J.B., and Cheng, J.S., "Cost-Effective Fatigue Crack Growth Analysis for Flight Spectrum Loading," NA-78-629, Rockwell International, Los Angeles, California, 1978
53. Poe, C.C., Jr., "Stress Intensity Factor for a Cracked Sheet With Riveted and Uniformly Spaced Stringers," NASA-TR-R-358, Washington, D.C., May 1971
54. Chang, J.B., and Hiyama, R., "Improved Methods for Predicting Spectrum Loading Effects - Seventh Quarterly Interim Report," NA-78-491-7, Rockwell International, Los Angeles, California, 1980
55. Anon, "User's Manual for VDEP II, Computer Program to Assess Impact of Fatigue and Fracture Criteria on Weight and Cost of Transport Aircraft," CASD-CIH-75-001, General Dynamics, Convair Division, San Diego, California, 1974
56. Chang, J.B., and K-W Liu, "Improved Methods for Predicting Spectrum Loading Effects - Eighth Quarterly Interim Report," NA-78-491-8, Rockwell International, Los Angeles, California 1980
57. Chang, J.B., "Improved Methods for Predicting Spectrum Loading Effects - Ninth Quarterly Interim Report," NA-78-491-9, Rockwell International, Los Angeles, California 1980
58. Chang, J.B., "Improved Methods for Predicting Spectrum Loading Effects - Tenth Quarterly Interim Report," NA-78-491-10, Rockwell International, Los Angeles, California, 1981